

AD 602764

WL TDR-64-53

WL
TDR
64-53

A STUDY OF THE FEASIBILITY OF SHOCK ISOLATING
VERY LARGE MANNED UNDERGROUND STRUCTURES

TECHNICAL DOCUMENTARY REPORT NO. AFWL TDR-64-53

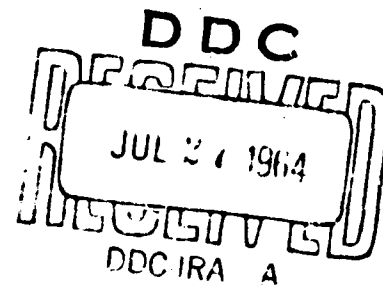
June 1964



Research and Technology Division
AIR FORCE WEAPONS LABORATORY
Air Force Systems Command
Kirtland Air Force Base.
New Mexico

Project No. 8811

20041215 102



BEST AVAILABLE COPY

(Prepared under Contract AF 29(601)-6053
by H. R. Saffell, J. G. Ved, L. S. Thomas
The Ralph M. Parsons Company, Los
Angeles, California)

Research and Technology Division
Air Force Systems Command
AIR FORCE WEAPONS LABORATORY
Kirtland Air Force Base
New Mexico

When Government drawings, specifications, or other data are used for any purpose other than in connection with a definitely related Government procurement operation, the United States Government thereby incurs no responsibility nor any obligation whatsoever; and the fact that the Government may have formulated, furnished, or in any way supplied the said drawings, specifications, or other data, is not to be regarded by implication or otherwise as in any manner licensing the holder or any other person or corporation, or conveying any rights or permission to manufacture, use, or sell any patented invention that may in any way be related thereto.

This report is made available for study upon the understanding that the Government's proprietary interests in and relating thereto shall not be impaired. In case of apparent conflict between the Government's proprietary interests and those of others, notify the Staff Judge Advocate, Air Force Systems Command, Andrews AF Base, Washington 25, DC.

This report is published for the exchange and stimulation of ideas; it does not necessarily express the intent or policy of any higher headquarters.

DDC AVAILABILITY NOTICE

Qualified requesters may obtain copies of this report from DDC.

FOREWORD

This study was undertaken to investigate the feasibility of isolating a very large underground structure from the effects of severe ground motion resulting from nuclear explosions. While size per se should not be a critical parameter in the performance of a shock isolation system, the oversight of practical design requirements tend to become more serious as size is increased. In view of the lack of an accepted and comprehensive standard of performance which might serve as a guide to the design of such systems, the question of feasibility is approached in this study by a close examination of all factors which previous experience with smaller systems has shown to be of significance. In particular, damping, flexibility of the supported load, sloshing of liquid filled tanks, control sensitivity, and other special design considerations frequently given only cursory attention are investigated here in detail. The study is then carried to the point where the basic concepts are established and the equations of motion of the complete system formulated and presented in a form permitting final optimization and refinement.

The authors wish to extend their appreciation to Dr. S. T. Epure, Daniel Freze and R. H. F. Boothe of The Ralph M. Parsons Company for their technical contributions; to G. S. Rasmussen & Associates for developing, programming and solving the equations for determining the unrestrained mode frequencies of the cage; and to R. T. Frankian & Associates for their assistance in formulating the time histories of the ground motions. In addition, the invaluable assistance rendered by Major Robert Crawford, Captain Douglas Merkle and Lt. John Flory of the Air Force Weapons Laboratory is gratefully acknowledged.

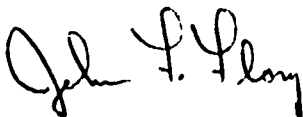
Data on liquid springs were obtained through the generous cooperation of the Cleveland Pneumatic Tool Company, H. W. Loud Machine Works, Inc., Menasco Manufacturing Company, Taylor Devices, Inc., and the Westinghouse Electric Corporation.

ABSTRACT

The feasibility of shock-isolating very large manned underground structures from the intense ground motions generated by a nuclear blast was investigated. The structure under consideration housed personnel living quarters, and communications and survival equipment, including large liquid-filled tanks, and was suspended within a concrete-lined underground cavity. Various suspension configurations, isolators, and damping devices were investigated and their performance characteristics compared with the specific requirements of this facility. It is concluded that an inclined, elastic, pendular suspension system incorporating fluid-filled isolators and force-limited dampers provides satisfactory control over the body motions without exceeding acceptable accelerations. Conventional cage structure and liquid storage techniques are found to be acceptable if careful attention is given to their design.

PUBLICATION REVIEW


This report has been reviewed and is approved.



JOHN F. FLORY
Lt USAF
Project Officer



THOMAS J. LOWRY, JR.
Colonel USAF
Chief, Civil Engineering Branch



PERRY L. HUIE
Colonel USAF
Chief, Research Division

TABLE OF CONTENTS

	Page
SECTION 1.0 INTRODUCTION	1
SECTION 2.0 DEFINITION OF GROUND SHOCK	5
SECTION 3.0 SUSPENSION SYSTEM CONFIGURATION	11
3.1 Isolation System Requirements.	11
3.2 Evaluation of Types of Suspension Systems	14
3.3 Selection of Recommended System	34
3.4 Damping Effects	53
Appendix 3A Derivation of Equations of Motion for Three-Degrees-of-Freedom Pendulum Suspension System	71
Symbols and Notations	85
SECTION 4.0 SHOCK ISOLATION DEVICES	89
4.1 Isolator Requirements.	90
4.2 Liquid Spring Concept.	95
4.3 Pneumatic Spring Concept	127
4.4 Sway Damper Concept	139
4.5 Cable/Isolator Interaction	174
Sybols and Notations.	191
SECTION 5.0 RIGID BODY ANALYSIS	197
5.1 Introduction	197
5.2 Reference Systems.	198
5.3 Equations of Motion	200
5.4 Dynamic Response	205
5.5 Leveling and Load Balancing Control	209
Appendix 5A Development of Equations of Motion.	223
Appendix 5B Air Resistance	239
Appendix 5C The Effect of Liquid Sloshing on the Response of the Container and Supporting Structure	248
Symbols and Notations.	265

	Page
SECTION 6.0 CAGE STRUCTURAL ANALYSIS	271
6.1 Introduction...	271
6.2 Structural Arrangement	275
6.3 Member Sizes.	277
6.4 Weight and Balance	278
6.5 Stiffnesses.	283
Appendix 6A Response of a Space Frame Structure. .	284
Symbols and Notations	315
SECTION 7.0 SUMMARY AND RECOMMENDATIONS.	317
7.1 Principal Conclusions	317
7.2 Recommendations	318
7.3 Problem Areas	320
REFERENCES	321
Distribution	323

1.0 INTRODUCTION

In the past decade, a great many shock isolation systems have been built to protect equipment and personnel housed in underground structures from the severe loads imposed by ground motions due to nuclear explosions. Although the systems vary widely with respect to size, type, environment, and attenuation their design in general has been governed by the same basic requirements for static and dynamic performance operation, maintenance, and reliability. Despite these common objectives, however, the wealth of accumulated design and operational experience has yielded no comprehensive accepted definition of ultimate usage requirements in terms of system design criteria.

As a result, many existing systems have been plagued by numerous deficiencies which have detracted from the convenience and flexibility of operation, have increased maintenance, have reduced reliability, or have compromised the desired attenuation. In most instances these deficiencies have been corrected at least in part by later modifications. The net effect, however, has been a reduction in confidence not only in the ability to engineer completely satisfactory designs but also in the practicality of shock isolation systems themselves.

In extending the use of shock isolation systems to even greater supported loads and ground accelerations, these earlier experiences have raised the question as to whether or not there exists a practical limit to the size of reliable systems. The doubt implied by the question stems from a simple extrapolation of the magnitude of the problems encountered in existing designs to larger and more expensive systems. It is recognized that size per se is not a critical factor in the performance of a shock isolation system. However, larger sizes do amplify the seriousness of the omission of features which should be included in all designs whatever their size. The more fundamental question, then, is whether or not thorough and systematic engineering techniques are sufficient to achieve reliable and economically feasible designs and to avoid the problems encountered in the past.

The design procedure for a shock isolation system can be divided into three phases, selection of configuration and isolator elements, analysis of dynamic response, and detail mechanical design. While there is some overlapping, in general, these three phases are carried out consecutively in the order shown. It is believed that the principal problems arise from a lack of thoroughness in formulating the basic concepts of the system, that is, in the first phase of the design procedure. The selection of system components and their arrangement must be made not only on the basis of output acceleration and/or rattlespace requirements but also on the considerations of sensitivity to input, static stability, effects of loading and temperature changes, damping characteristics, controllability and other factors relating to performance. In addition, the elements themselves must be compared with regard to mechanical

reliability, effects of manufacturing tolerances and aging on performance, and development cost and time. Only when a system and each of its components has passed a critical examination from each of these viewpoints should an analysis of the dynamic response of the system as a whole be attempted.

This study was undertaken specifically to investigate the feasibility of shock isolating very large underground structures. To demonstrate feasibility, a typical structure was assumed and a shock isolation system was selected on the basis of detailed studies of configurations and components. Equations of motion for the complete assembly were then formulated but not solved, there being sufficient confidence placed in the results of the preliminary analyses to assume that the final analysis would consist essentially of refinement and optimization.

The specific problem areas which experience has shown to be of particular importance and which were given special attention here are:

- . Selection of suspension system configuration
- . Effect of amount and type of damping
- . Selection of shock isolator
- . Requirements for leveling control
- . Effect of cage flexibility
- . Effect of sloshing fluids
- . Effect of air pressure loads on oscillating body
- . Transient response of pendulum

The shock isolated structure selected for consideration as typical of one which might be used in a large, deep underground protective facility consists of a cylindrical cage, 75 feet in diameter and 145 feet high, divided vertically into eleven stories. The cage is assumed to house personnel, their living quarters, and communications and other light electronic gear. The bottom floor contains waste storage equipment.

The cage is enclosed in a thick walled cylindrical capsule with a spherical dome and ellipsoidal bottom. The capsule is made of heavily reinforced concrete of sufficient strength to resist the ground motions and to carry the isolator loads.

To provide some basis for calculating weight, weight distribution, structural rigidity and other parameters of the physical configuration, a structural arrangement has been assumed and is described in Section 6. Conventional structural design practices have been employed wherever possible in order to preserve the general applicability of the conclusions.

The peak motions of the shock to which the facility is considered to be subjected were furnished by the Air Force Weapons Laboratory and were established quite arbitrarily. For the most part, the details of the ground motion are of little significance as far as the design approach

2.0 DEFINITION OF GROUND SHOCK

For a given shock strength, the size of the shock isolated level should not be a factor in determining whether or not the system is feasible. However, within broad ranges, the suitability of a particular type of isolation system may be dependent on the magnitudes of various parameters of the input motion. To enhance the usefulness of the studies of particular isolation system elements, therefore, peak capsule motions were selected so as to be representative of the order of magnitudes of those that might be expected in a practical design. These motions, furnished by the Air Force Weapons Laboratory (Reference 1) are shown in Table 2-1.

Table 2-1 Assumed Peak Motions of Capsule

	Displacement inches	Velocity feet /second	Acceleration Gravities
Horizontal	22	32	71
Vertical	34	38	64

Reference 1 also suggested that the general shape of the waveform be assumed to be as shown in Figure 2-1. If it is assumed that the permanent set of the capsule after the shock is negligible, the areas under the positive and negative parts of the velocity curve are equal

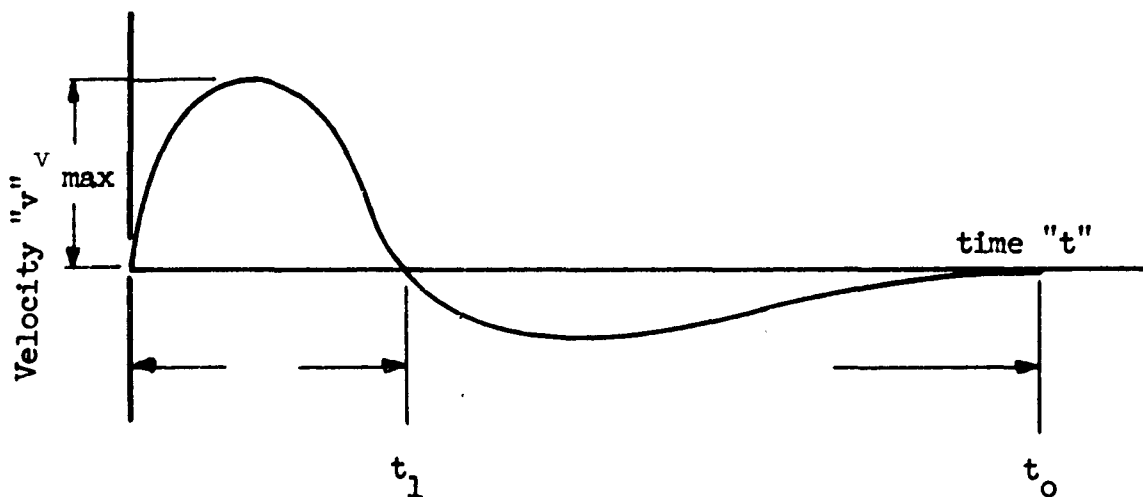


Figure 2-1. Suggested Waveform Shape for Capsule Motion; Velocity vs. Time.

and it is only necessary to estimate t_1 and t_0 . In the final analysis of the dynamic response of the isolation system, t_1 and t_0 would be varied to find the combination which was most critical for the system. For this preliminary analysis, it was considered sufficient to assume t_1 was about 0.1 seconds and t_0 was approximately $3t_1$. The shape of the curves were then adjusted to give the required peak displacement and acceleration.

The resulting velocity curves are shown in Figures 2-2 and 2-3 and their response spectra in Figure 2-4.

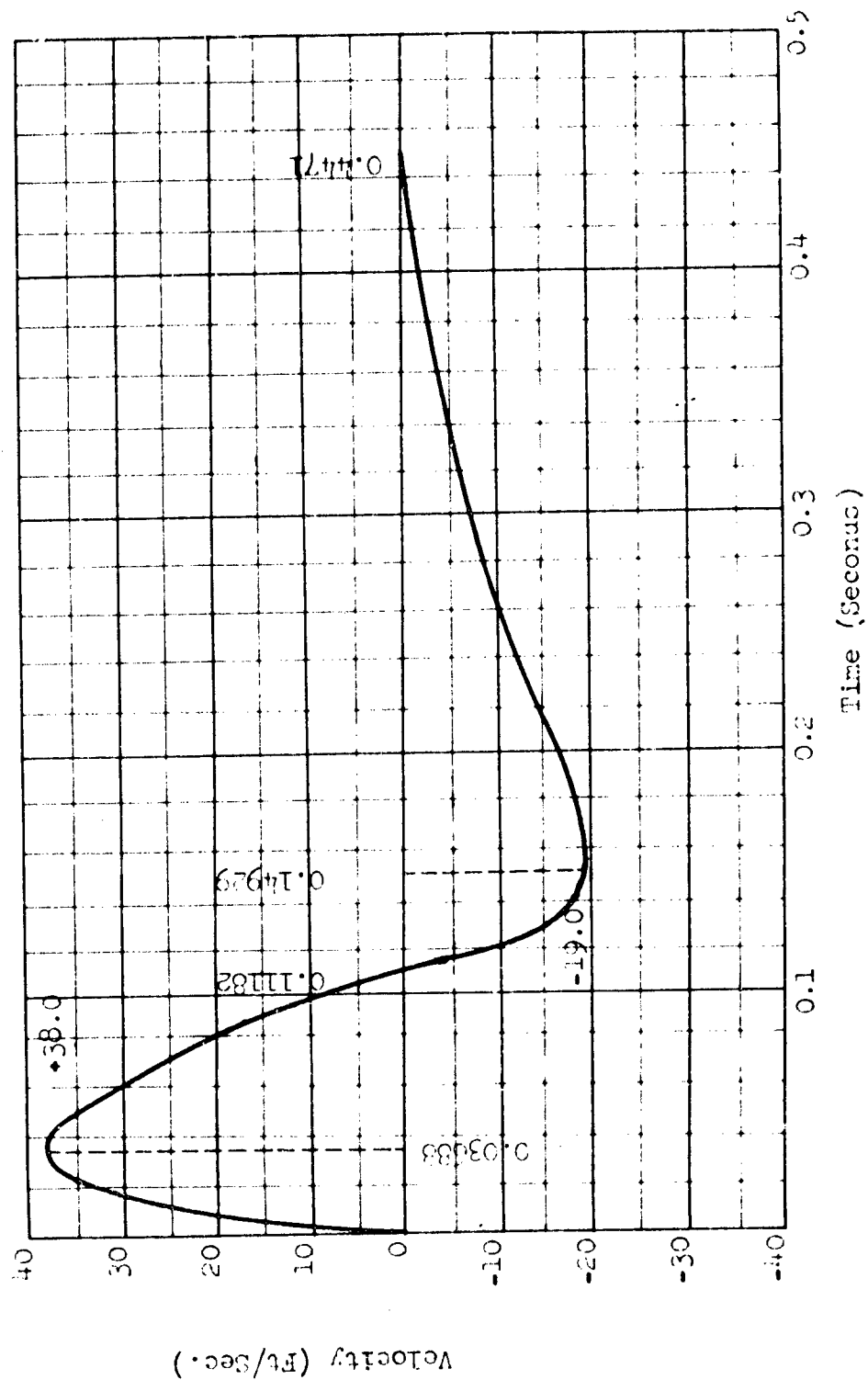


Figure 2-2. Vertical Ground Velocity Waveform.

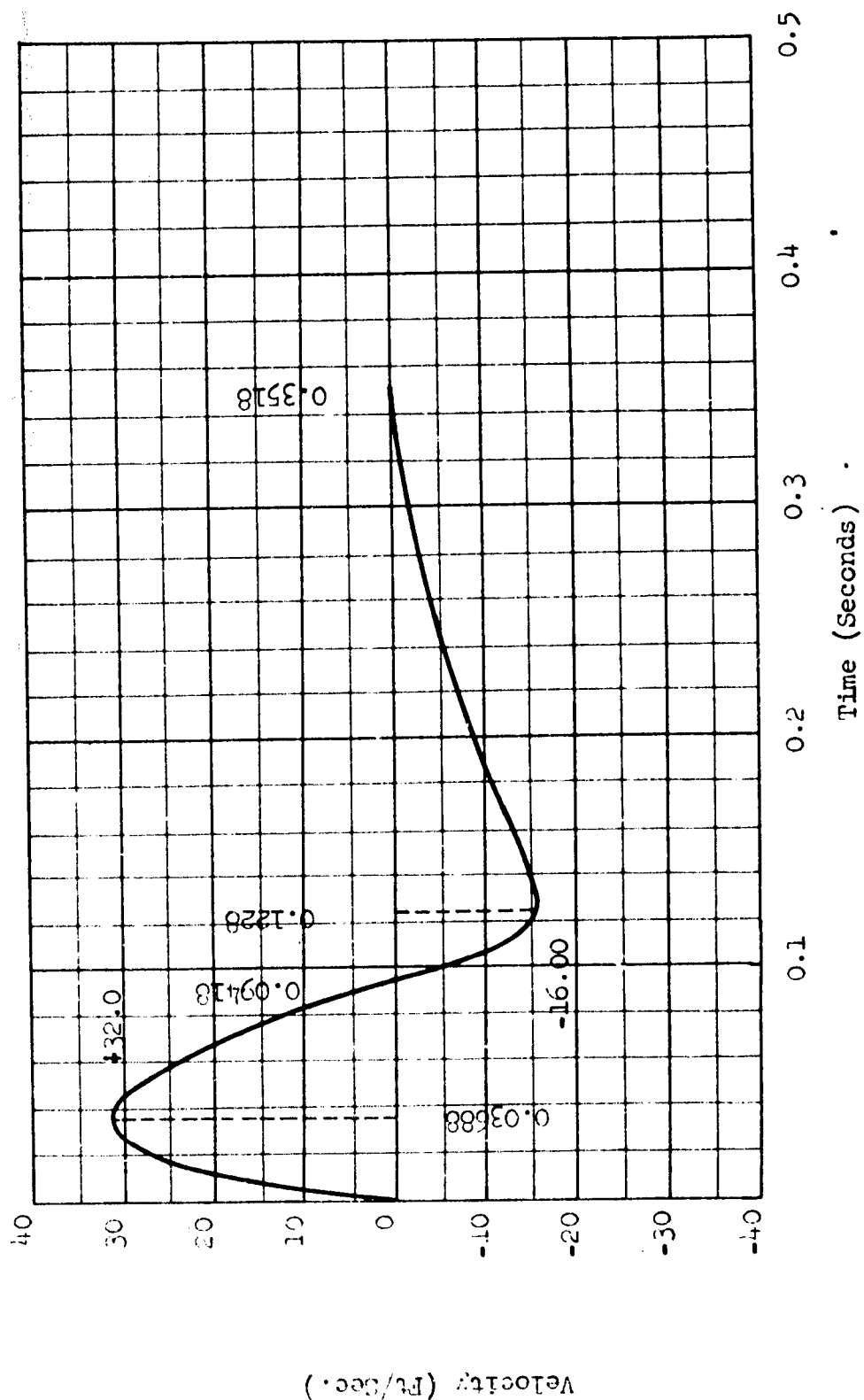


Figure 2-3. Horizontal Ground Velocity Waveform.

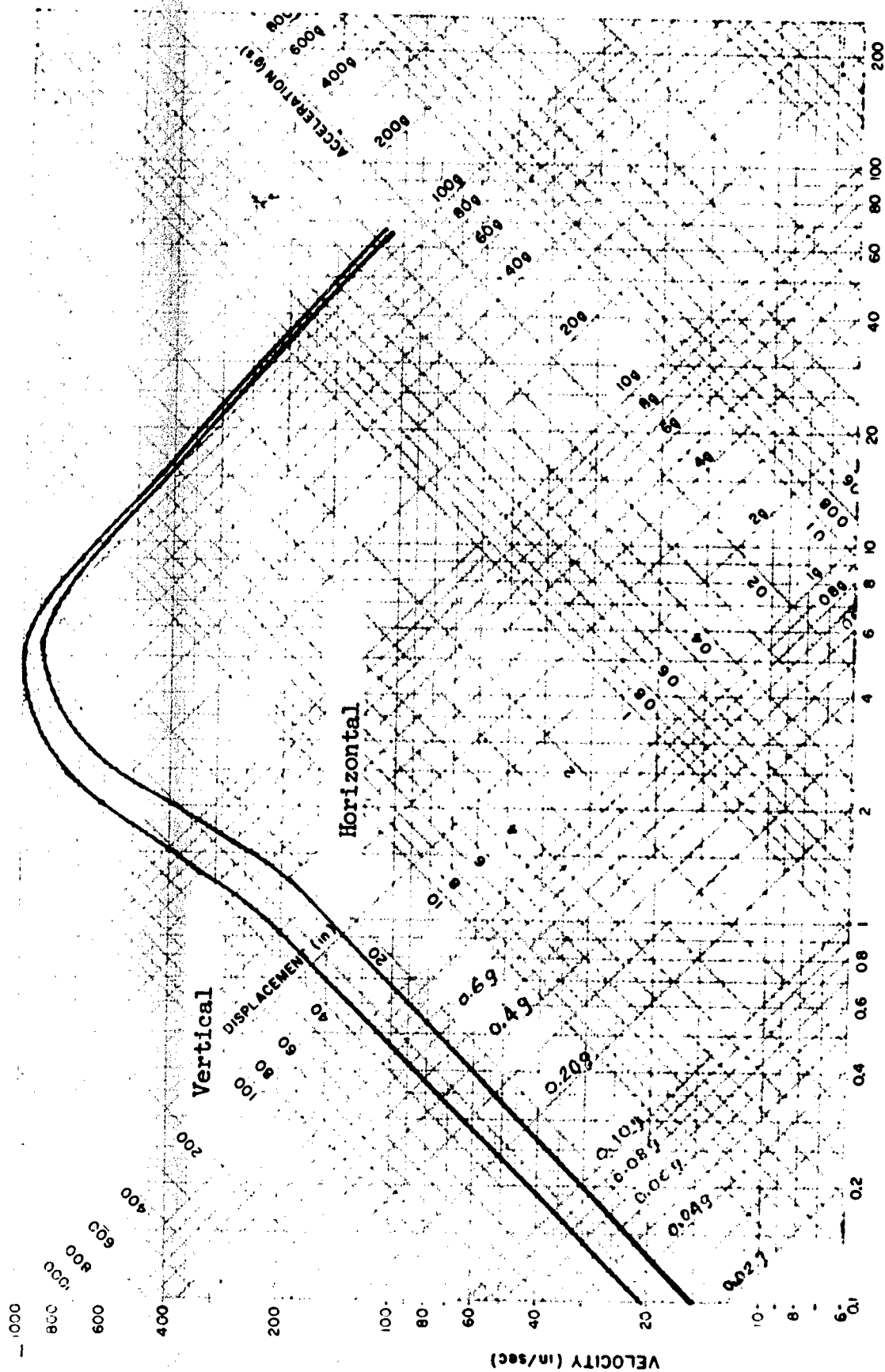


Figure 2-4. Shock Response Spectra For Vertical and Horizontal Waveforms.

3.0 SUSPENSION SYSTEM CONFIGURATION

3.1 Isolation System Requirements

Optimum performance of an isolation system is usually considered, in applications of this type, as a condition of minimum displacement of the isolated body relative to its surroundings yet remaining within an acceleration limit at any point on the body. Performance must be optimized not only for a single set of shock and body conditions, but also for the effects of variations in the shock, load, center-of-gravity location, component tolerances, and similar factors which theory and practice have shown to be significant.

The selection of relative displacement as a measure of optimum performance is based on the assumption that the cost of otherwise unused space in a capsule is much higher than the cost of the additional refinements needed in the isolation system to obviate the requirement for the rattlespace. Obviously there must be a limit as to how far a design optimized with respect to economy and reliability can proceed in this direction. An arbitrary limit, implied in many design criteria, fixes the maximum permissible rattlespace equal to the single-degree-of-freedom response of a linear isolation system in that direction.

It is evident that this criterion has no direct relation to either of the more fundamental optimization parameters--economy and reliability. Instead it represents the minimum possible relative displacement of a completely uncoupled linear undamped system. Since, from a practical viewpoint, it is almost impossible to avoid all coupling in a system, the linear, uncoupled, undamped rattlespace allowance must be viewed as a goal which can be achieved only at considerable expense.

In a given six-degree-of-freedom system incorporating linear or near-linear isolators, the increase in maximum relative displacement of the isolated body over the single-degree-of-freedom value, obviously, is related to the coupling between its modes of oscillation. The coupling in turn is dependent on the geometry of the suspension system. It would appear then that the optimization process would consist only of selecting a geometry such that the coupling is reduced essentially to zero.

As noted above, it is rarely, if ever, possible to achieve this desirable goal. Excursions of the center of gravity of the body, manufacturing tolerances, and the angular displacements of the lines of action of the restoring forces during oscillations all introduce coupling into an otherwise uncoupled system. It is important to note, however, that minimum energy transfer between modes does not necessarily lead to minimum rattlespace. Of equal importance is the stiffness of the mode into which the energy is transferred.

For example, consider a system subjected simultaneously to translatory shocks along the three major axes. Although the translational modes may be only slightly coupled with the rotational modes, the stiffness in

rotation may be very small. Thus the introduction of even small amounts of energy into the rotational modes may produce greater excursions at points far from the center of rotation than are introduced at the same points by pure translation. Rearranging the geometry of the suspension may result in more coupling energy in rotation, but at the same time increase the resistance in rotation in a greater proportion with a net effect of reducing the peak relative displacement at the critical location.

Whether or not a shock isolation system is to be fully optimized from the viewpoint of economy as an integrated element of a complete facility, it is evident that the design must begin by establishing the limits of feasibility of suspension system configurations. At this stage of the development it is sufficient to base comparison on criteria which, in general engineering practice, are usually found to be valid. Such criteria might be:

1. For a given total number of isolators, the fewer the number of different sizes, the less the unit cost.
2. A near-linear force-displacement characteristic is to be preferred to a highly nonlinear one.
3. Passive systems, in general, are more reliable than active systems.
4. Tension ties are less costly than columns.

Section 3.0 deals with the selection of a suspension system configuration for a facility of the assumed size and loads and, for the recommended system, establishes isolator performance criteria. Three isolation systems are compared, all of the overhead pendulum type. The overhead pendulum type of system has two distinct advantages. First, it utilizes gravity as a horizontal restoring force, thus minimizing or eliminating the need for added horizontal stiffness. Second, by proper design the pendulum arms are always in tension, thus minimizing their weight and cost. While the load must be carried eventually in compression to the base of the structure, the thickness of the enclosing capsule, dictated by requirements other than shock isolation, is usually well suited and easily adequate to support this additional burden. The only areas requiring more than nominal special attention are the locations where the pendulum loads are transferred to the capsule.

Although straightforward enough, it is believed that the approach taken here to compare the three suspension configurations is unique to this application. Since even with a slightly eccentric center-of-gravity location, rotation about the vertical axis does not contribute significantly to the horizontal rattlespace requirement, it was considered to be

justified to reduce the systems for preliminary comparison to three degrees of freedom, translation in the vertical and horizontal modes, and rotation about the horizontal axis. Equations are then formulated which not only indicate the coupling between modes, but also system stability. The equations are then compared, term for term, and numerical values are established for the two most promising systems.

The amount and type of damping are evaluated as to their applicability to shock isolation systems. Specific damping recommendations are then made.

The work of Section 3.0 establishes, tentatively, the system geometry and the performance characteristics required of its elements to attenuate the design shock to the acceptable level within a space envelope believed to be near optimum from the viewpoint of overall simplicity of design. Final verification of the capability of the selected system to perform as expected can be obtained only by numerical solutions of the complete equations of motion.

3.2 Evaluation of Types of Pendulum Suspension Systems

3.2.1 Types of Suspension Systems

The response of a shock isolated body is directly dependent upon the arrangement of the suspension system and the characteristics of the elastic elements. For bodies of different proportions different isolation systems are needed to minimize the response. In many applications the most suitable system consists of suspending the body by an elastic spherical pendulum, thus offering isolation in the three principal directions. Because of the limitations usually imposed on the space allowed for the movements (rattlespace), the engineer is faced with selecting the isolation system which will require minimum rattlespace without exceeding at any point on the body a maximum permissible acceleration.

The response of any isolated body consists of translation of and rotation about the center of gravity. Even though the ground motion is usually considered to induce only translation without rotation, the suspended body may be excited in the rotational mode by coupling with the translational mode. The selection of the suspension system and the rattlespace is usually governed by this coupling. For example, if the body to be isolated is spherical in shape, translation of the center of gravity governs the rattlespace allowance. If the body is oblong along one of the horizontal axes, like a thin rectangular plate, rotation about the vertical axis usually governs the requirements for rattlespace; while for a body oblong along the vertical axis, like a long vertical cylinder, rotations about the horizontal axis play an important part in defining rattlespace.

For a tall cage structure, as in the case assumed here, the suspension system should satisfy the following objectives:

1. Minimize the coupling between translational and rotational modes.
2. Increase the stiffness in rotational modes.
3. Stabilize the system over a wide range.

Three basic types of suspension systems to achieve the above purpose are considered here.

1. One level suspension with vertical pendulum arms and horizontal isolators (Figure 3-1a).

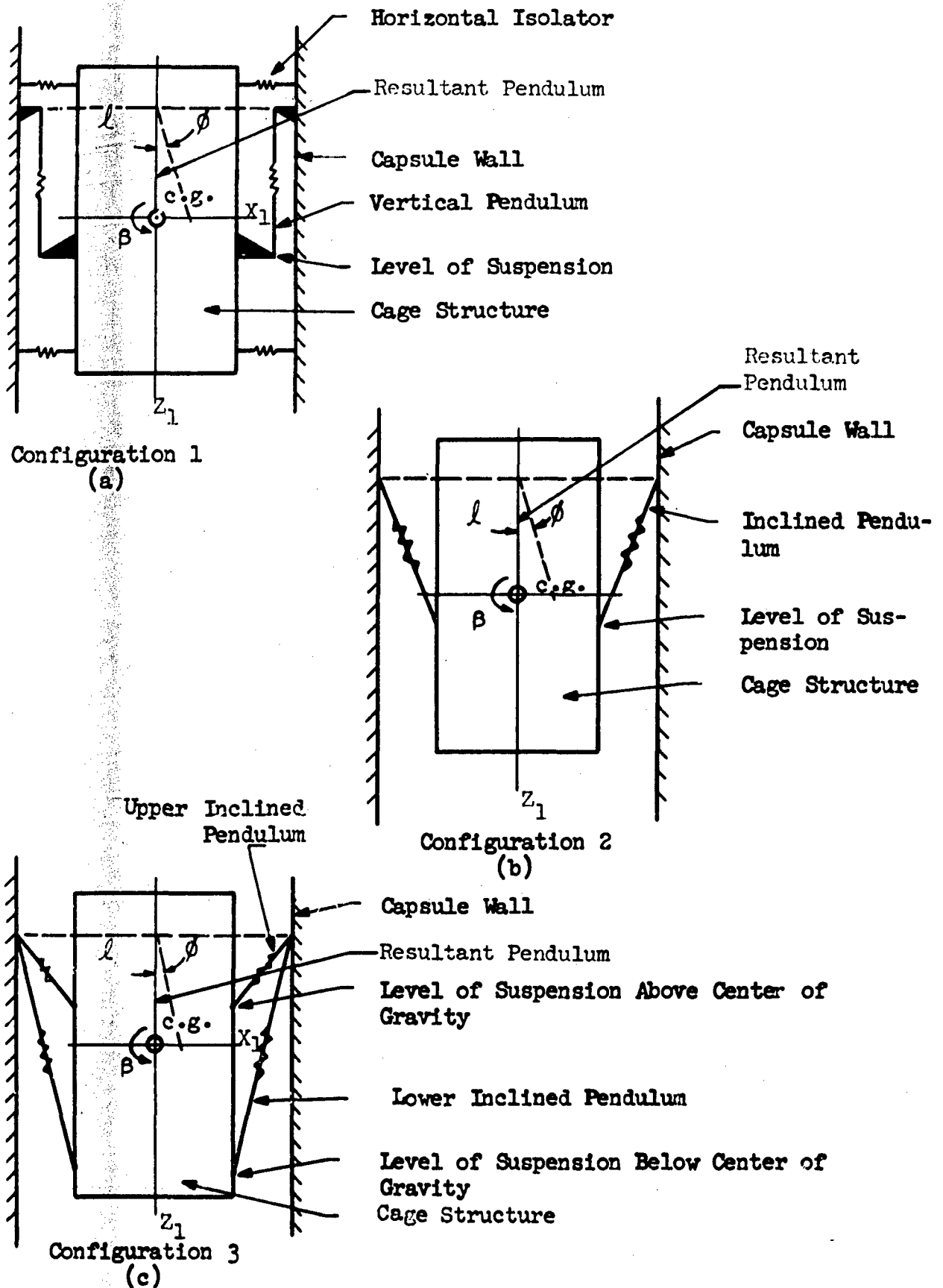


Figure 3-1. Suspension System Configurations.

2. One level suspension with inclined pendulums (Figure 3-1b). The horizontal isolators are eliminated by inclining the vertical isolators, which are attached to the body at the same level.

3. Two level suspension with inclined pendulums (Figure 3-1c). The body is suspended by means of two series of isolators: one series attached at a level above the center of gravity and the other at a level below the center of gravity. The attachments of both series of isolators at the capsule wall are at the same level. In configuration 1 and 2, the center of gravity is shown above the level of suspension to account for its highest possible position.

As the evaluation of the three configurations is based upon a qualitative rather than a quantitative analysis, the complexity of the system is reduced by limiting consideration to fewer, but important, parameters affecting the response of the system. The rotation about the vertical axis does not affect the rattlespace requirements because of the cylindrical shape of the cage structure. Hence, the system is reduced to three degrees of freedom in a plane configuration. Furthermore, damping is neglected in this analysis since it does not affect the coupling between different modes. This leads to a conservative estimate of stability. The equations of motion for a general case, and for each of the particular cases, are derived in Appendix 3A.

3.2.2 Equations of Motion for Three-Degree-of-Freedom Configurations

The generalized coordinates chosen for the three-degree-of-freedom system are as follows:

- l = instantaneous length of the resultant pendulum
- ϕ = inclination angle of the resultant pendulum with respect to the vertical axis.
- β = rotation of the supported mass about the center of gravity.

The general equations of motion are presented here with the following simplifications:

1. Damping is not included.
2. Effect of rotation of the body about the center of gravity on stiffness is of second order, hence neglected.
3. Centrifugal and coriolis' accelerations are neglected, because of their second order effect.
4. Spring stiffness is linear.

The general equations of motion in the Cartesian reference system, including centrifugal and coriolis' accelerations, can be represented as follows:

$$\begin{aligned} & (m\ddot{l} - m\dot{\phi}^2) \cos \phi - (2m\dot{l}\dot{\phi} + m\ddot{\phi}) \sin \phi \\ & + \sum \{K_n \cos \phi_n (\dot{l}_n - \dot{l}_{no})\} \\ & + \beta \sum \{K_n \cos \phi_n (r_3 \sin \phi_n - r_1 \cos \phi_n)\} + (m\ddot{Z}_0 - m\dot{g}) = 0 \end{aligned} \quad (\text{Eq. 3.1})$$

$$\begin{aligned} & (m\ddot{l} - m\dot{\phi}^2) \sin \phi + (2m\dot{l}\dot{\phi} + m\ddot{\phi}) \cos \phi \\ & + \sum \{K_n \sin \phi_n (\dot{l}_n - \dot{l}_{no})\} \\ & + \beta \sum \{K_n \sin \phi_n (r_3 \sin \phi_n - r_1 \cos \phi_n)\} + (m\ddot{X}_0) = 0 \end{aligned} \quad (\text{Eq. 3.2})$$

$$\begin{aligned} & I\ddot{\phi} + \sum \left\{ K_n \left[r_3 \sin \phi_n (\dot{l}_n - \dot{l}_{no}) - r_1 \cos \phi_n (\dot{l}_n - \dot{l}_{no}) \right] \right\} \\ & + \beta \sum \left\{ K_n \left[r_3 \sin \phi_n - r_1 \cos \phi_n \right]^2 \right\} = 0 \end{aligned} \quad (\text{Eq. 3.3})$$

where the following conditions are to be satisfied for \dot{l}_n and $\dot{\phi}_n$ for n^{th} isolator

$$\begin{aligned} \dot{l}_n \sin \phi_n &= \dot{l} \sin \phi + \dot{l}_{ns} \sin \phi_{ns} \\ \dot{l}_n \cos \phi_n &= \dot{l} \cos \phi + \dot{l}_{ns} \cos \phi_{ns} - \dot{l}_s \end{aligned} \quad (\text{Eq. 3.4})$$

The above equations are transformed into polar coordinates, neglecting centrifugal and coriolis' accelerations, as follows:

$$\ddot{\rho} + \rho \left\{ \sum_I \frac{K_n \cos \phi_{ns}}{m} \right\} + \ddot{U}_O \cos (\phi_O - \phi) = 0 \quad (\text{Eq. 3.5})$$

$$\begin{aligned} \ddot{\phi} + \phi \left\{ \left[\sum_I \frac{K_n \cos \phi_{ns}}{m(\ell_s + r_3)} - \sum_I \frac{K_n \cos \phi_{ns}}{m \ell_s} \right] \rho + \left[\sum_H \frac{K_n}{m} + \sum_I \frac{K_n \cos \phi_{ns} \delta_{ns}}{m(\ell_s + r_3)} \right] \right\} \\ + \rho \left\{ \sum_H \frac{K_n r_3}{m \ell_s} + \sum_I \frac{K_n [b']}{m \ell_s} \right\} + \ddot{U}_O \sin (\phi_O - \phi) = 0 \quad (\text{Eq. 3.6}) \end{aligned}$$

$$\begin{aligned} \ddot{\beta} + \phi \left\{ \left[\sum_I \frac{K_n \ell_s [d]}{m R^2 (\ell_s + r_3)} + \sum_H \frac{K_n r_3 \ell_s}{m R^2} + \sum_I \frac{K_n \delta_{ns} \ell_s [d]}{m R^2 (\ell_s + r_3)} \right] \right\} \\ + \rho \left\{ \sum_H \frac{K_n r_3^2}{m R^2} + \sum_I \frac{K_n [c]}{m R^2} \right\} = 0 \quad (\text{Eq. 3.7}) \end{aligned}$$

where $\rho = (\ell - \ell_s)$

$$(\ddot{U}_O)^2 = (\ddot{Z}_O)^2 + (\ddot{X}_O)^2$$

$$\tan \phi_O = \frac{\ddot{X}_O}{\ddot{Z}_O}$$

$$[b] = \sin \phi_{ns} (r_3 \sin \phi_{ns} - r_1 \cos \phi_{ns})$$

$$[c] = (r_3 \sin \phi_{ns} - r_1 \cos \phi_{ns})^2$$

$$[d] = (r_3 \cos \phi_{ns} + r_1 \sin \phi_{ns})$$

If $\phi_O \gg \phi$, then

$$\ddot{U}_O \cos (\phi_O - \phi) \cong \ddot{U}_O \cos \phi_O = \ddot{Z}_O$$

$$\text{and } \ddot{U}_O \sin (\phi_O - \phi) \cong \ddot{U}_O \sin \phi_O = \ddot{X}_O$$

The coefficients in the above set of equations are evaluated for each configuration and are shown in Table 3-1.

Table 3-1

Coefficients for Equations of Motion

$$\ddot{\rho} + D_0 \rho = -\ddot{Z}_0 \quad (\text{Eq. 3.8})$$

$$\ddot{\phi} + \phi \{ D_1 \rho + D_2 \} + \beta \{ D_3 \} = -\ddot{X}_0 / \ell_s \quad (\text{Eq. 3.9})$$

$$\ddot{\beta} + \phi \{ D'_1 \rho + D'_2 \} + \beta \{ D'_3 \} = 0 \quad (\text{Eq. 3.10})$$

Where

$$D_0 = \sum_I \frac{K_n \cos \phi_{ns}}{m}$$

$$D_1 = \sum_I \frac{K_n \cos \phi_{ns}}{m(\ell_s + r_3)} - \sum_I \frac{K_n \cos \phi_{ns}}{m(\ell_s)}$$

$$D_2 = \sum_H \frac{K_n}{m} + \sum_I \frac{K_n \cos \phi_{ns} \cdot \delta_{ns}}{m(\ell_s + r_3)}$$

$$D_3 = \sum_H \frac{K_n r_3}{m \ell_s} + \sum_I \frac{K_n [b]}{m \ell_s}$$

$$D'_1 = \sum_I \frac{K_n [d] \ell_s}{m R^2 (\ell_s + r_3)}$$

$$D'_2 = \sum_H \frac{K_n r_3 \ell_s}{m R^2} + \sum_I \frac{K_n [d] \delta_{ns} \ell_s}{m R^2 (\ell_s + r_3)}$$

$$D'_3 = \sum_H \frac{K_n r_3^2}{m R^2} + \sum_I \frac{K_n [c]}{m R^2}$$

$$[b] = \sin \phi_{ns} (r_3 \sin \phi_{ns} - r_1 \cos \phi_{ns})$$

$$[c] = (r_3 \sin \phi_{ns} - r_1 \cos \phi_{ns})^2$$

$$[d] = (r_3 \cos \phi_{ns} + r_1 \sin \phi_{ns})$$

Table 3-1 (Continued)

Coefficients for Equations of Motion

Configuration 1

$$D_0 = \frac{2K_v}{m}$$

$$D_1 = \frac{2K_v}{m} \left\{ \frac{1}{l_s + a_2} - \frac{1}{l_s} \right\}$$

$$D_2 = \frac{4K_H}{m} + \frac{2K_v \delta_s}{m(l_s + a_2)}$$

$$D_3 = \frac{2K_H(a_4 - a_3)}{m l_s}$$

$$D'_1 = \frac{2K_v a_2 l_s}{m R^2 (l_s + a_2)}$$

$$D'_2 = \frac{2K_H(a_4 - a_3) l_s}{m R^2} + \frac{2K_v \delta_s a_2 l_s}{m R^2 (l_s + a_2)}$$

$$D'_3 = \frac{2K_H(a_3^2 + a_4^2)}{m R^2} + \frac{2K_v r^2}{m R^2}$$

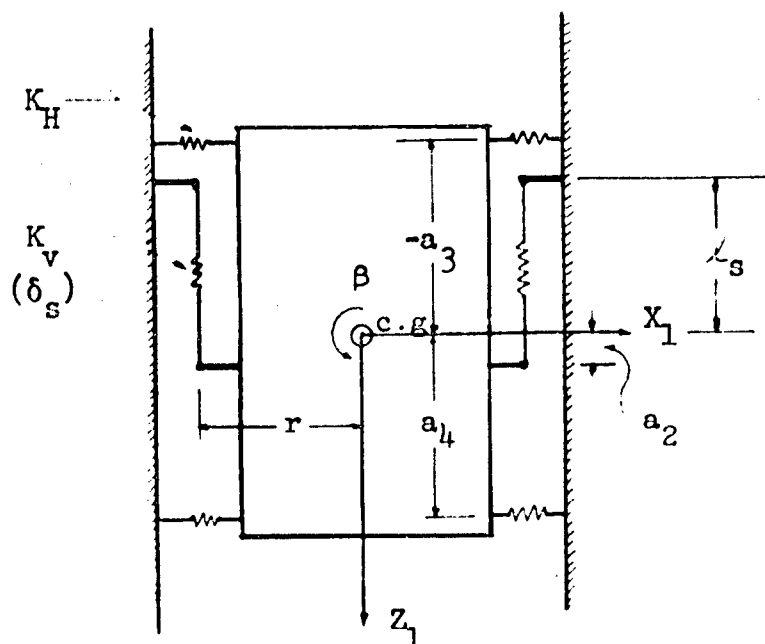


Table 3-1 (Continued)

Coefficients for Equations of Motion

Configuration 2

$$D_0 = \frac{2K}{m}$$

$$D_1 = \frac{2K}{m} \left\{ \frac{1}{l_s + a_2} - \frac{1}{l_s} \right\}$$

$$D_2 = \frac{2K\delta_s}{m(l_s + a_2)}$$

$$D_3 = \frac{2K\phi_2(r + a_2\phi_2)}{m l_s}$$

$$D'_1 = \frac{2K(a_2 - r\phi_2)l_s}{mR^2(l_s + a_2)}$$

$$D'_2 = \frac{2K\delta_s(a_2 - r\phi_2)l_s}{mR^2(l_s + a_2)}$$

$$D'_3 = \frac{2K(r + a_2\phi_2)^2}{mR^2}$$

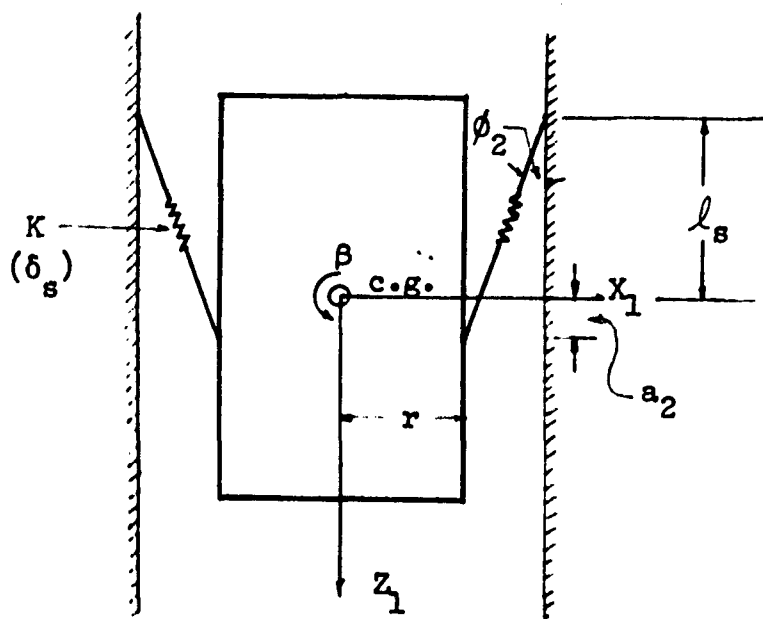


Table 3-1 (Continued)

Coefficients for Equations of Motion
Configuration 3

$$D_0 = \frac{2(K_1 + K_2)}{m}$$

$$D_1 = \frac{2}{m} \left\{ \frac{K_1}{l_s - a_1} + \frac{K_2}{l_s + a_2} - \frac{K_1 + K_2}{l_s} \right\}$$

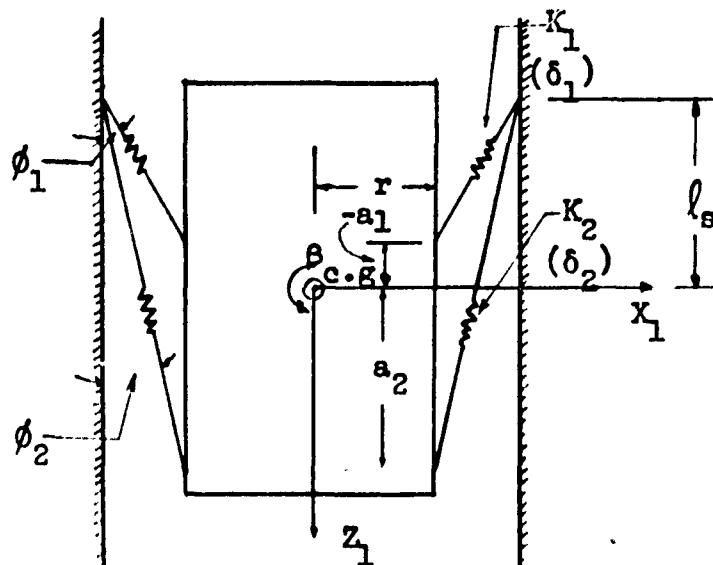
$$D_2 = \frac{2}{m} \left\{ \frac{K_1 \delta_{1s}}{l_s - a_1} + \frac{K_2 \delta_{2s}}{l_s + a_2} \right\}$$

$$D_3 = \frac{2}{m l_s} \left\{ K_1 \phi_1 (r - a_1 \phi_1) + K_2 \phi_2 (r + a_2 \phi_2) \right\}$$

$$D'_1 = \frac{2 l_s}{m R^2} \left\{ \frac{K_1 (-a_1 - r \phi_1)}{l_s - a_1} + \frac{K_2 (a_2 - r \phi_2)}{l_s + a_2} \right\}$$

$$D'_2 = \frac{2 l_s}{m R^2} \left\{ \frac{K_1 \delta_{1s} (-a_1 - r \phi_1)}{l_s - a_1} + \frac{K_2 \delta_{2s} (a_2 - r \phi_2)}{l_s + a_2} \right\}$$

$$D'_3 = \frac{2}{m R^2} \left\{ K_1 (r - a_1 \phi_1)^2 + K_2 (r + a_2 \phi_2)^2 \right\}$$



3.2.3 Evaluation of Types by Comparison of Coefficients

Eq. 3.8 indicates that, in a first approximation,

$$\ddot{\rho} + D_0 \rho = -\ddot{Z}_0$$

is uncoupled with either ϕ or β , which means that the effect of horizontal oscillations on the vertical mode is of second order. As the natural period of the system is long with respect to the period of the shock, it can be reasonably assumed that the critical conditions occur during residual oscillations. In which case, Eq. 3.8 becomes

$$\ddot{\rho} + D_0 \rho = 0$$

which is a linear differential equation of second order with a particular solution

$$\rho = \rho_0 \cos \omega t$$

where ρ_0 is the maximum amplitude of ρ .

Eq. 3.9

$$\ddot{\phi} + \phi (D_1 \rho + D_2) + \beta (D_3) = -\frac{\ddot{X}_0}{l_s}$$

is coupled with ρ and β , which means that ϕ mode is excited by the ground acceleration \ddot{X}_0 and part of the energy is transferred in β mode. The flow of energy to β mode can be reduced to zero by making coefficients $D_3 = 0$, or can be minimized in proportion to minimization of D_3 .

For Configuration 1, D_3 can be made zero only when $a_3 = a_4$. For the fixed location of center of gravity it is possible to maintain the equality between a_3 and a_4 . Unfortunately for the structures of the type considered here, the center of gravity can be expected to shift from its nominal position, which in turn makes $a_3 \neq a_4$ and coupling is introduced.

For Configuration 2, D_3 can be zero when $\phi_2 = 0$ or

$$r + a_2 \phi_2 = 0$$

$$\therefore \phi_2 = \frac{r}{-a_2}$$

which means that the point of attachment should be at $-a_2 = \frac{r}{\phi_2}$, above the center of gravity. If ϕ_2 is small, a_2 can be extremely large and may be beyond the limits of the structure. For large values of ϕ_2 , a_2 may be within the structure, but the condition $r + a_2 \phi_2 = 0$ cannot be maintained when the center of gravity shifts.

For Configuration 3, it does not seem possible to reduce D_3 to zero, but by proportioning the values of K_1 and K_2 , ϕ_1 and ϕ_2 , a_1 and a_2 , it is possible to reduce D_3 to minimum; not only for the nominal position of center of gravity, but also under the condition of shift of the center of gravity. This is discussed in detail in Paragraph 3.3.2.

If D_3 is reduced to the extent that it becomes negligible, then Eq. 3.2 becomes

$$\ddot{\phi} + \phi (D_2 + D_1 \rho) = - \frac{\ddot{x}_o}{l_s}$$

$$\ddot{\phi} + \phi (D_2 + D_1 \rho_o \cos \omega t) = - \frac{\ddot{x}_o}{l_s}$$

For steady-state oscillations, this equation is known as Mathieu's equation and the condition for stability is

$$\frac{D_2}{\omega^2} + \frac{D_1 \rho_o}{2 \omega^2} \leq \frac{1}{4}$$

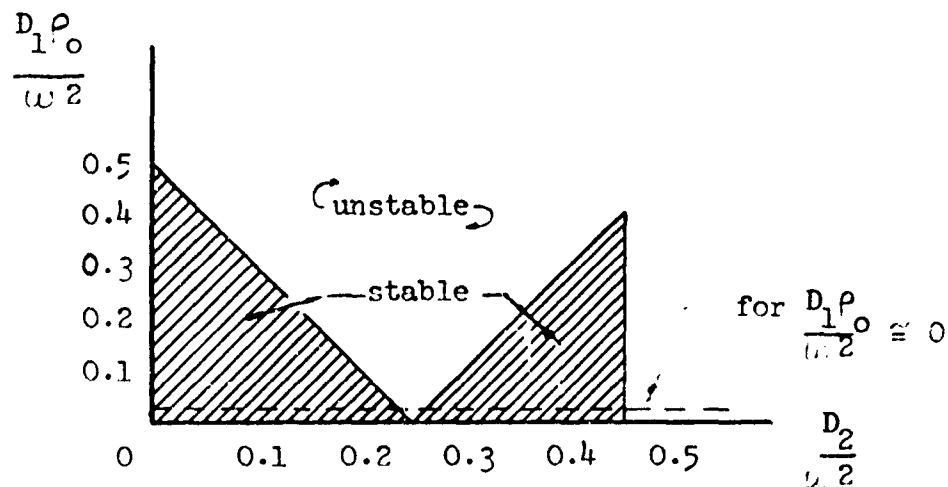


Figure 3-2. Ince-Strutt Diagram for Stability.

Referring to Figure 3-2, it can be seen that it is desirable to

reduce $\frac{D_1 \rho_o}{\omega^2}$ to zero, or close to zero, so that the suspension system is stable for all values of $\frac{D_2}{\omega^2}$. As $\frac{\rho_o}{\omega^2}$ is finite for a given system, D_1 should be close to zero.

For Configuration 1, D_1 will be zero only when a_2 is zero. As discussed earlier, this is not possible when the center of gravity is shifted from its design location.

For Configuration 2, D_1 will be zero when a_2 is zero which is not possible as stated above.

For Configuration 3, D_1 can be zero by properly proportioning a_1 and a_2 . For a small shift of the center of gravity, the summation of

$$\frac{K_1}{l_s - a_1} + \frac{K_2}{l_s + a_2}$$

can be kept fairly close to its initial value by properly selecting a_1 and a_2 . For example, if a_2 is large and a_1 small, compared to l_s , small variations in the values of a_1 and a_2 will not change the value of the summation appreciably.

Equation 3.10 is

$$\ddot{\beta} + \beta D'_3 + \phi(D'_1 \rho + D'_2) = 0$$

If D'_1 is made zero, the β -mode is uncoupled with ρ -mode which indicates that the maximum amplitude of β is reduced.

For Configuration 1, D'_1 can be made zero only when $a_2 = 0$ which is impractical due to possible shifts of the center of gravity as discussed earlier.

For Configuration 2, D'_1 can be zero when $a_2 - r\phi_2 = 0$; i.e., $\phi_2 = \frac{a_2}{r}$ which is contrary to the condition needed for minimizing D_3 , that is, uncoupling the ϕ -mode from the β -mode.

For Configuration 3, D'_1 can be zero by proportioning the values of K_1 , K_2 , a_1 , a_2 and ϕ_1 , ϕ_2 . Due to the shift of center of gravity, one of the terms of the expression

$$\frac{K_1(-a_1 - r\phi_1)}{l_s - a_1} + \frac{K_2(a_2 - r\phi_2)}{l_s + a_2}$$

increases while the other term decreases keeping the summation fairly constant. Thus, if D_1 is close to zero for the nominal position of the center of gravity, it will remain close to zero even when center of gravity is shifted.

If D'_2 is made zero, the β -mode is uncoupled with the ϕ -mode, which means the maximum amplitude of β will be further reduced.

For Configuration 1, D'_2 can be zero only when $a_3 = a_4$ and $a_2 = 0$, which is impractical as discussed before.

For Configuration 2, D_2' can be zero only when $a_2 - r\phi_2 = 0$; i.e.,

$$\phi_2 = \frac{a_2}{r},$$

which is contrary to condition required for reducing D_3 to zero.

For Configuration 3, D_2' can be zero by proportioning the values of K_1 , K_2 , a_1 , a_2 and δ_{1s} , δ_{2s} . Due to the shift of the center of gravity, one of the terms of the expression

$$\frac{K_1 \delta_{1s} (-a_1 - r\phi_1)}{l_s - a_1} + \frac{K_2 \delta_{2s} (a_2 - r\phi_2)}{l_s + a_2}$$

increases while the other term decreases, maintaining the summation fairly constant.

In reviewing the above comparison of coefficients of three configurations, it can be seen that Configuration 3 offers the maximum flexibility in reducing the required coefficients to zero or to the minimum needed to uncouple the various modes. The principal advantage of Configuration 3 suspension over the other two types is the larger number of parameters available for system adjustment to given requirements. This in turn makes the system less sensitive to shifts of the center of gravity, as compared to the other configurations.

3.2.4 Evaluation of Types by Comparison of Stability

The stability criteria of the system subjected to vertical and horizontal input simultaneously are very complex to derive. For preliminary sizing, a simple approach is taken by considering vertical and horizontal inputs separately. For inclined inputs (i.e., vertical and horizontal inputs acting simultaneously), the method of derivation of stability criteria is outlined.

3.2.4.1 Stability for Vertical Input

The equations of motion are:

$$\ddot{\rho} + D_0 \rho = -\ddot{Z}_0 \quad (\text{Eq. 3.11a})$$

$$\ddot{\phi} + \phi(D_1 \rho + D_2) + \beta(D_3) = 0 \quad (\text{Eq. 3.11b})$$

$$\ddot{\beta} + \phi(D_1' \rho + D_2') + \beta(D_3') = 0 \quad (\text{Eq. 3.11c})$$

For residual oscillations,

$$\phi = \phi_0 \cos \omega t \quad \text{where } \omega^2 = \frac{\sum K_n}{m}$$

If D_3 in Eq. 3.11b is negligible, then Eq. 3.11b becomes

$$\ddot{\phi} + \phi(D_2 + D_1 \phi_0 \cos \omega t) = 0 \quad (\text{Eq. 3.12})$$

This equation can be converted into the form of Mathieu's equation.

$$\ddot{y} + y(\lambda \pm 2h \cos 2x) = 0$$

$$\text{Let } \omega t = 2x, \therefore \frac{dx}{dt} = \frac{\omega}{2}$$

$$\begin{aligned} \frac{d^2 \phi}{dt^2} &= \frac{d}{dt} \cdot \frac{d\phi}{dt} \\ &= \frac{d}{dt} \left(\frac{d\phi}{dx} \cdot \frac{dx}{dt} \right) \\ &= \frac{d}{dx} \left(\frac{d\phi}{dx} \cdot \frac{dx}{dt} \right) \frac{dx}{dt} \\ &= \frac{d^2 \phi}{dx^2} \left(\frac{dx}{dt} \right)^2 \\ &= \frac{\omega^2}{4} \cdot \frac{d^2 \phi}{dx^2} \end{aligned}$$

Hence Eq. 3.11b becomes

$$\frac{\omega^2}{4} \cdot \frac{d^2 \phi}{dx^2} + \phi(D_2 + D_1 \phi_0 \cos 2x) = 0$$

$$\frac{d^2 \phi}{dx^2} + \phi \frac{4D_2}{\omega^2} + \frac{4D_1 \phi_0}{\omega^2} (\cos 2x) = 0$$

(Eq. 3.13)

The condition for stability is:

$$\frac{4D_2}{\omega^2} + \frac{2D_1 \phi_0}{\omega^2} < 1$$

$$\text{or } \frac{D_2}{\omega^2} + \frac{D_1 \phi_0}{2\omega^2} < 1/4$$

(Eq. 3.14)

Configuration 1

$$\frac{2K_H}{K_V} + \frac{\delta_s}{\ell_s + a_2} + \frac{\rho_o}{2} \left\{ \frac{1}{\ell_s + a_2} - \frac{1}{\ell_s} \right\} < \frac{1}{4}$$

$$\therefore \frac{2K_H}{K_V} + \frac{1}{\ell_s + a_2} \left\{ \delta_s + \frac{\rho_o}{2} \right\} - \frac{\rho_o}{2\ell_s} < \frac{1}{4} \quad (\text{Eq. 3.15})$$

Configuration 2

$$\frac{\delta_s}{\ell_s + a_2} + \frac{\rho_o}{2} \left\{ \frac{1}{\ell_s + a_2} - \frac{1}{\ell_s} \right\} < \frac{1}{4}$$

$$\therefore \frac{1}{\ell_s + a_2} \left\{ \delta_s + \frac{\rho_o}{2} \right\} - \frac{\rho_o}{2\ell_s} < \frac{1}{4} \quad (\text{Eq. 3.16})$$

Configuration 3

$$\frac{K_1}{K_1 + K_2} \cdot \frac{\delta_{1s}}{\ell_s - a_1} + \frac{K_2}{K_1 + K_2} \cdot \frac{\delta_{2s}}{\ell_s + a_2} + \frac{\rho_o}{2(K_1 + K_2)} \left\{ \frac{K_1}{\ell_s - a_1} + \frac{K_2}{\ell_s + a_2} - \frac{K_1 + K_2}{\ell_s} \right\} < \frac{1}{4}$$

$$\therefore \frac{K_1}{K_1 + K_2} \cdot \frac{1}{\ell_s - a_1} \left\{ \delta_{1s} + \frac{\rho_o}{2} \right\} + \frac{K_2}{K_1 + K_2} \cdot \frac{1}{\ell_s + a_2} \left\{ \delta_{2s} + \frac{\rho_o}{2} \right\} - \frac{\rho_o}{2\ell_s} < \frac{1}{4} \quad (\text{Eq. 3.17})$$

Comparing expressions Eq. 3.15 and 3.16 for stability, it can be seen that they are comparable, except that Eq. 3.15 contains the additional term

$$\frac{2K_H}{K_V}$$

Configuration 1 can be made stable by satisfying the relationship expressed by Eq. 3.15. Configuration 2 will be more stable than Configuration 1 for the same values of a_2 , K_n and δ_s .

3.2.4.2 Stability for Horizontal Input

The equations of motion become

$$\ddot{\rho} + D_0 \rho = 0 \quad (\text{Eq. 3.18a})$$

$$\ddot{\phi} + \phi (D_1 \rho + D_2) + \beta (D_3) = - \frac{\ddot{x}_o}{l_s} \quad (\text{Eq. 3.18b})$$

$$\ddot{\beta} + \phi (D'_1 \rho + D'_2) + \beta (D'_3) = 0 \quad (\text{Eq. 3.18c})$$

In the first approximation, it seems reasonable to assume that because of zero vertical input the ρ -mode remains unexcited, in which case Eq. 3.18 b and c become

$$\ddot{\phi} + \phi (D_2) + \beta (D_3) = - \frac{\ddot{x}_o}{l_s} \quad (\text{Eq. 3.19a})$$

$$\ddot{\beta} + \phi (D'_2) + \beta (D'_3) = 0 \quad (\text{Eq. 3.19b})$$

Taking the Laplace Transform, we get

$$\begin{aligned} s^2 \bar{\phi} + D_2 \bar{\phi} + D_3 \bar{\beta} &= - \mathcal{L} \frac{\ddot{x}_o}{l_s} \\ s^2 \bar{\beta} + D'_3 \bar{\beta} + D'_2 \bar{\phi} &= 0 \end{aligned}$$

The frequency determinant is

$$\begin{vmatrix} s^2 + D_2 & D_3 \\ D'_2 & s^2 + D'_3 \end{vmatrix} = 0$$

$$\therefore (s^2 + D_2)(s^2 + D'_3) - D'_2 D_3 = 0$$

$$\therefore s^4 + s^2 (D_2 + D'_3) + D_2 D'_3 - D'_2 D_3 = 0$$

$$\text{Let } a = D_2 + D'_3$$

$$\text{and } b = (D_2 D'_3 - D'_2 D_3)$$

The frequency equation becomes

$$s^4 + a s^2 + b = 0 \quad (\text{Eq. 3.20})$$

The solution of the equation gives

$$s^2 = -\frac{a}{2} \pm \sqrt{\left(\frac{a}{2}\right)^2 - b} \quad (\text{Eq. 3.21})$$

The stability or instability of the dynamical system depends upon the location of these roots in the complex S plane. The roots of the polynomial Eq. 3.20 are complex numbers of the form

$$S_1 = \delta_1 + i\omega_1,$$

which gives the solution of Eq. 3.19a and b in the form

$$\begin{bmatrix} \phi \\ \beta \end{bmatrix} = \begin{bmatrix} A_1 \\ A_2 \end{bmatrix} e^{\delta_1 t} \quad (\text{Eq. 3.22})$$

If the real part δ_1 of the roots S_1 is negative numbers, the term, $e^{\delta_1 t}$, acts as a decrement factor in the solution of ϕ and β and the solution is stable. If, however, one or more roots, S_1 , has a positive real part, the solution for Eq. 3.22 will contain the exponentially increasing factor

$$e^{\delta_1 t}$$

and the system is unstable. If the real part of the root, S_1 , is zero, the system is on the borderline between stability and instability.

The Routh-Hurwitz stability criterion states that, for all the roots to have negative real parts, the coefficients a and b in Eq. 3.20 must be positive. This can be inferred directly from Eq. 3.21 when

$$b > 0$$

$$\frac{a}{2} > \sqrt{\left(\frac{a}{2}\right)^2 - b}$$

and S will have two distinct roots. The particular solution of Eq. 3.20 will give the roots containing an imaginary part only because of the absence of damping in Eq. 3.19a and b.

Condition 1

$$a > 0$$

$$\therefore (D_2 + D'_3) > 0$$

Configuration 2

$$\frac{2K\delta_s}{m(\ell_s + a_2)} + \frac{2K}{mR^2} (r + a_2\phi_2)^2 > 0 \quad (\text{Eq. 3.23a})$$

Configuration 3

$$\frac{2}{m} \left\{ \frac{K_1 \delta_{1s}}{\ell_s - a_1} + \frac{K_2 \delta_{2s}}{\ell_s + a_2} \right\} + \frac{2}{mR^2} \left\{ K_1 (r - a_1\phi_1)^2 + K_2 (r + a_2\phi_2)^2 \right\} > 0 \quad (\text{Eq. 3.23b})$$

It can be seen that these conditions are satisfied by both configurations.

Condition 2

$$b > 0$$

$$\therefore (D_2 D'_3 - D'_2 D_3) > 0$$

Configuration 2

$$\frac{4}{m^2} \left\{ \frac{K\delta_s}{\ell_s + a_2} \cdot \frac{K}{R^2} (r + a_2\phi_2)^2 - \frac{K\delta_s (a_2 - r\phi_2)}{R^2 (\ell_s + a_2)} K\phi_2 (r + a_2\phi_2) \right\} > 0 \quad (\text{Eq. 3.24a})$$

Configuration 3

$$\begin{aligned} \frac{4}{m^2} \left\{ \left[\frac{K_1 \delta_{1s}}{\ell_s - a_1} + \frac{K_2 \delta_{2s}}{\ell_s + a_2} \right] \left[\frac{K_1}{R^2} (r - a_1\phi_1)^2 + \frac{K_2}{R^2} (r + a_2\phi_2)^2 \right] \right. \\ \left. - \left[\frac{K_1 \delta_{1s} (-a_1 - r\phi_1)}{R^2 (\ell_s - a_1)} + \frac{K_2 \delta_{2s} (a_2 - r\phi_2)}{R^2 (\ell_s + a_2)} \right] \left[K_1 \phi_1 (r - a_1\phi_1) \right. \right. \\ \left. \left. + K_2 \phi_2 (r + a_2\phi_2) \right] \right\} > 0 \quad (\text{Eq. 3.24b}) \end{aligned}$$

Comparing Eq. 3.24a with Eq. 3.24b, it can be seen that Configuration 2 will satisfy the conditions of Eq. 3.24a up to certain limits of a_2 , after which $D_2 D'_3 > D'_2 D_3$ and the system will become unstable. Configuration 3 will satisfy the conditions of Eq. 3.24b without any limit on a_2 , as D'_2 also contains $-a_1$ to compensate for high values of a_2 , if any.

Another interesting basis for comparison is the range of stabilities. As it is evident that both configurations are stable within certain limits, the criterion that one of the two configurations is more stable or is stable within a wider range than the other can be used as an additional basis for comparison and selection. Condition 2 states that $b = (D_2 D'_3 - D'_2 D_3) > 0$, which can be interpreted thus: the larger the value of $(D_2 D'_3)$ up to the limit,

$$b = \frac{a^2}{4},$$

the better the system will be from the viewpoint of stability.

For the configurations under consideration, the values of D_2 and D'_3 are always positive. Hence, the greatest value of b will be achieved when either D'_2 or D_3 is zero;

$$\therefore b_m = D_2 D'_3$$

$$\therefore S^2 = -\left(\frac{D_2 + D'_3}{2}\right) \pm \sqrt{\left(\frac{D_2 + D'_3}{2}\right)^2 - D_2 D'_3}$$

$$\therefore S_1^2 = -D_2, (S_1)_{1,2} = \pm i \sqrt{D_2}$$

$$S_2^2 = -D'_3, (S_2)_{1,2} = \pm i \sqrt{D'_3}$$

$$\therefore \phi = A_1 \cos \sqrt{D_2} t$$

$$\text{and } \beta = A_2 \cos \sqrt{D'_3} t$$

This shows that Eq. 3.19a is uncoupled with β and Eq. 3.19b is uncoupled with the pendulum angle, ϕ . A similar conclusion has been drawn by comparing only the coefficients in Paragraph 3.2.3, in which it is shown that Configuration 3 is better than Configuration 2 due to various parameters available to make D'_2 and D_3 close to zero.

Hence, from the above discussion it seems that Configuration 3 offers a wider region of stability than Configuration 2. In addition it minimizes the flow of energy from one mode to another when various parameters are properly proportioned.

3.2.4.3 Stability for Inclined Input

For a shock input which has both horizontal and vertical components, the equations of motion become

$$\ddot{\rho} + D_0 \rho = -\ddot{Z}_0 \quad (\text{Eq. 3.25a})$$

$$\ddot{\phi} + \phi (D_1 \rho + D_2) + \beta(D_3) = \frac{\ddot{X}_0}{L_s} \quad (\text{Eq. 3.25b})$$

$$\ddot{\beta} + \phi (D'_1 \rho + D'_2) + \beta (D'_3) = 0 \quad (\text{Eq. 3.25c})$$

For residual oscillations, Eq. 3.25a gives

$$\rho = \rho_0 \cos \omega t$$

Hence, Eq. 3.25 b and c become

$$\ddot{\phi} + \phi (D_1 \rho_0 \cos \omega t + D_2) + \beta(D_3) = -\frac{\ddot{X}_0}{L_s} \quad (\text{Eq. 3.26a})$$

$$\ddot{\beta} + \phi (D'_1 \rho_0 \cos \omega t + D'_2) + \beta(D'_3) = 0 \quad (\text{Eq. 3.26b})$$

The above equations can be reduced to first order by making the substitution

$$\phi = \phi_1, \quad \dot{\phi}_1 = \phi_2$$

$$\beta = \beta_1, \quad \dot{\beta}_1 = \beta_2$$

Eq. 3.26 a and b become

$$\dot{\phi}_2 + \phi_1 (D_1 \rho_0 \cos \omega t + D_2) + \beta_1(D_3) = -\frac{\ddot{X}_0}{L_s}$$

$$\dot{\phi}_1 - \phi_2 = 0$$

$$\dot{\beta}_2 + \phi_1 (D'_1 \rho_0 \cos \omega t + D'_2) + \beta_1(D'_3) = 0$$

$$\dot{\beta}_1 - \beta_2 = 0$$

This can be represented in matrix form as follows:

$$\begin{bmatrix} \ddot{\phi}_1 \\ \ddot{\beta}_1 \\ \ddot{\phi}_2 \\ \ddot{\beta}_2 \end{bmatrix} + \begin{bmatrix} 0 & 0 & -1 & 0 \\ 0 & 0 & 0 & -1 \\ (D_1 \phi_0 \cos \omega t + D_2) & D_3 & 0 & 0 \\ (D_1' \phi_0 \cos \omega t + D_2') & D_3' & 0 & 0 \end{bmatrix} \begin{bmatrix} \phi_1 \\ \beta_1 \\ \phi_2 \\ \beta_2 \end{bmatrix} = \begin{bmatrix} 0 \\ 0 \\ -\ddot{x}_0 / \lambda_s \\ 0 \end{bmatrix} \quad (\text{Eq. 3.27})$$

These equations can be written in the general form

$$\frac{d}{dt} \left\{ \lambda \right\} + [u] \left\{ \lambda \right\} = \left\{ -\ddot{x}_0 / \lambda_s \right\} \quad (\text{Eq. 3.28})$$

Where $\{\lambda\}$ is the general column vector of n elements $\phi_1, \phi_2, \beta_1, \beta_2$, and $[u]$ is the square matrix of n^{th} order. In general, the elements, U_{ij} , of the matrix $[u]$ are either functions of the independent variable t or constants or both.

The differential equation 3.28 may be integrated by means of the Peano-Baker method. Let the initial conditions of the system be such that

$$\{\lambda\} = \{\lambda\}_0 \quad \text{at } t = 0$$

where $\{\lambda\}_0$ is the column vector of initial values of elements of $\{\lambda\}$. Direct integration of Eq. 3.28 gives the following integral equation:

$$\{\lambda\} = \{\lambda\}_0 - \int_0^t \left[[u(\xi)] \left\{ \lambda \right\} + \left\{ \frac{\ddot{x}_0}{\lambda_s} \right\} \right] d\xi \quad (\text{Eq. 3.29})$$

where ξ is a subsidiary variable of integration. This integral equation may be solved by repeated substitutions of $\{\lambda\}$ from the left hand member of Eq. 3.29 into the integral. Because of the repetitive and tedious method involved in the solution of the equations as shown above, an attempt has not been made to solve Eq. 3.26 a and b. The method of approach is indicated, however.

3.3 Selection of Recommended System

3.3.1 Basis for Selection

Based upon the discussion in the preceding paragraphs, the isolation system of Configuration 3 is recommended because of the following advantages:

1. Reduction in coupling between different modes, assuming proper selection of critical parameters, which reduces rotations.

2. Insensitivity of the system to shifts in location of the center of gravity.
3. Increased stability due to two levels of suspension.
4. Reduction in the effect of eccentricity.
5. Rapid restoration of the system, even when highly disturbed in rotations.

3.3.2 Design Parameters

The discussion of Section 3.2.3 shows that, for Configuration 3 to have these advantages, it is necessary that

- a. D_3 should be zero or minimum
- b. D_1 should be zero or minimum
- c. D_1' should be zero or minimum
- d. D_2' should be zero or minimum.

However, it is not possible to satisfy all the conditions simultaneously. The most important condition is that D_3 should be minimized, which means reducing the coupling between translational and rotational modes. For Configuration 3

$$D_3 = K_1 \sin \phi_1 (r \cos \phi_1 - a_1 \sin \phi_1) + K_2 \sin \phi_2 (r \cos \phi_2 + a_2 \sin \phi_2).$$

The variables of this function are not independent, but are related by the following equation:

$$D_4 = K_1 \delta_1 \cos \phi_1 + K_2 \delta_2 \cos \phi_2 - \frac{mg}{2} = 0$$

To find the minimum value of the function D_3 , Lagrange's Method of Undetermined Multipliers can be used.

$$\text{Let } D_3 = f_1 (K_1, K_2) \quad (\text{Eq. 3.30a})$$

$$\text{and } D_4 = f_2 (K_1, K_2) = 0 \quad (\text{Eq. 3.30b})$$

If D_3 is to have a maximum or minimum, it is necessary that

$$\frac{\partial D_3}{\partial K_1} = 0, \quad \frac{\partial D_3}{\partial K_2} = 0$$

Hence

$$\left(\frac{\partial D_3}{\partial K_1} \right) dK_1 + \left(\frac{\partial D_3}{\partial K_2} \right) dK_2 = 0 \quad (\text{Eq. 3.31})$$

Differentiating the functional relation D_4 , we get

$$\left(\frac{\partial D_4}{\partial K_1} \right) dK_1 + \left(\frac{\partial D_4}{\partial K_2} \right) dK_2 = 0 \quad (\text{Eq. 3.32})$$

Multiplying Eq. 3.32 by the parameter λ and adding the results to Eq. 3.31, we obtain

$$\left[\frac{\partial D_3}{\partial K_1} + \lambda \frac{\partial D_4}{\partial K_1} \right] dK_1 + \left[\frac{\partial D_3}{\partial K_2} + \lambda \frac{\partial D_4}{\partial K_2} \right] dK_2 = 0$$

This equation is satisfied if

$$\frac{\partial D_3}{\partial K_1} + \lambda \frac{\partial D_4}{\partial K_1} = 0 \quad \text{and} \quad \frac{\partial D_3}{\partial K_2} + \lambda \frac{\partial D_4}{\partial K_2} = 0 \quad (\text{Eq. 3.33})$$

For the unique value of λ , the following condition is to be satisfied:

$$\frac{\partial D_3 / \partial K_1}{\partial D_4 / \partial K_1} = \frac{\partial D_3 / \partial K_2}{\partial D_4 / \partial K_2} \quad (\text{Eq. 3.34})$$

Now

$$\frac{\partial D_3}{\partial K_1} = \sin \phi_1 (r \cos \phi_1 - a_1 \sin \phi_1)$$

$$\frac{\partial D_3}{\partial K_2} = \sin \phi_2 (r \cos \phi_2 + a_2 \sin \phi_2)$$

$$\frac{\partial D_4}{\partial K_1} = \delta_1 \cos \phi_1$$

$$\frac{\partial D_4}{\partial K_2} = \delta_2 \cos \phi_2$$

The relation of Eq. 3.34 gives

$$\frac{\sin \phi_1 (r \cos \phi_1 - a_1 \sin \phi_1)}{\sin \phi_2 (r \cos \phi_2 + a_2 \sin \phi_2)} = \frac{\delta_1 \cos \phi_1}{\delta_2 \cos \phi_2}$$

$$\frac{\delta_1}{\delta_2} = \frac{\tan \phi_1}{\tan \phi_2} \left\{ \frac{r \cos \phi_1 - a_1 \sin \phi_1}{r \cos \phi_2 + a_2 \sin \phi_2} \right\} \quad (\text{Eq. 3.35})$$

As the function D_3 is linear in K_1 and K_2 , the above relation obtained by Lagrange's Method of Undetermined Multipliers is not adequate to obtain the minimum with K_1 and K_2 as variables, hence the following additional relation is introduced.

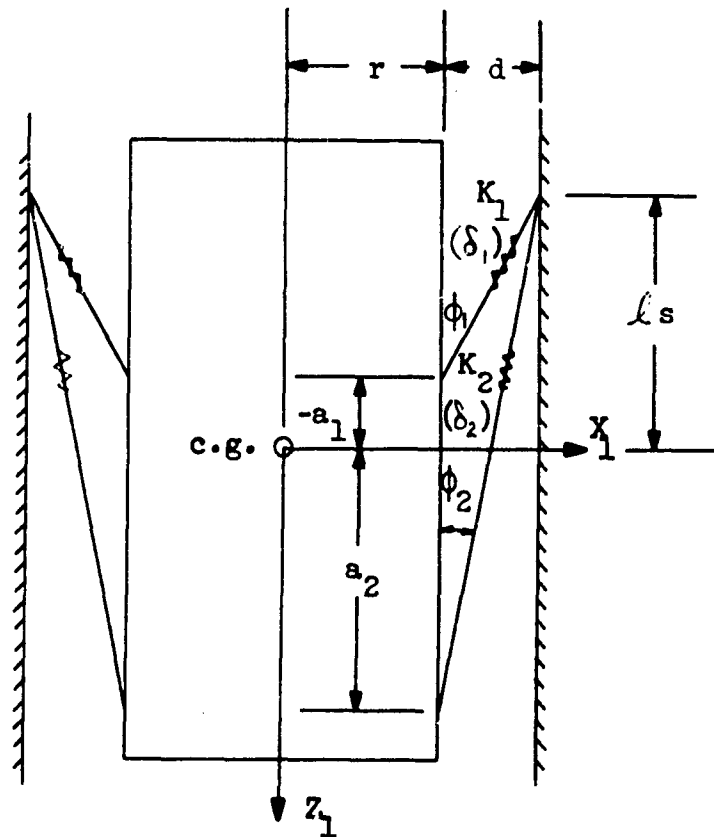


Figure 3-3. Configuration 3 Notation.

$$K_1 \delta_1 \cdot \sin \phi_1 \cdot a_1 = K_2 \delta_2 \sin \phi_2 \cdot a_2$$

$$\therefore \frac{\delta_1}{\delta_2} = \frac{K_2 \sin \phi_2 \cdot a_2}{K_1 \sin \phi_1 \cdot a_1} \quad (\text{Eq. 3.36})$$

Using Eq. 3.35, we obtain

$$\frac{\tan \phi_1}{\tan \phi_2} \left\{ \frac{r \cos \phi_1 - a_1 \sin \phi_1}{r \cos \phi_2 + a_2 \sin \phi_2} \right\} = \frac{K_2}{K_1} \frac{\sin \phi_2}{\sin \phi_1} \frac{a_2}{a_1}$$

$$\therefore \frac{K_1}{K_2} \cdot \frac{a_1}{a_2} \cdot \frac{\sin \phi_1}{\sin \phi_2} \cdot \frac{\tan \phi_1}{\tan \phi_2} \cdot \frac{r \cos \phi_1 - a_1 \sin \phi_1}{r \cos \phi_2 + a_2 \sin \phi_2} = 1 \quad (\text{Eq. 3.37})$$

Compiling the conditions to be satisfied, we obtain

- a. D_3 should be zero or minimum

Eq. 3.37 gives

$$\frac{K_1}{K_2} \cdot \frac{a_1}{a_2} \cdot \frac{\sin \phi_1}{\sin \phi_2} \cdot \frac{\tan \phi_1}{\tan \phi_2} \cdot \frac{r \cos \phi_1 - a_1 \sin \phi_1}{r \cos \phi_2 + a_2 \sin \phi_2} = 1$$

or for small angles

$$\frac{K_1}{K_2} \cdot \frac{a_1}{a_2} \cdot \left(\frac{\phi_1}{\phi_2}\right)^2 \cdot \frac{r - a_1 \phi_1}{r + a_2 \phi_2} = 1 \quad (\text{Eq. 3.38a})$$

- b. D_1 should be zero or minimum

$$\frac{K_1}{l_s - a_1} + \frac{K_2}{l_s + a_2} - \frac{K_1 + K_2}{l_s} = 0 \quad (\text{Eq. 3.38b})$$

- c. D'_1 should be zero or minimum

$$\frac{K_1(-a_1 - r\phi_1)}{l_s - a_1} + \frac{K_2(a_2 - r\phi_2)}{l_s + a_2} = 0 \quad (\text{Eq. 3.38c})$$

- d. D'_2 should be zero or minimum

$$\frac{K_1 \delta_{1s}(-a_1 - r\phi_1)}{l_s - a_1} + \frac{K_2 \delta_{2s}(a_2 - r\phi_2)}{l_s + a_2} = 0 \quad (\text{Eq. 3.38d})$$

3.3.3 Calculations of Design Parameters

To reduce the coupling between modes and to increase the stability of the system, it is desirable to meet the criteria in Eq. 3.38 a through d. Owing to limitations on the various parameters arising from practical considerations, it may not be possible to satisfy all the criteria simultaneously. An attempt is made to satisfy most of the criteria as closely as possible.

Rattlespace is one of the parameters which is limited for economic reasons. This in turn restricts the inclination of top and bottom isolators. Considering various factors such as intensity of horizontal shock, movements of extreme points of the suspended mass due to rotations about the center of gravity, and the space required for structural and mechanical connections of isolators to the cage structure, a rattlespace of 112 in. seems to be a reasonable choice. With a rattlespace greater than 112 in., it is possible to reduce the coupling to minimum, possibly to zero; but then the motion of the suspended mass will be contained within a space much less than 112 in., which means that the available rattlespace is not used effectively. On the other hand, if a rattlespace of less than 112 in. is chosen, the coupling may increase and the movements of the mass may not be contained within the given space, hence the isolation may prove ineffective.

By a method of trial and error, the following parameters are selected which appear to satisfy criteria, Eq. 3.38 a through d, closely.

$$a_1 = 10.0 \text{ ft.}$$

$$a_2 = 60.0 \text{ ft.}$$

$$\phi_1 = 0.155 \text{ rad.} = 8.88 \text{ degrees}$$

$$\phi_2 = 0.072 \text{ rad.} = 4.12 \text{ degrees}$$

$$K_1 = 2K_2$$

Following are the constants of the system:

$$r = 37.5 \text{ ft.}$$

$$l_s = 70.0 \text{ ft.}$$

Criterion Eq. 3.38a

$$\frac{K_1}{K_2} \cdot \frac{a_1}{a_2} \left(\frac{\phi_1}{\phi_2} \right)^2 \cdot \frac{r - a_1 \phi_1}{r + a_2 \phi_2} = 1$$

$$\frac{2}{1} \cdot \frac{10}{60} \cdot \left(\frac{0.155}{0.072} \right)^2 \cdot \frac{37.5 - (10)(0.155)}{37.5 + (60)(0.072)} = 1.33$$

Criterion Eq. 3.38b

$$\frac{K_1}{l_s - a_1} + \frac{K_2}{l_s + a_2} - \frac{K_1 + K_2}{l_s} = 0$$

$$\frac{2}{70-10} + \frac{1}{70+60} - \frac{3}{70}$$

$$= 0.0333 + 0.0077 - 0.0428$$

$$= -.0018 \cong 0$$

Criterion Eq. 3.38c

$$\frac{K_1(-a_1 - r\phi_1)}{l_s - a_1} + \frac{K_2(a_2 - r\phi_2)}{l_s + a_2}$$

$$\frac{2 \{-10 - (37.5)(0.155)\}}{70 - 10} + \frac{1 \{60 - (37.5)(.072)\}}{70 + 60}$$

$$= - 0.526 + 0.440$$

$$= - 0.086 \cong 0$$

Criterion Eq. 3.38d reduces to equation 3.38c when

$$\delta_{1s} = \delta_{2s}$$

Figure 3-4 shows the parameters of suspension system Configuration 3.

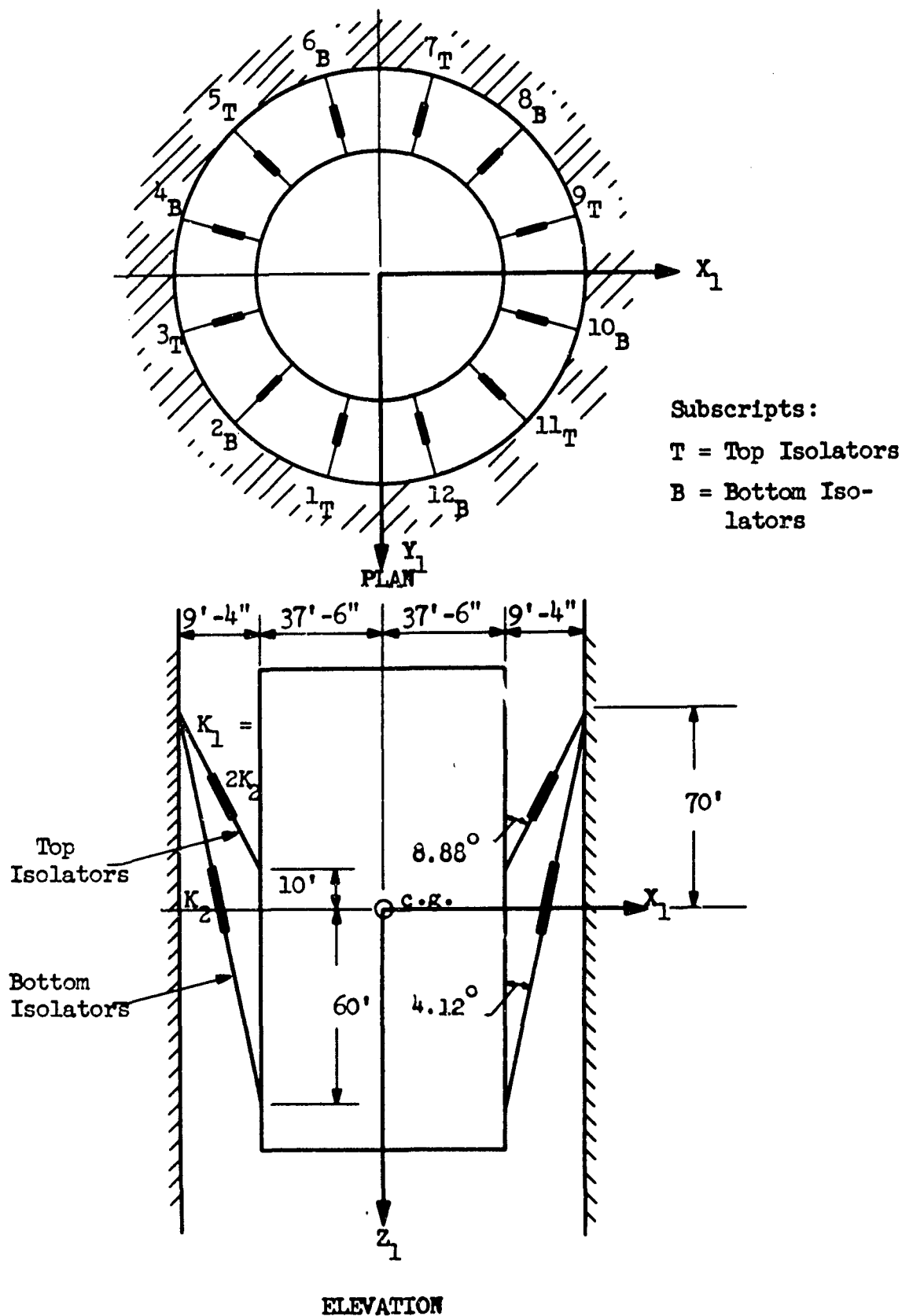


Figure 3-4. Suspension System Configuration 3.

3.3.4 Numerical Evaluation of System Stability

From the viewpoint of pendulum stability as described in Reference 2, it is essential, if resonance effects are to be avoided, to insure that the pendulum frequency is less than one half the frequency of the radial mass-spring system of the pendulum arm. The farther the pendulum frequency is from this value, the greater the stability of the system.

A good first approximation of the stability of the configuration can be obtained by reducing the system to the simple two-degree-of freedom, undamped spring pendulum shown in Figure 3-5. By lumping masses and stiffnesses, this model may be considered somewhat representative of Configuration 1 without the horizontal sway dampers.

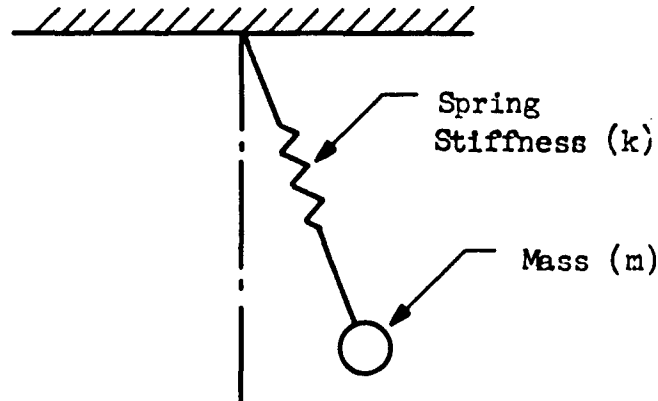


Figure 3-5. Simple Elastic Pendulum

In this facility, two factors are fixed: the mass of the supported structure and the maximum acceleration to which the structure and its contents may be exposed. These quantities then fix in a first approximation the uncoupled axial frequency of the pendulum-spring combination at:

$$\omega_1^2 = \frac{k}{m}$$

where the k is the stiffness of the spring incorporated in the

pendulum arm.

Referring to the shock response spectrum of Figure 2-4, a linear undamped system of a frequency $f = .35$ cps will respond with a relative displacement of $3\frac{1}{4}$ inches with an absolute acceleration of 0.42 gravities. Then the stiffness of a single isolator is

$$k = m\omega_1^2 = 5.25 \times 10^3 \text{ pounds per inch}$$

where

$$m = \text{mass supported by each isolator} = 1.09 \times 10^3 \text{ lb. sec}^2 \text{ inch}^{-1}.$$

The natural frequency of the simple unsprung pendulum is

$$\omega^2 = \frac{g}{l}$$

where l is the pendulum length; in this case the distance from the center of gravity of the suspended mass to the pendulum upper attachment point.

If a spring is incorporated in the pendulum arm, Reference 2 gives the equivalent natural frequency as

$$\omega_o^{*2} = \frac{g}{l^*}$$

where

$$l^* = \frac{l + R^2}{l}$$

$$R^2 = \frac{I_{c.g.}}{m}$$

$I_{c.g.}$ = Moment of inertia of the mass about its center of gravity.

From a consideration of the geometry of the cage and the surrounding capsule, there appears to be a limit of about 70 feet to the permissible length of the pendulum arm. Since the vertical position of the center of gravity of the mass may vary plus or minus 5 feet from the nominal position, we have for the limits of length:

$$l = \begin{Bmatrix} 780 \\ 900 \end{Bmatrix} \text{ inches}$$

Using these numerical values

$$I_{c.g.} \text{ (total system)} = 3.62 \times 10^6 \text{ lb. sec. in.}$$

$$m \text{ (total system)} = 13.1 \times 10^3 \text{ lb. sec.}^2 \text{ in.}^{-1}$$

$$R^2 = 276 \text{ in.}^2$$

we obtain

l (In.)	l^* (In.)	ω_o^{*2} (Rad./Sec.) ²	ω_o^* (Rad./Sec.)	$\omega_o^{*2} / \omega_1^2$
780	783.5	0.493	0.702	0.102
900	903.0	0.428	0.654	0.089

The ratio $(\omega_o^{*2} / \omega_1^2)$ is a criterion of the energy exchange between the vertical and the horizontal modes, the critical condition being

$$\frac{\omega_o^{*2}}{\omega_1^2} = 0.250$$

It may be noted that the values given for this configuration fall much below the critical value.

The degree of stability of the system can be shown graphically by use of an Ince-Strutt diagram which employs the parameters

$$a = \left(\frac{2\omega_o^*}{\omega_1} \right)^2$$

$$q = \frac{2\rho_o}{l^*}$$

Letting $\rho_0 = 34$ inches

ℓ (in.)	a	q
780	0.408	0.082
900	0.356	0.071

In Figure 3-6 these points are shown in the Ince-Strutt diagram.

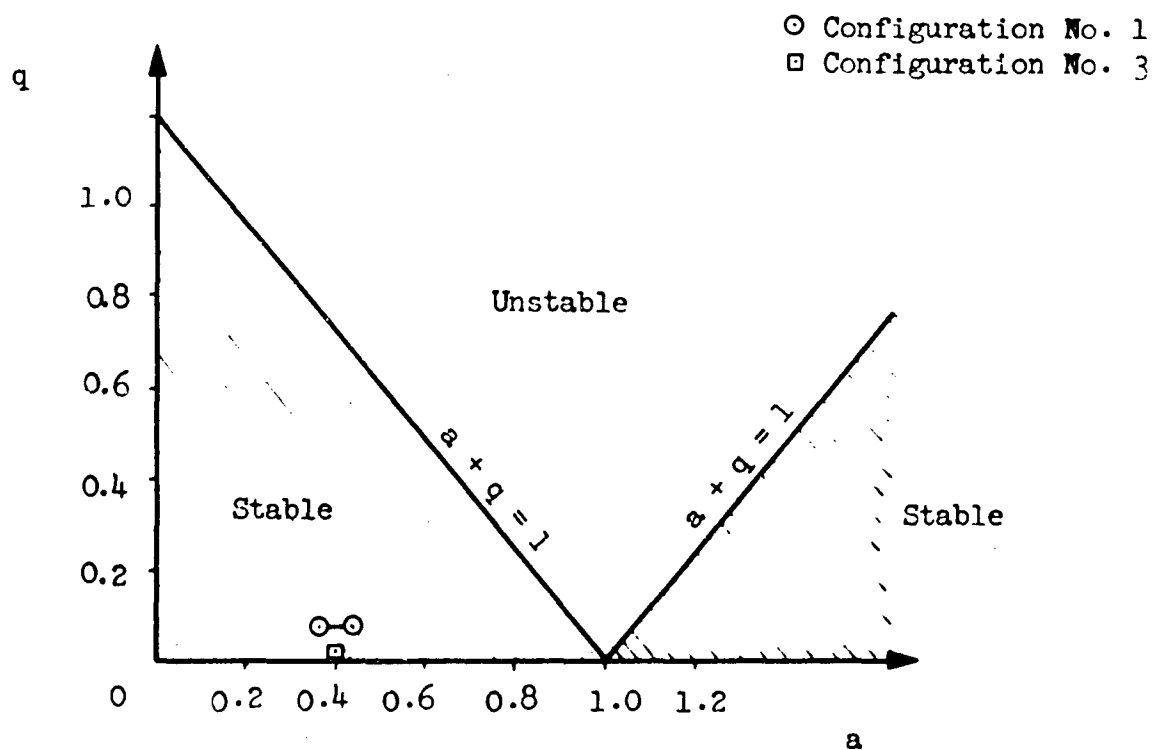


Figure 3-6. Ince-Strutt Stability Diagram Showing Relationship of the Facility Configuration.

It is evident from the diagram that on the basis of this simple, two-degree-of-freedom, undamped approximation, the configuration selected for this facility is highly stable. It is believed to be unlikely that with moderate amounts of damping and coupling to other modes, the complete six-degree-of-freedom damped system will respond appreciably differently insofar as stability is concerned. The actual stability of the system, of course, can be determined from the results of a complete rigid body analysis.

For Configuration 2, the condition of stability is given by Eq. 3.16

$$a + q \leq 1$$

$$\therefore \frac{4\delta_s}{l_s + a_2} + 2\rho_0 \left\{ \frac{1}{l_s + a_2} - \frac{1}{l_s} \right\} \leq 1$$

Using the following numerical constants

$$\delta_s = 7'$$

$$l_s = 70'$$

$$a_2 = -5'$$

$$\rho_0 \approx 3'$$

we obtain

$$\frac{(4)(7)}{65} + 6 \left\{ \frac{1}{65} - \frac{1}{70} \right\}$$

$$= 0.43 + 0.0066 < 1$$

Hence the system is stable.

For Configuration 3, the condition of stability is given by Eq. 3.17

$$a + q \leq 1$$

$$4 \left(\frac{K_1}{K_1 + K_2} \cdot \frac{\delta_{1s}}{l_s - a_1} + \frac{K_2}{K_1 + K_2} \cdot \frac{\delta_{2s}}{l_s + a_2} \right) + 2\rho_o \left(\frac{K_1}{K_1 + K_2} \cdot \frac{1}{l_s - a_1} + \frac{K_2}{K_1 + K_2} \cdot \frac{1}{l_s + a_2} - \frac{1}{l_s} \right) \leq 1$$

Using the following numerical constants

$$\begin{aligned} K_1 &= 2K_2 \\ \delta_{1s} &= \delta_{2s} = 7' \\ l_s &= 70' \\ a_1 &= 10' \\ a_2 &= 60' \\ \rho_o &= 3' \end{aligned}$$

we obtain

$$4 \left(\frac{2}{3} \cdot \frac{7}{60} + \frac{1}{3} \cdot \frac{7}{130} \right) + 6 \left(\frac{2}{3} \cdot \frac{1}{60} + \frac{1}{3} \cdot \frac{1}{130} - \frac{1}{70} \right) = 0.384 - 0.004 \leq 1$$

Hence the system is stable.

3.3.5 Calculations for Suspension System of Configuration 2.

In the discussion so far, only a qualitative approach has been used to arrive at the selection of Configuration 3. However, it is desirable to obtain quantitatively the responses of the

systems of Configurations 2 and 3 as a better comparison. Hence, it is desirable to solve the equations of motion by a numerical integration method on a digital computer to obtain the responses of the two configurations.

Suspension System Configuration 2 is shown in Figure 3-7. The stiffnesses and polar co-ordinates (ℓ_{ns} , ϕ_{ns} , θ_{ns}) for all isolators are calculated and presented in Tables 3-2 and 3-3.

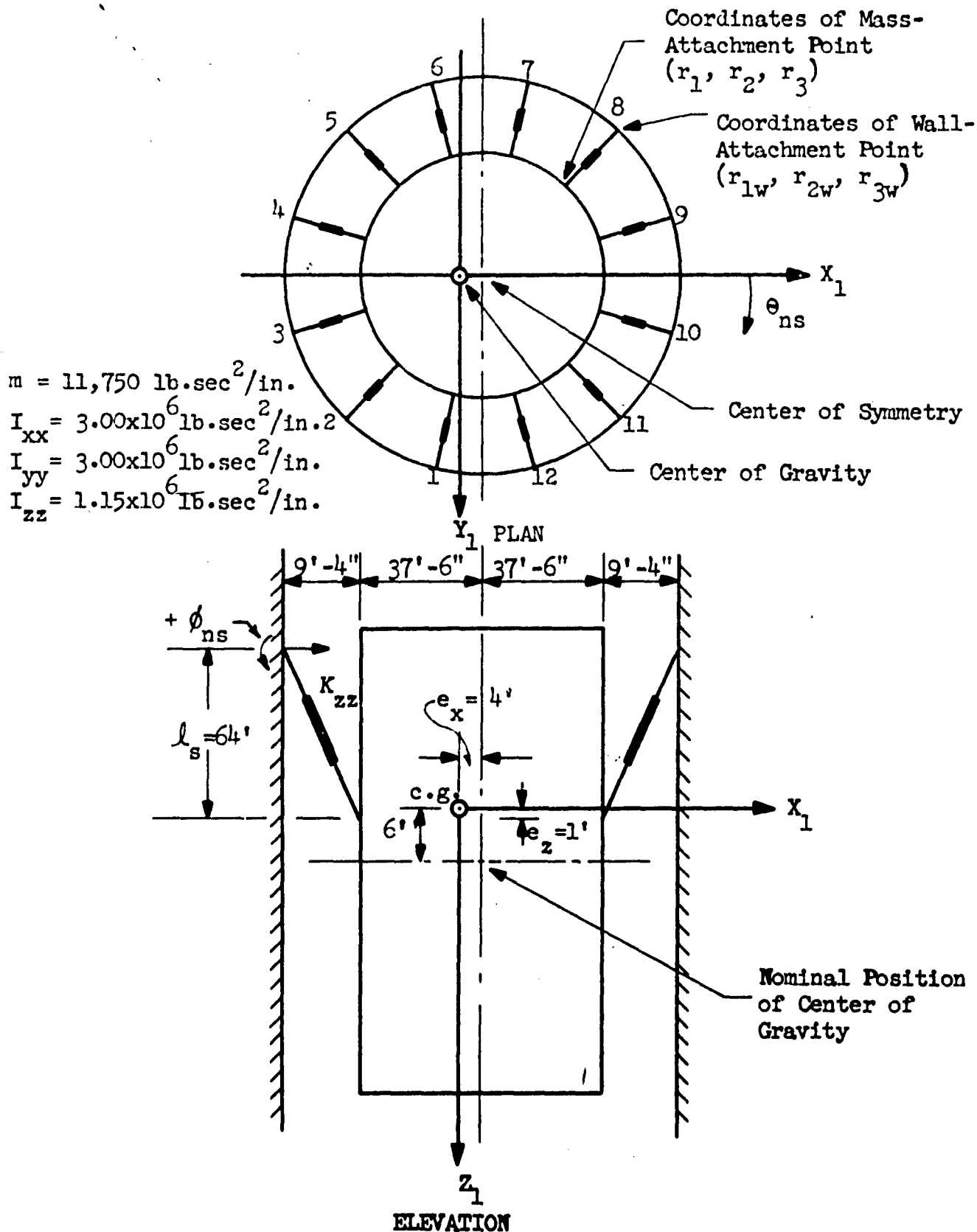


Figure 3-7. Suspension System Configuration 2

Table 3-2

Computed Data for Stiffness of All Isolators of Configuration 2

Iso- lator	C_n	$W e_x \frac{C_n}{I_i}$	$\left(\frac{W/N \pm W e_x \frac{C_n}{I_i}}{\cos \phi_{ns}} \right) (K_{zz})'_n$		$(K_{zz})_n$	δ_{ns}	ℓ_{no}	
	In.	Lbs.	Lbs.	Lbs.	Lb/In	Lb/In	In.	In.
1	144	2.60×10^4	40.5×10^4	41.0×10^4	5.10×10^3	4.82×10^3	84.9	705
2	318	5.73×10^4	43.6×10^4	44.2×10^4	5.50×10^3	5.28×10^3	84.0	706
3	425	7.65×10^4	45.6×10^4	46.2×10^4	5.74×10^3	5.52×10^3	83.8	706
4	425	7.65×10^4	45.6×10^4	46.2×10^4	5.74×10^3	5.52×10^3	83.8	706
5	318	5.73×10^4	43.6×10^4	44.2×10^4	5.50×10^3	5.28×10^3	84.0	706
6	144	2.60×10^4	40.5×10^4	41.0×10^4	5.10×10^3	4.82×10^3	84.9	705
7	-144	-2.60×10^4	35.3×10^4	35.7×10^4	4.44×10^3	4.32×10^3	83.0	707
8	-318	-5.73×10^4	32.2×10^4	32.6×10^4	4.05×10^3	3.84×10^3	85.0	705
9	-425	-7.65×10^4	30.2×10^4	30.6×10^4	3.80×10^3	3.70×10^3	82.9	707
10	-425	-7.65×10^4	30.2×10^4	30.6×10^4	3.80×10^3	3.70×10^3	82.9	707
11	-318	-5.73×10^4	32.2×10^4	32.6×10^4	4.05×10^3	3.84×10^3	85.0	705
12	-144	-2.60×10^4	35.3×10^4	35.7×10^4	4.44×10^3	4.32×10^3	83.0	707

Table 3-3

Numerical Data for Isolators of Configuration 2

Iso- lator	l no	r ₁	r _{1w}	r ₂	r _{2w}	r ₃	r _{3w}	φ _{ns}	θ _{ns}	(K _{zz}) _n
		In.	In.	In.	In.	In.	In.	Deg.Min.	Deg.Min.	Lb./In.
1	705	- 96	-132	425	532	12	-768	-8° 15'	108° 40'	4.82 x 10 ³
2	706	-270	-350	318	398	12	-768	-8° 15'	135°	5.28 x 10 ³
3	706	-378	-484	144	180	12	-768	-8° 15'	161° 20'	5.52 x 10 ³
4	706	-378	-484	-144	-180	12	-768	-8° 15'	198° 40'	5.52 x 10 ³
5	706	-270	-350	-318	-398	12	-768	-8° 15'	225°	5.28 x 10 ³
6	705	- 96	-132	-425	-532	12	-768	-8° 15'	251° 20'	4.82 x 10 ³
7	707	192	228	-425	-532	12	-768	-8° 15'	288° 40'	4.32 x 10 ³
8	705	366	446	-318	-398	12	-768	-8° 15'	315°	3.84 x 10 ³
9	707	474	580	-144	-180	12	-768	-8° 15'	341° 20'	3.70 x 10 ³
10	707	474	580	144	180	12	-768	-8° 15'	18° 40'	3.70 x 10 ³
11	705	366	446	318	398	12	-768	-8° 15'	45°	3.84 x 10 ³
12	707	192	228	425	532	12	-768	-8° 15'	71° 20'	4.32 x 10 ³

Due to eccentricity, e_x , of the center of gravity, the body in the static position will not remain symmetrical with respect to the capsule, but there will be small initial translations and rotations. As the purpose of this analysis is only to compare the responses of various configurations, it seems reasonable to neglect the initial translations and rotations, and the system is treated as if it were symmetrical.

The numerical values are as follows:

W	= Weight of the body (nominal minus 10 per cent)	= 4.545×10^6 lbs.
e_x	= Eccentricity of c.g. on x axis	= 48 in.
N	= Number of isolators	= 12
C_n	= Distance from center of symmetry to mass-attachment point of n^{th} isolator, in x_1 direction (as shown in table 3-2)	
I	= Moment of inertia of 12 mass-attachment points of isolators	= $6 R^2$ = 1.21×10^6 in. ²
ω_v	= Natural frequency in vertical direction	= 2.19 rad./sec.
$(K_{zz})'_n$	= Stiffness of the n^{th} isolator	= $\frac{\omega_v^2}{g \cos \phi_{ns}} \left\{ \frac{W}{n} + \frac{W e_x C_n}{I} \right\}$ lb./in.
K_c	= Stiffness of the cable	= 13.7×10^4 lb./in.
$(K_{zz})_n$	= Combined stiffness of cable plus n^{th} isolator in series	= $\frac{(K_{zz})'_n K_c}{(K_{zz})'_n + K_c}$ lb./in.
δ_{ns}	= Static deflection of n^{th} isolator	= $(l_{ns} - l_{no})$ in.
l_{ns}	= Total length of n^{th} isolator in static position	= 790 in.
l_s	= Length of the pendulum in static position	= 768 in.

3.4 Damping Effects

3.4.1 Damping Requirements

The incorporation of damping in a shock isolation system can be beneficial on several counts. First, the system is quickly restored to a near equilibrium position where it is prepared to sustain a second attack. Second, damped systems in general are less sensitive to details of the shock input than are undamped systems. Third, damping in the translational modes reduces the amount of energy transferred by coupling to the rotational modes, thus reducing the angular displacements and the requirement for rattle space.

Despite these very significant advantages, only in a very few actual designs has there been made a systematic attempt to optimize the damping both as to type and amount. Perhaps this lack of deliberate attention has been prompted, at least in part, by the absence in many design criteria documents of specific damping instructions or objectives.

Insofar as the first advantage listed above is concerned, it is the agency using the facility which must fix the time within which the facility must be restored to readiness. Admittedly, since the optimum readiness time from the users point of view is zero seconds, the selection of any finite time simply represents a reluctant relaxation of desired performance. On the other hand it would appear to be desirable to know the time required by all the shock isolation systems in the facility to regain readiness and to insure that a significant proportion of this time is not due to slowly decaying oscillations of only one or two systems.

In establishing performance criteria for the facility studied here, a tentative minimum damping requirement was established which specified that all systems be damped to 0.1 amplitude in 30 seconds. It was not intended that this requirements should impose severe design conditions on the system, but rather that it be used as a target point which could be made more severe or relaxed if justified by more detailed analysis. In any case, the specification of an explicit damping requirement would provide a common basis for the design of all systems within the facility.

Specific damping requirements to achieve an optimum displacement relative to the capsule can be established only after a comprehensive analysis of the system has been made and the influence of significant system parameters, including the cost of damping and rattle space have been evaluated. If the resulting damping requirement from this consideration is less severe than that required to restore the system in the specified time, the larger amount of damping should be employed.

In Reference 2, it was suggested that an upper limit of damping needed to provide optimum insensitivity to the input waveform could be established by evaluating the damping required to reduce the response amplification factors of a moderately decaying sinusoid to values comparable to those for the undamped response to a regular pulse. Thus, even though the ground shock waveform were radically different from the predicted shape, the shock isolation system would still survive without exceeding rattlespace and acceleration limitations.

Viscous damping ratios needed to achieve this degree of insensitivity range from 10 per cent to 15 per cent of critical. The attendant damping forces then may be very large and care must be taken to ensure that severe transient ground motions do not introduce large accelerations into the isolated mass.

In this respect it is especially important not only that the amount of damping be investigated, but also the type of damping. Some types of damping, even in apparently small amounts, can produce conditions so undesirable as to offset completely the advantages of damping. For this reason several different types of damping are reviewed here and their characteristics compared with the requirements of this application.

The requirements for damping incorporated in a shock isolation system design, then, are that it must

1. Inhibit quasi-resonances from being generated in the system by unexpected oscillations in the input shock.
2. Attenuate the oscillations by a specified amount in a specified period of time.
3. Permit the mass to return to or near to its initial position.
4. Exert a minimum force on the mass during both transient and residual motions.

As bases for comparing quantitatively the effectiveness of different types of damping in fulfilling these requirements, the following indices of performance are established.

Peak force required to damp the free oscillations of a system from initial amplitude X_0 to reduced amplitude αX_0 in time t_1 .
(Index of attenuation)

Peak force required to dissipate a given amount of energy in a single, forced steady-state cycle. (Index of sensitivity)

Ratio of rest force (i.e. damping force at $\dot{X}(0)$) to stiffness (Index of Terminal Excursion).

Ratio of peak transient damping force to peak damping force during residual motion.

3.4.2 Types of Damping

Mechanical devices to dissipate energy may produce a constant damping force with relative displacement, a force proportional to \dot{X}^n where $1 \leq n \leq 2$, a force proportional to \dot{X} or a force which is a function of several or all of these. In many dampers, however, a single type of damping is sufficiently predominant to permit a representation of the damping characteristic by a single function.

Some of the more usual types of damping are

$F_d = C_1 \operatorname{sgn} \dot{X}$	coulomb	
$F_d = C_2 \dot{X}$	viscous	} velocity damping
$F_d = C_3 \dot{X}^{1.75}$	hydraulic	
$F_d = C_4 \dot{X}^2$	quadratic	

where

F_d = damping force

X = displacement

C = a constant

In addition to devices exhibiting these properties, there is a class of practical dampers whose principle of operation involves the flow of a compressible fluid and which produces damping forces dependent in varying percentages on displacement, velocity and time. Both liquid and pneumatic springs fall in this latter category.

3.4.2.1 Equivalent Viscous Damping Ratio

Of the types of damping noted above, it is only the viscous damping which with a linear restoring force yields a linear differential equation of motion for the system of which it is a component. Thus, it is convenient for the purpose of analysis to relate the performances of systems containing nonlinear damping with an "equivalent" viscous case. The use of an "equivalent viscous damping ratio"

as an indication of the effect on a system of nonviscous energy dissipative mechanisms can lead to erroneous conclusions, however, unless interpreted in strict accordance with the definition of the term. The damping ratio of a linear, viscously damped system is defined,

$$\zeta = \frac{c}{2\omega m}$$

where

ζ = viscous damping ratio

c = viscous damping coefficient

ω = $\sqrt{k/m}$

k = stiffness of restoring element

m = supported mass

The viscous damping force, a linear function of velocity, is

$$F_{dv} = c\dot{x} = 2\zeta\omega m\dot{x}$$

For the linear system, the damping ratio, ζ , is the ratio of the damping coefficient, c , to that damping coefficient, c_r , which produces a damping force which will just inhibit an oscillatory motion of the supported mass.

It is sometimes convenient in dealing with systems which have non-viscous damping, and linear restoring forces and which are exposed to steady vibrations to relate their peak responses to the viscous case by the means of an "equivalent viscous damping ratio", ζ_e . To determine ζ_e it is assumed that if the energy dissipated by damping in a nonviscous system during a non-decaying forced cycle is the same as that dissipated during an equivalent cycle by a viscously-damped system of the same damping ratio, the peak responses of the systems will be identical.

The work done or energy dissipated by damping during one nondecaying cycle of a viscously damped system is

$$W = \pi c \omega X_0^2 = 2\pi \zeta m (\omega X_0)^2$$

(Eq. 3.39)

Consider, now, a system with a constant friction force F_{dc} such that

$$F_{dc} = K \operatorname{sgn} \dot{x}$$

The work done by such a system per cycle is

$$W = 4F_{dc}X_0 \quad (\text{Eq. 3.40})$$

Equating Eq. 3.39 with Eq. 3.40, we obtain an equivalent viscous damping ratio for the constant friction system

$$\zeta_{e1} = \frac{2F_{dc}}{\pi m \omega^2 X_0}$$

which implies equal energy dissipation per cycle for the two systems.

Similarly, if we consider a system with a linear restoring force but a damping force proportional to the square of the velocity, thus

$$F_{dq} = c_2 \dot{x}^2$$

the work per non-decaying cycle is

$$W = \frac{8c_2 X_0^3 \omega^2}{3}$$

and the equivalent damping ratio ζ_{e2} is

$$\zeta_{e2} = \frac{4c_2 X_0}{3\pi m}$$

Note that we stipulate only that if $\zeta = \zeta_{e1} = \zeta_{e2}$ the energy dissipation per steady state cycle of these three systems is the same. Nothing is said about the comparative rates of decay of oscillations of the systems nor about the relative magnitudes of their damping forces. Also note that the equivalent viscous damping ratio for nonviscous systems, as defined above, is not the ratio of damping of the system to the critical damping of that same nonviscous system.

3.4.2.2 Index of Insensitivity

We defined the energy dissipation for a single steady state cycle as the index of insensitivity of the system to the shock input. Thus the "equivalent viscous damping coefficient" is this index. Comparing peak damping forces needed to achieve the same equivalent viscous damping coefficients, we find

$$\frac{F_{dc}}{F_{dv}} = \frac{\pi}{4} = 0.785$$

$$\frac{F_{dc}}{F_{dv}} = \frac{3\pi}{8} = 1.178$$

Thus for the three systems, coulomb damping will provide the same degree of insensitivity with a lower damping force.

To gain some idea of the magnitude of the coulomb damping force needed in the vertical direction in the system proposed for the facility considered in this study, in order to obtain an equivalent viscous damping ratio of 0.10, we let

$$\zeta_{e1} = 0.10$$

$$\omega = 2.20 \text{ radians/seconds}$$

$$X_0 = 2.833 \text{ feet}$$

$$g = 32.2 \text{ feet/seconds}^2$$

then

$$\frac{F_{dc}}{\text{Weight}} = \frac{\pi \zeta_{e1} \omega^2 X_0}{2g} = 0.0668$$

Thus the acceleration of the mass due to the damping force would be 0.0668 g.

3.4.2.3 Index of Attenuation

The second basis selected for comparison is the peak force required to attenuate the residual oscillations by an amount $X_0(1 - \alpha)$ in a time t_1 . For the viscous system with small damping ratios; i.e., $\zeta < 0.20$,

$$F_{dv} \approx \frac{2m\omega X_0 \ln\left(\frac{1}{\alpha}\right)}{t_1}$$

For the coulomb damped system

$$F_{dc} = \frac{\pi m \omega X_0 (1 - \alpha)}{2t_1}$$

then

$$\frac{F_{dc}}{F_{dv}} = \frac{\pi}{4} = \left[\frac{1 - \alpha}{\ln \frac{1}{\alpha}} \right]$$

Since the ratio $\left[\frac{1 - \alpha}{\ln \frac{1}{\alpha}} \right]$ is less than unity for all values of α less than 1.0, the peak damping force required to produce the same attenuation in a coulomb damped system is always less than that needed in a viscous system. A similar comparison will show that the peak damping force of the quadratic system will be higher than that of the viscous system for the same attenuation.

Using the system dimensions of the previous example and letting $\alpha = 0.10$, $t_1 = 30$ seconds we obtain

$$\frac{F_{dc}}{W} = \frac{\pi \omega X_0 (1 - \alpha)}{2t_1 g} = 0.00912$$

The acceleration due to the damping force needed to attenuate the system to 10 percent amplitude in 30 seconds then is small. Thus, if the system is to incorporate 10 per cent equivalent viscous damping in order to provide the insensitivity specified, the time to damp free oscillations to 0.1 of their peak oscillation will be much less than 30 seconds.

3.4.2.4 Index of Terminal Excursion

It is desirable for the system to return near to its initial position at the cessation of motion. The difference between the initial and terminal positions is called here, the index of terminal excursion. For all types of damping forces which are functions only of motion, the terminal excursion, of course, is zero. For the coulomb damping case, however, the final position of the system is dependent on the details of the system and the input, but it will fall between limits which may be defined:

$$\delta_{max} = \pm \frac{F_{dc}}{k}$$

In terms of the equivalent viscous damping ratio

$$\delta_{\max} = \pm \frac{\pi \zeta_e X_o}{2}$$

Substituting values from the previous examples,

$$\delta_{\max} = \pm 0.445 \text{ ft.}$$

For an equivalent viscous damping ratio of 0.10, then, the friction band for the coulomb damped system will be about one foot.

3.4.2.5 Transient Forces

The peak damping forces which have been considered in the previous paragraphs are the maxima which occur during the residual oscillations of the mass; i.e., after the shock motion has ceased. During the transient period of the oscillation, however, large relative velocities and accelerations can occur and damping devices which generate forces as functions of these motion parameters may produce forces during this period which greatly exceed the forces occurring later during the free oscillation.

For example, consider a viscously damped system of the dimensions used earlier; i.e., with a damping ratio of 0.10. The peak acceleration in g's due to the damping force occurring during steady state oscillations is

$$\frac{F_{dv}}{W} = \frac{0.0668}{0.785} = 0.0851 \text{ g's}$$

During the transient phase, however, the peak ground velocity is given in Section 2.0 as 38 feet per second. If the motion of the mass at this instant is small, the peak acceleration introduced into the mass by the damper at the moment of peak ground velocity is

$$\frac{F_{dv}}{W} = \frac{2\zeta \omega X_t}{g} = 0.519 \text{ g}$$

It is evident that it is undesirable to transfer accelerations of this magnitude to the load even though in the viscous case they occur out-of-phase with the peak accelerations occurring during residual oscillations.

For a quadratic-damped system of the same equivalent viscous damping ratio, the transient acceleration is much higher. Thus,

$$\frac{F_{dQ}}{W} = \frac{3\pi \zeta_e \dot{x}^2}{4X_0 g} = 3.73 g$$

The maximum force that can be transferred to the mass during the transient phase by a coulomb damper, of course, is (F_{dc}/W) , which was calculated previously for the conditions of the example as 0.0668 g.

3.4.2.6 Summary of Coulomb and Velocity Damping

From the above discussion, it is evident that neither coulomb nor velocity damping, incorporated in a system rigidly connected to the shock source, meets all of the requirements established as desirable in this application. While use of the coulomb-damped system results in lower forces transmitted to the mass and in rapid attenuations, it does not permit the system to return sufficiently near to its initial position. On the other hand velocity-damped systems which have a terminal excursion of zero, transmit very high accelerations if the transient ground velocities are high. This latter point is of particular significance when it is noted that in practical systems, few damping mechanisms give a damping force linearly proportional to velocity, but that their characteristic is much closer to the quadratic case.

If the isolator is not rigidly attached to the ground and the mass, but is in turn supported by a flexible element such as a cable which will not take a compressive load, and if the transient ground acceleration is in the downward direction, a high transient damping force cannot be transmitted through the isolator to the mass. In this case, however, a high velocity damping characteristic in the isolator will reduce the response of the isolator possibly below that of the input and tend to cause the flexible element to slacken. High accelerations are introduced into the system, then, as the cable again becomes taut. This problem is discussed more fully in Section 4.0.

3.4.2.7 Other Damping Systems

In exploring other damping systems whose characteristics might approach our requirements more closely, we start basically with a velocity-type damping function since we wish the system always to return to its initial position. Our principal objective is to reduce the effect of the transfer of high transient accelerations from the ground.

Consider, for example, the visco-elastic system shown in Figure 3-8. Here a spring of stiffness Nk has been inserted between the viscous damper and the supporting structure. For residual oscillations where the damping forces are small, the system behaves essentially like the simpler viscously-damped system discussed earlier. At large values of \dot{z} , however, the deflections of spring Nk increase, mitigating the transient damping force transferred to the mass, m .

In Figure 3-9, the system has been altered by replacing the linear spring k with a nonlinear one, changing the damping force F_D to the more general expression $c(\dot{x} - \dot{y})^n$ and adding coulomb friction. This type of system is essentially the mechanical analog of those compressible fluid-filled devices in which damping is obtained by the viscous flow of the fluid. Such devices include both liquid and pneumatic springs.

The differential equations of motion for this system are of the third order, and the presence of the nonlinear elements precludes their solution in closed form. However, something of the system behavior can be noted by inspection of the system shown in Figure 3-10 and the analog shown in Figure 3-9. The nonlinear spring provides the basic static force-displacement relationship for the fluid stored in the cylinder and tank, while the combination of the spring k_2 in series with the damper is representative of the effect of the rate of flow of fluid through the throttling device. The coulomb friction is no longer the principle source of energy dissipation and has been included in Figure 3-9 only because some friction is inherent in all these devices.

Since by careful mechanical design the coulomb friction can be made small, the system will always return very near to its initial position. The spring k_2 -damper combination can be sized to provide the needed residual damping; their relative proportions will govern the peak transient damping force. It is still desirable, of course, to keep n , the exponent of velocity in the damping term as close to unity as possible. Several methods for controlling to some extent the value of n are described in Section 4, as are the limits of obtaining desired performance characteristics with given load, frequency, damping, and stroke requirements, using a given fluid.

An isolator employing damping in this manner, then, is considered to be most promising for use in facilities of this type.

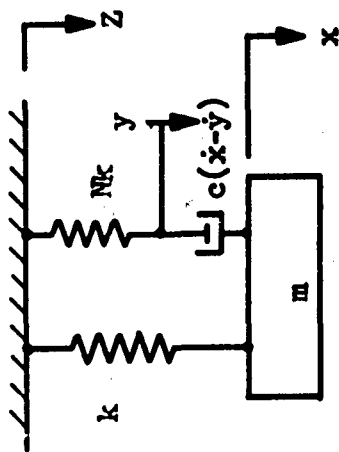


Figure 3-8. Visco-Elastic System.

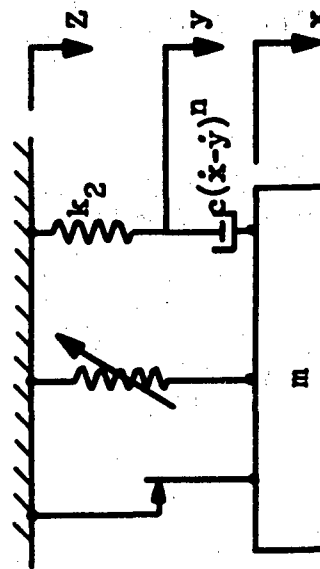


Figure 3-9. Mechanical Analog of Viscous-Fluid Filled System.

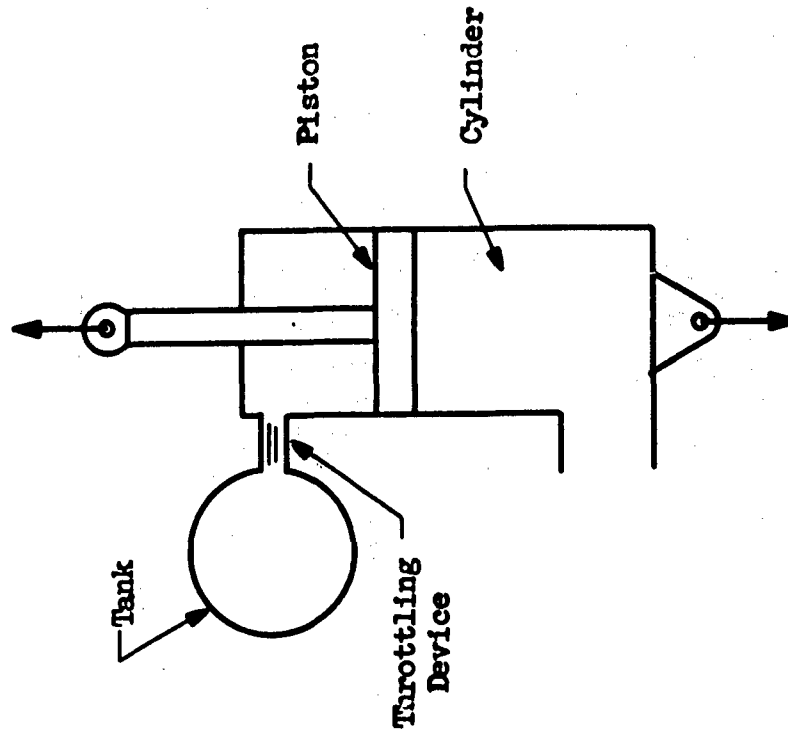


Figure 3-10. Schematic of Liquid or Pneumatic Spring With Energy Dissipation.

3.4.3 Damping in Inclined Isolators

If the vertical and horizontal isolators are essentially independent, as in Suspension System Configuration 1, then individual damping characteristics can be selected to satisfy the damping requirements listed earlier in this section. If only a single set of isolators is used, however, and the isolators are installed in the inclined pendulum arms as in Configurations 2 and 3, they must provide the damping both in the vertical and the horizontal directions. Thus, additional constraints are imposed on the damping attainable in the two directions which are functions of the dynamic characteristics of the body, the angle of inclination of the pendulum arms and the pendulum attachment points.

The following simplified analysis has been made to provide an indication of the damping ratios which can be obtained horizontally for a given vertical damping ratio. As in the evaluation of types of suspension systems presented earlier, the springs are assumed to be linear and, in addition, an equivalent viscous damping coefficient has been employed. The calculated ratios, then are indicative of sensitivity to input shock characteristics, but not necessarily of attenuation or response to transient motions of the capsule.

This analysis is intended to serve only as a guideline in selecting damping characteristics for final evaluation in the rigid body analysis of Section 5.0..

Referring to Paragraph 5A-7, it is shown that the damping force can be represented as

$$[F]_n^D = [\bar{C}]_n^D [\dot{\delta}]_n$$

where $[\bar{C}]_n^D$ = Damping stiffness matrix having elements representing force/unit velocity

$[\dot{\delta}]_n$ = Velocity matrix having elements representing rate of change of displacement

Neglecting effect of rotation on stiffness matrix, we get

$$[F]_H^D = [D]_{pn} [K]_N^D \left\{ [\dot{S}]_{pn} + [D]_{pn}^{-1} [-r_a] [\dot{\phi}] \right\}$$

For a two-dimensional figure, this can be written as

$$\begin{aligned}
 \begin{bmatrix} F_H^D \\ F_V^D \end{bmatrix}_n &= \begin{bmatrix} \cos \phi_n & \sin \phi_n \\ -\sin \phi_n & \cos \phi_n \end{bmatrix} \begin{bmatrix} 0 & 0 \\ 0 & K_n^D \end{bmatrix} \left\{ \begin{bmatrix} l_n \dot{\phi}_n \\ \dot{l}_n \end{bmatrix} \right. \\
 &+ \left. \begin{bmatrix} \cos \phi_n & -\sin \phi_n \\ \sin \phi_n & \cos \phi_n \end{bmatrix} \begin{bmatrix} r_3 \dot{\beta} \\ -r_1 \dot{\beta} \end{bmatrix} \right\} \\
 &= \begin{bmatrix} 0 & K_n^D \sin \phi_n \\ 0 & K_n^D \cos \phi_n \end{bmatrix} \left\{ \begin{bmatrix} l_n \dot{\phi}_n \\ \dot{l}_n \end{bmatrix} + \dot{\beta} \begin{bmatrix} r_3 \cos \phi_n + r_1 \sin \phi_n \\ r_3 \sin \phi_n - r_1 \cos \phi_n \end{bmatrix} \right\} \\
 &= K_n^D \left\{ \begin{bmatrix} \dot{l}_n \sin \phi_n \\ \dot{l}_n \cos \phi_n \end{bmatrix} + \dot{\beta} \begin{bmatrix} \sin \phi_n (r_3 \sin \phi_n - r_1 \cos \phi_n) \\ \cos \phi_n (r_3 \sin \phi_n - r_1 \cos \phi_n) \end{bmatrix} \right\}
 \end{aligned}$$

Therefore, horizontal damping force for the system

$$F_H^D = K_n^D \left\{ \dot{l}_n \sin \phi_n + \dot{\beta} \sin \phi_n (r_3 \sin \phi_n - r_1 \cos \phi_n) \right\}$$

Referring to Paragraph 3.A.2,

$$\begin{aligned}
 \sin \phi_n &\approx \sin \phi_{ns} + \cos \phi_{ns} \cdot \frac{l}{l_n} \phi \\
 \cos \phi_n &\approx \cos \phi_{ns} - \sin \phi_{ns} \cdot \frac{l}{l_n} \phi \\
 \therefore \sin^2 \phi_n &= \sin^2 \phi_{ns} + \cos^2 \phi_{ns} \left(\frac{l}{l_n} \phi \right)^2 + 2 \sin \phi_{ns} \cos \phi_{ns} \cdot \frac{l}{l_n} \phi \\
 \sin \phi_n \cdot \cos \phi_n &= \sin \phi_{ns} \cdot \cos \phi_{ns} \left\{ 1 - \left(\frac{l}{l_n} \phi \right)^2 \right\} - \sin^2 \phi_{ns} \cdot \frac{l}{l_n} \phi \\
 &\quad + \cos^2 \phi_{ns} \cdot \frac{l}{l_n} \phi
 \end{aligned}$$

Substituting the above values in the expression for F_H^D , we obtain

$$F_H^D = K_n^D \left\{ l_n \left(\sin \phi_{ns} + \cos \phi_{ns} \cdot \frac{l}{l_n} \cdot \phi \right) + \dot{\beta} r_3 \left[\sin^2 \phi_{ns} + \cos^2 \phi_{ns} \left(\frac{l}{l_n} \phi \right)^2 + 2 \sin \phi_{ns} \cdot \cos \phi_{ns} \cdot \frac{l}{l_n} \phi \right] - \dot{\beta} r_1 \left[\sin \phi_{ns} \cdot \cos \phi_{ns} \left(1 - \frac{l^2 \phi^2}{l_n^2} \right) - \sin^2 \phi_{ns} \cdot \frac{l}{l_n} \phi + \cos^2 \phi_{ns} \frac{l}{l_n} \phi \right] \right\}$$

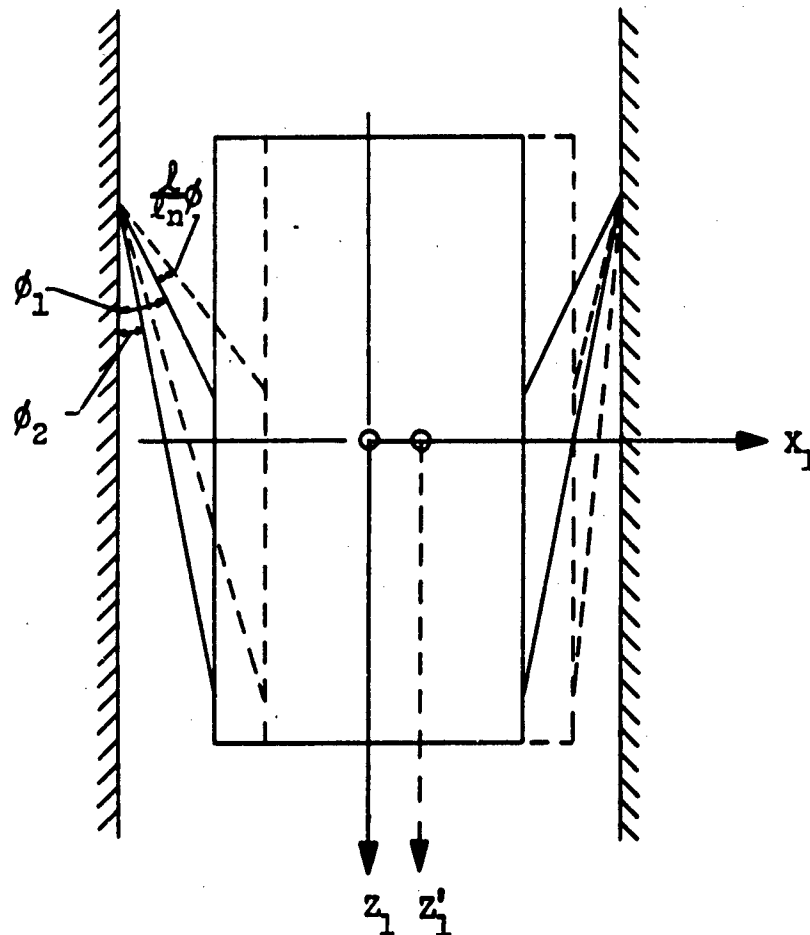


Figure 3-11. Change in Length of Isolators for Lateral Displacement

Referring to Figure 3-11, for isolators on left side

$$\begin{aligned}
 l_n &= \frac{l_s + r_3}{\cos \left(\phi_n + \frac{l}{l_n} \phi \right)} \\
 \therefore \frac{d}{dt} (l_n) &= \frac{d}{d\phi} \left\{ \frac{l_s + r_3}{\cos \left(\phi_n + \frac{l}{l_n} \phi \right)} \right\} \cdot \frac{d\phi}{dt} \\
 &= \frac{\tan \left(\phi_n + \frac{l\phi}{l_s + r_3} \right)}{\cos \left(\phi_n + \frac{l\phi}{l_s + r_3} \right)} \cdot (l_s + r_3) \cdot \frac{l}{l_s + r_3} \cdot \dot{\phi} \\
 &\approx \left(\phi_n + \frac{l\phi}{l_s + r_3} \right) l \dot{\phi}, \quad \text{for small angles} \\
 &\approx l_s \phi_n \dot{\phi} \quad \text{when } \frac{l\phi}{l_s + r_3} \ll \phi_n \text{ and } l \approx l_s
 \end{aligned}$$

For isolators on right side

$$\begin{aligned}
 l_n &= \frac{l_s + r_3}{\cos \left(\phi_n - \frac{l}{l_n} \phi \right)} \\
 \therefore \frac{d}{dt} (l_n) &= - \left(\phi_n - \frac{l\phi}{l_s + r_3} \right) l_s \dot{\phi} \\
 &= - l_s \phi_n \dot{\phi} \\
 \therefore -(\dot{l}_n)_L &= (\dot{l}_n)_R
 \end{aligned}$$

where subscripts refer to left and right sides. Therefore,

$$\begin{aligned}
F_H^D = & 2K_1^D \left\{ \dot{l}_1 \sin \phi_1 - \dot{\beta} a_1 \left[\sin^2 \phi_1 + \cos^2 \phi_1 \left(\frac{l}{l_n} \phi \right)^2 \right] \right. \\
& + \dot{\beta} r \left[\sin \phi_1 \cos \phi_1 \left(1 - \frac{l^2 \phi^2}{l_n^2} \right) \right] \left. \right\} \\
& + 2K_2^D \left\{ \dot{l}_2 \sin \phi_2 + \dot{\beta} a_2 \left[\sin^2 \phi_2 + \cos^2 \phi_2 \left(\frac{l}{l_n} \phi \right)^2 \right] \right. \\
& + \dot{\beta} r \left[\sin \phi_2 \cos \phi_2 \left(1 - \frac{l^2 \phi^2}{l_n^2} \right) \right] \left. \right\}
\end{aligned}$$

Neglecting $\frac{l^2 \phi^2}{l_n^2}$, and for small angles, we obtain

$$\begin{aligned}
F_H^D = & 2K_1^D \left\{ l_s \phi_1^2 \dot{\phi} + \dot{\beta} \phi_1 (-a_1 \phi_1 + r) \right\} \\
& + 2K_2^D \left\{ l_s \phi_2^2 \dot{\phi} + \dot{\beta} \phi_2 (a_2 \phi_2 + r) \right\} \\
= & 2K_1^D \phi_1 \left\{ l_s \phi_1 \dot{\phi} + \dot{\beta} (r - a_1 \phi_1) \right\} \\
& + 2K_2^D \phi_2 \left\{ l_s \phi_2 \dot{\phi} + \dot{\beta} (r + a_2 \phi_2) \right\}
\end{aligned}$$

Substituting the following numerical values:

$$\begin{aligned}
l_s &= 840 \text{ inches} \\
\phi_1 &= 0.155 \text{ radians} \\
\phi_2 &= 0.072 \text{ radians} \\
r &= 450 \text{ inches} \\
a_1 &= 120 \text{ inches} \\
a_2 &= 720 \text{ inches} \\
K_1^D &= 2K_2^D \text{ pounds per inch}
\end{aligned}$$

$$\begin{aligned} F_H^D &= 2K_1^D (0.155) \{ (840)(0.155)\dot{\phi} + \dot{\beta} [450 - (120)(0.155)] \} \\ &\quad + K_1^D (0.072) \{ (840)(0.072)\dot{\phi} + \dot{\beta} [450 + (720)(0.072)] \} \\ &= K_1^D (44.7\dot{\phi} + 170.2\dot{\beta}) \end{aligned}$$

The vertical natural frequency $\omega_v = 0.35$ cycle per second
 $= 2.19$ radians/second

$$\begin{aligned} \omega_v^2 &= \frac{K}{m} \\ \therefore 2(K_1 + K_2) &= m\omega_v^2 \quad \text{where } K = 2(K_1 + K_2) \\ &= 4.8 \text{ m} \\ \therefore 3K_1 &= 4.8 \text{ m} \quad \text{where } 2K_2 = K_1 \\ \therefore K_1 &= 1.6 \text{ m} \quad \text{and } K_2 = 0.8 \text{ m} \end{aligned}$$

Horizontal component of the stiffness

$$\begin{aligned} K_H &= 2 (K_1 \sin^2 \phi_1 + K_2 \sin^2 \phi_2) \\ &= 2 \{ 1.6 \text{ m } (0.155)^2 + 0.8 \text{ m } (0.072)^2 \} \\ &= 0.0851 \text{ m} \end{aligned}$$

$$\text{Now } \omega_H = \sqrt{\frac{K_H}{m} + \frac{g}{l_s}} = \sqrt{0.0851 + \frac{386}{840}} = 0.74 \text{ radians/second}$$

For steady state vibrations, let

$$\begin{aligned} \phi &= \phi_m \sin \omega_H t \\ \dot{\phi} &= \omega_H \phi_m \cos \omega_H t \end{aligned}$$

From the shock spectrum (Figure 2-4), the maximum horizontal displacement of the center of gravity is 24 inches.

$$\therefore \phi_m = \frac{24}{840} = 0.0286 \text{ radians}$$

Assuming the magnitude of maximum rotation β_m is the same as ϕ_m , that is

$$\dot{\phi} \cong \dot{\beta}$$

For vertical motion, damping ratio

$$\begin{aligned}\xi_v &= \frac{2(K_1^D + K_2^D) \dot{l}}{2 \omega_v m \dot{l}} \\ &= \frac{3K_1^D}{2 \omega_v m}\end{aligned}$$

$$K_1^D = \frac{2}{3} \xi \omega_v m$$

For horizontal motion, damping ratio

$$\xi_H = \frac{K_1^D (44.7 \dot{\phi} + 170.2 \dot{\beta})}{2 \omega_H m \cdot l_s \dot{\phi}}$$

Substituting the values of K_1^D and $\dot{\beta}$, we obtain

$$\begin{aligned}\xi_H &= \frac{2}{3} \xi_v \cdot \omega_v m \cdot \frac{(44.7 \dot{\phi} + 170.2 \dot{\phi})}{2 \omega_H m \cdot l_s \cdot \dot{\phi}} \\ &= \frac{70.16}{840} \frac{\omega_v}{\omega_H} \cdot \xi_v \\ &= 0.085 \frac{\omega_v}{\omega_H} \cdot \xi_v \\ \frac{\xi_H}{\xi_v} &= 0.085 \frac{\omega_v}{\omega_H} \\ &= 0.085 \times \frac{2.19}{0.74} \\ &= 0.25\end{aligned}$$

SECTION 3 APPENDIX3A DERIVATION OF EQUATIONS OF MOTION FOR THREE-DEGREES-OF-FREEDOM
PENDULUM SUSPENSION SYSTEM3A-1 Reduction of Equations of Motion from Six Degrees of Freedom
to Three Degrees of Freedom

The equations of motion in full for a six-degree-of-freedom system are shown in Paragraph 5.3. These are reduced here to describe the three-degree-of-freedom system by setting θ , θ_n , r_2 , α , γ equal to zero. In order to reduce the complexity, the damping and the effect of rotation of the body about its center of gravity on the stiffnesses are not included.

The equations become:

$$\begin{aligned}
 & \begin{bmatrix} \cos \phi & 0 & \sin \phi \\ 0 & 0 & 0 \\ -\sin \phi & 0 & \cos \phi \end{bmatrix} \begin{bmatrix} 2m\ddot{\phi} + m\dot{\phi}^2 \\ 0 \\ m\ddot{l} - m\dot{\phi}^2 \end{bmatrix} \\
 & + \sum \left\{ \begin{bmatrix} \cos \phi_n & 0 & \sin \phi_n \\ 0 & 0 & 0 \\ -\sin \phi_n & 0 & \cos \phi_n \end{bmatrix} \begin{bmatrix} 0 & 0 & 0 \\ 0 & 0 & 0 \\ 0 & 0 & K_n \end{bmatrix} \begin{bmatrix} 0 \\ 0 \\ l_n - l_{no} \end{bmatrix} + \begin{bmatrix} \cos \phi_n & 0 & -\sin \phi_n \\ 0 & 0 & 0 \\ \sin \phi_n & 0 & \cos \phi_n \end{bmatrix} \begin{bmatrix} 0 & r_3 & 0 \\ r_3 & 0 & r_1 \\ 0 & -r_1 & 0 \end{bmatrix} \begin{bmatrix} 0 \\ \beta \\ 0 \end{bmatrix} \right\} \\
 & + \begin{bmatrix} m \ddot{X}_o \\ 0 \\ m \ddot{Z}_o - mg \end{bmatrix} = 0
 \end{aligned}
 \tag{Eq. 3A-1}$$

and

$$\begin{aligned}
 & \begin{bmatrix} 0 \\ I \ddot{\beta} \\ 0 \end{bmatrix} + \sum \left\{ \begin{bmatrix} 0 & -r_3 & 0 \\ r_3 & 0 & -r_1 \\ 0 & r_1 & 0 \end{bmatrix}_n \begin{bmatrix} \cos \phi_n & 0 & \sin \phi_n \\ 0 & 0 & 0 \\ -\sin \phi_n & 0 & \cos \phi_n \end{bmatrix} \begin{bmatrix} 0 & 0 & 0 \\ 0 & 0 & 0 \\ 0 & 0 & K_n \end{bmatrix} \right\} x \\
 & \left\{ \begin{bmatrix} 0 \\ 0 \\ l_n - l_{no} \end{bmatrix} \begin{bmatrix} \cos \phi_n & 0 & -\sin \phi_n \\ 0 & 0 & 0 \\ \sin \phi_n & 0 & \cos \phi_n \end{bmatrix} \begin{bmatrix} 0 & r_3 & 0 \\ -r_3 & 0 & r_1 \\ 0 & -r_1 & 0 \end{bmatrix} \begin{bmatrix} 0 \\ \beta \\ 0 \end{bmatrix} \right\} = 0
 \end{aligned}
 \tag{Eq. 3A-2}$$

Now

$$\begin{bmatrix} \cos \phi_n & 0 & \sin \phi_n \\ 0 & 0 & 0 \\ -\sin \phi_n & 0 & \cos \phi_n \end{bmatrix} \begin{bmatrix} 0 & 0 & 0 \\ 0 & 0 & 0 \\ 0 & 0 & K_n \end{bmatrix} \begin{bmatrix} \cos \phi_n & 0 & -\sin \phi_n \\ 0 & 0 & 0 \\ \sin \phi_n & 0 & \cos \phi_n \end{bmatrix} \begin{bmatrix} 0 & r_3 & 0 \\ -r_3 & 0 & r_1 \\ 0 & -r_1 & 0 \end{bmatrix} \begin{bmatrix} 0 \\ \beta \\ 0 \end{bmatrix}$$

$$= \begin{bmatrix} \beta K_n \sin \phi_n (r_3 \sin \phi_n - r_1 \cos \phi_n) \\ 0 \\ \beta K_n \cos \phi_n (r_3 \sin \phi_n - r_1 \cos \phi_n) \end{bmatrix}$$

The equations become

$$\begin{aligned} & (2m\ddot{\phi} + m\dot{\phi}^2) \cos \phi + (m\ddot{l} - m\dot{\phi}^2) \sin \phi \\ & + \sum \left\{ K_n \sin \phi_n (\dot{l}_n - \dot{l}_{no}) \right\} + \beta \sum \left\{ K_n \sin \phi_n (r_3 \sin \phi_n - r_1 \cos \phi_n) \right\} + (m\ddot{x}_o) = 0 \end{aligned}$$

(Eq. 3A-3)

$$\begin{aligned} & (m\ddot{l} - m\dot{\phi}^2) \cos \phi - (2m\ddot{\phi} + m\dot{\phi}^2) \sin \phi \\ & + \sum \left\{ K_n \cos \phi_n (\dot{l}_n - \dot{l}_{no}) \right\} + \beta \sum \left\{ K_n \cos \phi_n (r_3 \sin \phi_n - r_1 \cos \phi_n) \right\} + (m\ddot{z}_o - mg) = 0 \end{aligned}$$

(Eq. 3A-4)

$$\begin{aligned} & I\ddot{\beta} + \sum \left\{ (r_3)_n K_n \left[\sin \phi_n (\dot{l}_n - \dot{l}_{no}) + \beta \sin \phi_n (r_3 \sin \phi_n - r_1 \cos \phi_n) \right] \right. \\ & \left. - (r_1)_n K_n \left[\cos \phi_n (\dot{l}_n - \dot{l}_{no}) + \beta \cos \phi_n (r_3 \sin \phi_n - r_1 \cos \phi_n) \right] \right\} = 0 \end{aligned}$$

(Eq. 3A-5)

Multiplying Eq. 3A-3 by $\sin \phi$ and Eq. 3A-4 by $\cos \phi$ and adding, we get

$$\begin{aligned} & (m\ddot{l} - m\dot{\phi}^2) + \sum \left\{ K_n (\dot{l}_n - \dot{l}_{no}) [\sin \phi \cdot \sin \phi_n + \cos \phi \cdot \cos \phi_n] \right\} \\ & + \beta \sum \left\{ K_n (r_3 \sin \phi_n - r_1 \cos \phi_n) [\sin \phi \cdot \sin \phi_n + \cos \phi \cdot \cos \phi_n] \right\} \\ & + (m\ddot{x}_o) \sin \phi + (m\ddot{z}_o - mg) \cos \phi = 0 \end{aligned}$$

(Eq. 3A-6)

Neglecting centrifugal acceleration, $m\dot{\phi}^2$, with respect to longitudinal acceleration $m\ddot{l}$, Eq. 3A-6 becomes

$$\begin{aligned} m\ddot{l} + \sum \{ K_n \cos(\phi_n - \phi) [(\ell_n - \ell_{no}) + \beta(r_3 \sin\phi_n - r_1 \cos\phi_n)] \} \\ + (m\ddot{X}_0) \sin\phi + (m\ddot{Z}_0 - mg) \cos\phi = 0 \end{aligned} \quad (\text{Eq. 3A-7})$$

Multiplying Eq. 3A-3 by $\cos\phi$ and Eq. 3A-4 by $\sin\phi$ and subtracting the latter from the former, we get

$$\begin{aligned} (2m\dot{\phi} + m\ddot{\phi}) + \sum \{ K_n (\ell_n - \ell_{no}) [\cos\phi \sin\phi_n - \sin\phi \cos\phi_n] \} \\ + \beta \sum \{ K_n (r_3 \sin\phi_n - r_1 \cos\phi_n) [\cos\phi \sin\phi_n - \sin\phi \cos\phi_n] \} \\ + (m\ddot{X}_0) \cos\phi - (m\ddot{Z}_0 - mg) \sin\phi = 0 \end{aligned} \quad (\text{Eq. 3A-8})$$

Neglecting Coriolis' acceleration $2m\dot{\phi}$, with respect to tangential acceleration $m\ddot{\phi}$, Eq. 3A-8 becomes

$$\begin{aligned} m\ddot{\phi} + \sum \{ K_n \sin(\phi_n - \phi) [(\ell_n - \ell_{no}) + \beta(r_3 \sin\phi_n - r_1 \cos\phi_n)] \} \\ + (m\ddot{X}_0) \cos\phi - (m\ddot{Z}_0 - mg) \sin\phi = 0 \end{aligned} \quad (\text{Eq. 3A-9})$$

Equation 3A-5 becomes

$$\begin{aligned} I\ddot{\phi} + \sum \{ K_n (\ell_n - \ell_{no}) (r_3 \sin\phi_n - r_1 \cos\phi_n) + K_n \beta (r_3 \sin\phi_n - r_1 \cos\phi_n)^2 \} \\ \therefore I\ddot{\phi} + \sum \{ K_n (r_3 \sin\phi_n - r_1 \cos\phi_n) [(\ell_n - \ell_{no}) + \beta(r_3 \sin\phi_n - r_1 \cos\phi_n)] \} = 0 \end{aligned} \quad (\text{Eq. 3A-10})$$

For ℓ_n and ϕ_n of the n^{th} isolator, the following conditions are to be satisfied:

$$\ell_n \sin \phi_n = \ell \sin \phi + \ell_{ns} \sin \phi_{ns} \quad (\text{Eq. 3A-11a})$$

$$\ell_n \cos \phi_{ns} = \ell \cos \phi - \ell_s + \ell_{ns} \cos \phi_{ns} \quad (\text{Eq. 3A-11b})$$

3A-2 General Equations of Motion for Three Configurations

The general equations of motion are derived for Configurations 1 through 3 (Figures 3-1 a, b, and c). The following assumptions are made for simplicity:

(1) Pendulum angle ϕ is small

$$\sin \phi \approx \phi$$

(2) $\frac{l_{ns}}{l_n} \approx 1$

(3) Second order nonlinear coupling terms (e.g., ϕ^2 , $\beta\phi$, etc.) are neglected.

(4) The body is assumed to be symmetrically suspended
 $\therefore \phi_{ns}$ and r are equal and opposite in sign.

From Eq. 3A-11a and b

For inclined isolators

$$l_n \phi_n = l\phi + l_{ns} \phi_{ns} \quad (\text{Eq. 3A-12a})$$

$$\text{and } l_n = l + l_{ns} - l_s \quad (\text{Eq. 3A-12b})$$

$$\phi_n = \frac{l}{l_n} \phi + \frac{l_{ns}}{l_n} \phi_{ns} = \frac{l}{l_n} \phi + \phi_{ns} \quad (\text{Eq. 3A-13})$$

$$\text{and } l_n = l + l_{no} + \delta_{ns} - l_s, \text{ as } l_{ns} = l_{no} + \delta_{ns}$$

$$\begin{aligned} \therefore (l_n - l_{no}) &= (l - l_s) + \delta_{ns} \\ &= \rho + \delta_{ns} \text{ where } \rho = l - l_s \end{aligned} \quad (\text{Eq. 3A-14})$$

For horizontal isolators, which are assumed to remain horizontal during dynamic motion, Eq. 3A-11 a and b give

$$\phi_n = \phi_{ns}$$

$$l \sin \phi = (l_n - l_{ns}) \sin \phi_{ns}$$

as the horizontal isolators do not carry vertical load

$$\delta_{ns} = 0, \quad l_{ns} = l_{no}$$

$$l \sin \phi = (l_n - l_{no}) \sin \phi_{ns} = (l_n - l_{no})$$

$$\text{as } \phi_{ns} = \frac{\pi}{2} \quad (\text{Eq. 3A-15})$$

Eq. 3A-7, 3A-9 and 3A-10 can be written as follows:

$$m\ddot{z} + F_z + (m\ddot{x}_o) \sin \phi + (m\ddot{z}_o - mg) \cos \phi = 0 \quad (\text{Eq. 3A-16a})$$

$$m\ddot{\phi} + F_\phi + (m\ddot{x}_o) \cos \phi - (m\ddot{z}_o - mg) \sin \phi = 0 \quad (\text{Eq. 3A-16b})$$

$$I\ddot{\beta} + M_\beta = 0 \quad (\text{Eq. 3A-16c})$$

where

$$F_\ell = \sum \{ K_n \cos(\phi_n - \phi) [(\ell_n - \ell_{no}) + \beta(r_3 \sin \phi_n - r_1 \cos \phi_n)] \} \quad (\text{Eq. 3A-17a})$$

$$F_\phi = \sum \{ K_n \sin(\phi_n - \phi) [(\ell_n - \ell_{no}) + \beta(r_3 \sin \phi_n - r_1 \cos \phi_n)] \} \quad (\text{Eq. 3A-17b})$$

$$M_\beta = \sum \{ K_n (r_3 \sin \phi_n - r_1 \cos \phi_n) [(\ell_n - \ell_{no}) + \beta(r_3 \sin \phi_n - r_1 \cos \phi_n)] \} \quad (\text{Eq. 3A-17c})$$

The terms F_ℓ , F_ϕ , and M_β can be broken down into the horizontal and inclined categories of the isolators.

$$F_\ell = F_\ell(H) + F_\ell(I)$$

$$F_\phi = F_\phi(H) + F_\phi(I)$$

$$M_\beta = M_\beta(H) + M_\beta(I)$$

The following suboperations are performed to reduce the expressions in Eq. 3A-17:

$$\begin{aligned} \cos \phi_n &\cong \cos\left(\frac{\ell}{\ell_n} \phi + \phi_{ns}\right) \\ &\cong \cos \frac{\ell}{\ell_n} \phi \cdot \cos \phi_{ns} - \sin \frac{\ell}{\ell_n} \phi \cdot \sin \phi_{ns} \\ &\cong \cos \phi_{ns} - \frac{\ell}{\ell_n} \phi \cdot \sin \phi_{ns} \end{aligned} \quad (\text{Eq. 3A-18a})$$

$$\begin{aligned} \sin \phi_n &= \sin\left(\frac{\ell}{\ell_n} \phi + \phi_{ns}\right) \\ &= \sin \frac{\ell}{\ell_n} \phi \cdot \cos \phi_{ns} + \cos \frac{\ell}{\ell_n} \phi \cdot \sin \phi_{ns} \\ &= \frac{\ell}{\ell_n} \phi \cdot \cos \phi_{ns} + \sin \phi_{ns} \end{aligned} \quad (\text{Eq. 3A-18b})$$

$$\begin{aligned}
 \cos(\phi_n - \phi) &\cong \cos\left[\phi_{ns} + \phi\left(\frac{\ell}{\ell_n} - 1\right)\right] \\
 &\cong \cos \phi_{ns} \cdot \cos \phi\left(\frac{\ell}{\ell_n} - 1\right) - \sin \phi_{ns} \cdot \sin \phi\left(\frac{\ell}{\ell_n} - 1\right) \\
 &\cong \cos \phi_{ns} - \phi\left(\frac{\ell}{\ell_n} - 1\right) \cdot \sin \phi_{ns} \quad (\text{Eq. 3A-18c})
 \end{aligned}$$

$$\begin{aligned}
 \sin(\phi_n - \phi) &\cong \sin\left[\phi_{ns} + \phi\left(\frac{\ell}{\ell_n} - 1\right)\right] \\
 &\cong \sin \phi_{ns} \cdot \cos \phi\left(\frac{\ell}{\ell_n} - 1\right) + \cos \phi_{ns} \cdot \sin \phi\left(\frac{\ell}{\ell_n} - 1\right) \\
 &\cong \sin \phi_{ns} + \phi\left(\frac{\ell}{\ell_n} - 1\right) \cdot \cos \phi_{ns} \quad (\text{Eq. 3A-18d})
 \end{aligned}$$

$$\beta \cos(\phi_n - \phi) \cdot \cos \phi_n \cong \beta \cos^2 \phi_{ns} \quad (\text{Eq. 3A-18e})$$

$$\beta \cos(\phi_n - \phi) \cdot \sin \phi_n \cong \beta \sin \phi_{ns} \cdot \cos \phi_{ns} \quad (\text{Eq. 3A-18f})$$

$$\beta \sin(\phi_n - \phi) \cdot \cos \phi_n \cong \beta \sin \phi_{ns} \cdot \cos \phi_{ns} \quad (\text{Eq. 3A-18g})$$

$$\beta \sin(\phi_n - \phi) \cdot \sin \phi_n \cong \beta \sin^2 \phi_{ns} \quad (\text{Eq. 3A-18h})$$

Therefore

$$\begin{aligned}
 F_\ell &= F_\ell(H) + F_\ell(I) \\
 &= \sum_H \left\{ K_n \cos(\phi_n - \phi) \left[(\ell_n - \ell_{no}) + \beta(r_3 \sin \phi_n - r_1 \cos \phi_n) \right] \right\} \\
 &+ \sum_I \left\{ K_n \cos(\phi_n - \phi) \left[(\ell_n - \ell_{no}) + \beta(r_3 \sin \phi_n - r_1 \cos \phi_n) \right] \right\} \\
 &= \sum_H \left\{ -K_n \phi\left(\frac{\ell}{\ell_n} - 1\right) \left[\ell\phi + \beta(r_3 \sin \phi_n - r_1 \cos \phi_n) \right] \right\} \\
 &+ \sum_I K_n \left\{ \left[\cos \phi_{ns} - \phi\left(\frac{\ell}{\ell_n} - 1\right) \sin \phi_{ns} \right] \left[(\ell - \ell_s) + \delta_{ns} \right] + \beta \left[r_3 \sin \phi_{ns} \cos \phi_{ns} \right. \right. \\
 &\quad \left. \left. - r_1 \cos^2 \phi_{ns} \right] \right\} \\
 &= \sum_I K_n \left\{ (\rho + \delta_{ns}) \cos \phi_{ns} \right\} \\
 &\quad \because \sum \sin \phi_{ns} = 0, \text{ and } \sum r_1 = 0 \quad (\text{Eq. 3A-19})
 \end{aligned}$$

$$\begin{aligned}
 \therefore F_{\phi} &= \sum_H \left\{ K_n \sin(\phi_n - \phi) \left[(\ell_n - \ell_{no}) + \beta(r_3 \sin \phi_n - r_1 \cos \phi_n) \right] \right\} \\
 &+ \sum_I \left\{ K_n \sin(\phi_n - \phi) \left[(\ell_n - \ell_{no}) + \beta(r_3 \sin \phi_n - r_1 \cos \phi_n) \right] \right\} \\
 &= \sum_H K_n \{ [\ell \phi + \beta r_3] \} \\
 &+ \sum_I K_n \left\{ \left[\sin \phi_{ns} + \phi \left(\frac{\ell}{\ell_n} - 1 \right) \cos \phi_{ns} \right] [\rho + \delta_{ns}] + \beta [r_3 \sin^2 \phi_{ns} \right. \right. \\
 &\quad \left. \left. - r_1 \sin \phi_{ns} \cdot \cos \phi_{ns}] \right\} \\
 &= \sum_H \left\{ K_n (\ell \phi + \beta r_3) \right\} + \sum_I \left\{ K_n (\rho + \delta_{ns}) \left[\phi \left(\frac{\ell}{\ell_n} - 1 \right) \cos \phi_{ns} \right] + \beta [b] \right\} \\
 &\hspace{15em} (\text{Eq. 3A-20})
 \end{aligned}$$

$$\text{where } [b] = \sin \phi_{ns} (r_3 \sin \phi_{ns} - r_1 \cos \phi_{ns})$$

$$\begin{aligned}
 \therefore M_{\beta} &= \sum_H \left\{ K_n (r_3 \sin \phi_n - r_1 \cos \phi_n) \left[(\ell_n - \ell_{no}) + \beta(r_3 \sin \phi_n - r_1 \cos \phi_n) \right] \right\} \\
 &+ \sum_I \left\{ K_n (r_3 \sin \phi_n - r_1 \cos \phi_n) \left[(\ell_n - \ell_{no}) + \beta(r_3 \sin \phi_n - r_1 \cos \phi_n) \right] \right\} \\
 &= \sum_H \left\{ K_n (r_3) (\ell \phi + \beta r_3) \right\} \\
 &+ \sum_I K_n \left\{ \left[r_3 \left(\frac{\ell}{\ell_n} \phi \cdot \cos \phi_{ns} + \sin \phi_{ns} \right) - r_1 \left(\cos \phi_{ns} - \frac{\ell}{\ell_n} \phi \cdot \sin \phi_{ns} \right) \right] \times \right. \\
 &\quad \left. [(\rho + \delta_{ns}) + \beta(r_3 \sin \phi_{ns} - r_1 \cos \phi_{ns})] \right\} \\
 &= \sum_H \left\{ K_n \cdot r_3 (\ell \phi + \beta r_3) \right\} \\
 &+ \sum_I K_n \left\{ r_3 \left(\frac{\ell}{\ell_n} \phi \cdot \cos \phi_{ns} + \sin \phi_{ns} \right) (\rho + \delta_{ns}) \right\} \\
 &+ \sum_I K_n \left\{ (-r_1) \left(\cos \phi_{ns} - \frac{\ell}{\ell_n} \phi \cdot \sin \phi_{ns} \right) (\rho + \delta_{ns}) \right\} \\
 &+ \sum_I K_n \left\{ \beta r_3 \left(\frac{\ell}{\ell_n} \phi \cos \phi_{ns} + \sin \phi_{ns} \right) (r_3 \sin \phi_{ns} - r_1 \cos \phi_{ns}) \right\} \\
 &+ \sum_I K_n \left\{ \beta (-r_1) \left(\cos \phi_{ns} - \frac{\ell}{\ell_n} \phi \sin \phi_{ns} \right) (r_3 \sin \phi_{ns} - r_1 \cos \phi_{ns}) \right\} \\
 &= \sum_H \left\{ K_n r_3 (\ell \phi + \beta r_3) \right\} \\
 &+ \sum_I K_n \left\{ r_3 (\rho + \delta_{ns}) \left(\frac{\ell}{\ell_n} \phi \cdot \cos \phi_{ns} \right) \right\} \\
 &+ \sum_I K_n \left\{ r_1 (\rho + \delta_{ns}) \left(\frac{\ell}{\ell_n} \phi \cdot \sin \phi_{ns} \right) \right\} \\
 &+ \sum_I K_n \beta \left\{ (r_3 \sin \phi_{ns} - r_1 \cos \phi_{ns})^2 \right\} \\
 &= \sum_H \left\{ K_n r_3 (\ell \phi + \beta r_3) \right\} \\
 &+ \sum_I K_n \left\{ \frac{\ell}{\ell_n} \phi (\rho + \delta_{ns}) (r_3 \cos \phi_{ns} + r_1 \sin \phi_{ns}) + \beta (r_3 \sin \phi_{ns} - r_1 \cos \phi_{ns})^2 \right\}
 \end{aligned}$$

(Continued)

$$= \sum_H \{K_n r_3 (\ell\phi + \beta r_3)\} \\ + \sum_I K_n \left\{ \frac{\ell}{\ell_n} \phi (\rho + \delta_{ns}) [d] + \beta [c] \right\}$$

where

$$[c] = (r_3 \sin\phi_{ns} - r_1 \cos\phi_{ns})^2 \\ \text{and } [d] = (r_3 \cos\phi_{ns} + r_1 \sin\phi_{ns})$$

Substituting the expressions of F_ℓ , F_ϕ , and M_β obtained in Eq. 3A-19, 20 and 21 into Eq. 3A-16 a, b and c we get

$$m\ddot{\ell} + \sum_I \{K_n (\rho + \delta_{ns}) \cos\phi_{ns}\} + (m\ddot{X}_O) \sin\phi + (m\ddot{Z}_O - mg) \cos\phi = 0 \quad (\text{Eq. 3A-22a})$$

$$m\ell\ddot{\phi} + \sum_H \{K_n (\ell\phi + \beta r_3)\} + \sum_I K_n \left\{ (\rho + \delta_{ns}) \left[\phi \left(\frac{\ell}{\ell_n} - 1 \right) \cos\phi_{ns} \right] \right. \\ \left. + \beta [b] \right\} + (m\ddot{X}_O) \cos\phi - (m\ddot{Z}_O - mg) \sin\phi = 0 \quad (\text{Eq. 3A-22b})$$

$$I\ddot{\beta} + \sum_H \{K_n r_3 (\ell\phi + \beta r_3)\} + \sum_I K_n \left\{ \frac{\ell}{\ell_n} \phi (\rho + \delta_{ns}) [c] + \beta [b] \right\} = 0 \quad (\text{Eq. 3A-22c})$$

where

$$[b] = \sin\phi_{ns} (r_3 \sin\phi_{ns} - r_1 \cos\phi_{ns}) \\ \text{and } [c] = (r_3 \sin\phi_{ns} - r_1 \cos\phi_{ns})^2 \\ \text{and } [d] = (r_3 \cos\phi_{ns} + r_1 \sin\phi_{ns})$$

In the above equations

$$\sum_I K_n \cdot \cos\phi_{ns} \cdot \delta_{ns} - mg \cos\phi = 0 \\ \text{and } \sum_I K_n \cdot \cos\phi_{ns} \cdot \delta_{ns} \cdot \phi - mg \sin\phi = 0$$

$$\text{Let } \ddot{X}_O = \ddot{U}_O \sin\phi_O \quad \text{and} \quad \ddot{Z}_O = \ddot{U}_O \cos\phi_O$$

where \ddot{U}_O is the resultant acceleration acting at an angle ϕ_O with the vertical axis.

Hence Eq. 3A-22a, b and c reduce to

$$m \ddot{l} + \sum_I \left\{ K_n \rho \cos \phi_{ns} \right\} + m \ddot{U}_0 \cos(\phi_0 - \phi) = 0 \quad (\text{Eq. 3A-23a})$$

$$m l \ddot{\phi} + \sum_H \left\{ K_n (l \phi + \beta r_3) \right\} + \sum_I K_n \left\{ (\rho + \delta_{ns}) \left(\frac{l}{l_n} \phi \cdot \cos \phi_{ns} \right) - \rho \phi \cos \phi_{ns} + \beta [b] \right\} + m \ddot{U}_0 \sin(\phi_0 - \phi) = 0 \quad (\text{Eq. 3A-23b})$$

$$I \ddot{\beta} + \sum_H \left\{ K_n r_3 (l \phi + \beta r_3) \right\} + \sum_I K_n \left\{ \frac{l}{l_n} \phi (\rho + \delta_{ns}) [a] + \beta [c] \right\} = 0 \quad (\text{Eq. 3A-23c})$$

By making the approximation: $\rho \ll l_s$, we get

$$l = l_s + \rho \approx l_s$$

$$l_n = l + r_3 = l_s + \rho + r_3 \approx l_s + r_3$$

Also

$$\ddot{l} = (\dot{l}_s + \dot{\rho}) = \ddot{\rho}, \text{ and } I = mR^2$$

The equations then reduce to

$$\ddot{\rho} + \sum_I \left\{ \frac{K_n \cos \phi_{ns}}{m} \right\} \rho + \ddot{U}_0 \cos(\phi_0 - \phi) = 0 \quad (\text{Eq. 3A-24a})$$

$$\begin{aligned} \ddot{\phi} + \sum_H \left\{ \frac{K_n}{m} \right\} \phi + \sum_H \left\{ \frac{K_n}{m l_s} r_3 \right\} \beta + \sum_I \left\{ \frac{K_n \cos \phi_{ns}}{m(l_s + r_3)} - \frac{K_n \cos \phi_{ns}}{m l_s} \right\} \phi \rho \\ + \sum_I \left\{ \frac{K_n \delta_{ns} \cos \phi_{ns}}{m(l_s + r_3)} \right\} \phi + \sum_I \left\{ \frac{K_n [b]}{m l_s} \right\} \beta + \ddot{U}_0 \sin(\phi_0 - \phi) = 0 \end{aligned} \quad (\text{Eq. 3A-24b})$$

$$\begin{aligned} \ddot{\beta} + \sum_H \left\{ \frac{K_n r_3^2}{mR^2} \right\} \phi + \sum_H \left\{ \frac{K_n r_3^2}{mR^2} \right\} \beta + \sum_I \left\{ \frac{K_n l_s [a]}{mR^2(l_s + r_3)} \right\} \phi \rho \\ + \sum_I \left\{ \frac{K_n l_s \delta_{ns} [a]}{mR^2(l_s + r_3)} \right\} \phi + \sum_I \left\{ \frac{K_n [c]}{mR^2} \right\} \beta = 0 \end{aligned} \quad (\text{Eq. 3A-24c})$$

Let

$$\begin{aligned}
 D_0 &= \sum_I \left\{ \frac{K_n \cos \phi_{ns}}{m} \right\} \\
 D_1 &= \sum_I \left\{ \frac{K_n \cos \phi_{ns}}{m(\ell_s + r_3)} - \frac{K_n \cos \phi_{ns}}{m \ell_s} \right\} \\
 D_2 &= \sum_H \left\{ \frac{K_n}{m} \right\} + \sum_I \left\{ \frac{K_n \cdot \delta_{ns} \cdot \cos \phi_{ns}}{m(\ell_s + r_3)} \right\} \\
 D_3 &= \sum_H \left\{ \frac{K_n r_3}{m \ell_s} \right\} + \sum_I \left\{ \frac{K_n [b]}{m \ell_s} \right\} \\
 D'_1 &= \sum_I \left\{ \frac{K_n \ell_s [d]}{m R^2 (\ell_s + r_3)} \right\} \\
 D'_2 &= \sum_H \left\{ \frac{K_n \ell_s r_3}{m R^2} \right\} + \sum_I \left\{ \frac{K_n \ell_s \cdot \delta_{ns} [d]}{m R^2 (\ell_s + r_3)} \right\} \\
 D'_3 &= \sum_H \left\{ \frac{K_n r_3^2}{m R^2} \right\} + \sum_I \left\{ \frac{K_n [c]}{m R^2} \right\}
 \end{aligned}$$

Eq. 3A-24a, b and c become

$$\ddot{\phi} + D_0 \phi = -\ddot{U}_0 \cos(\phi_0 - \phi) \quad (\text{Eq. 3A-25a})$$

$$\ddot{\phi} + \phi(D_1 \phi + D_2) + \beta(D_3) = -\ddot{U}_0 \sin(\phi_0 - \phi) \quad (\text{Eq. 3A-25b})$$

$$\ddot{\beta} + \phi(D'_1 \phi + D'_2) + \beta(D'_3) = 0 \quad (\text{Eq. 3A-25c})$$

For the configurations under consideration, it seems reasonable to assume that $\phi_0 \gg \phi$

$$\therefore \phi_0 - \phi \approx \phi_0$$

$$\therefore \ddot{U}_0 \cos(\phi_0 - \phi) \approx \ddot{U}_0 \cos \phi_0 \approx \ddot{Z}_0$$

$$\text{and } \ddot{U}_0 \sin(\phi_0 - \phi) \approx \ddot{U}_0 \sin \phi_0 = \ddot{X}_0$$

Eq. 3A-25a, b and c further reduce to

$$\ddot{\phi} + D_0 \phi = - \ddot{Z}_0 \quad (\text{Eq. 3A-26a})$$

$$\ddot{\phi} + \phi(D_1 \phi + D_2) + \beta(D_3) = - \ddot{X}_0 \quad (\text{Eq. 3A-26b})$$

$$\ddot{\beta} + \phi(D'_1 \phi + D'_2) + \beta(D'_3) = 0 \quad (\text{Eq. 3A-26c})$$

3A-3 Evaluation of Coefficients for Each Configuration

The initial angles of inclination for pendulum in Configurations 2 and 3 are assumed to be small ($\phi_{ns} < \pi/6$), hence the following approximation is made:

$$\sin \phi_{ns} \approx \phi_{ns} \text{ and } \cos \phi_{ns} \approx 1$$

$$D_0 = \sum_I \frac{K_n \cos \phi_{ns}}{m}$$

$$\text{Configuration 1} \quad \frac{2K_v}{m}$$

$$\text{Configuration 2} \quad \frac{2K}{m}$$

$$\text{Configuration 3} \quad \frac{2(K_1 + K_2)}{m}$$

$$D_1 = \sum_I \frac{K_n \cos \phi_{ns}}{m(\ell_s + r_3)} - \sum_I \frac{K_n \cos \phi_{ns}}{m \ell_s}$$

$$\text{Configuration 1} \quad \frac{2K_v}{m} \left\{ \frac{1}{\ell_s + a_2} - \frac{1}{\ell_s} \right\}$$

$$\text{Configuration 2} \quad \frac{2K}{m} \left\{ \frac{1}{\ell_s + a_2} - \frac{1}{\ell_s} \right\}$$

$$\text{Configuration 3} \quad \frac{2}{m} \left\{ \frac{K_1}{\ell_s - a_1} + \frac{K_2}{\ell_s + a_2} - \frac{K_1 + K_2}{\ell_s} \right\}$$

$$D_2 = \sum_H \frac{K}{m} + \sum_I \frac{K_n \cos \phi_{ns} \phi_{ns}}{m(\ell_s + r_3)}$$

$$\text{Configuration 1} \quad \frac{4K_H}{m} + \frac{2K_V \delta_s}{m(\ell_B + a_2)}$$

$$\text{Configuration 2} \quad \frac{2K \delta_s}{m(\ell_s + a_2)}$$

$$\text{Configuration 3} \quad \frac{2}{m} \left\{ \frac{K_1 \delta_{1s}}{\ell_s - a_1} + \frac{K_2 \delta_{2s}}{\ell_s + a_2} \right\}$$

$$D_3 = \sum_H \frac{K_n r_3}{m \ell_s} + \sum_I \frac{K_n [b]}{m \ell_s}$$

$$\text{Configuration 1} \quad \frac{2K_H}{m \ell_s} (a_4 - a_3)$$

$$\begin{aligned} \text{Configuration 2} \quad \Sigma [b] &= \Sigma \sin \phi_{ns} (r_3 \sin \phi_{ns} - r_1 \cos \phi_{ns}) \\ &= \phi_2 \{a_2 \phi_2 - (-r)\} + (-\phi_2) \{a_2 (-\phi_2) - r\} \\ &= 2\phi_2 (r + a_2 \phi_2) \end{aligned}$$

$$\therefore D_3 = \frac{2K}{m \ell_s} \phi_2 (r + a_2 \phi_2)$$

$$\begin{aligned} \text{Configuration 3} \quad \Sigma [b] &= \phi_1 \{(-a_1) \phi_1 - (-r)\} + (-\phi_1) \{(-a_1) (-\phi_1) - r\} \\ &+ \phi_2 \{a_2 \phi_2 - (-r)\} + (-\phi_2) \{a_2 (-\phi_2) - r\} \\ &= 2\phi_1 (r - a_1 \phi_1) + 2\phi_2 (r + a_2 \phi_2) \end{aligned}$$

$$\therefore D_3 = \frac{2}{m \ell_s} \{K_1 \phi_1 (r - a_1 \phi_1) + K_2 \phi_2 (r + a_2 \phi_2)\}$$

$$D'_1 = \sum_I \frac{K_n [d] \ell_s}{m R^2 (\ell_s + r_3)}$$

$$\begin{aligned} \text{Configuration 1} \quad \Sigma [d] &= \Sigma (r_3 \cos \phi_{ns} + r_1 \sin \phi_{ns}) \\ &= 2a_2 \end{aligned}$$

$$\therefore D'_1 = \frac{2K_v a_2 l_s}{mR^2(l_s + a_2)}$$

Configuration 2 $\Sigma[d] = \{a_2 + (-r)(\phi_2)\} + \{a_2 + (r)(-\phi_2)\}$
 $= 2(a_2 - r\phi_2)$

$$\therefore D'_1 = \frac{2K(a_2 - r\phi_2)l_s}{mR^2(l_s + a_2)}$$

Configuration 3 $\Sigma[d] = \{-a_1 + (-r)(\phi_1)\} + \{-a_1 + (r)(-\phi_1)\}$
 $+ \{a_2 + (-r)(\phi_2)\} + \{a_2 + (r)(-\phi_2)\}$
 $= 2(-a_1 - r\phi_1) + 2(a_2 - r\phi_2)$

$$\therefore D'_1 = \frac{2l_s}{mR^2} \left\{ \frac{K_1(-a_1 - r\phi_1)}{l_s - a_1} + \frac{K_2(a_2 - r\phi_2)}{l_s + a_2} \right\}$$

$$D'_2 = \sum_H \frac{K_n r_3 l_s}{mR^2} + \sum_I \frac{K_n [d] \delta_{ns} l_s}{mR^2(l_s + r_3)}$$

Configuration 1 $\frac{2K_H(a_4 - a_3)l_s}{mR^2} + \frac{2K_v a_2 \delta_s l_s}{mR^2(l_s + a_2)}$

Configuration 2 $\frac{2K(a_2 - r\phi_2)\delta_s l_s}{mR^2(l_s + a_2)}$

Configuration 3 $\frac{2l_s}{mR^2} \left\{ \frac{K_1(-a_1 - r\phi_2)\delta_{1s}}{l_s - a_1} + \frac{K_2(a_2 - r\phi_2)\delta_{2s}}{l_s + a_2} \right\}$

$$D'_3 = \sum_H \frac{K_n r_3^2}{mR^2} + \sum_I \frac{K_n [c]}{mR^2}$$

$$\text{Configuration 1 } \Sigma[c] = \Sigma(r_3 \sin \phi_{ns} - r_1 \cos \phi_{ns})^2$$

$$= 2r^2$$

$$\therefore D'_3 = \frac{2K_H(a_3^2 + a_4^2)}{mR^2} + \frac{2K_V r^2}{mR^2}$$

$$\begin{aligned} \text{Configuration 2 } \Sigma[c] &= \{a_2 \phi_2 - (-r)\}^2 + \{a_2(-\phi_2) - r\}^2 \\ &= 2(r + a_2 \phi_2)^2 \end{aligned}$$

$$\therefore D'_3 = \frac{2K}{mR^2} (r + a_2 \phi_2)^2$$

$$\begin{aligned} \text{Configuration 3 } \Sigma[c] &= \{(-a_1)(\phi_1) - (-r)\}^2 + \{(-a_1)(-\phi_1) - r\}^2 \\ &\quad + \{a_2 \phi_2 - (-r)\}^2 + \{a_2(-\phi_2) - r\}^2 \\ &= 2(r - a_1 \phi_1)^2 + 2(r + a_2 \phi_2)^2 \end{aligned}$$

$$\therefore D'_3 = \frac{2}{mR^2} \{K_1(r - a_1 \phi_1)^2 + K_2(r + a_2 \phi_2)^2\}$$

SECTION 3 SYMBOLS AND NOTATIONS

Generalized Coordinates

- l : Instantaneous length of the resultant pendulum
- ϕ : Inclination of resultant pendulum with vertical axis
- β : Rotation about the axis through center of gravity perpendicular to plane of the figure.

Reference Systems

- $\left. \begin{matrix} X_0 \\ Z_0 \end{matrix} \right\}$: Ground reference system and ground motion
- $\left. \begin{matrix} X \\ Z \end{matrix} \right\}$: Capsule reference system (parallel to $X_0 - Z_0$)
- $\left. \begin{matrix} X_1 \\ Z_1 \end{matrix} \right\}$: Inertial reference system, origin at center of gravity (parallel to X-Z)

Ground Accelerations

- $\left. \begin{matrix} \ddot{X}_0 \\ \ddot{Z}_0 \end{matrix} \right\}$: Ground accelerations along X_0 and Z_0 axes respectively.

Physical Constants for Suspension System

- l_s : Length of the resultant pendulum in static condition (with dead load)
- $\left. \begin{matrix} l_{ns} \\ \phi_{ns} \end{matrix} \right\}$: Polar coordinates of n^{th} isolator in static position
- $\left. \begin{matrix} l_n \\ \phi_n \end{matrix} \right\}$: Polar coordinates of n^{th} isolator at time 't' due to translation of center of gravity.

- l_{no} : Length of the n^{th} isolator with zero load
- R : Radius of gyration of the suspended mass
- $\left. \begin{matrix} r_1 \\ r_2 \\ r_3 \end{matrix} \right\}_n$: Coordinates of mass-attachment-point of the n^{th} isolator in $X_1 - Y_1 - Z_1$ directions, respectively
- $\left. \begin{matrix} r_{1w} \\ r_{2w} \\ r_{3w} \end{matrix} \right\}_n$: Coordinates of the wall-attachment-point of the n^{th} isolator in $X_1 - Y_1 - Z_1$ directions, respectively
- δ_{ns} : Static deflection of the n^{th} isolator
- r : X coordinate of an isolator
- a_1 : Z_1 coordinate of the level of suspension above center of gravity.
- a_2 : Z_1 coordinate of the level of suspension below center of gravity.
- a_3 : Z_1 coordinate of the top horizontal isolators.
- a_4 : Z_1 coordinate of the bottom horizontal isolators
- K_n : Axial stiffness of the n^{th} isolator.
- K : Axial stiffness of isolators of configuration 2.
- K_v : Axial stiffness of the vertical isolators.
- K_H : Axial stiffness of the horizontal isolators.
- K_1 : Axial stiffness of top series of isolators of configuration 3.
- K_2 : Axial stiffness of bottom series of isolators of configuration 3.

m	: Mass of the suspended body
W	: Weight of the suspended body
ρ	: Axial extension of the resultant pendulum
ρ_0	: Maximum value of ρ
g	: Acceleration due to gravity
\ddot{U}_0	: Resultant ground acceleration
ϕ_0	: Inclination of \ddot{U}_0 with vertical axis
ϕ_1	: Static inclination of top isolator, configuration 3
ϕ_2	: Static inclination of bottom isolator, configuration 3
ϕ_m	: Maximum value of ϕ
ω	: Natural frequency
ω_v	: Natural frequency in vertical direction
ω_H	: Natural frequency in horizontal direction
ω_1	: Natural frequency of the pendulum spring
ω_0^*	: Equivalent natural frequency of the pendulum
δ_s	: Static deflection of isolators, configurations 1 and 2
δ_{1s}	: Static deflection of top isolators, configuration 3
δ_{2s}	: Static deflection of bottom isolators, configuration 3
D_0	} : Refer to Table 3-1
D_1	
D_2	
D_3	
D'_1	
D'_2	
D'_3	

F_d	: Damping force
F_H^D	: Damping force in horizontal direction
ξ, ζ	: Damping ratio or subsidiary variable of integration
c	: Damping coefficient
I	: Moment of inertia of the suspended body about the axis through center of gravity perpendicular to plane
I_i	: Moment of inertia of 12 mass attachment points of isolators
\sum_H	: Summation applicable to horizontal isolators
\sum_I	: Summation applicable to inclined isolators
λ	: Undetermined multiplier used in Lagrange's method
k	: Stiffness of restoring element
l	: Pendulum length
l^*	: Equivalent pendulum length
e_x	: Eccentricity in X_1 direction
e_z	: Eccentricity in Z_1 direction
N	: Total number of isolators
C_N	: Distance from center of symmetry to mass-attachment point of n^{th} isolator in X_1 direction (see Table 3-2)
$(K_{zz})'_n$: Axial stiffness of n^{th} isolator
$(K_{zz})_n$: Combined axial stiffness of cable plus n^{th} isolator in series
θ_{ns}	: Inclination of vertical plane containing n^{th} isolator in static position with X-axis
K_1^D	: Damping coefficient for top isolators, configuration 3
K_2^D	: Damping coefficient for bottom isolators, configuration 3

4.0 SHOCK ISOLATION DEVICES

Despite the large number of shock isolation systems which have been designed to support personnel in underground protective structures, there yet remain to be established complete criteria which will ensure performance which is acceptable from the viewpoints of dynamic response, static stability, adjustability, and maintenance. Yet until standards of performance can be defined quantitatively in each of these areas, there is little likelihood that the system will meet all the expectations of the using agency. On the other hand, the problem of identifying and assigning specific target values to the various performance parameters is exceedingly difficult, if not impossible. Not only are physical data lacking in many of the areas, but frequently operational experience with these types of systems has not been sufficient to provide the broad basis needed to support general conclusions. With regard to the latter, psychological reaction to the system's behavior by operating personnel can be as significant as the physical reaction.

The basic requirements of the shock isolator itself are dictated by the needs of the complete isolation system. Load capacity, stiffness, damping, stroke and overall length have been discussed in the previous section and tentative criteria established from the viewpoint of system performance and simplicity. Near-linear force-displacement characteristics, a type of damping which allows the system to return to its initial position but yields low transient forces, and load and stiffness adjustability were judged to be preferred qualities in an isolator.

While these qualities were not selected completely irrespective of the behavior of practical devices, they do represent idealizations which, particularly for a facility of this size, may be difficult to achieve with the confidence and reliability also demanded. No existing isolation device is of sufficient size to meet the requirements of a large facility by a significant margin.

In this section, promising isolator and damper principles are reviewed and their potential for meeting the requirements are compared. In addition, their capability for withstanding the environment to which they might be exposed and for meeting operational requirements are examined.

The study of isolation devices has been limited to liquid and pneumatic springs as these types of devices have been found in the past to be most flexible in tailoring to the needs of a particular requirement. As noted in Section 3.0, the restoring-force and energy dissipative characteristics of compressible fluid-filled isolators can be easily controlled in design and the load and stiffness adjustability is ideally suited to installations where a wide range of loading conditions must be met.

In suspension Configurations 2 and 3, damping is provided in all modes by the isolators installed in the pendulum arms. In Configuration 1 separate sway dampers are provided in the horizontal direction. Thus this section also presents concepts of general devices which function to attenuate lateral oscillations of the cage.

The design of suitable hardware for shock isolation however is not limited to the selection of devices which yield the desired restoring force and energy dissipation. Other design problems, equally important, must be solved. Structural integrity, dynamic response of the isolators themselves and their interaction with the supported mass, adjustability, definition of control requirements and other functions must be thoroughly explored before all critical parameters can be identified and a final solution obtained. Several of these problems which experience has shown to be of particular importance have been studied further in this section and in Section 5.0.

Considerable attention is given to the pendulum-isolator system. The configuration considered to be best suited for this application consists of the isolator attached at its base to the cage structure by means of a spherical bearing or gimbal and a flexible cable assembly connecting the top of the piston rod with the capsule. The capsule attachment could comprise open bridge sockets and plate weldments. A typical cable assembly would consist of three $2\frac{1}{2}$ -inch diameter wire ropes each of 6 x 19 classification.

The very strong ground motions to which the capsule-end of the pendulum system is exposed not only can induce large forces in the attachments but can also transmit very high loads into the cable-isolator combination. In particular, as the cable can support no axial compression, care must be taken to ensure that it never goes slack. Otherwise high accelerations are introduced when it retightens. The dynamic interaction of the isolator-cable assembly is examined in this section and critical parameters ensuring satisfactory operation evaluated.

4.1 Isolator Requirements

In addition to the performance requirements specified in Section 3.0, the isolator must perform reliably when exposed to shock, temperature, humidity, and radiation. Further, it must resist aging, require minimum maintenance, and remain stable over long periods of time. And it must be economically feasible.

These requirements are reviewed here in detail.

4.1.1 Attenuation Level

The most severe attenuation requirement is dictated by the shock tolerance of personnel housed within the supported cage.

Personnel occupancy is considered necessary in all areas of these facilities, even though such occupancy may be limited in power capsules to maintenance functions. Therefore the degree of isolation required is based on personnel capability. Vertical and horizontal accelerations will be held below 0.5g and 0.2g, respectively.

4.1.2 Temperature and Humidity

The shock isolators for all capsules will be located in the space between the capsule structure and the suspended cage. It is assumed that no temperature or moisture control is provided in this space; therefore, the temperature of the capsule will govern and, to be conservative, the air should be assumed to be saturated. The capsule temperature is a function of depth of burial, and for this study, the estimated temperature is 100 degrees F. The maintenance of a proper equilibrium position requires that temperature compensation be included for all systems experiencing changes in temperature and employing devices sensitive to temperature changes. Changes in temperature can cause significant changes in shock isolator length for both the liquid and the pneumatic springs. Shock isolators for use in weapons systems are normally exposed to temperature changes of as much as 35 to 40 degrees F., during which their operational characteristics must be maintained. However, the available literature for facilities similar to those being considered here, indicates that the ambient temperature rise at the shock isolators will not be more than about 20 degrees F.

4.1.3 Load and Load Variation Capacity

Each of the three cages will incorporate a multifilar pendulum suspension, as discussed in Section 3.0. The load to be supported by each isolator can vary significantly, depending upon the load to be supported and the particular suspension system used. In the two-level suspension with inclined pendulum (Configuration 3), the upper springs support twice the load of the lower springs, while in the one-level suspension system, all springs support essentially equal loads.

The total weight and center of gravity of each system can be located only within finite tolerances during preliminary design; in addition the weights and center of gravity locations in a particular facility may change due to functional modifications and growth considerations. Therefore, each shock isolator must incorporate generous change capacity based upon maintaining structural integrity, dynamic response and ability to hold the static position of any system at the predetermined equilibrium position.

Best Available Copy

For isolator load differences significantly beyond the magnitude estimated in Section 6.0, development of multiple isolator designs appear to be warranted. Three shock isolator static loads with estimated load adjustabilities are tabulated in Table 4-1.

Table 4-1 Static Spring Load Capacity

System	Nominal Spring Load (Kips)	Number of Springs	Spring Load Range Maximum Load (Kips)	Minimum Load (Kips)
Single Plane (Configuration 2)	421	12	557	302
Double Plane (Configuration 3)	282 560	6 6	371 742	201 402

The load adjustability was made plus or minus 10 per cent plus the effect of the center of gravity shift estimated in Section 6.0.

4.1.4 Stiffness Variation

In addition to the requirement to hold the static equilibrium position constant while the supported masses vary, there is also the need to minimize coupling by holding the dynamic equilibrium conditions constant. Thus as the load on each isolator is varied, the stiffness of the isolators should vary in proportion to the load so that each isolator element maintains the same natural frequency as before the change. Stiffnesses and the capacity for stiffness adjustability should be made in the same proportions as the load capacity and spring load range indicated in Table 4-1.

The vertical to horizontal frequency ratio should be maintained as large as practicable in order to avoid the energy transfer effects which occur upon approaching a ratio of two, the pendulum instability discussed in Section 3.0 and Reference 2.

4.1.5 Stroke

The stroke required of the shock isolator is a function of the motion of the suspended cage relative to the capsule and must be obtained from results of an analysis of the dynamic response of the system. The analysis determines the maximum displacements and combinations of displacements in the vertical and horizontal directions and rotation about all three principal axes. A second variable, the rattlespace needed between the capsule structure and the suspended cage, is also determined by the dynamic analysis. Once the rattlespace is fixed by the results of the rigid body analysis, enough shock isolator

stroke is provided to allow the isolated body complete freedom within the rattlespace.

The space allowed for the two-level suspension derives primarily from inclining the isolators to obtain horizontal damping. For this case the stroke should not be made dependent on the rattlespace but should be fixed at values determined from analysis plus an allowance to account for uncertainties of input and response. Preliminary estimates indicate that shock isolator stroke should be 70 inches, single amplitude.

4.1.6 Damping

As indicated in Section 3.0 damping is required to minimize amplification effects, coupling between modes of oscillation and continued oscillations. The amount of damping required in the vertical and horizontal directions is obtained from the results of a rigid body analysis of the suspension system.

The two devices considered here for vertical shock isolation devices, liquid and pneumatic springs, are particularly adapted to obtain damping as a function of piston motion. The characteristics of the damping available in these devices are analyzed in this section.

Preliminary estimates indicate that an equivalent viscous damping ratio of 0.10 should be provided in the vertical direction. An equivalent viscous damping ratio of 0.025 should be provided in the horizontal direction, based on obtaining equal energy dissipation in the single and double plane suspension systems.

4.1.7 Mass Limitations

The size, weight and flexibility of shock isolator components are of great significance during the high acceleration and high velocity portions of the ground motion. Significant accelerations can be generated in the components by both the horizontal and vertical components of the ground motion.

The shock isolator components which connect the shock isolator to the capsule structure are directly exposed to the high accelerations and velocities and can become open paths for transmission of sizable amounts of energy into or through the shock isolator. For example, if the shock isolator connector were a stiff column member, the vertical high velocity input would be transmitted directly to the shock isolator piston. In the liquid spring, the piston orifices sized for handling nominal fluid velocities at low piston velocity, would generate excessive forces when exposed to high-velocity motions. In addition, high-velocity horizontal motions at the top of a stiff column member connected to a shock isolator of significant mass will induce a severe

bending load in the column member. The most promising approaches which have been found to mitigate the problem of high energy transmission into the shock isolator are those of making connecting members that are flexible and of providing relieving mechanisms at the piston.

The effect of component mass and flexibility is considered for each device where it appears significant.

An added consideration is the effect of the mass and stiffness of the connecting member coupling with the response of the elastic spring element. The high-velocity-input problem and the coupling consideration are analyzed in detail in this section under the paragraph entitled Cable-Isolator Interaction.

4.2 Liquid Spring Concept

4.2.1 Basic Principle

The liquid spring principle consists of a solid plunger moving into a volume that is already completely filled with a fluid. The motion of the plunger into the chamber displaces the fluid, raising its pressure and increasing the reactive force in the spring. This concept developed from the research work of several experts in high pressure technology, in particular, the work of P. W. Bridgman, Hollis Professor of Mathematics and Natural Philosophy, Harvard University. Professor Bridgman discusses the basic sealing mechanism which makes possible all high pressure fluid devices in Reference 3. This sealing mechanism is referred to as the unsupported area principle and is shown in Figure 4-1. Figure 4-1 shows the piston and seal mechanism used extensively by Professor Bridgman in his high pressure research. The features and operation of the unsupported area seal mechanism are:

- . The area of the moving plug piston exposed to fluid pressure is larger than the area of the seal by the area of the plug extension, which passes through a hole in the soft packing seal, and the steel anti-extrusion rings.
- . The pressure of the liquid on the stud is supported by the force developed in the seal, and since the seal area is smaller than the loaded stud area, the pressure developed in the seal is larger than the fluid pressure loading the stud.
- . The excess seal pressure produces the curious effect wherein the seal tends to leak both to the outside of the device and back into the fluid. This seal leakage effect produces the need for anti-extrusion rings.

The first commercial liquid springs were developed by Dowty Equipment, Ltd., England, for use on landing gears for British military aircraft. It should be noticed that the seal is a modified version of Professor Bridgman's seal. This first liquid spring application took the form shown in Figure 4-2. The piston shown in the Dowty spring is not a necessary part of the spring since the fluid compression occurs due to fluid displacement as the rod moves into the device. The piston is used to carry fluid flow control devices which provide damping or control piston speed, or both. Therefore, the piston provides functions auxiliary to the primary spring function, making the liquid spring a more versatile device. The fluid displacement is accommodated by compression of the fluid and by deflections of the plunger and housing parts. The fluid compression contributes the major portion of the displacement, the deflections are usually quite small and are normally neglected. If extreme accuracy is required of the spring, a prototype can be built and calibrated over its useful stroke, which accounts for all effects.

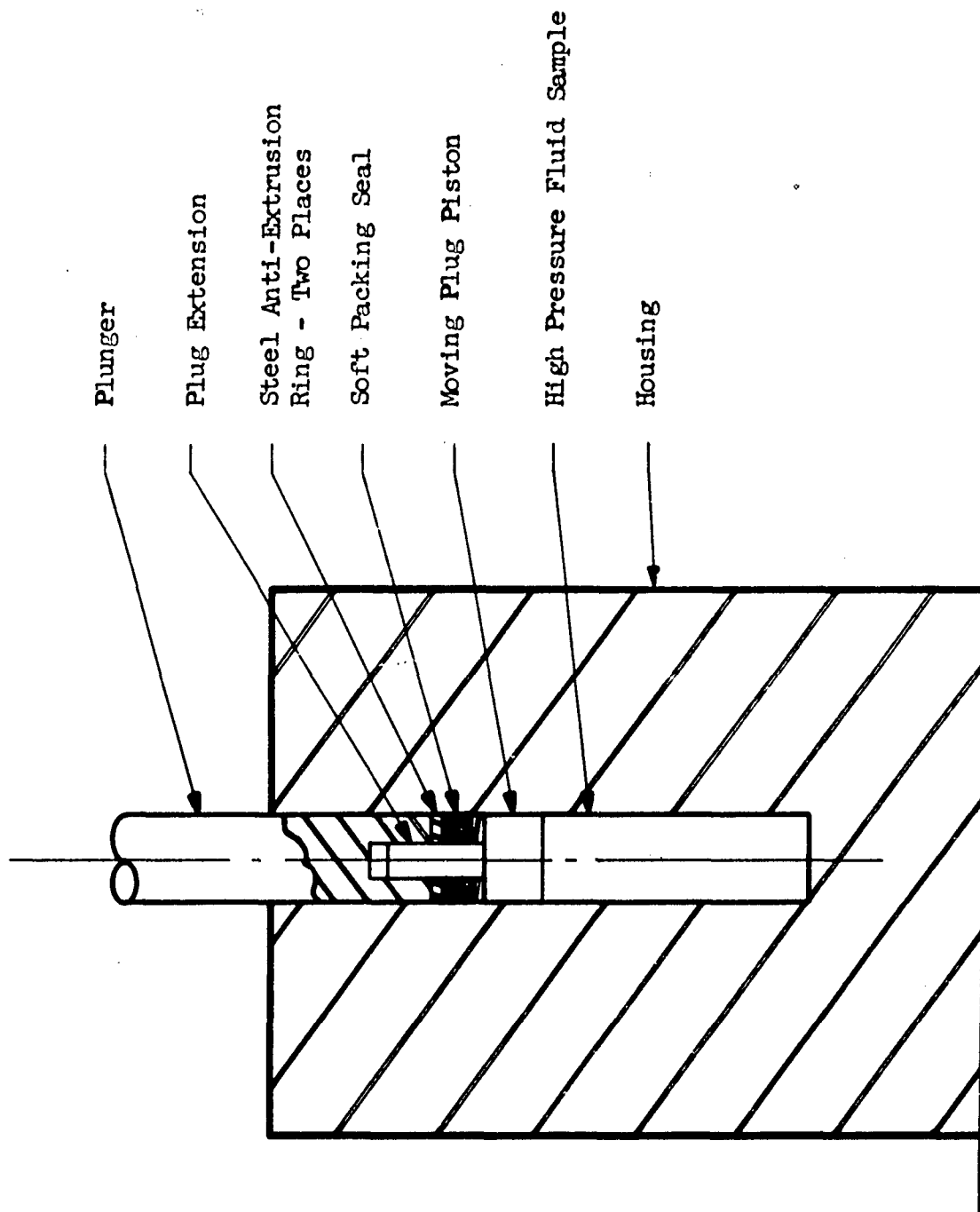


Figure 4-1. Bridgman High Pressure Seal Concept.

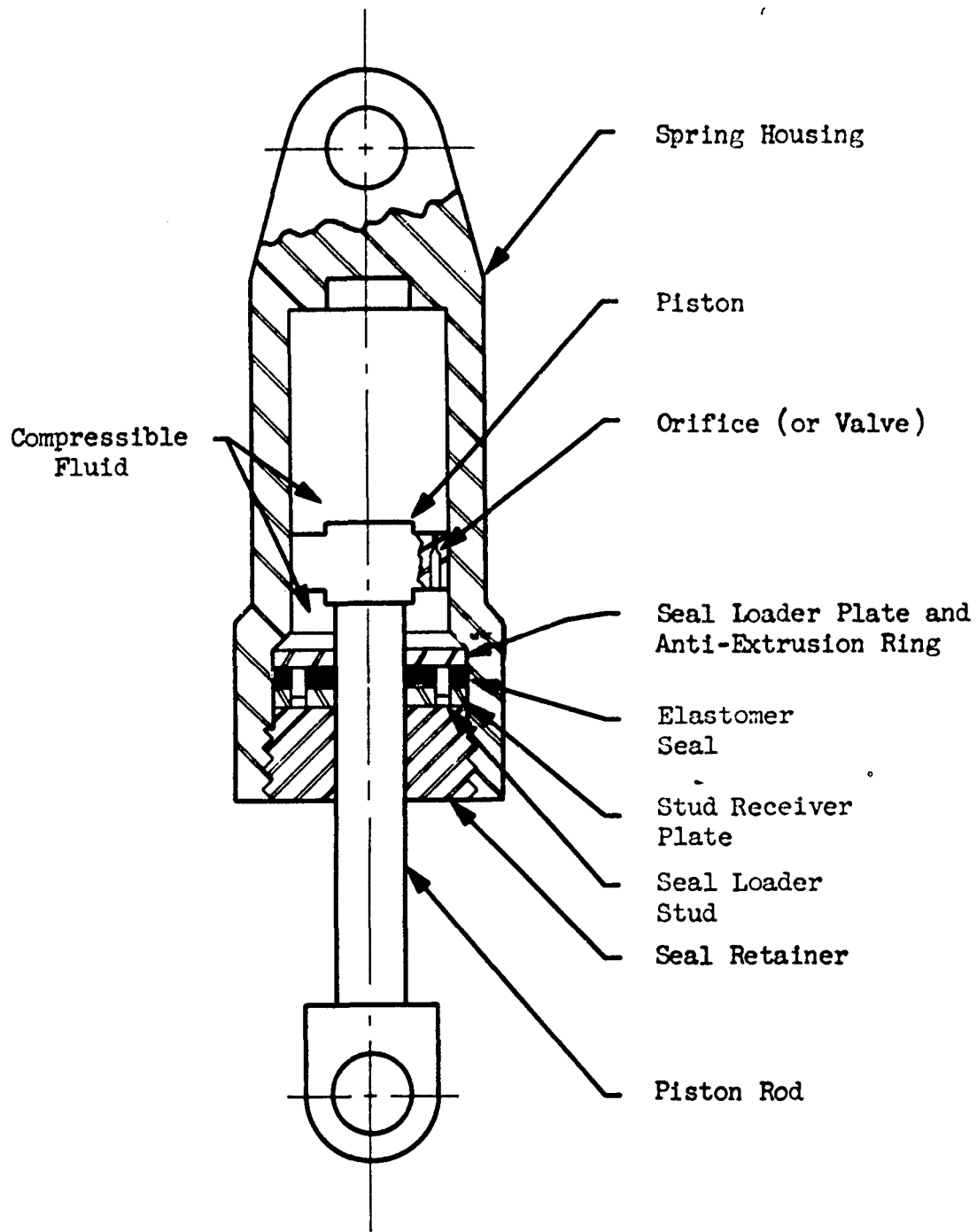


Figure 4-2. Dowty Liquid Spring Concept for Landing Gear.

4.2.2 Liquid Spring Design Concepts

The first liquid spring concept (shown in Figure 4-2) employed in this country was similar to the Dowty landing gear device. This design was used on the Lockheed F-104 fighter aircraft and in the design and manufacture of die springs. Taylor Devices, Inc., has developed a novel design concept (Figure 4-3) employing a stepped cylindrical piston operating over an internal stud and piston closure. The differential area between the inside diameter of the larger portion of the cylindrical piston and the outside diameter of the smaller portion of the cylindrical piston is displaced during extension of the spring, raising the fluid pressure and providing restoring force.

The Taylor Devices design can be easily adapted to accommodate a position limiter, damping orifices and valve devices between the stepped cylinder piston and the stud.

The combined tension and compression spring concept (Figure 4-4) was used in a preloaded condition on the Polaris missile system. The preload was about half the total static load experienced by the spring at full deflection. For this application, the simple tension spring design shown in Figure 4-5, the inverted compression spring with yoke shown in Figure 4-6, and the Taylor Devices design shown in Figure 4-3 are most useful.

4.2.3 Fluids and Fluid Properties

Fluids recommended for application in liquid springs are silicones of relatively moderate viscosity. These fluids are, in general, clear colorless liquids of variable viscosity which are distinguished by:

- . high compressibility
- . excellent thermal and oxidative stability
- . relative inertness and nontoxicity
- . resistance to shear stress breakdown
- . small viscosity change over wide temperature change
- . low pour point
- . low to high flash point
- . lubricity problems

Five manufacturers of liquid springs contacted in regard to a spring design suitable for this application reported using silicone fluids in their liquid springs. These were:

. The Cleveland Pneumatic Tool Company - uses a mixture of silicone fluids of unspecified constituents and characteristics (proprietary). Dow Corning bulletin entitled, "Engineering Guide to Silicone Fluids," indicates that CPT uses Dow Corning fluids.

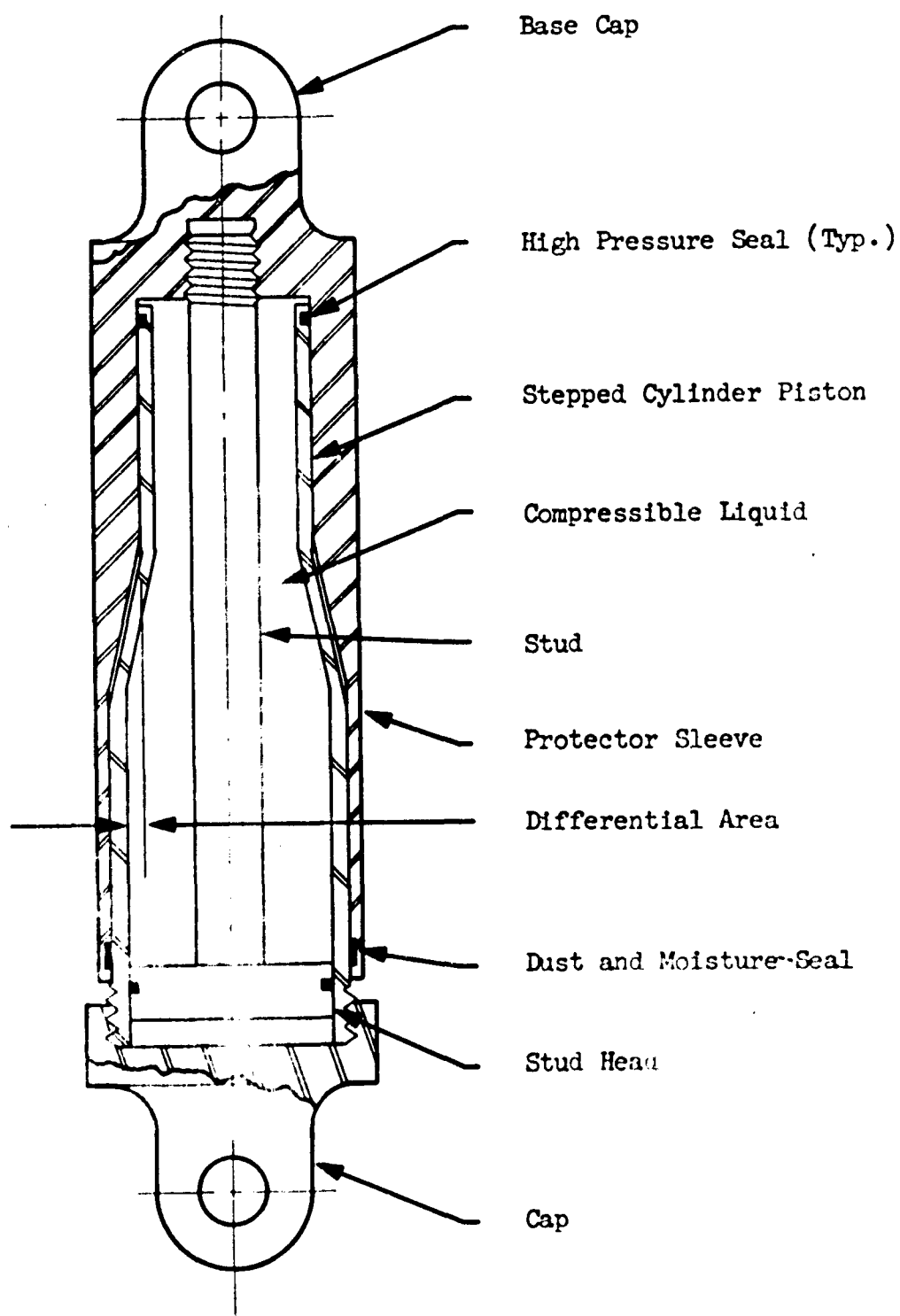


Figure 4-3. Stepped Cylindrical Tension Spring Concept.
(Proprietary with Taylor Devices, Inc.)

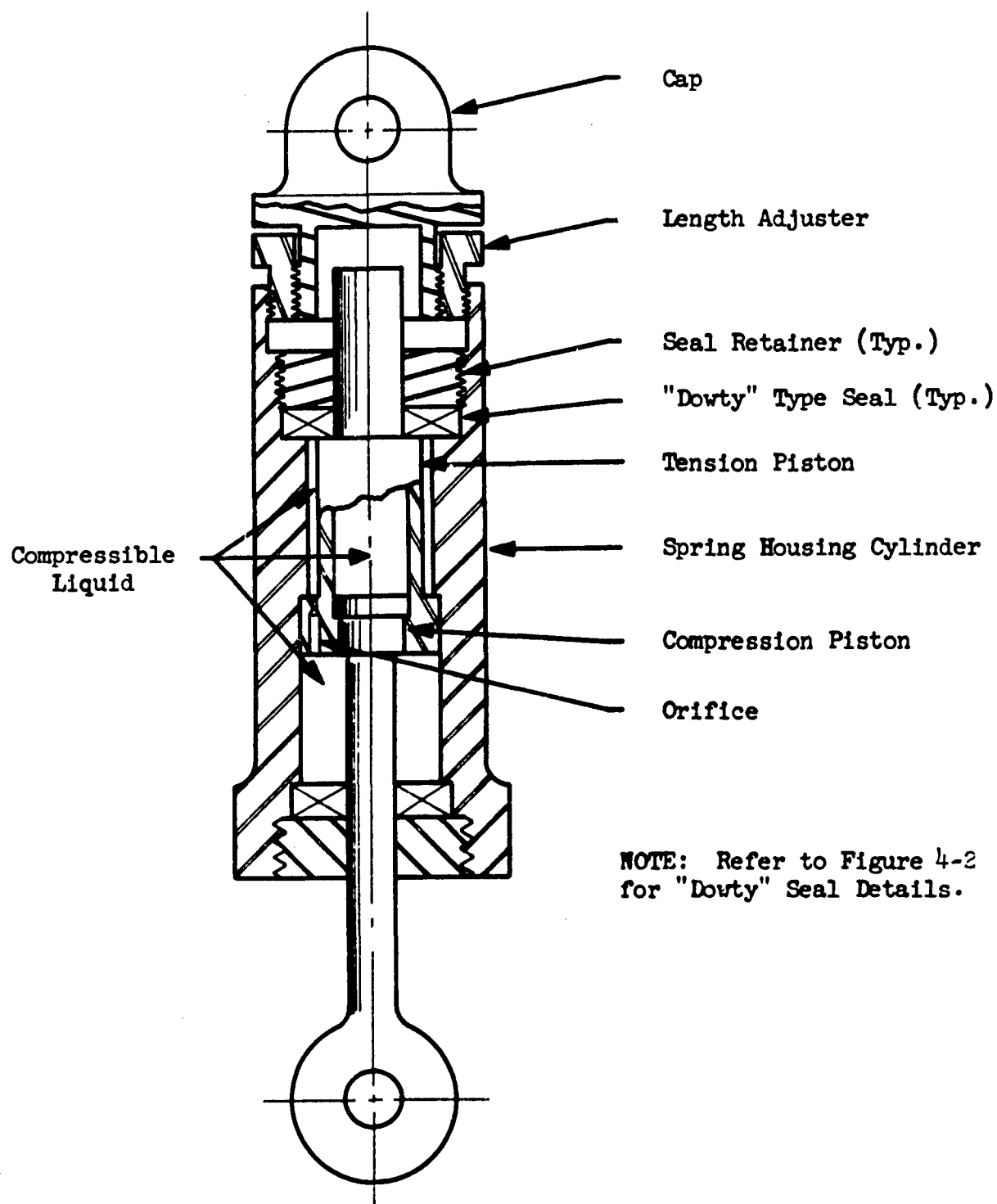


Figure 4-4. Tension Spring Concept Used in Polaris Missile System. (Proprietary with Westinghouse Electric Corporation)

NOTE: Refer to
Figure 4-2
for "Dowty" Seal
Details.

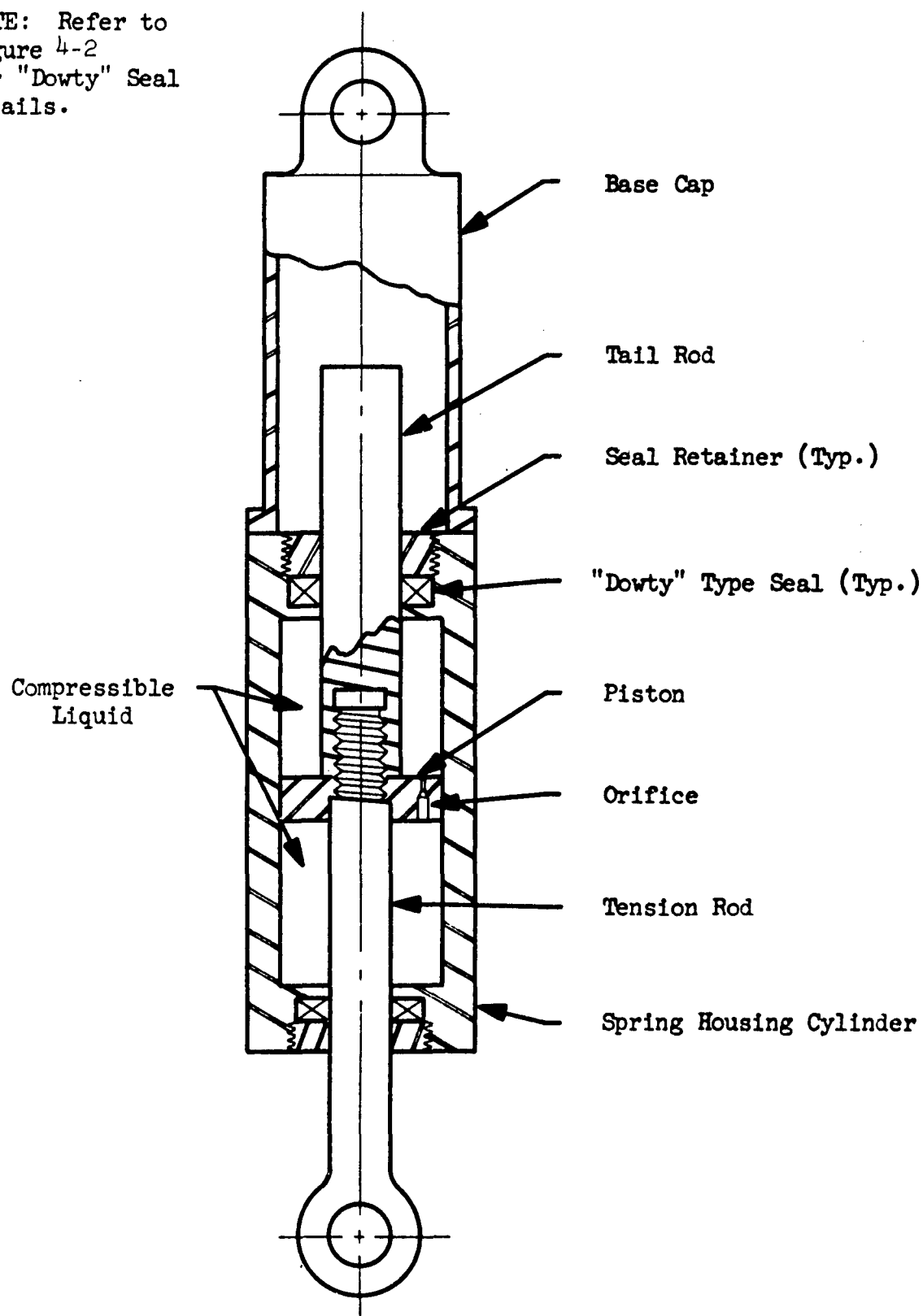


Figure 4-1. Simple Tension Spring.

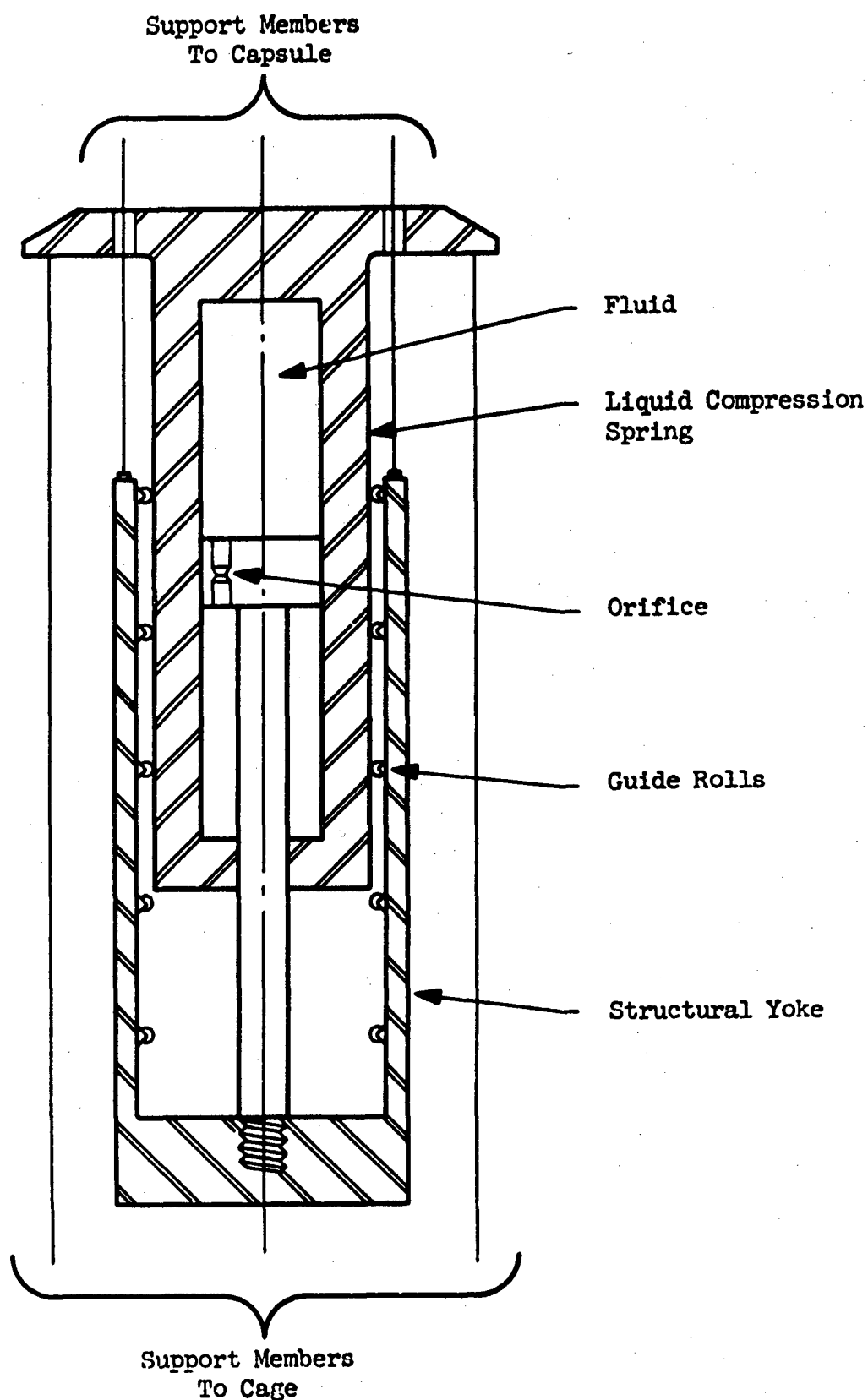


Figure 4-6.

Schematic of Liquid Compression Spring Used to Support Tension Loads.

. H. W. Loud Machine Works, Inc. - has used a mixture of Dow Corning fluids; 70 per cent F 4029 and 30 per cent 510-50 centistoke, by volume. They suggest using 100 per cent F 4029 for this application.

. Menasco Manufacturing Company - uses Dow Corning fluid 200-50 centistokes.

. Taylor Devices, Inc.-report development of a patented silicone blend which they call Piezoil 602.

. Westinghouse Electric Corporation-specifies MIL-F-21568-50 centistokes for use in their liquid springs. MIL-F-21568-50 centistokes fluid has published characteristics which are identical to those published by Dow Corning Corporation for their 200-50 centistokes fluid and Union Carbide Corporation for their L-45 50 centistokes fluid. These will be considered identical fluids for this study. The characteristics of these fluids and others shown in the literature are presented in Table 4-2 and Figure 4-7.

The compressibilities of several silicone fluids are shown on Figure 4-7, and are compared with that of water. The highest compressibility shown is for fluids with a very low viscosity and low flash point (0.65 centistokes and 30°F, respectively). These fluids are not considered applicable here, but their compressibility is shown for comparative purposes. The next highest compressibility shown is for the Dow Corning F 4029 fluid. These data show that compressibility of 10 to 11 per cent can be obtained at 20,000 psi with proven fluids. Note that the higher the compressibility, the smaller the volume needed to obtain the same frequency spring.

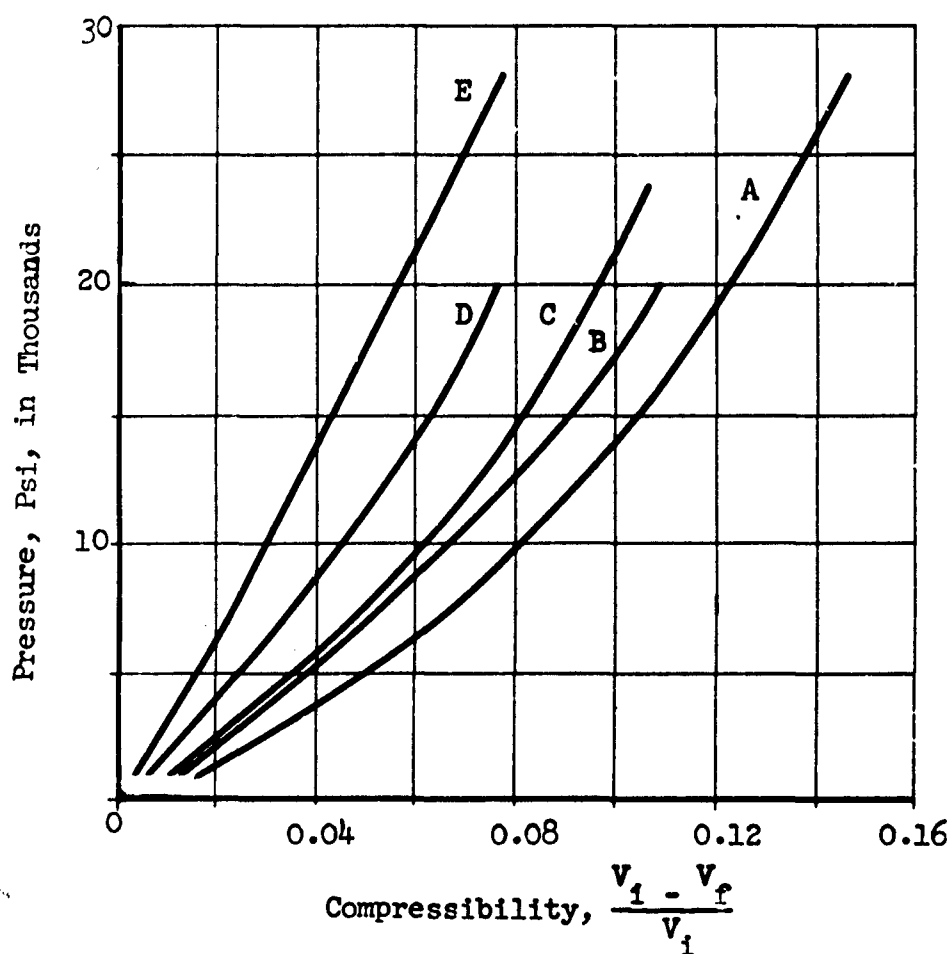
Viscosity stability of the silicone fluids studied are generally much better than normal lubricating oils and hydraulic fluids. Comparing the two silicone fluids appearing to be most promising for this application, MIL-F-21568 and Dow Corning F 4029, the F 4029 fluid has slightly better viscosity stability with variation in temperature. The viscosity is reduced 59 per cent and 55 per cent for the MIL-F-21568 and F 4029 fluids, respectively, when the temperature is increased from 100 to 210°F. Employment of the more stable material will provide more nearly constant damping forces with changing temperature.

The thermal expansion of liquids used in the liquid spring is particularly significant, since fluid expansion will change either the load or the position of a liquid spring. The coefficient of thermal expansion for silicone fluids is about 1×10^{-3} cubic inch per cubic inch--degree Centigrade.

The silicone fluids are rated in Reference 4 as having mediocre radiation stability. The fluids of 10 centistokes viscosity and above gel at an exposure of 1×10^{10} ergs/gm and the low viscosity grades, 10 centistokes and lower, experience an increase in viscosity of about 50 per cent for the same radiation exposure. Since the radiation exposure

Table 4-2 Properties of Silicone Fluids

Property	Fluid									
	Water	Mineral Oil	Dow Corning Fluids				Union Carbide Corp.		Taylor Devices	
			200-0.65	200-50	F 4029	510-50	L-45-50	L-45-100		
Viscosity at 25° C in Centistokes	0.89	-	0.65	50	100	50	50	100	110	-
Compressibility at 5,000 psi	0.017	-	-	-	-	-	-	0.033	0.023	0.036
10,000 psi	0.030	0.033	0.081	-	0.065	0.050	-	0.057	0.044	0.061
15,000 psi	0.042	0.048	0.103	-	0.089	0.066	-	0.076	0.063	0.081
20,000 psi	0.056	0.060	0.121	-	0.104	0.079	-	0.093	0.076	0.097
25,000 psi	0.067	-	-	-	-	-	-	-	-	0.109
Coefficient of Expansion x 103	-	-	-	1.04	1.17	0.96	1.04	0.97	0.75	-
Flash Point °F.	-	-	30	535	150	525	535	575	410	-
Pour Point °F. (Freeze Point in Parenthesis)	-	-	(-90)	-67	-58	(-76)	-67	-67	-56	-
Specific Gravity	1	-	-	0.96	0.875	0.99-1001	0.96	0.97	0.99	-
Data Source	Ref. 3 page 143	Ref. 5	Ref. 6 and 7	Ref. 7	Ref. 5	Ref. 6 and 7	Ref. 8	Ref. 8 and 9	Ref. 8 and 9	Ref. 10



- Curve A - Dow Corning, Fluids 200 and 500 (0.65 centistokes)
- B - Dow Corning, Fluid F-4029
- C - Taylor Devices, Fluid Piezoil B-602
- D - Union Carbide, Fluid L-527
- E - Water

Figure 4-7. Fluids Compressibility

within these facilities is many orders of magnitude lower than the critical range, 10^8 to 10^{10} ergs/gm, no significant problems are anticipated. Therefore considering the range of radiation exposure permitted for these facilities, these fluids are expected to perform satisfactorily.

The lubricating properties of silicone fluids deviate significantly from those of hydraulic fluids and lubricants in general. The silicone fluids do not provide adequate lubrication for steel-on-steel or steel in combination with many other metals, such as brass, copper, babbitt, magnesium, tin, chromium, zinc, aluminum and stainless steel. Nylon inserts or coatings, when used with steel or plastics, are satisfactorily lubricated by the silicone fluids.

Silicone fluids exhibit higher leakage rates than the more conventional fluids because of lower surface tension and slight shrinkage experienced by most elastomers when in contact with the silicone fluids. These sealing problems may be eliminated by the selection of specially compounded elastomers or by adding components to the fluids to counteract their tendency to cause shrinkage.

The literature indicates that the silicone materials of moderate viscosity, Dow Corning F 4029, 200-50 centistokes and Union Carbide L-45, are stable indefinitely below 300°F . The use of these fluids, under conditions of high pressure, total enclosure, and operating temperatures of 100 to 140 degrees F., should present no thermal stability problems.

The silicone fluids are generally noncorrosive to materials used in liquid springs. Small quantities of impurities, such as water can, however, cause problems. Additives are available to eliminate the corrosion problems which might arise from water and other contaminants.

The Dow Corning F 4029 fluid has the best compressibility property of the fluids compared that have suitable viscosity and satisfactory flash points. The Dow Corning 200 and Union Carbide L-45 fluids of 50 and 100 centistokes viscosity have good coefficients of expansion, flash and pour points and viscosity-temperature coefficients. These are the recommended fluids with the Dow Corning F 4029 having the better compressibility and viscosity-temperature stability while the other fluids have the most beneficial coefficient of expansion. On these bases the F 4029 fluid will be used where exact fluid properties are required.

Temperature sensitivity of the liquid spring depends on the fluid employed. Having selected the Dow Corning F 4029 fluid, the effect of temperature changes on the liquid spring can be estimated. It will be assumed that the liquid volume is 40,000 cubic inches, and the piston rod and tail rod diameters are 4-1/2 and 8 inches, respectively.

The change in length of the liquid spring is

$$\Delta L = \frac{\text{Fluid Volume} \times \text{Fluid Coefficient of Expansion}}{\text{Effective Area of Piston}}$$

The fluid coefficient of expansion is

$$\frac{0.001 \text{ Inch}^3}{\text{Inch}^3 \text{ } ^\circ\text{C.}} \times \frac{5^\circ\text{C.}}{9^\circ\text{F.}} = \frac{0.00056 \text{ Inch}^3}{\text{Inch}^3 \text{ } ^\circ\text{F.}}$$

For a 20°F. change

$$\Delta L = \frac{40,000 \times 0.00056 \times 20}{(50.3 - 16)} = 13.1 \text{ inches}$$

An uncontrolled displacement of thirteen inches in a system designed to accept about 40 inches of vertical displacement is obviously unacceptable, and means to eliminate such an occurrence must be found. This problem is covered under Section 5.0 under the paragraph entitled Leveling and Load Balancing Control.

4.2.4 Leakage

Leakage has been shown by Bridgman and others to be easily handled by the unsupported area seal principle, for static and quasi-static conditions. Other precautions must be observed in order to eliminate dynamic leakage. Surface roughness and imperfections of shafts, such as hairline cracks and porosity can produce significant leakage for relative motion between shaft and seal. The fluid collects in the hills and valleys of the surface roughness and in the pores of porous material. When the seal moves past these discontinuities the highly compressed fluid is free to expand and appears on the shaft as if the shaft were sweating. This form of leakage is minimized by careful control of materials and surface quality. Several vendors provided drawings which showed chrome-plated piston rods; however, one vendor reports that leakage through porosity of chrome plating caused enough trouble to induce him to eliminate chromeplating from his design.

Surface finishes of the order of two to four microinches, rms, are recommended by liquid spring manufacturers coupled with the suggestion that the tool marks be oriented parallel with the direction of motion of the part through the seal.

One manufacturer, Taylor Devices, Inc., reports obtaining excellent wear and sealing characteristics from a coating of nylon fused on the steel parts which slide against the seals.

The five manufacturers dismiss leakage as negligible. Westinghouse, Cleveland Pneumatic and the Menasco Manufacturing Company employ the "Dowty" seal or modified versions. Taylor Devices and the H. W. Loud Machine Works, Inc., have developed their own seal designs.

The Taylor Devices, Inc. seal configuration was not disclosed in their literature. A statement in one of their brochures, however, indicates that they have had seal problems resulting from excessive seal pressure. It was stated in a discussion of friction and leakage related to the use of a fluid blend:

"What makes this performance more remarkable is the fact that more seal pressure is exerted with the new liquid mixture. We discovered this when early experiments with the new fluid showed a "chewing" on the front lip of the seal, the liquid pressure side. Obviously, the seal was growing into the high pressure fluid; that is, because it was exerting a greater pressure than the fluid it contained, the seal was extruding backward into the fluid (adding an anti-extrusion member solved this problem)."

The H. W. Loud Machine Works, Inc. seal is shown in Figure 4-8. The seal configuration is patented and its use by others, notably Dowty Equipment of Canada, Ltd., is licensed by Loud. It may be noticed that this design incorporates loading and shielding members of standard "O" rings and plastic and steel turned parts. The seal ring and "O" rings provide the initial or low pressure seal; as pressure increases the sealing function shifts to the wedge ring which becomes pressurized in excess of the fluid pressure by the combined effect of the seal and "O" rings. The washer, backing up the wedge ring, provides protection for the wedge ring from wear and ingestion of dust and other foreign materials.

4.2.5 Damping

From the basic operating principle of the liquid spring it is evident that damping will result from friction between sliding elements and from energy losses associated with the flow of the fluid during stroke. Since the number of individual mechanisms contributing to the total energy loss are many, it is most convenient to represent the total dissipative force grossly as the sum of two or three terms, each term containing all the effects of a given type. For example, the equation representing the total dissipative force for a given unit might be assumed to contain three terms representing coulomb friction, capillary flow and quadratic flow, the weights proportioned to each of the terms being based on the results of experiments of that particular design.

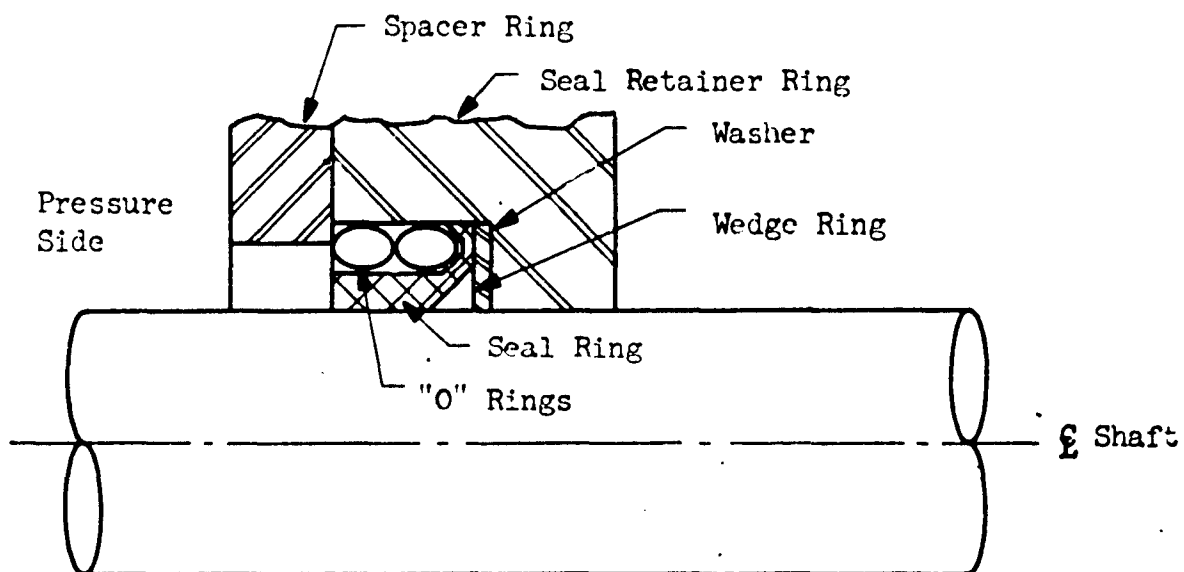


Figure 4-3. Liquid Spring Seal. Patented by H.W. Lou Machine Works, Inc. of Pomona, California.

The effect of the coulomb friction term is considered detrimental to the proper static balancing of the system; therefore, considerable effort must be expended in minimizing such effects. The friction is inherent in the seals used to contain the high pressure fluid of the liquid spring. The seal designs employed in liquid springs make use of materials having the lowest known coefficients of friction, Teflon on polished steel or on polished nylon. Little improvement is expected in the near future from the use of improved materials.

The geometry of the seal design is carefully controlled to provide a considerably higher seal pressure than the contained fluid pressure. A normal consequence of such a design is the excess friction which must be accepted in order to ensure positive sealing. Reduction of this seal overpressure is the same as reducing the sealing safety factor, and should be avoided.

Reduction in the effective width of the seal would be an effective means for obtaining reduced friction since the seal friction varies linearly with the contact area of the seal on the shaft which in turn varies directly with seal width. As the seal width is reduced, there will be found some critical width where wear becomes excessive. Considerable development effort may be required in order to hold the required seal longevity while minimizing seal friction.

The normal liquid spring configuration for tensile loads employs an extended tail rod and two seals; whereas the configuration for compressive load employs only one seal. This creates the opportunity to halve the friction loads due to sealing, since the compression spring may be used for tensile applications by adding a yoke, as shown in Figure 4-6, guided on the exterior of the liquid spring. This approach, while it halves the seal friction force, adds any friction due to guide loads. However, since the guide load friction may be made very small by application of antifriction guide bearings, coulomb friction for the spring assembly can be reduced to essentially the compression spring value.

The literature indicates that the coefficient of friction for Teflon on steel increases as rubbing speed increases from below 0.1 for static friction to 0.3 for dynamic friction. Assuming a seal pressure of 125 per cent of the contained fluid pressure, the friction force can be derived in terms of the supported load. The seal force acting normal to the surface of the spring rod is:

$$F_f = 1.25 P (\pi D) l_s;$$

where P is the contained fluid pressure, D is the inside diameter of the seal and l_s is the seal width.

The nominal supported load is

$$W = \frac{\pi D^2}{4} P$$

Therefore

$$D = \sqrt{\frac{4W}{\pi P}}$$

and

$$P = \frac{4WF}{\pi D^2}$$

$$F_f = 1.25 \mu_s \sqrt{WP} \pi = 4.43 \mu_s \sqrt{WP}$$

The friction load parallel with the spring rod will be

$$\begin{aligned} F_c &= \mu F_f = (0.1)(4.43) \mu_s \sqrt{WP} \\ &= 0.443 \mu_s \sqrt{WP} \end{aligned}$$

where the friction factor is taken as 0.1.

Assuming an equilibrium pressure of 20,000 psi for a nominal spring load of

$$\frac{5.052 \times 10^6 \text{ pounds}}{12 \text{ springs}} = 42.1 \times 10^4 \text{ pounds/spring}$$

$$F_c = 0.443 \times 9.17 \times 10^4 \mu_s = 4.06 \times 10^4 \mu_s$$

Converting this force into a percentage of the total supported load, we obtain

$$\frac{F_c}{W} = \frac{12(4.06 \times 10^4 \mu_s)(100)}{5.052 \times 10^6} = 9.65 \mu_s \text{ per cent}$$

which is plotted in Figure 4-9 as a function of seal width. If two seals are used, the total width of both seals will indicate the total friction.

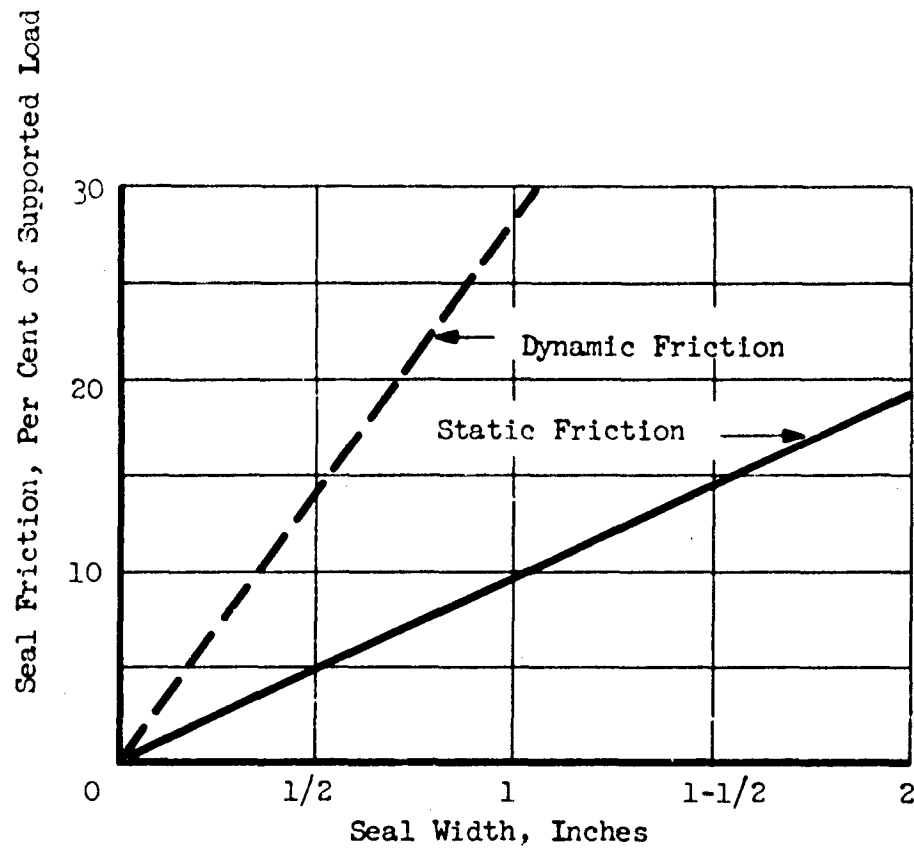


Figure 4-9. Seal Friction.

The other mechanisms contributing to the total coulomb friction are the possible rubbing of the piston on the inside of the spring housing, or of the shaft on the seal backing parts, and the loads developed in ball joint connectors. These loads are minor (assuming adequate design and manufacturing quality control) and will be neglected.

The flow of the fluid within the spring during stroking is accompanied by losses due to either or both of two fundamental mechanisms: viscous or fluid shear stress losses are due to laminar flow and to the laminar boundary layer present in turbulent flow over smooth surfaces; turbulence losses govern when the flow occurs over surfaces of sufficient roughness to eliminate the laminar film and for sudden contractions and expansions of the flow passages.

Laminar flow occurs in a particular device for flow below a critical rate defined by a Reynolds number between 2000 and 4000. Above the critical Reynolds number the flow becomes turbulent; however, for most flow systems there is a transition region where a laminar fluid layer exists at the fluid boundary over a thickness which decreases with increasing flow rate. Above a second critical Reynolds number the laminar boundary layer is disrupted and the flow becomes purely turbulent.

The losses resulting from coulomb friction and these several mechanisms are as follows:

. Coulomb friction loss	$= C_1 \frac{\dot{X}}{X}$
. Laminar flow losses	$= C_2 \dot{X}$
. Laminar film flow losses	$= C_3 [\dot{X}]^{1.75}$
. Turbulent flow and orifice flow losses	$= C_4 [\dot{X}]^2$

where C_1 , C_2 , C_3 , and C_4 are constants which depend on seal, fluid, thermal, geometrical or other system parameters and \dot{X} is the fluid flow velocity.

The fluid flows, and the motion of solid objects within the fluid, which generate energy losses are:

- . Fluid flow through the piston orifices
- . Fluid flow through the piston passages leading to the piston orifices

- . Fluid flow through the annular gap between the exterior of the piston and the inside of the spring housing
- . Motion of the piston rod through the fluid.

All of these flow paths are normally made quite smooth when the liquid spring is fabricated to obtain proper fits, smooth operation and spring longevity. In most hydraulic devices and in the liquid springs developed to date, the orifice losses predominate, especially at higher velocities.

It has been shown in Section 3.0 that viscous damping is preferable to "square law" damping since equal energy dissipation is obtained with smaller maximum forces. For this system, viscous damping may be employed by making the piston similar to a bundle of tubes. This minimizes the velocity squared component. By selection of the piston length and diameter of the tubes the fraction of critical damping can be controlled.

Combining all of the energy dissipative terms which can occur in the liquid spring the following expression is obtained:

$$F_D = C_1 \frac{\dot{X}}{|\dot{X}|} + C_2 \dot{X} + C_3 (\dot{X})^{1.75} + C_4 (\dot{X})^2$$

The effect of these terms can be modified as follows:

- . The coulomb friction term, $C_1 \frac{\dot{X}}{|\dot{X}|}$, can be minimized, but not eliminated.
- . The viscous damping term, $C_2 \dot{X}$, can be optimized through selective design.
- . The laminar boundary layer term, $C_3 (\dot{X})^{1.75}$, will be insignificant since very short boundary lengths are involved.
- . The turbulent flow term, $C_4 (\dot{X})^2$, can be minimized through selective design.

4.2.6 Stiffness of Liquid Spring

Unlike the wire helical spring, torsion bar or beam, the stiffness of the liquid spring varies with the load it supports. In fact, it is this variation in stiffness with load, and, thus, with displacement which characterizes the liquid spring as being nonlinear. While nonlinearity per se may not be particularly useful or even desirable in a given application, the stiffness variation can act in some instances to reduce coupling in shock isolation systems where the coupling is the result of asymmetric loading.

Consider, for example, an isolation system supported by several linearly elastic elements. The stiffness, k , and the static deflection, X_0 , of each of the units is fixed during design such that the sum of the static forces of all the elements and the first moment of their stiffnesses about the center of gravity is zero. By this means the coupling with the vertical mode of the system is minimized.

If the center of gravity of the system is displaced from its original position for any reason, the sum of the static forces of the elements about the new center of gravity location can be returned to zero by adjusting X_0 to produce the required loads. However, the stiffness of the isolators is fixed and cannot be altered to yield a zero moment. This coupling, in addition to any that may already exist in the system, is magnified.

This situation can be improved materially by the selection of isolation elements whose stiffnesses change proportionally with the load they support. As the load on each element is adjusted to account for a change in center of gravity location, the stiffness is automatically altered proportionately and the system is always balanced.

For any fluid spring, the conditions under which this balance can be achieved can be easily shown by the following relationships. The force, F , supporting the load is equal to the fluid pressure, P , multiplied by the area, A , on which the pressure acts. If the area is independent of the displacement, X , then

$$k = \frac{dF}{dX} = A \frac{dP}{dX}$$

To obtain a balanced element, we require only that the ratio of the stiffness to the load remain constant.

Then

$$\frac{k}{F_0} = \text{Constant} = \frac{dP/dX}{P_0}$$

where the subscript, 0 , indicates equilibrium conditions.

This is equivalent to specifying that the uncoupled natural frequency of the element must remain constant under all loading conditions since

$$\omega_o^2 = \frac{k}{m} = \frac{g}{F_0} \frac{dF/dX}{1} = \frac{g}{P_0} \frac{dP/dX}{1}$$

A diagram showing the essential elements of a liquid spring is given in Figure 4-10.

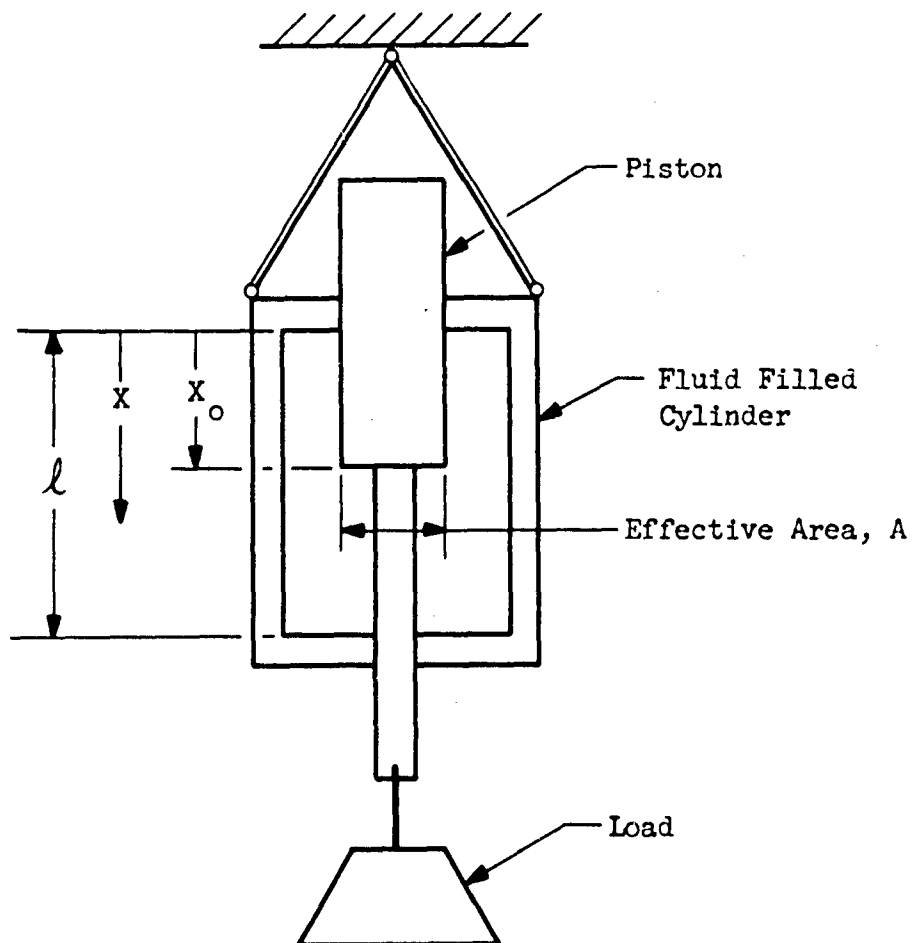


Figure 4-10. Schematic of Liquid Spring Isolator.

The cylinder is filled with fluid to an initial pressure, P_o , such that the equilibrium displacement of the piston is always X_o . Designating the volume of the system when the piston displacement, X , is zero as V_* , the volume of the system at $0 \leq X \leq X_o$ is

$$V = V_* - A X$$

and when $X = X_o$

$$V_o = V_* - A X_o$$

To evaluate the relationship between the pressure of the fluid and its volume, the characteristics of the particular fluid must be known. In Table 4-3 the compressibility of Dow Corning Fluid F 4029 is given. This fluid is recommended for the liquid spring application by several manufacturers and its compressibility is typical of most fluids used for liquid spring isolators.

Pressure, P (Psi)	Volume Change, $\Delta V/V$
10,000	0.065
20,000	0.104
30,000	0.132
40,000	0.155
50,000	0.174

Table 4-3. Compressibility Data for Dow Corning F 4029 Silicone Fluid.

It may be noted that in the table the volume changes are based on the free or unpressurized volume of fluid. In practice, however, the volume of the isolator in its equilibrium position, V_o , is held constant, while the free volume of the fluid is dependent on the equilibrium pressure. Noting that the equilibrium pressure recommended by most manufacturers is about 20,000 psi, the data of Table 4-3 have been normalized to this value and are plotted in a more convenient form in Figure 4-11. The relationship is then approximated by a curve defined by the binomial

$$\frac{P}{P_o} = a + b \left(\frac{V}{V_o} \right) + c \left(\frac{V}{V_o} \right)^2,$$

the curve being shown in the figure. In the equation, the coefficients have been evaluated

$$\begin{aligned} a &= + 79.6793 \\ b &= -143.1976 \\ c &= + 64.5183 \end{aligned}$$

△ Dow Corning Data Points

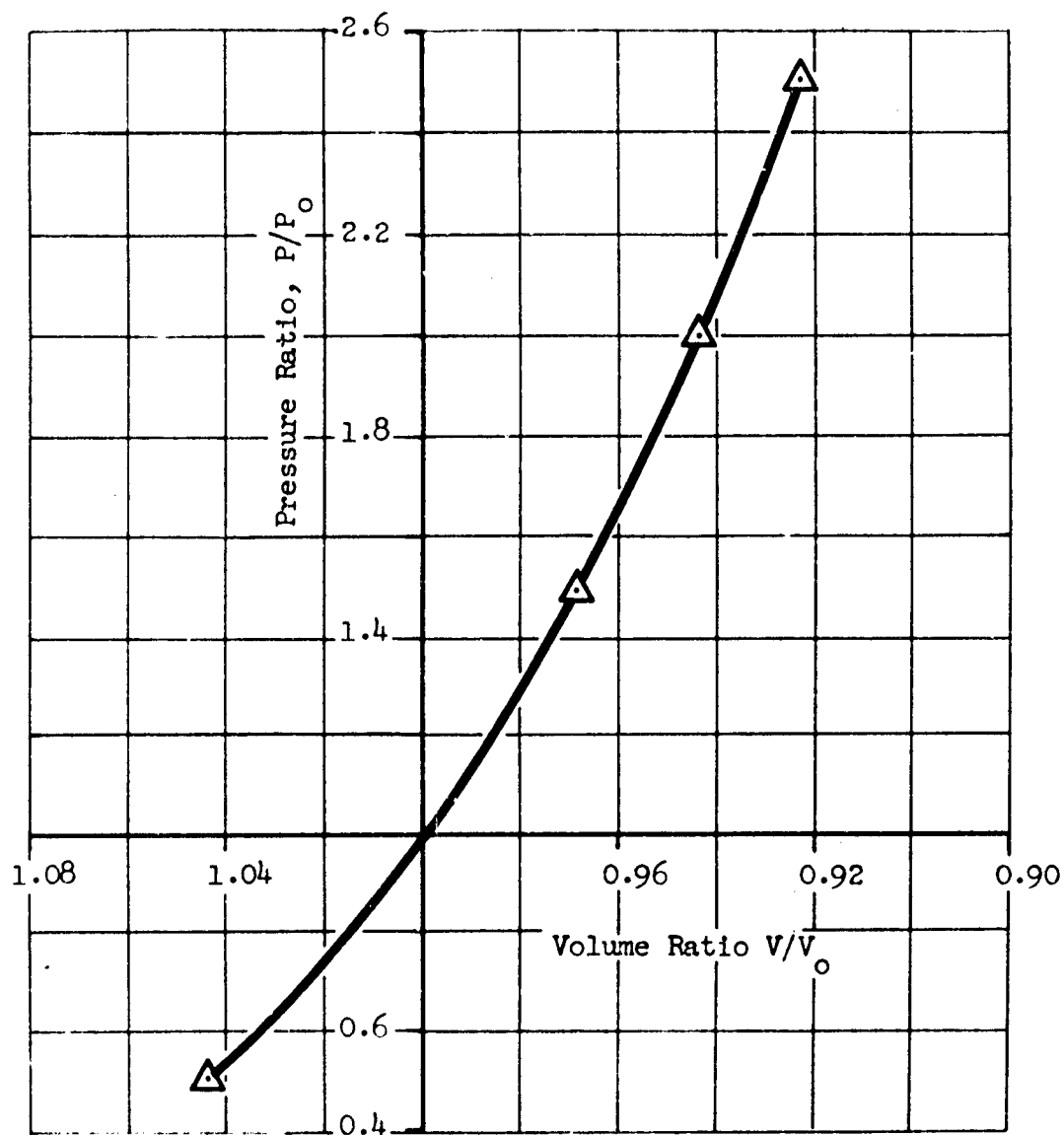


Figure 4-11. Pressure-Volume Relationship for Dow Corning, Fluid F-4029 Normalized to $P_0 = 20,000$ Psi.

Then

$$\omega^2 = - \frac{A g}{V_0} \left[b + 2c \left(\frac{V}{V_0} \right) \right]$$

It can be readily seen from this equation that ω varies with V and thus with the displacement of the system. Of more significance, however, is the variation in ω with load about the equilibrium position. Then as $V \rightarrow V_0$

$$\omega_0^2 \rightarrow - \frac{A g}{V_0} \left[b + 2c \right]$$

which is constant for a given system; i.e., it is independent of the load.

For a system employing this type of element then, a compensation in load or load distribution will result in an automatic stiffness compensation at the equilibrium position.

The instantaneous stiffness of the isolator is given by

$$\frac{dF}{dX} = A \frac{dP}{dV} \frac{dV}{dX} = - A^2 \frac{dP}{dV} = - F_0 \left(\frac{A}{V_0} \right) \left[b + 2c \left(\frac{V}{V_0} \right) \right]$$

But

$$\frac{V}{V_0} = \frac{V_* - AX}{V_* - AX_0} = 1 - \left(\frac{A}{V_0} \right) (X - X_0)$$

Then

$$\frac{dF}{dX} = - F_0 \left(\frac{A}{V_0} \right) \left\{ b + 2c \left[1 - \left(\frac{A}{V_0} \right) (X - X_0) \right] \right\}$$

And since

$$\frac{A}{V_0} = \frac{-\omega_0^2}{g (b + 2c)}$$

$$\frac{dF}{dX} = \frac{F_0 \omega_0^2}{g (b + 2c)} \left\{ b + 2c \left[1 + \left(\frac{\omega_0^2}{g (b + 2c)} \right) (X - X_0) \right] \right\}$$

Calculation of Stiffness of Three Isolators

In Section 3.0 three methods of suspending the cage are considered. Configuration 2 consists of twelve identical isolators attached at a single transverse plane through the vertical center line of the cage

while Configuration 3 consists of six identical isolators attached to the cage in an upper plane and six identical isolators attached in a lower plane. The isolators for the single plane system will be designated No. 2, while the upper and lower isolators for the two-plane system will be designated No. 3U and No. 3L, respectively.

Each of the isolators is intended to perform satisfactorily at static load variations indicated in Table 4-1. The static loads on the isolators are

Isolator No.	No. 2	No. 3U	No. 3L
Nominal Load (Kips)	421	560	282

At the equilibrium position, X_0 , the uncoupled circular frequency, ω_0 , of all isolators is fixed at 2.199 radians per second. Then for all three isolators

$$\frac{A}{V_0} = - \frac{(2.199)^2}{386 [-143.197 + (2 \times 64.518)]} = 8.846 \times 10^{-4} \text{ inch}^{-1}$$

and

$$\frac{dF}{dX} = F_0 [0.01252 + 0.00009 (X - X_0)]$$

where X and X_0 are in inches and dF/dX is in pounds per inch.

The second term within the brackets in the equation above is the nonlinear contribution to the stiffness. In this case, it may be seen that the nonlinearity is relatively small. For example, at an excursion of the system of as much as 30 inches, the change in stiffness from its equilibrium value is only about 20 per cent.

4.2.7 Manufacturers' Preliminary Data and Designs

Basic shock isolator functional requirements were estimated early in the progress of this study. The following shock isolator functional requirements were based on the shock environment furnished by AFWL, and on the use of a sufficient number of isolators to support the full cage load:

Spring Rate	6,000 pounds/inch
Static Load	432,000 pounds
Dynamic Excursion	<u>±</u> 36 inches
Operating Cycles	40 cycles of 36-inch single amplitude and 1000 cycles of 1/2-inch single amplitude

Five industrial organizations provided preliminary designs, budget costs and damping and minimum friction data for liquid springs. They were:

Cleveland Pneumatic Tool Company, Cleveland, Ohio (CPT)
H. W. Loud Machine Works, Inc., Pomona, California (LMW)
Menasco Manufacturing Company, Burbank, California (MMC)
Taylor Devices, Inc., North Tonawanda, New York (TD)
Westinghouse Electric Corporation, Sunnyvale, California (WEC)

A summary of the design features evident from the data furnished is shown in Table 4-4 and a summary of procurement data is shown in Table 4-5.

The design concepts employed by the five manufacturers are shown in Figures 4-3 and 4-5.

Figure 4-3 depicts the concept employed by Taylor Devices, Inc., and is described in a preceding paragraph.

Taylor Devices reports that this concept provides significant advantages. They are:

- . The cylindrical piston and stud closure concept has less tendency toward transverse deflection; it is more stable than the simple cylinder, piston and piston rod configuration of Figure 4-2.
- . Secondly, the seals operate against the inside diameter of a tube rather than on the outside diameter of a rod (which they claim improves seal life by a factor of three).
- . The device provides an annular area between the closure stud and the piston cylinder inside diameter which may be used to locate damping orifices, valves and stroke limiting devices.

Figure 4-5 shows a simple, extended rod, piston and cylinder device. This design was recommended by Cleveland Pneumatic Tool, Menasco, Loud and Westinghouse. The design concept consists of a piston and a stepped rod, housed within a thick wall cylinder. The load is supported by means of fluid pressure acting on the differential area of the step in the piston rod. The piston is used to carry orifices so

Table 4-4 Liquid Spring Functional Data

Summary of Manu- fac- turers	Physical Details			Operational Details			
	Weight (Kips)	Length (feet)	Outside Diameter (Inches)	Static Pressure (Psig, Thousands)	Thermal Expansion (Inch Per Degree F.)	Friction	
						Nominal Sliding Friction (%Equili- brium Force)	Minimum Sliding Friction (%Equili- brium Force)
Maxi- mum	31.4	27.3	40	25.7	0.6	10	5
Mini- mum	9.17	20.8	19	19	0.3	2.8	1.4
Average	22.4	22.3	30.2	21.8	0.43	5.1	2.5

Table 4-5 Liquid Spring Procurement Data

Summary of Manufacturers	Shipping Time - One (1) Spring (Weeks)	Shipping Time - Twelve Springs (Weeks)	Engineering Cost (Dollars)	Total Cost Twelve Springs (Dollars)
Maximum	39	52	50,000	1,500,000
Minimum	20	36	8,000	302,000
Average	30	40.4	26,000	710,000

that fluid damping can be incorporated. The five manufacturers were asked to provide a mathematical representation of the damping inherent in their liquid spring design and estimates regarding minimizing seal friction. They reported as follows:

Menasco Manufacturing Company

Damping is nonlinear and consists primarily of a velocity squared term, $C_1 \dot{X}^2$. To treat this mathematically, Menasco normally uses an equivalent viscous damping term, $C_2 \dot{X}$, where C_2 is the coefficient of equivalent damping. The coefficient is obtained by determining experimentally the energy dissipated by a prototype and equating the actual energy loss to the linear viscous damping loss.

Seal friction in the basic Menasco design is about three per cent of the load at equilibrium. Seal friction can be reduced by a factor of about two, from three per cent to one-and-a-half per cent without significant research expenditure. This may be accomplished by reducing the length of the seal, which reduces the total radial seal load on the piston rod. This method of reducing friction is a trade-off of life for low friction since reduction in seal length lowers seal life. Menasco states that the nominal design life is well in excess of the specified life of 40 cycles of 36-inch single amplitude and 1,000 cycles of 1/2-inch single amplitude, and that reduced seal life resulting from lowered seal length and friction will still exceed the specified life by a comfortable margin.

Taylor Devices, Inc.

The damping force is described by the equation:

$$C_1 \frac{\dot{X}}{|\dot{X}|} (X + C_2) + C_3 \dot{X} + C_4 \dot{X}^2 + C_5 M_f \ddot{X}$$

where

- C_1 and C_2 = Coefficients of coulomb friction of seal
- C_3 = Coefficient of viscous damping
- C_4 = Coefficient of hydraulic damping
- C_5 = Coefficient of liquid inertial damping
- M_f = Liquid mass
- X = Displacement

Taylor Devices is not able to furnish the values of the coefficients and suggests that a separate study program be initiated to obtain a set of empirical curves to describe the liquid spring characteristics. The range of total friction force in the Taylor Devices design may be represented as sketched in Figure 4-12 for the conditions of this study.

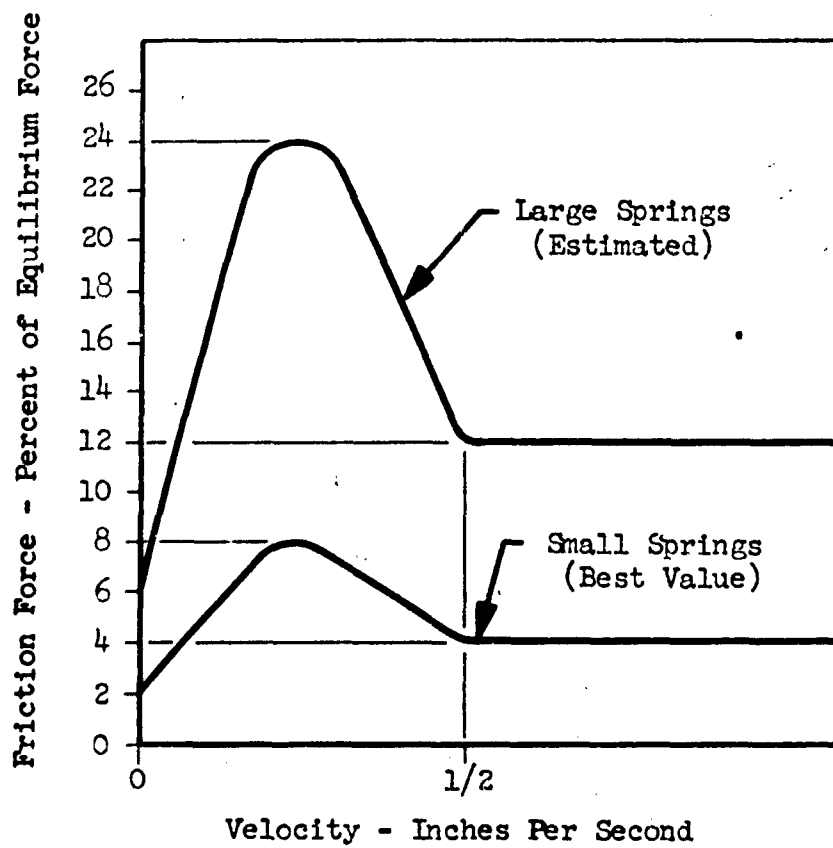


Figure 4-12.

Range of Friction with Velocity in Taylor Devices
Liquid Spring

Westinghouse Electric Corporation

Liquid spring damping will consist of coulomb, viscous and velocity squared components. Westinghouse normally linearizes this to viscous damping by the same means reported by Menasco. A discussion of this treatment may be found in Reference 11.

Friction may be reduced by the same means indicated by the Menasco Manufacturing Company, and with the same reduction in spring life. Westinghouse states that friction tends to increase during breakaway followed by a reduction as velocity increases.

Figure 4-13 shows a median force displacement curve for the five isolator designs. No curve deviated from the median by more than four per cent at minimum stroke and two per cent at maximum stroke. Also shown for comparison is a linear characteristic. It may be noted that the deviation of the median from the linear curve at maximum stroke is about three per cent.

The wide variation in estimated cost figures shown in Table 4-5 is attributed to the fact that only preliminary concepts were solicited and thus the development and testing programs considered by each supplier may be far from similar.

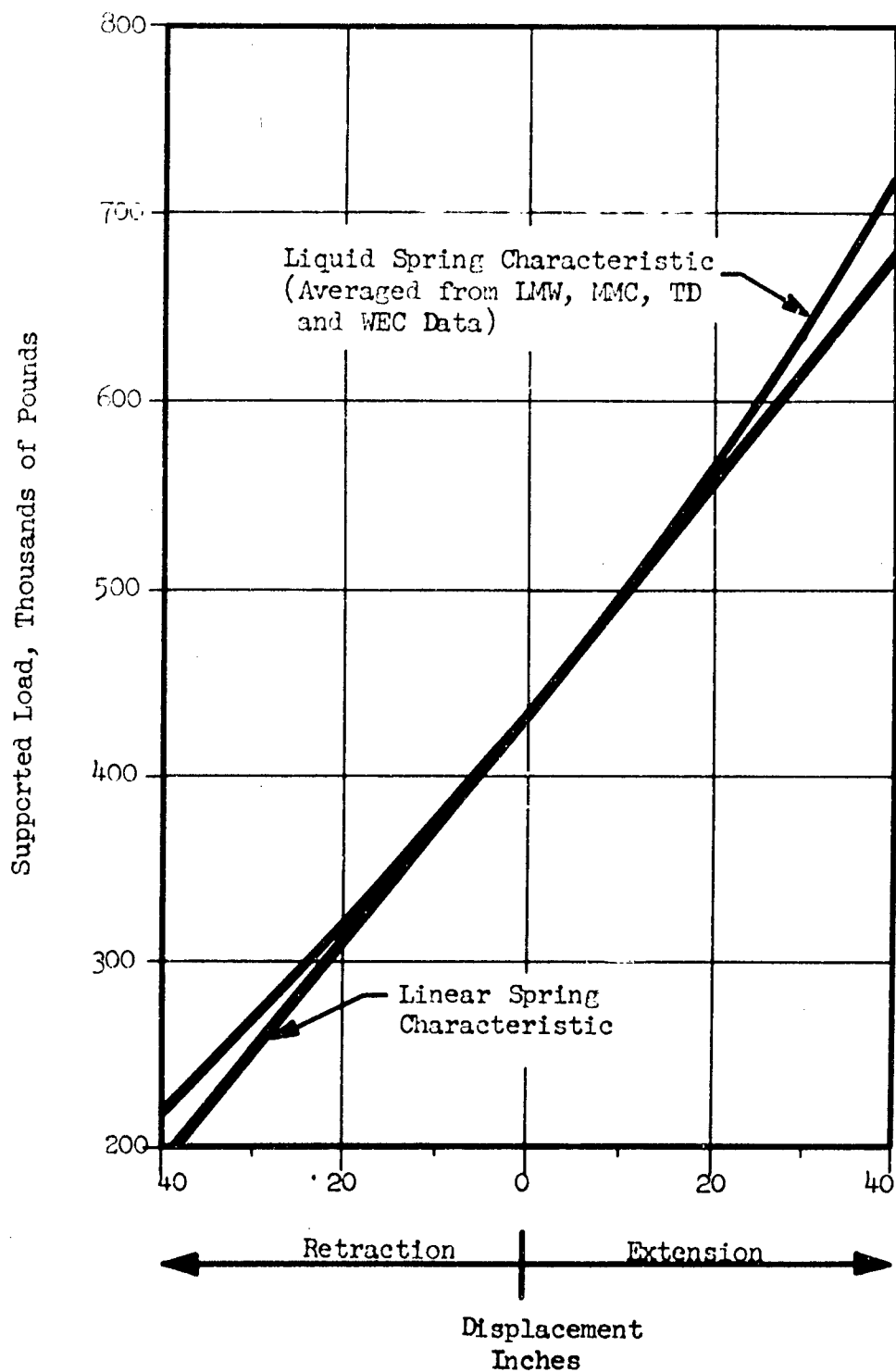


Figure 4-13. Shock Isolator Average Spring Rate.

4.3 Pneumatic Spring Concept

4.3.1 Introduction

Many of the advantages, both in size and performance, of fluid isolation devices have been mentioned in previous sections. Of particular interest, insofar as performance is concerned, is the ease with which load adjustments can be made, the inherent stiffness compensation, and the integral damping features.

From the viewpoint of operating principle, the pneumatic spring need be no different from the liquid spring. In its simplest concept it consists only of an air-filled cylinder and a piston. Its stiffness characteristic then is near to the slope of an adiabatic compression curve. It is evident, of course, that this simple arrangement is unidirectional; that is, it will always produce a force in one direction like the liquid springs discussed earlier in this section.

A large number of different methods of employing the pneumatic principle to shock isolation have been in use for many years. Only recently, however, has concerted attention been given to the application of pneumatic devices to use in underground protective structures. Only in one known instance, the Launch Control Center suspension system for WS133A, has the pneumatic spring been adapted to the particular needs of protection from the severe ground shock resulting from nuclear explosions. Test and operating experience with the WS133A Launch Control Center system has led to several advanced concepts which achieve less friction and fluid leakage and, in the smaller sizes, incorporate a variable effective area piston, whose area-stroke relationship can be tailored to match a broad range of desirable performance characteristics. One unit, the Parsons Model 133B Pneumatic Isolator, is shown schematically in Figure 4-14.

The advantage of the variable area feature is that it provides an additional parameter for the control of the instantaneous stiffness of the system. It is particularly useful in minimizing excursions from the equilibrium position due to otherwise uncompensated temperature or load changes. In this facility an isolator position controller is to be provided. Thus, the need for area variation with stroke is obviated.

4.3.2 Description of Pneumatic Isolator

A schematic diagram of the pneumatic isolator to be used as a model in this analysis is shown in Figure 4-15. The isolator is essentially a cylinder-piston system, except that the piston seals have been replaced by an elastomeric sleeve, which is permanently attached both to the piston and to the cylinder wall. The fold in the sleeve "rolls" in the annular clearance between the piston and cylinder with relative motion of these parts. The advantages of the rolling sleeve over the conventional sliding pressure seal are that it reduces leakage to an almost negligible value, eliminates friction due to sealing and reduces the number of parts requiring precision machining.

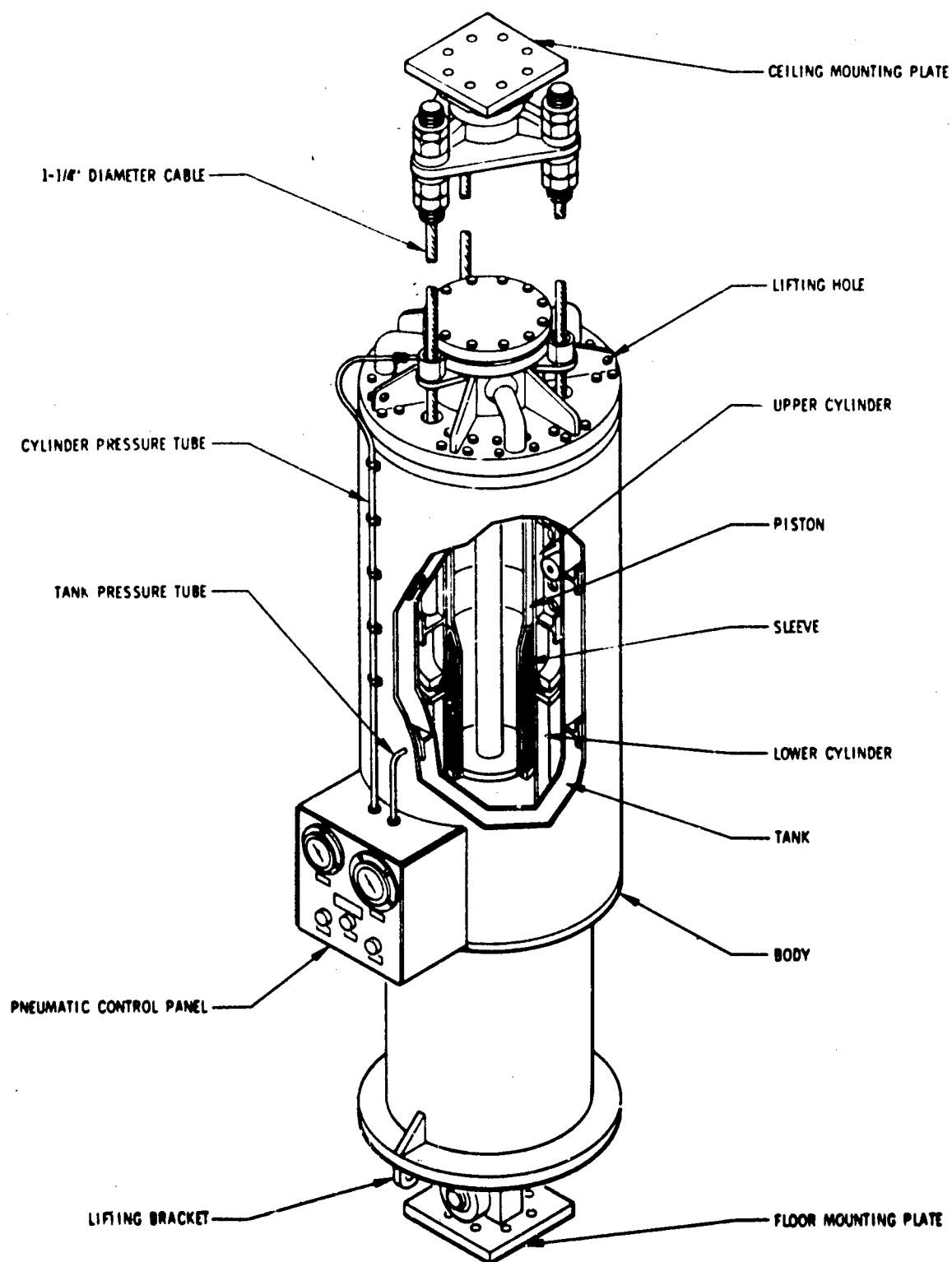


Figure 4-14. Parsons Model 133-B Pneumatic Isolator (Patent Applied For).

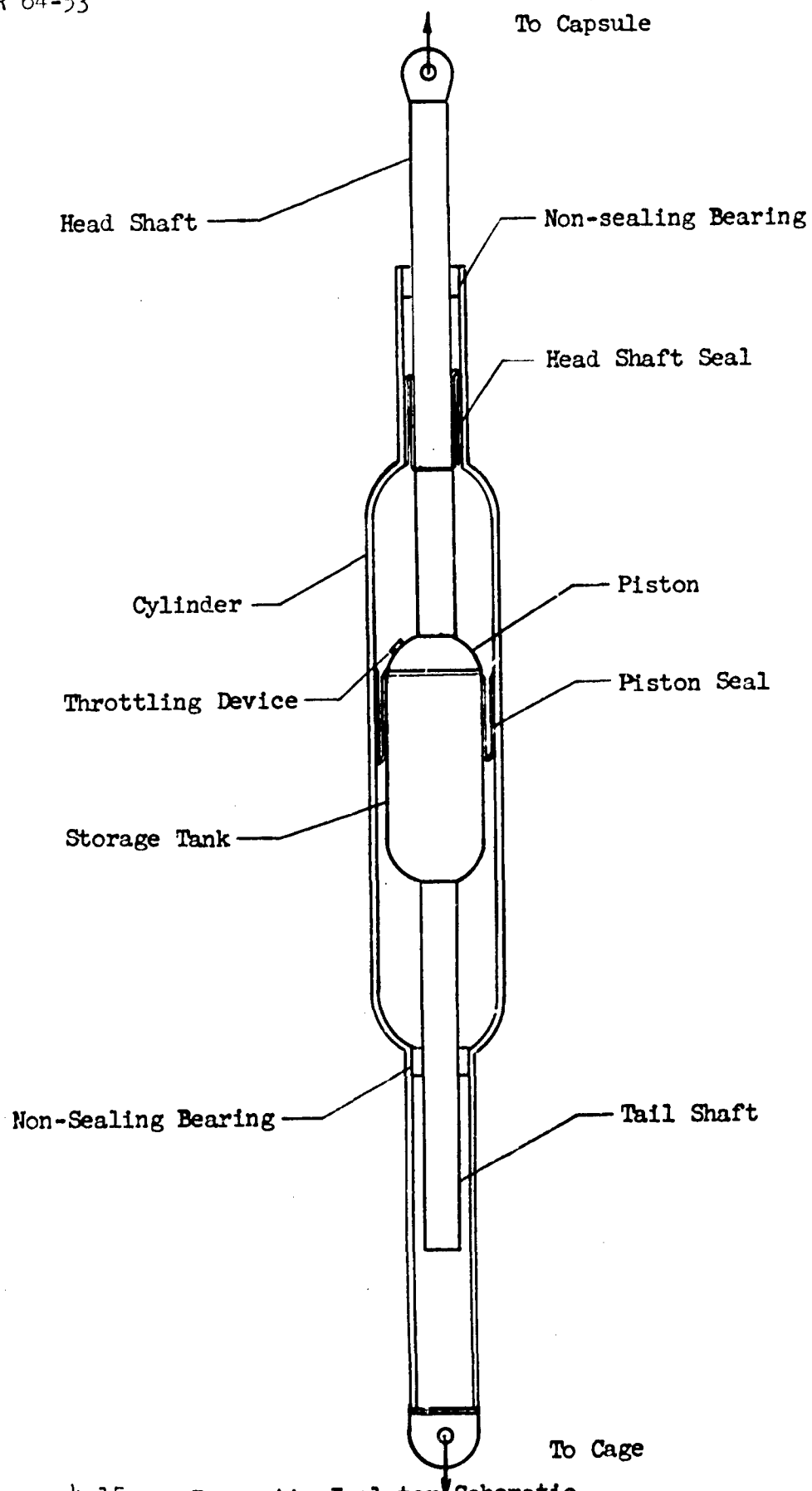


Figure 4-15. Pneumatic Isolator Schematic.

Neglecting powers of c greater than one,

$$V_i \approx \pi r(ru + 2ch)$$

$$dV_i = \pi r(r - c)du$$

4.3.5 Stiffness at Equilibrium

The force exerted by the isolator is

$$F = (P_i - P_a)A$$

where

F = force

P_i = cylinder pressure

P_a = atmospheric pressure

A = effective area of piston

The stiffness is given by

$$\frac{dF}{du} = A \frac{dP}{du}$$

To evaluate dP/du , the flow characteristics of the throttling device between the cylinder and the tank must be defined. If it consists of a valve which is closed when the isolator is in the equilibrium position, the rate of change of pressure with displacement is dependent only on the cylinder volume. If on the other hand, throttling is accomplished by a capillary, orifice or similar device which is always open to permit a small but finite flow of air between the cylinder and the tank, the equilibrium stiffness can be best defined by considering both volumes. To make the analysis more general it will be assumed that both volumes are effective.

For small excursions from equilibrium, then, the variation in pressure with volume is

$$\frac{dP_i}{dV_i} = -n P_{i_o} \left[\frac{(V_{i_o} + V_T)^n}{(V_{i_o} + V_T)^{n+1}} \right]$$

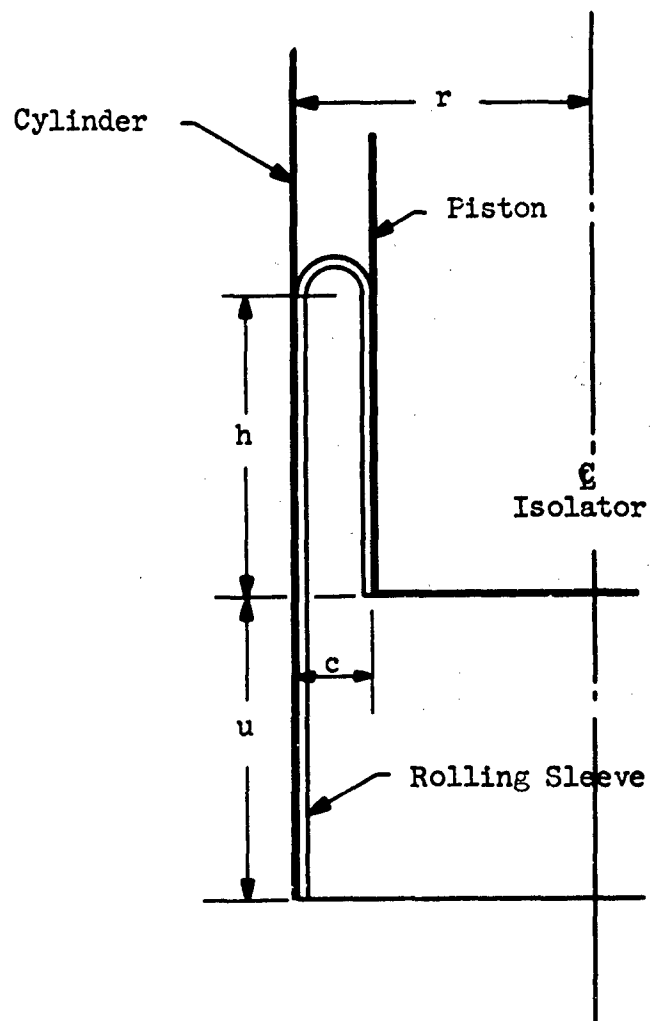


Figure 4-16 . Geometry of Rolling Sleeve Seal

Table 4-6 Summary of Isolator Requirements

Requirement	Configura- tion 2	Configuration 3	
		Upper	Lower
Circular Frequency (nominal), Radians/Second	2.20	2.20	2.20
Maximum Load (Static), Kips	557	742	371
Maximum Load (Dynamic), Kips	836	1113	557
Minimum Load (Static), Kips	302	402	201
Maximum Relative Displacement, Inches	± 70	± 70	± 70
Stiffness at Maximum Static Load, Pounds/Foot	83,700	111,500	55,860
Stiffness at Minimum Static Load, Pounds/Foot	45,380	60,400	30,260
Temperature Variation, °F.	± 10	± 10	± 10

The length of the rolling sleeve is

$$L = u + 2h + \frac{\pi c}{2}$$

As the sleeve is elastic, there will be some change in length with pressure. Thus,

$$dh = -\frac{du}{2} + dL(P)$$

However, the strain in the sleeve due to pressure is important only in that it results in some variation in the system volume with pressure. If $c \ll r$, this effect on system performance may be neglected.

The volume of gas contained within the cylinder is

$$V_1 = \pi \left\{ r^2(u + h) - (r - c)^2 h + \frac{\pi c^2}{2} \left(r - \frac{c}{2} \right) \right\}$$

Neglecting powers of c greater than one,

$$V_i \approx \pi r(ru + 2ch)$$

$$dV_i = \pi r(r - c)du$$

4.3.5 Stiffness at Equilibrium

The force exerted by the isolator is

$$F = (P_i - P_a)A$$

where

F = force

P_i = cylinder pressure

P_a = atmospheric pressure

A = effective area of piston

The stiffness is given by

$$\frac{dF}{du} = A \frac{dP}{du}$$

To evaluate dP/du , the flow characteristics of the throttling device between the cylinder and the tank must be defined. If it consists of a valve which is closed when the isolator is in the equilibrium position, the rate of change of pressure with displacement is dependent only on the cylinder volume. If on the other hand, throttling is accomplished by a capillary, orifice or similar device which is always open to permit a small but finite flow of air between the cylinder and the tank, the equilibrium stiffness can be best defined by considering both volumes. To make the analysis more general it will be assumed that both volumes are effective.

For small excursions from equilibrium, then, the variation in pressure with volume is

$$\frac{dP_i}{dV_i} = -n P_{i_o} \left[\frac{(V_{i_o} + V_T)^n}{(V_{i_o} + V_T)^{n+1}} \right]$$

where

n = polytropic index for appropriate gas process

V_{i0} = initial volume of cylinder

V_T = volume of tank

P_{i0} = initial pressure in cylinder

Then for small displacements, $V_i \rightarrow V_{i0}$

$$\frac{dP_i}{dV_i} \rightarrow - \frac{n P_o}{V_{i0} + V_T}$$

And by substitution, the stiffness at the equilibrium position is given by

$$\frac{dF}{du} = \frac{-n F_o A}{(V_{i0} + V_T)}$$

where F_o is the equilibrium load on the isolator.

The value of n is dependent upon the velocities of the excursions from equilibrium. For example, if the excursion takes place very slowly, the compression process is essentially isothermal and $n=1.0$. If, further, the throttle will permit a small flow of air to maintain equal pressures in tank and cylinder, the slow response frequency of the isolator is

$$\omega_s^2 = \frac{Ag}{V_{i0} + V_T}$$

If the excursion occurs rapidly, the value of n approaches 1.4. To determine the frequency in this case, the characteristic of the flow throttling device must be defined in greater detail. As an upper limit, however, if the device closed off completely the flow between tank and cylinder, the frequency would be

$$\omega_f^2 = \frac{-nAg}{V_{i0}}$$

4.3.6 Temperature Sensitivity

The excursions of the piston from its equilibrium position due to changes in the temperature of the environment can be obtained by considering the state of the gas in the cylinder and tank. If the throttle is closed and no gas is permitted to enter or to leave the cylinder,

$$\frac{dV_i}{V_i} = \frac{dT}{T}$$

$$du = \left\{ \frac{V_i}{\pi r(r - c)} \right\} \frac{dT}{T}$$

If the gas is permitted to flow freely between cylinder and tank

$$du = \left[\frac{V_i + V_T}{\pi r(r - c)} \right] \frac{dT}{T}$$

If a controller is used to maintain the equilibrium position during temperature changes, the weight flow of air required to maintain the position is

$$\frac{dw}{dt} = - \frac{w_o}{T_o} \frac{dT}{dt}$$

4.3.7 Calculation of Isolator Sizes

Although the stiffnesses and frequencies presented in the previous paragraphs can be used to estimate with good accuracy the behavior of the system for small oscillations about the equilibrium position, the period of the pneumatic isolator, a nonlinear device, is dependent on the amplitude of oscillation as well as on the parameters shown in the equations. It is desirable from the viewpoint of pendulum suspension system stability to ensure that the period of oscillations of the isolator does not fall far below the value of 1/0.35 in order to minimize coupling with the pendulum mode (section 3.0). To determine the actual period of the pneumatic isolator, however, particular flow characteristics must be assigned to the valves and the nonlinear differential equations of motion solved for a range of response amplitudes and input shocks.

This analysis has not been carried to this degree of detail since the feasibility of the isolator is not critically dependent on variations in dimensions or flow characteristics of the magnitude introduced by this effect.

On the basis of the simple equations presented for static equilibrium conditions, the gross sizes of the isolator elements are determined. It is assumed that the throttling device for all isolators is such that while the flow characteristics may be arbitrary, even to the extent of being dependent on flow direction, the pressures in the tank and cylinder will equalize soon after relative motion between the piston and cylinder has ceased. The maximum air pressure is fixed at 1000 psi at a dynamic load of 110 percent of the maximum values shown in Table 4-6 and the gap width, c , at 1-1/2 inches.

The basic isolator dimensions are shown in Table 4-7. Whether or not the tank volumes indicated are sufficient to provide the damping required can only be determined by analysis of the complete system. In any case, the volume ratio could be increased appreciably and the throttle setting adjusted to yield essentially the same dynamic frequency.

Table 4-7 Basic Pneumatic Isolator Dimensions

	Configuration 2	Configuration 3	
		Upper	Lower
Effective Area (Square Inches)	920	1225	613
Maximum Equilibrium Pressure (Psia)	620	620	620
$V_i + V_t$ (Cubic Inches)	102,800	136,900	71,500
Cylinder Inside Radius (r) (Inches)	17.86	20.50	14.70
Approx. Cylinder Volume (Cubic Inches)	80,000	110,000	55,000
Ratio Tank Volume/Cylinder Volume	0.28	0.24	0.30

4.3.8 Pneumatic Spring Stiffness Equations

The stiffness of the pneumatic isolator was given earlier as

$$\frac{dF}{du} = A \frac{dP}{du}$$

Under dynamic conditions the simple expression used earlier to relate pressure to displacement is no longer valid due to the flow of air through the throttle. To determine the cylinder pressure at any time, it is necessary to know the state of the gas both in the cylinder and the tank. The derivation of the stiffness equation given in Reference 13 is presented here.

Thus,

$$\frac{dP_i}{P_i} = \frac{dw_i}{w_i} + \frac{dT_i}{T_i} - \frac{du}{u}$$

$$\frac{dP_T}{P_T} = \frac{dw_T}{w_T} + \frac{dT_T}{T_T}$$

where $dV_i/V_i \cong du/u$

The energy equation for the gas in the cylinder is

$$dq_i = C_p dT_i - v_i dP_i$$

where

q_i = heat transferred to or from gas in isolator

C_p = specific heat of gas in isolator

Letting $dq = 0$ and since $v_i = \frac{V_i}{w_i}$, $\frac{dT_i}{T_i} = \left(\frac{\gamma - 1}{\gamma} \right) \frac{dP_i}{P_i}$

where γ = ratio of specific heats for air

Substituting in the equation of state, we get

$$\frac{dP_i}{P_i} - \gamma \left[\frac{dw_i}{w_i} - \frac{du}{u} \right]$$

Similarly

$$\frac{dP_T}{P_T} = \gamma \left[\frac{dw_T}{w_T} \right] = -\gamma \left[\frac{dw_i}{w_T} \right]$$

Note that $dw_T = -dw_i$, but to evaluate the flow of gas between the tank and cylinder, the characteristics of the throttling device must be defined. If the expression for the flow rate is a timewise continuous function, however, it will be dependent on the state of the gas upstream and downstream but not on the derivatives of the gas properties.

Substituting in the stiffness equation, we obtain

$$\frac{dF}{du} = -\gamma AP_i \left[\frac{1}{u} - \frac{\dot{w}_i}{w_i u} \right]$$

Note that the first term in the brackets gives the stiffness of the closed cylinder as shown previously, while the contribution to the instantaneous stiffness provided by the gas flow is indicated by the second term.

4.4 Sway Damper Concepts

The elimination of post attack horizontal oscillations and the reduction of resonant and coupling effects dictate the need for damping in the horizontal direction. Horizontal damping may be obtained by:

- . Inclining the vertical isolators so that a portion of their spring and damping effect acts in the horizontal direction
- . Providing separate damping devices, oriented to operate horizontally

These damping concepts are discussed in section 3.0, and devices for use with the second approach are covered here. Three devices are considered; pneumatic and hydraulic dashpots, coulomb dampers and polyurethane foam collars.

Recent studies on similar projects resulted in a shock isolation system similar to the one being considered here (Reference 14); a cylindrical cage, supported in a multifilar pendulum arrangement within a domed cylindrical capsule (Figure 4-17). In that system, rattlespace was minimized; the vertical isolators were slightly inclined, and separate horizontal sway dampers were provided, located symmetrically at the top and bottom of the cage. Ten shock isolators were provided, located at equal intervals around the circumference of the suspended cage. Ten sway dampers were also provided with five in a horizontal plane above the top and five in a horizontal plane below the bottom of the cage. The sway dampers were cylinder and piston devices, connected at the piston rod end to the capsule and at the cylinder end to the suspended cage. The connections were made by means of spherical bearings. As shown in Figure 4-17, the sway dampers did not lie in a radial direction, but were oriented more nearly tangentially to the suspended cage. This orientation was felt to be necessary so that the sway dampers could be effective against cage rotations.

Although no detailed cost analysis was made of the system, rough estimates indicated that the cost of the sway dampers would be appreciable. Further, due to their large size and weight, they would be cumbersome to install and to maintain. The earliest work done on the subject of sway damping in this study was to find means for simplifying the system and reduce its cost. The study on polyurethane collars and the concept of sway damping by the component of inclined isolators resulted from this work.

It would be beneficial for the damping device design to be such as to permit simple adjustment of its characteristics. The need for adjustability derives from the isolator requirements of load and stiffness variation and temperature sensitivity and adjustability.

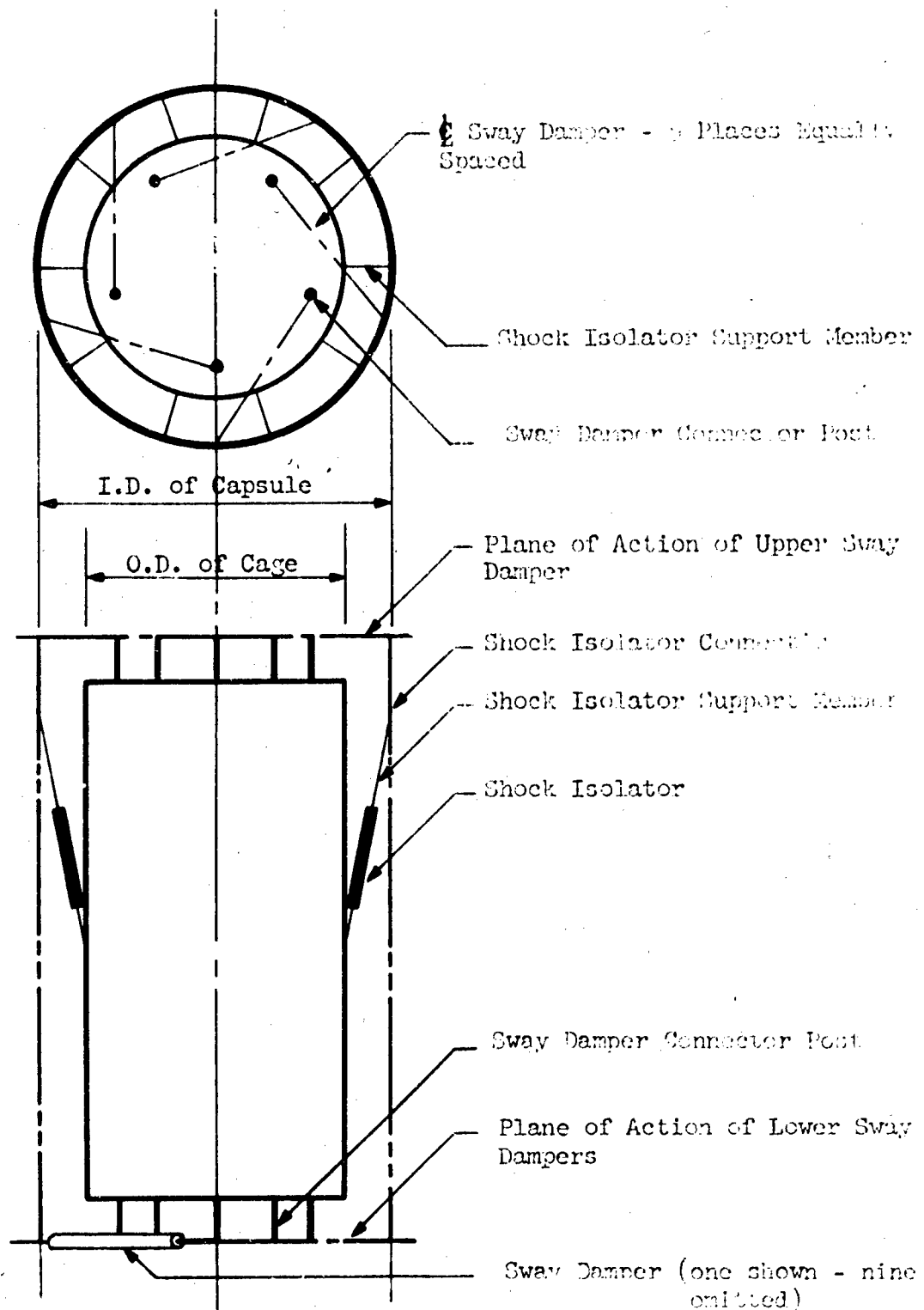


Figure 4-17. Shock Isolation System With Separate Sway Dampers.

Best Available Copy

A damper of adjustable characteristics will permit overall system adjustment to hold the relationship between vertical and horizontal characteristics equal.

At the equilibrium position of the suspension systems considered here, friction is considered to be objectionable. Friction is particularly troublesome for the horizontal direction in pendular systems, since the restoring forces are much smaller than for the vertical direction (Figure 4-24). Therefore, it is concluded that friction forces at the equilibrium position or center position should be small in order to prevent malpositioning.

It has been shown in Reference 2 that the shock isolation system will become unstable if the ratio of the system's vertical and horizontal frequencies is close to two. The stiffness of the horizontal sway dampers will be in parallel with the effective horizontal stiffness of the pendular system. Holding the vertical to horizontal frequency ratio at 2.0 or higher requires setting an upper limit to the stiffness of the sway dampers.

The vertical frequency has been fixed at 0.35 cps based on overall system needs. The horizontal frequency must be held to

$$\omega_{sn} \leq \frac{\omega_v}{2} \leq \frac{0.70\pi}{2} \leq 1.1 \text{ radians per second}$$

For the small fraction of equivalent viscous damping to be supplied in this application, the damped natural frequency can be assumed equal to the undamped frequency. The horizontal frequency can be shown to be

$$\omega_{sn} = \sqrt{\frac{K_{sd}g}{W} + \frac{g}{R}} \leq 1.1 \text{ radians per second}$$

for the single plane pendular system, which is considered for use with separated sway dampers. In this system R is seventy feet and the nominal weight, W, is 5.052×10^6 pounds. Solving for K_{sd} ,

$$K_{sd} \leq \frac{(1.1)^2 - \frac{386}{840}}{386} \left[5.052 \times 10^6 \right] \leq 9830 \text{ pounds per inch}$$

This fixes the upper limit of effective sway damper stiffness at 9,830 pounds per inch.

4.4.1 Pneumatic and Coulomb Damper Concepts

Pneumatic sway dampers normally take the form of simple double-acting dashpots, vented at appropriate positions along their stroke.

Pneumatic dampers obtain their energy dissipating characteristics in part from coulomb friction but primarily from the discharge of the contained gas after compression. These dampers normally operate by means of relative motion of a piston device within some form of cylindrical housing. Each of the two basic damping forces can be modified significantly by appropriate design and manufacture of the parts.

The working medium used in the pneumatic sway damper tends to dry out lubricants; hence, it tends to produce more and more friction with time. This effect can be eliminated by design and maintenance; however, designing to employ friction and to preclude lubrication and maintenance would appear to be a more desirable approach.

Coulomb Friction

A friction force is generated in a piston and cylinder device between the piston and the internal surface of the cylinder and between the piston rod and its bearing and seal.

These forces may be increased by controlling lubrication (or the lack of lubrication), normal force of the piston or piston seals on the cylinder wall, normal force of the rod seal on the piston rod, and selection of the rubbing materials. These forces may be decreased to very small magnitudes by careful design and materials selection, but friction cannot be completely eliminated.

When designing a device with the intention of employing coulomb friction as a component of the damping force, the following precautions should be observed:

- . Select a configuration which provides zero or near zero force over the critical stroke region near the system equilibrium position.
- . Select materials with frictional characteristics which do not change with exposure to dust, aging, temperature change, wear.
- . Protect the design from contaminants which will alter its friction force capability.

- . Preload the wearing surfaces so that the friction force remains essentially constant as the wear surface is removed, and so that the friction force can be altered by adjustment of the preload.
- . Select a fine enough surface finish so that the friction force does not change as the surface gets smoother with wear.

Two devices employing coulomb friction are shown in Figures 4-18 and 4-19 along with their load stroke characteristics. These devices are not recommended for use here; they are shown only to illustrate existing designs employing the principles discussed. The simple vented dashpot was used in the Launch Equipment Room shock isolation system in the WS 133A Weapons System. The load stroke characteristic shown was obtained from a load stroke test with a 2 cps sinusoidal stroke input of 10-inch double amplitude. It was estimated that coulomb friction produced most of the energy dissipation from this device and resulted in badly worn piston cups after about one thousand inches of travel. The force due to compression of the air is significant only at the extremity of the stroke.

The Coulomb Friction Damper shown in Figure 4-19, a development of Houdaille Industries, Inc., of Buffalo, New York, is an attractive damping device with one significant exception. It will cause system malposition. A similar device, eliminating the zero position friction load is discussed in a later paragraph.

Pneumatic Damping

The pneumatic dashpot makes use of the gas compression relationship $p v^n = \text{constant}$. The pneumatic damping device does work in compressing the enclosed gas. At the end of the compression stroke, the gas is discharged from the device and the compression force drops to zero. Then on the return stroke the air in the opposite side of the device is compressed, then released. This action provides the load stroke relationship shown in Figure 4-20. If the stroke occurs in a short time interval, and assuming no leakage and constant specific heat of the gas, the polytropic compression exponent approaches 1.4, the adiabatic exponent for air. However, as the stroke is slowed down so that heat transfer occurs and also as the system leaks, the compression will have an effective exponent between 0 and 1.4.

Maximum energy will be dissipated from the oscillating system when adiabatic compression is achieved and when the compressed, heated gas is discharged from the device at the end of the compression stroke. The adiabatic compression will be approached at the piston velocities expected here and with normal commercial cup seals. The gas discharge

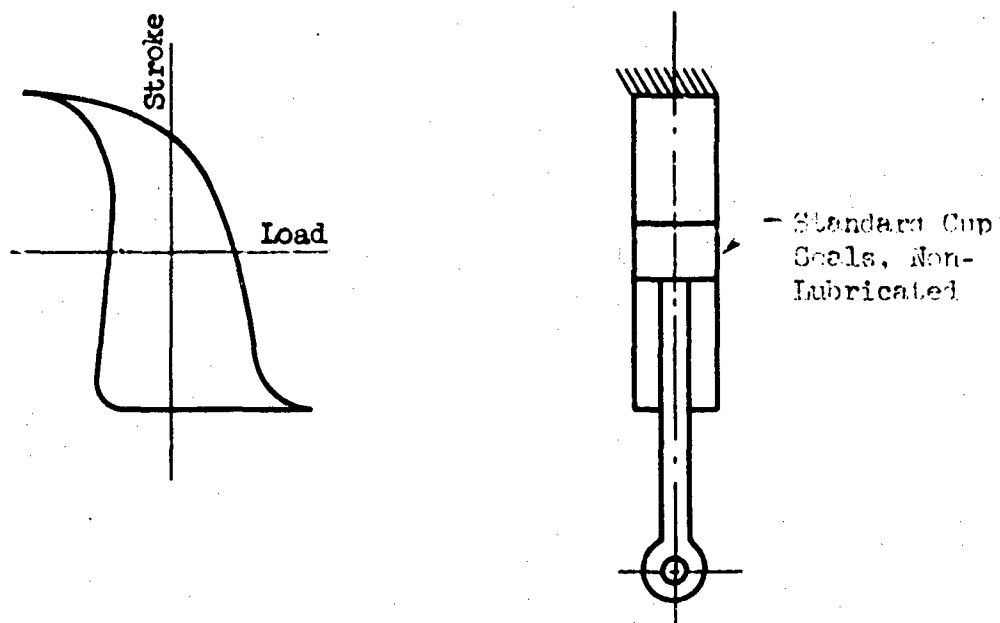
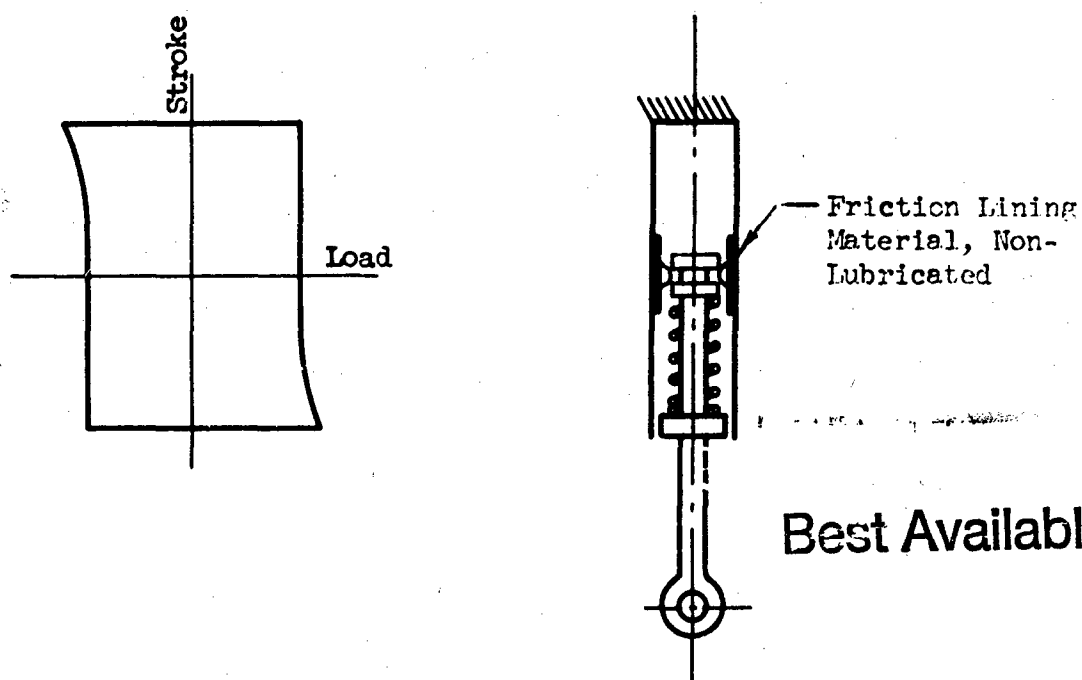


Figure 4-18. Vented Dashpot With Coulomb Friction.



Best Available Copy

Figure 4-19. Coulomb Friction Damper. (Proprietary with Houdaille Industries, Inc.)

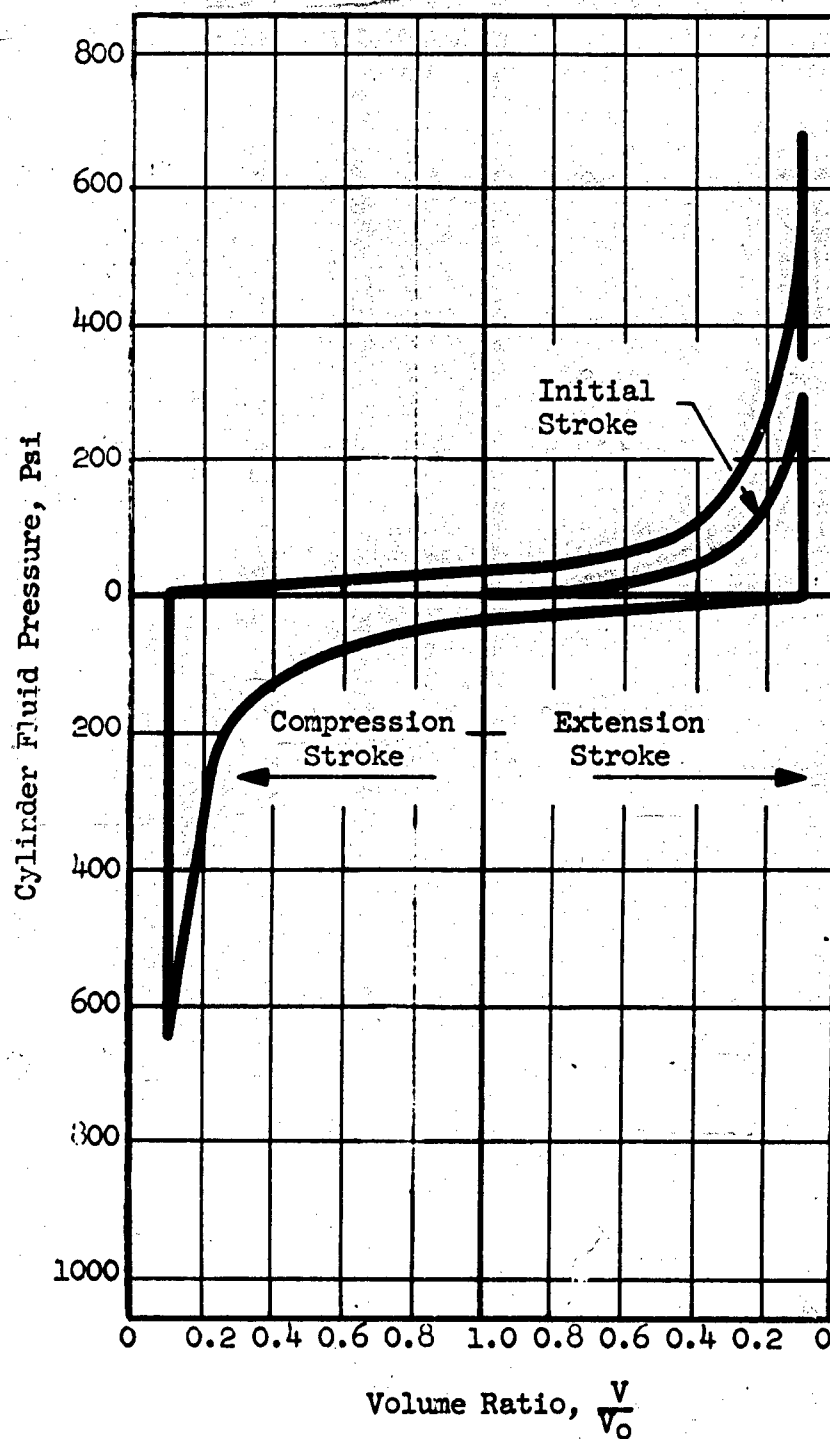


Figure 4-20. Load Stroke Characteristic for Pneumatic Dashpot With Quick Air Release Device.

can be realized by incorporating suitable valving in the system. A pneumatic damper incorporating a slide valve was used in the Launch Control Center Shock isolation system on the WS 133A Weapon System. This concept is shown in Figure 4-21. The slide valve contains the

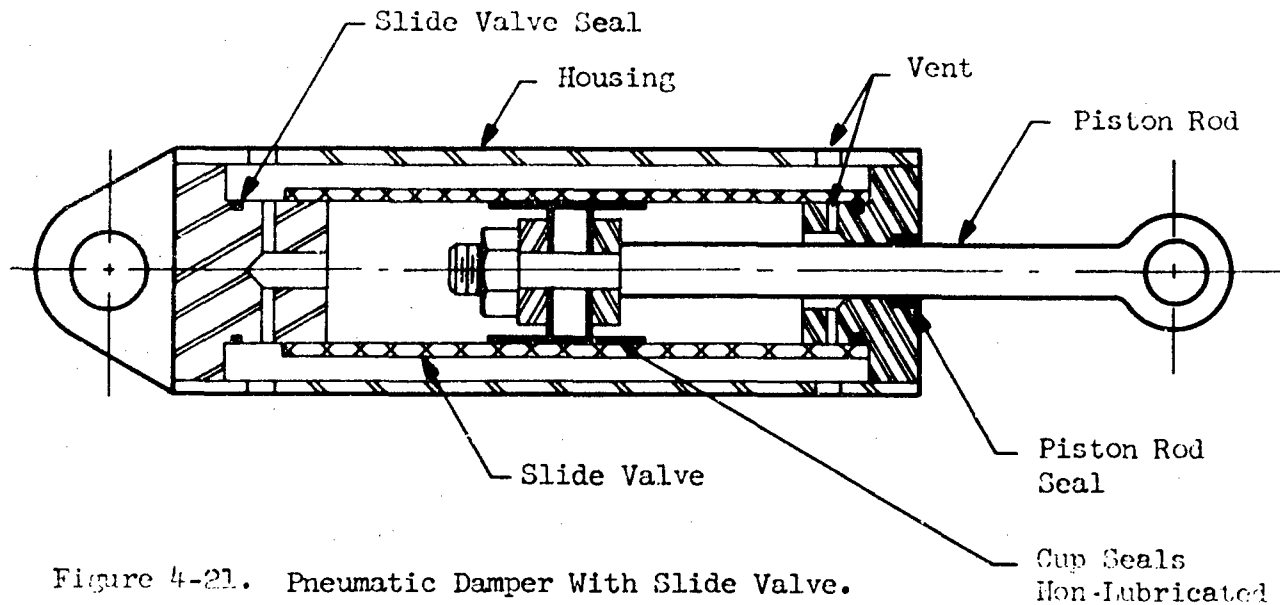


Figure 4-21. Pneumatic Damper With Slide Valve.

compressed gases until the direction of motion reverses, then gas discharge occurs. This concept suffers from coulomb forces at the equilibrium position, as do those shown in the preceding figures. The expected optimum damping from the pneumatic damper is evident from Figure 4-20. For construction of Figure 4-20, the polytropic exponent was taken as 1.3 and relative volumes were taken from Figure 4-21. Comparison of the load stroke characteristic of the coulomb damping effect and the damping due to venting of compressed gas indicates that use of the vented pneumatic device is inefficient.

4.4.2 Coulomb Damper Concept

A coulomb damping device incorporating means for eliminating the problems normally encountered with coulomb damping is shown in Figures 4-22 and 4-23. It consists of a spring loaded moving shoe, rubbing against constrained automotive brake band lining. The brake-band lining is housed within a structural steel frame.

The problems normally encountered with coulomb friction in low frequency suspension systems are due to lack of predictability of the friction load and failure of the system to return to the equilibrium position.

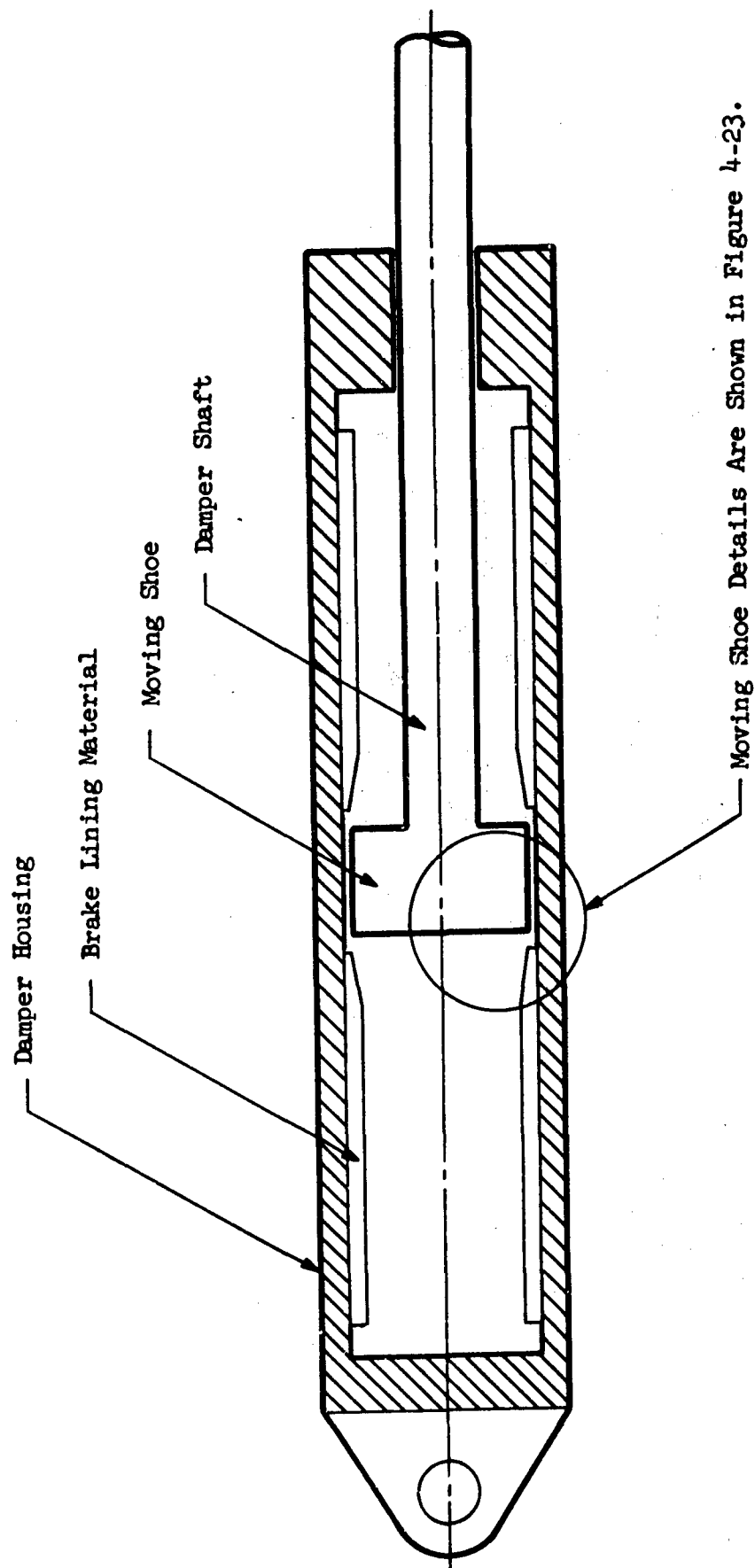


Figure 4-22. Coulomb Damper Concept.

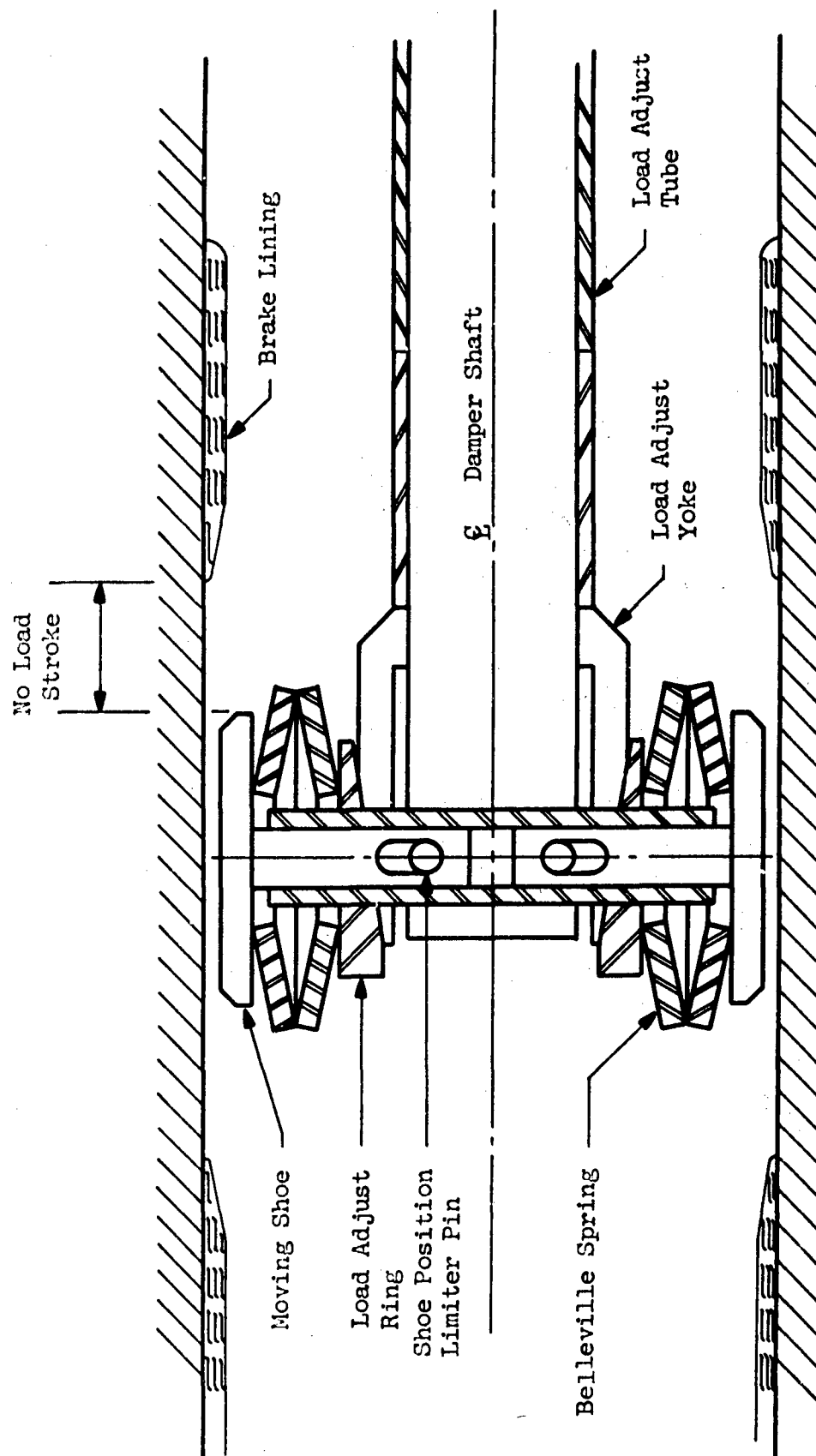


Figure 4-23. Coulomb Damper Moving Shoe Details.

The predictability of the coulomb friction may be optimized by providing a design wherein the forces applied to the friction-producing surfaces remain approximately constant during dimensional changes due to wear and inaccuracies of manufacture. In addition, it is required that the force-deflection characteristic be adjustable. These can be obtained in the concept shown here by applying the load by means of Belleville springs of cone height to disc thickness ratio of about 1.25. This cone-height to disc-thickness ratio will provide a spring of variable stiffness where the stiffness is sizable, then becomes quite small and then increases rapidly. This will permit designing the device to a preload where minor changes in preload deflection do not significantly modify the coulomb force; however, there is retained the capability to significantly modify the coulomb force by adjustment of spring deflection. Selection of a cone-height to disc-thickness ratio of 1.25 also eliminates the secondary Belleville spring problem of "pop through," where the spring suddenly deflects under load without addition of load.

Failure of a system to return to the equilibrium position when friction is present results from the friction force overcoming the restoring force of the system near the region of the equilibrium position. Therefore, to overcome this problem, the coulomb damper force must be made smaller than the restoring force over the full displacement of the system so that the system will be self-centering. For pendulum systems, the restoring force is zero at the equilibrium position and increases approximately linearly, for small angular displacements, as shown in Figure 4-24. The nominal system weight was used to construct the restoring force curve of Figure 4-24.

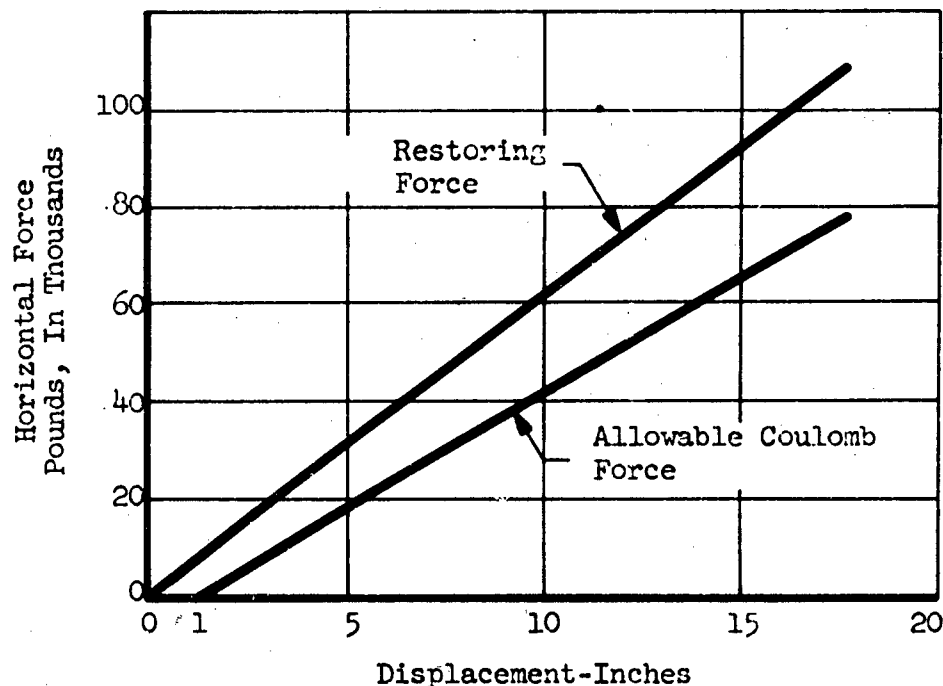


Figure 4-24. Assumed Force Relationship For An Underdamped Pendulum System.

Allowing 5,000 pounds for total miscellaneous friction in connections and bearings and allowing 33 per cent over the total coulomb damper force for static friction of the device, the total allowable coulomb force in Figure 4-24 was constructed. This defines the upper limit of allowable sway damper force.

Allowing a no load displacement of 3-1/2 inches, the total allowable damper force is about 11,200 pounds. Assuming constant force in the coulomb damper the load deflection characteristics of a single damper is shown in Figure 4-25.

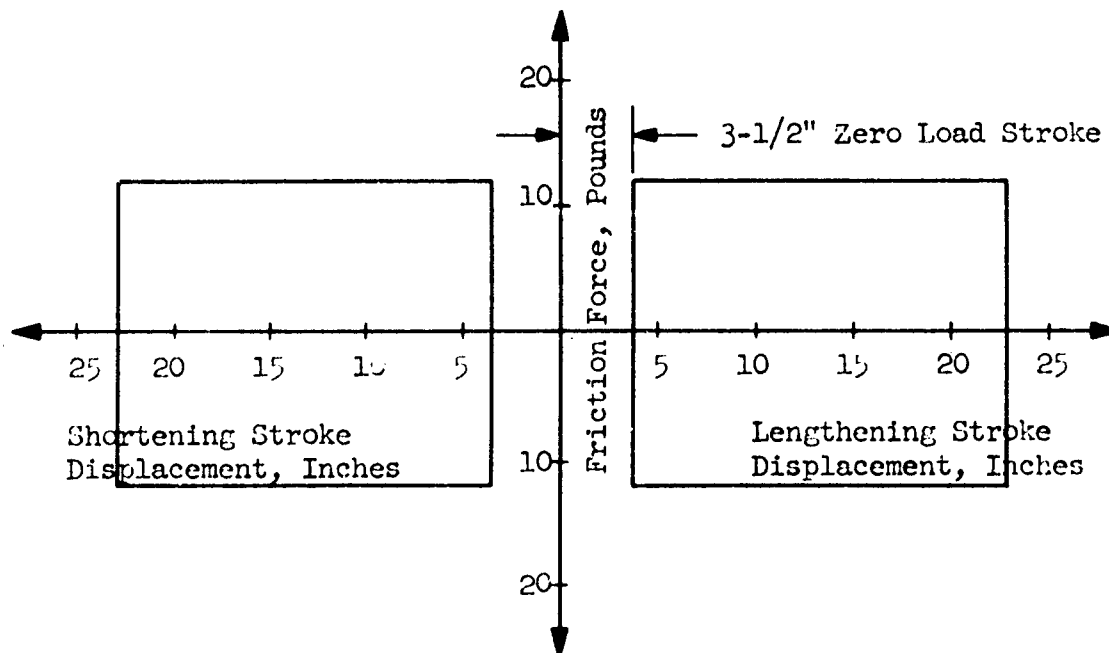


Figure 4-25. Coulomb Damper With Stepped Load-Displacement Characteristic.

The work done in one cycle of all the coulomb dampers required by a system, described by the characteristics of Figure 4-25 is $4 \times 11,200 \times (22 - 3.5) = 828,800$ pounds-inches. This is about two per cent of equivalent viscous damping for a 22-inch single amplitude.

The zero load stroke about the system equilibrium position is obtained in the device shown in Figure 4-22 by providing clearance between the moving shoe and the brake lining material over the desired zero load stroke. The load stroke characteristic of Figure 4-25 shows an instantaneous rise to peak friction force. The actual load stroke characteristics of the real device will have a finite rise time and

the step function shown will be some curve depending on the clearances between parts, surface irregularities and a slight change in spring force with shoe deflection. These effects are expected to be quite small, and are neglected in this study. The stepped load-displacement characteristic will cause jerkiness of the system and will probably cause detrimental accelerations. This problem can be mitigated by designing the friction damper with minimized spring preload on the moving shoe and tapering the brake lining material so that the normal force of moving shoe on the friction material increases over the critical initial few inches of stroke to the selected damping force. The resulting optimized load deflection characteristic is shown in Figure 4-26.

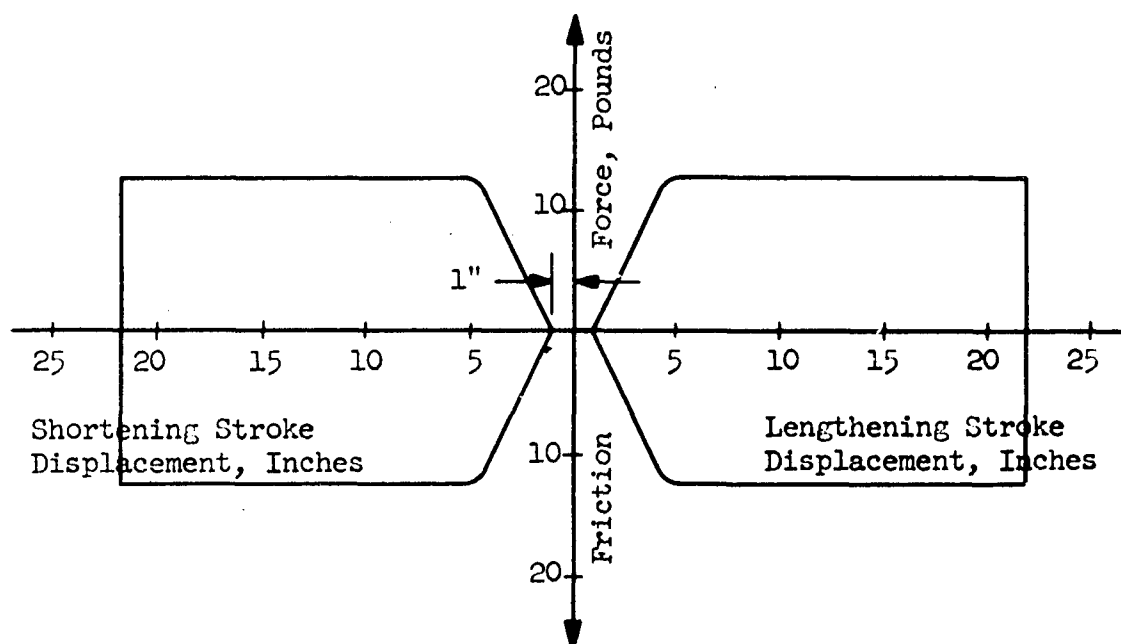


Figure 4.26. Coulomb Damper With Optimized Load-Displacement Characteristic.

A second benefit is obtained with the optimized characteristic compared with the stepped characteristic: the zero load stroke can be minimized and maximum damping can be achieved with a device meeting the characteristics of Figure 4-26.

4.4.3 Hydraulic Sway Damper Concepts

The hydraulic sway damper concepts are similar in principle to the liquid spring, except that the sway damper designs normally operate at much lower pressures.

The energy dissipation mechanisms found in hydraulic sway dampers are the same as those discussed in the section on liquid spring damping, coulomb friction and fluid flow losses. The coulomb friction was shown to be quite significant in the liquid spring; however, this resulted from the assumed initial pressure of 20,000 psi. In the normal hydraulic device, the seal friction losses will be minor.

The hydraulic energy-dissipating devices normally take either of two forms: linear motion piston and cylinder devices or rotary devices. Most commercially available devices employ orifices and valving to obtain damping. The damping is obtained by losses occurring when the fluid is forced through orifices and valves and varies with the square of velocity. When these devices are used in applications subject to high-velocity input, blowoff valves are normally incorporated to eliminate serious excessive pressures. In this application, it is desired to obtain damping during free pendulum oscillations and yet not introduce excessive acceleration during exposure to the high-velocity portion of the ground motion. Therefore, the hydraulic sway damper must be designed to produce the desired damping for a piston velocity of about 334 inches per second, but not generate excessive loads at the peak velocity of about 300 inches per second.

Of the three kinds of damping (coulomb, viscous and hydraulic), the coulomb damper requires least peak force, followed by the viscous and lastly by the hydraulic, assuming equal energy dissipation. A linear motion piston and cylinder device will be analyzed for a damper application. Since viscous damping is considered more desirable than hydraulic damping, the device will be configured to make use of the viscous characteristic. Consider the simple piston and cylinder configuration shown in Figure 4-27. The piston and hole variables will be sized to obtain laminar flow.

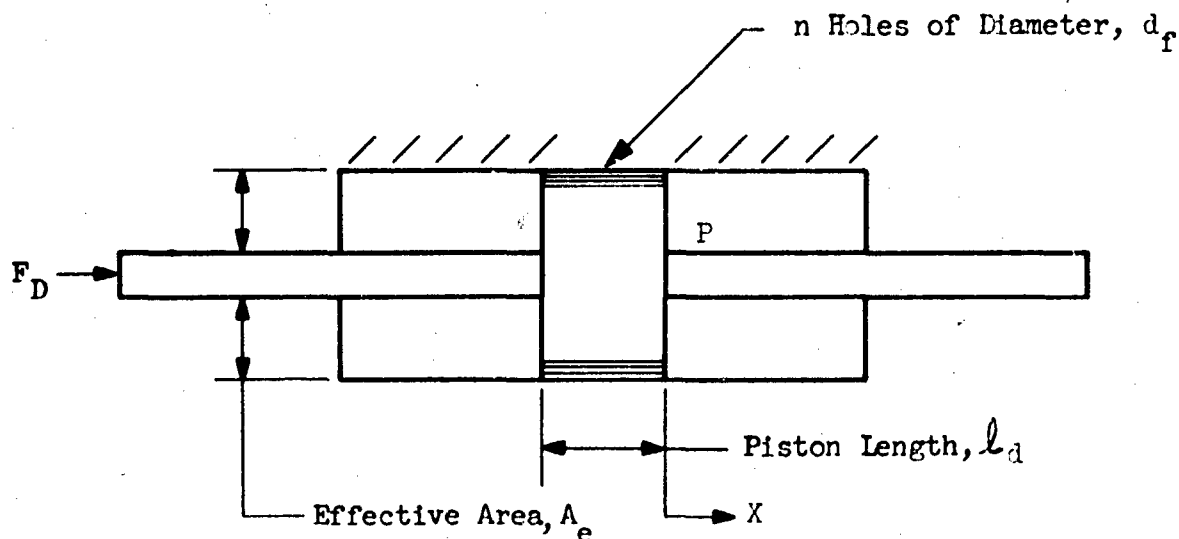


Figure 4-27. Schematic of a Simple Linear Motion Damper.

It is assumed that the fluid is incompressible, all surfaces are smooth with no abrupt discontinuities, and the total peak damping force applies 0.1 g on the suspended cage. In addition to the maximum damping force assumption, a design Reynolds number of 1300 will be used for a piston velocity of 18 inches per second. The Reynolds number is fixed at 1300 so that under conditions of increased temperature the flow will remain laminar.

It is further assumed that twelve dampers are installed in a system similar to the one shown in Figure 4-17. In this case, there would be six dampers at the top and six at the bottom of the cage. The maximum damping force in a sway damper will be, from geometry, one-eighth of the total force; then

$$F_d = P A_e = \frac{0.1W}{8}$$

The fluid flow that occurs for any displacement, X, is

$$A_e X$$

and the flow rate will be

$$A_e \frac{dX}{dt} = A_e V_p$$

where V_p is the piston velocity. Then the fluid velocity, V_f , through the holes in the piston will be

$$V_f = \frac{4 A_e V_p}{n \pi d_f^2}$$

The frictional head loss across the piston will follow the Darcy equation,

$$h_L = f \frac{l_d}{d_f} \frac{V_f^2}{2g}$$

For laminar flow, the friction factor f , is $64/N_R$. Since the Reynolds number has been defined at 1300, the frictional head loss becomes

$$h_L = \frac{64 l_d V_f^2}{2600 d_f g}$$

The velocity head will be determined, assuming that the entrance of each piston hole is rounded to avoid initial flow disturbances, and that the entrance loss is negligible. The flow distribution in the entrance will be uniform except for a thin fluid film at the surface of the hole which

is considered to be at rest. The kinetic energy of the flow increases from $\frac{V^2}{2g}$ at the entrance to $\frac{2V^2}{2g}$ at a location in the piston holes where

$$l'_d \approx 0.058 N_R d_f \quad (\text{Reference 15}).$$

V is the average velocity determined by dividing the volumetric flow rate by the sum of the hole areas. The location in the piston represented by l'_d is that location where the fluid velocity profile across the hole is a parabola.

Since the fluid is discharged into a region of essentially zero fluid velocity, the exit loss is considered equal to the flow kinetic energy. Therefore, the damping force becomes

$$F_d = PA_e = wA_e \left(h_L + \frac{2V_f^2}{2g} \right) = 63,200 \text{ pounds}$$

Substitution of h_L and V_f results in

$$wA_e \left[\left(\frac{64 l_d}{2600 d_f g} \right) \left(\frac{16A_e^2 V_p^2}{n^2 \pi^2 d_f^4} \right) + \frac{16A_e^2 V_p^2}{n^2 \pi^2 d_f^4 g} \right] = 63,200 \text{ pounds}$$

which can be reduced to

$$\frac{16w A_e^3 V_p^2}{n^2 \pi^2 d_f^4 g} \left[\frac{64 l_d}{2600 d_f} + 1 \right] = 63,200 \text{ pounds}$$

Noting that the first term in the bracket is the viscous contribution to the damping force, it is clear that the dominance of viscous effect can be controlled by selection of piston length, l_d , and hole diameter, d_f .

For a fluid having a specific gravity of 1.0, this equation becomes

$$\frac{A_e^3}{n^2 d_f^4} \left[\frac{64 l_d}{2600 d_f} + 1 \right] = 1.3 \times 10^6 \text{ square inches}$$

Selecting a piston length of 10 inches, a piston diameter of 6 inches, a rod size of 3 inches, and piston hole sizes of less than 1/8-inch diameter, the ratio of viscous to hydraulic damping for this configuration is about 2.

As the Reynolds number is reduced, the ratio of viscous to hydraulic damping is increased. By employing the very high viscosity silicone fluids recently developed, a linear motion damper having essentially no hydraulic damping can be obtained.

The holes should be arranged symmetrically about the piston rod center-line so as to minimize development of side loads. Inaccuracies of hole size and location and contamination will tend to produce side loads. The larger the number of holes selected the smaller will be the unbalance effect due to any one hole. An example using a piston diameter of six inches, and twenty holes of 0.10 inch diameter will be used. The next step is to select a fluid of proper kinematic viscosity.

$$N_R = \frac{V_f d_f}{\gamma} = 1300$$

$$\gamma = \frac{4 A_e V_p}{1300 \pi d_f}$$

$$\gamma = \frac{4 \times 21.2 \times 18}{26,000 \pi \times 0.10} = 0.187 \text{ inches}^2/\text{second}$$

$$\frac{0.187}{1.54 \times 10^{-3}} = 121 \text{ centistokes}$$

This is easily obtained by blending Dow Corning 510 fluids of 100 and 500 centistokes viscosity.

The available data indicate that this viscosity will be reduced to about 100 centistokes for a temperature rise of 20 degrees F. and to 80 centistokes for a temperature rise of 40 degrees F. Using an assumed fluid temperature rise of 40 degrees F., the Reynolds number becomes 1970 and the maximum damping force is reduced to 41,700 pounds.

Next, the problem of excessive pressures under high frequency input must be dealt with. It is suggested that the simplest, and most effective, method of preventing high transient pressures is to shock-isolate the piston on the piston rod by means of a near zero rate Belleville spring design, preloaded to develop the maximum working forces, but deflecting under shock loads. This device now meets all the necessary conditions for system damping, save the possible need for alteration of the damping characteristic to satisfy changed system parameters. This need can be met in practice by keying the piston to the housing, adding perforated plates at the ends of the piston which can be controlled by overtravel, and, then, rotating the spring loader tubes. The perforated plates would be rotated to line up with more or less holes in the piston by this means modifying the damping characteristics.

The completed concept is shown in Figure 4-28.

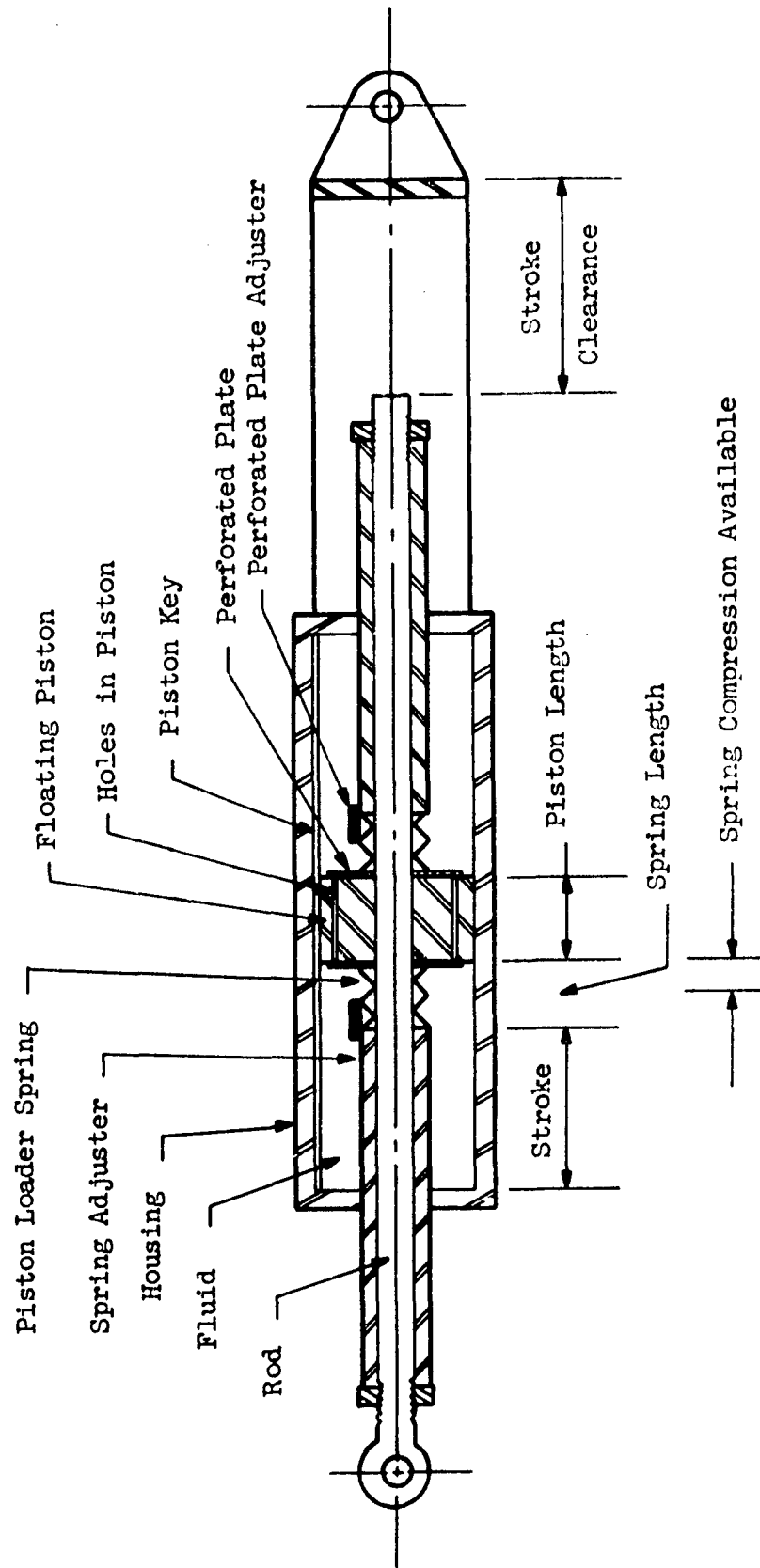


Figure 4-28. Concept for Viscous Damper With Force Limiting and Adjustable Damping Characteristics.

4.4.4 Polyurethane Collar Sway Dampers

4.4.4.1 Polyurethane Collar Sway Dampers Concepts

The concept of encircling the suspended cage structure with resilient polyurethane collars, one at the top and one at the bottom of the cage, is shown in Figure 4-29. As shown in the figure, the collars are not continuous, but rather are twelve segments, fifteen to twenty feet long, and approximately five feet thick, leaving gaps in width of approximately five feet. The gaps are required for two reasons:

- . To permit free movement of the shock isolator support members
- . To provide for air flow from the dome to the base of the capsule

The first requirement for gaps derives from suspension systems where the shock isolator connections are above the upper collar.

The polyurethane raw material is made from either of two raw materials: polyester or polyether. The polyether material is a relatively new development of lower raw material cost, which has improved aging and resiliency characteristics. The polyester-based material seems to have the advantage with respect to fabrication cost. This advantage derives from the "one-shot" process, which is reported in Reference 16 to be suitable for the polyester-based material only. Development of a similar process for the polyether-based material would appear to offer economic advantage.

The one-shot process consists of feeding the several mixtures used into a mixing nozzle, which mixes and delivers the mix into a moving mold. The foaming takes place after delivery of the liquid into the mold and is the result of a gas release due to the reaction of the liquid. As indicated above, manufacture of the polyether material has not been developed into a continuous process, but consists of machine-mixing in stages and mold-curing.

The flexible foamed polyurethanes exhibit considerable variation in load-deflection properties. Reference 16 shows four foams of 6 pound density where the stress at a strain level of 0.7 inch per inch varies between 3-1/2 psi and about 13 psi. It is also reported that the material can be compounded so that it returns to its initial shape very slowly after deflection. This characteristic could be employed to maximize damping characteristics; however, no published

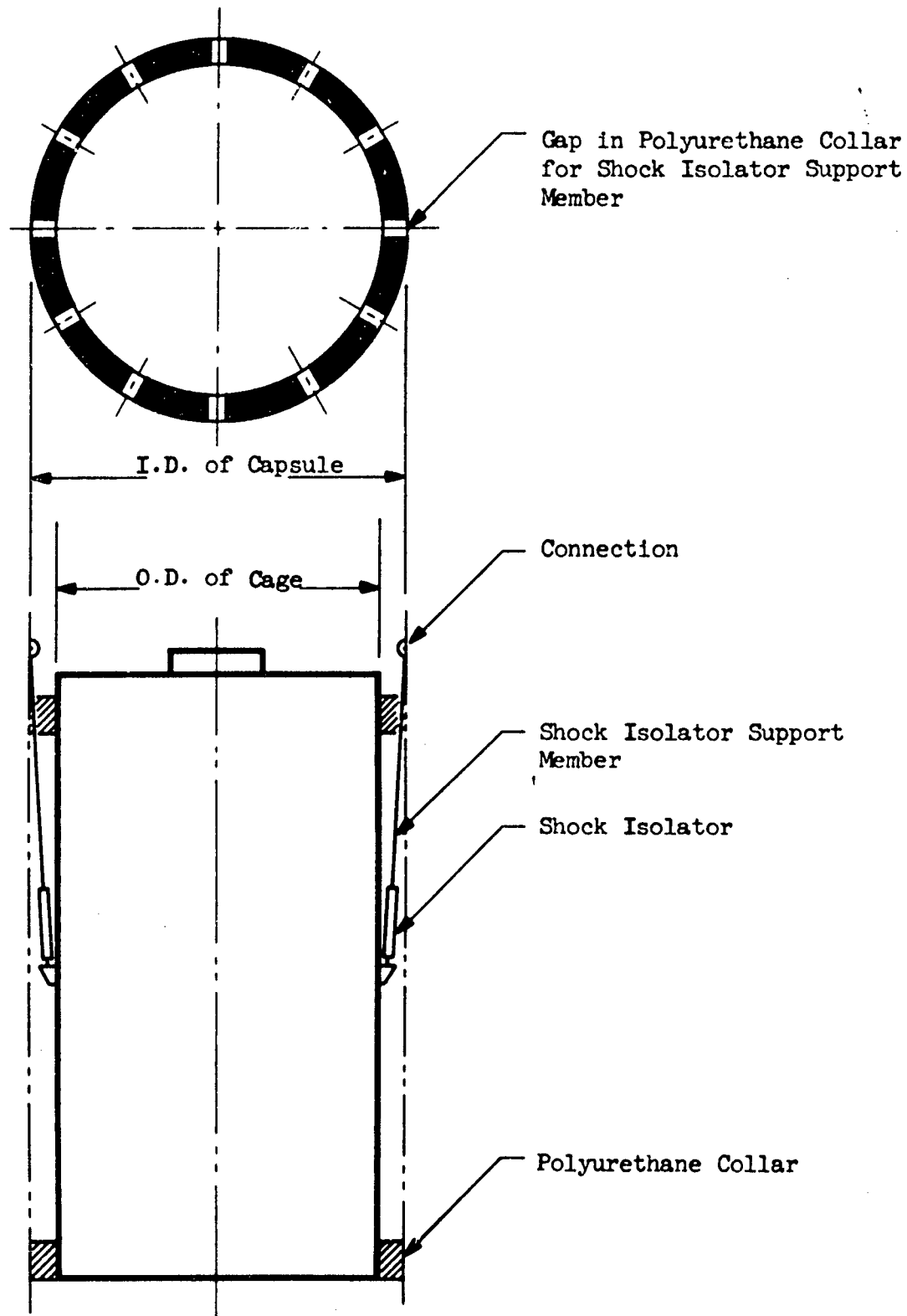


Figure 4-27. Polyurethane Collar Sway Dampers.

data are available to enable the designer to make use of this property. The stress-strain characteristic of three densities of foam are shown in Figure 4-30.

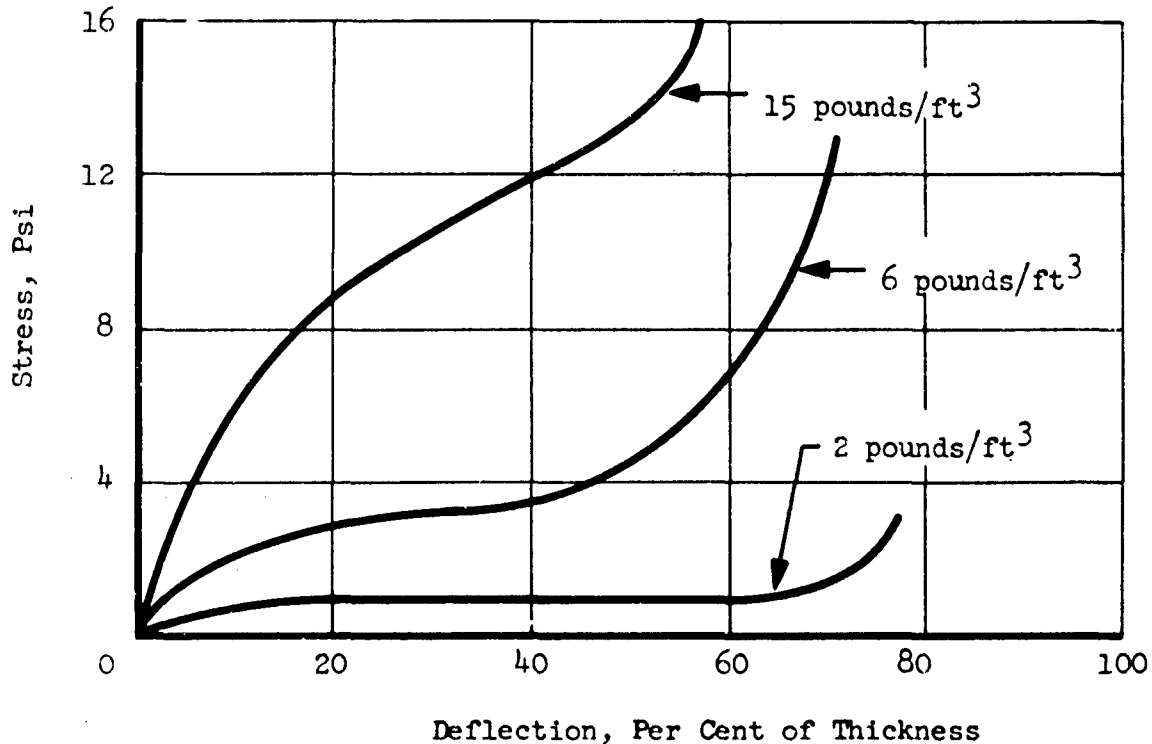


Figure 4-30. Stress-Strain Characteristics of Polyurethane Foams.

The stress-strain curves of these foams provide the following general characteristics:

- The initial slope of the curve is larger than successive slopes until the 50 per cent strain region is approached.
- The slope approaches zero and the load remains constant, in the 20-to-40 per cent strain region for low density foams (2 to 6 pounds per cubic foot).
- The slope approaches a constant value in the 20-to-40 per cent strain region for higher density foams (6 to 15 pounds per cubic foot).

- . The stiffness increases rapidly in the region of 60-to-80 per cent strain. The lower density foams exhibit the higher maximum strain, and the higher density foams exhibit higher stiffness.

The stress-strain curve used to determine scaled stiffness properties was obtained from averaged data of the loading and unloading curve of Sample No. 22 of Reference 17. These averaged data were used as follows to obtain a representative load deflection characteristic for the system shown in Figure 4-29.

- . The load deflection curve for Sample No. 22 of Reference 17 was averaged and plotted in Figure 4-31.
- . A layout of the cage-capsule-foam collar geometry was made.
- . The layout of the cage was displaced horizontally in 5-inch increments.
- . The average compression of each foam collar segment was determined.
- . The pressure response of each segment due to its average compression was determined from the averaged load deflection data of Sample No. 22 of Reference 17.
- . The total force resulting from compression of the foam collar segments was calculated for each 5-inch increment of displacement and plotted as total sway damper force versus deflection in Figure 4-32.

The averaged load deflection curve shown in Figure 4-32 was employed in paragraph 4.4.4.2.

The work done in scaling the damping effects (paragraph 4.4.4.2) resulted in a damping ratio which is disappointingly low. It must be emphasized, however, that this result cannot be applied generally to polyurethanes, since the low damping ratio was obtained from the data of tests on one sample which were reported in terms that are not amenable for direct scaling. Even more significant, the spring effect indicated by the averaged data of Figure 4-32 was assumed operable on the return stroke. The literature indicates that the total area under the load deflection curve can be used for energy dissipation by material compounding. In general, few data are available from which damping can be calculated.

The polyurethanes exhibit excellent aging characteristics, and oxidation resistance (up to 250°F.), and can be made fire-retardant or self-extinguishing. The polyester material loses its tensile strength under prolonged high humidity, while the polyether is only slightly affected. The ambient conditions of these facilities would provide excellent conditions for obtaining longevity from foam materials.

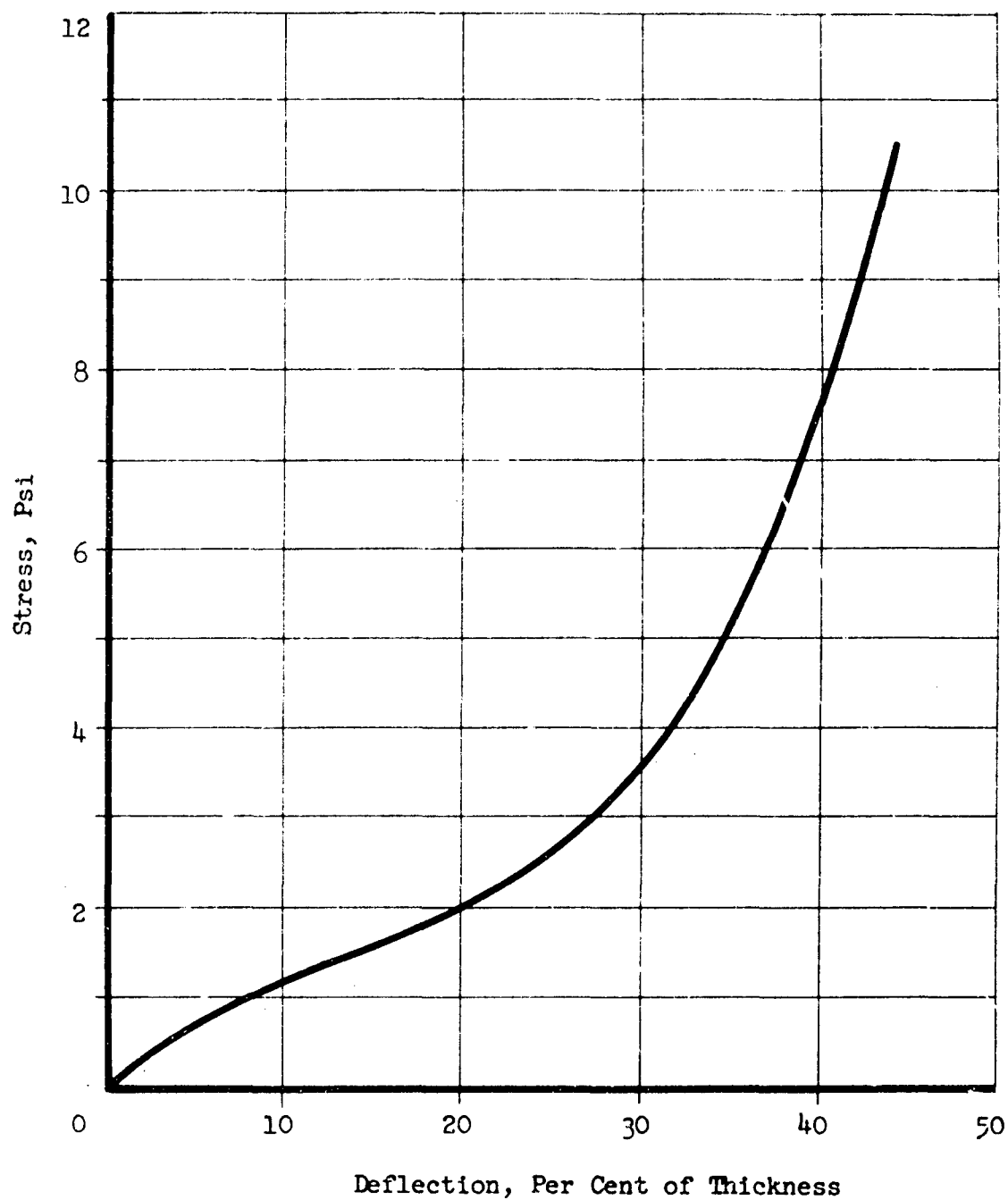


Figure 4-31. Averaged Load Deflection Characteristics of a Six Pound Density Polyurethane Foam.

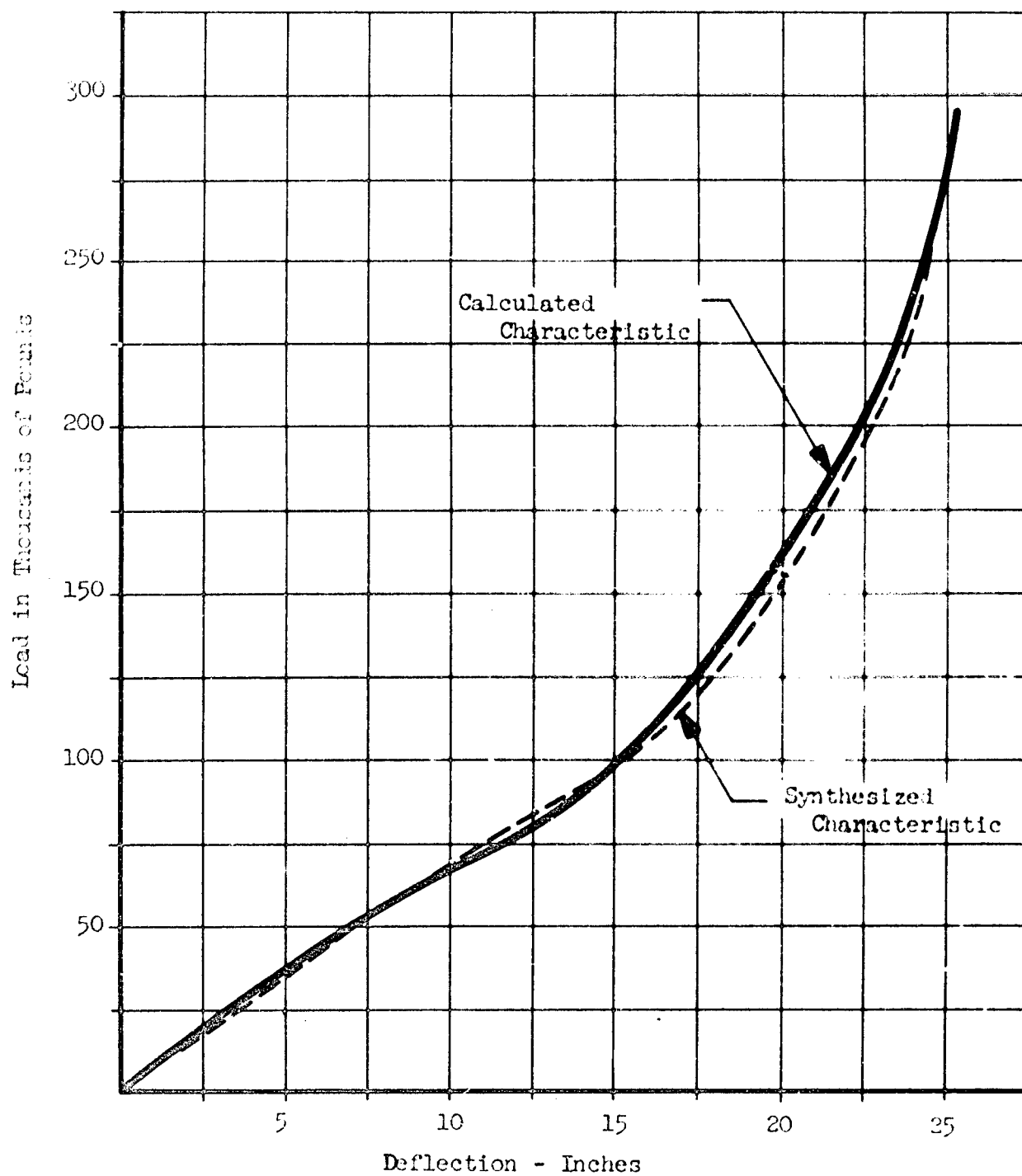


Figure 4-32. Polyurethane Sway Damper Load Deflection Characteristics.

Two configurations were examined: the first configuration consisted of bulk polyurethane material enclosed in an elastomer bag; the second configuration consisted of slabs of the raw material cemented together to form a collar segment of suitable dimensions and to a metal backing plate and an antifriction material.

The bagged-foam concept was employed by Westinghouse Electric Corporation in one design for the horizontal restraining members in a missile suspension system. The bags were made airtight and were filled with a foam of approximately four pounds per cubic foot density. It was found that the effect of the entrapped air could be represented by $p v^n = \text{constant}$, where $n = 1.3$ (Reference 18). It was reported that "the effect of variation in foam 'ventilation' properties is essentially masked or overridden by the cover effects under dynamic conditions," and "damping was reduced considerably by the segmented covers." Since the foam's ventilation properties are considered the only characteristic of significance regarding damping, then a device which degrades and masks the effect of changes in this characteristic will not be particularly useful in this application.

The WEC test results indicate that, in the bagged configuration, the horizontal mounts are "relatively insensitive to velocity. The only difference noted is the increased displacement and higher force due to the increased energy of the higher impact velocity. The stiffness remains the same for the spectrum of velocities....."

The air spring effect will produce excessive stiffness for this application and would hamper efforts to maximize damping. Secondly, elimination of the airtight bag would achieve a savings in cost.

The bulk material concept is shown in Figure 4-33 and consists of four slabs of foam, 15 feet long, 3 feet high, and 14 inches thick, cemented together, forming a 4-foot, 8-inch thick collar. This collar thickness is based on an estimate of rattlespace required for Configuration 1 which was made early in the progress of this study.

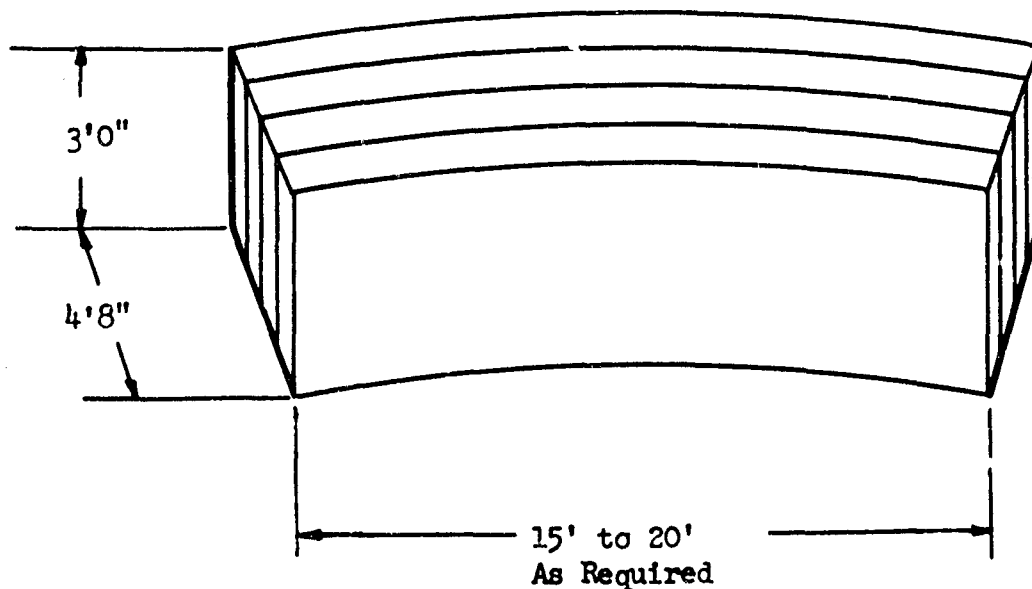


Figure 4-33. Polyurethane Sway Damper Collar Segment.

Slabs of this size are manufactured commercially in both the polyester and polyether materials. The design and use of large blocks of foamed plastics should avoid cementing more than two layers of material in more than one direction. If this precaution is not observed, a slab of the material will be isolated in the interior of the block. Such an isolated slab will act like a relatively stiff spring due to the compressibility of the trapped gas.

The face of the collar segment which rubs against the suspended cage should be coated with a film of Teflon to minimize friction loads. Assuming a friction factor of 0.1 and a pressure loading of about 8 psi on the heaviest loaded segment at a deflection of about 40 per cent, the shear stress is less than 1 psi. The shear capacity of the foam exceeds this load by approximately an order of magnitude.

Cost of bulk polyurethane material is reported in Reference 19 to be 60 to 70 cents per pound for the prepolymer-type and 45 to 55 cents per pound for the continuous mix process. Estimated costs for high density foam compounds, which now appear to be required here, vary between \$1.58 per pound by the CPR International Corporation to \$2.00 per pound by the American Urethane Division of Stauffer Chemical Corporation.

The system shown in Figure 4-29 and 4-33 will employ sixteen segments of 3-foot by 15-foot load area by 4 feet, 8 inches in thickness and eight slabs of 3-foot by 20-foot load area and 4 feet, 8 inches in thickness, for a total volume of 5,600 cubic feet. The raw slabs alone will cost approximately \$70,000.

4.4.4.2 Stiffness and Damping Characteristics of Polyurethane Collars

To determine the effectiveness of the polyurethane collars in damping and to compare their performance with those of other sway damper concepts, quantitative data on the fundamental damping parameters of polyurethane were needed. However, the very large number of different polyurethane foams which are commonly produced, coupled with an almost total lack of information on the dynamic properties of any of them, led, necessarily, to an effort to piece together data from several sources. The accuracy of the physical properties so obtained is questionable, but it is the only data now available to serve as a basis for gross comparisons with other damping methods.

Data Available

A fairly comprehensive examination of the literature on polyurethane foams and discussions with several manufacturers has led to the conclusion that there are few data available on its properties which characterize dynamic response. Not only are there a very large number of different compounds available, but the manufacturing techniques vary widely usually for the purpose of achieving a particular quality. Apparently there has been little effort made to standardize the foams so that even their static physical properties can be generalized.

In Reference 17 dynamic response data are given for 22 different types of resilient materials including polyurethanes and polyvinyls. The tests were conducted on very small samples and both stiffness and equivalent viscous damping coefficients are presented. However, the dynamic characteristics of most elastomers can be modeled more closely by a visco-elastic system than by the simple damped oscillator. In addition, other data indicate that under static conditions, the stiffness of polyurethane is nonlinear.

It was feared, then, that in scaling the data from the sample to the full-size installation, the use of linear stiffness and damping could lead to appreciable error in the results.

The approach adopted consisted of considering the test model as a visco-elastic system, assigning a nonlinear stiffness to the principal spring in accordance with static test data on polyurethanes, assuming a similar type of stiffness and quadratic damping function in the secondary circuit, and varying the parameters of the secondary circuit to obtain a dynamic response which agreed with that of the test sample. The coefficients obtained in this manner would then be used as a basis for extrapolation.

Reference 17 gives no time histories of the dynamic response of polyurethanes which could be used as a basis for comparison, but a curve is given for a polyvinyl of approximately the same physical characteristics and averaged dynamic response. Properties of the two materials are compared in Table 4-8.

Table 4-8. Comparison of Properties of Polyurethane and Polyvinyl

Property	F 506 Polyurethane	Soft Polyvinyl
Hardness, Shore Durometer	0 to 12	< 1
Density, lb/ft ³	6.2	5.9
Proportional Limit (% thickness)	21	15
Average Stiffness (lb/in)	51.9	30.8
Modulus of Elasticity (psi)	12	7.4
Average Damping Ratio	0.11 to 0.26	0.11 to 0.16

The sample was a rectangular parallelepiped 2 by 2 by 0.906 inches with a steel plate of 1.27 pounds, cemented to one face. The weighted assembly was dropped from a height of 10 inches. Accelerations were recorded.

Mathematical Model

To permit the extrapolation of experimental data to this application, a mathematical model of the polyurethane sample was constructed as shown in Figure 4-34 to determine by a trial and error method the nonlinear stiffness and damping coefficients which would give a response comparable to experimental data.

The equation of motion for this mathematical model was derived and solved on a Burroughs 205 Computer by numerical integration. Various trials were made with different coefficients for damping and stiffness, while the shape of the acceleration curve obtained from computer results compared grossly with that of the experiment. The equation of motion with its coefficients follows:

$$M_m \ddot{x}_1 = W - K_1(x_1 - x_3) - K_D(\dot{x}_1 - \dot{x}_2)$$

$$K_D(\dot{x}_1 - \dot{x}_2) = K_2(x_2 - x_3)$$

$$K_D = (6.5 \times 10^{-3}) \left\{ |\dot{x}_1 - \dot{x}_2| \right\} \quad \text{Pounds Seconds per Inch}$$

$$K_1 = (33.6) \left[1 + \frac{|(x_1 - x_3)^3|}{(0.495)^4} \right] \quad \text{Pounds per Inch}$$

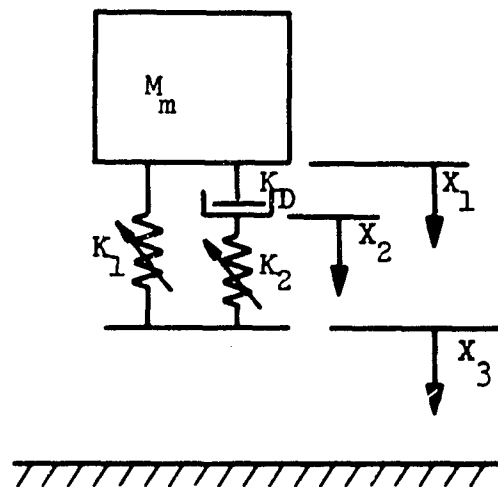


Figure 4-34. Drop Test Model for Determining the Nonlinear Characteristics of a Polyurethane Sample.

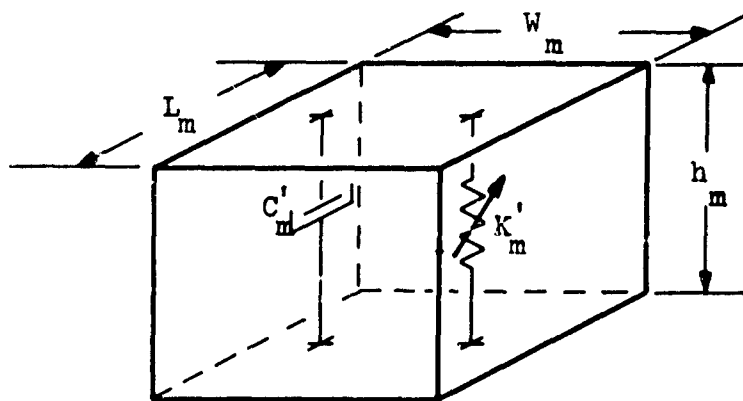


Figure 4-35. Linear Model of Elemental Polyurethane Sample.

$$K_2 = (16.8) \left[1 + \frac{|(x_2 - x_3)^3|}{(0.495)^4} \right] \text{ Pounds per Inch}$$

$$M_m = 3.29 \times 10^{-3} \text{ Pound Seconds}^2 \text{ per Inch}$$

The response obtained from the solution of this equation was plotted and the viscous damping ratios for an equivalent single-degree-of-freedom system were obtained by the logarithmic decrements. The maximum and average ratios observed were 0.20 and 0.12, respectively. The frequency for the first cycle was 27.8 cps and the average frequency was 18.6 cps. The above damping ratios were converted to viscous damping coefficients for the purpose of scaling the total system. The maximum viscous damping force is given by

$$F_{dm} = C_{max} (\dot{x}_1 - \dot{x}_2)$$

$$\text{where } C_{max} = 2 \zeta_m \omega_{nm} M_m$$

The natural frequency ω_{nm} is obtained from the frequency of the first cycle $\omega_{osc m}$

$$\begin{aligned} \omega_{nm} &= \frac{\omega_{osc m}}{\sqrt{1 - \zeta^2}} \\ &= \frac{(2\pi)(27.8)}{\sqrt{1 - (0.2)^2}} \\ &= 179 \text{ rad/sec.} \end{aligned}$$

$$\begin{aligned} C_{max} &= (2)(0.2)(179)(3.29 \times 10^{-3}) \\ &= 23.6 \times 10^{-2} \text{ Pound Seconds per Inch} \end{aligned}$$

The average damping ratio is

$$C_{ave} = 2 \zeta_{ave} \omega_{nm} M_m$$

Now,

$$\begin{aligned}\omega_{nm} &= \frac{\omega_{osc\ m}}{\sqrt{1 - \zeta_{ave}^2}} \\ &= \frac{(2\pi)(18.6)}{\sqrt{1 - (0.12)^2}} \\ &= 118 \text{ rad/sec.} \\ C_{ave} &= (2)(0.2)(118)(3.29 \times 10^{-3}) \\ &= 9.28 \times 10^{-2} \text{ Pound Seconds per Inch}\end{aligned}$$

Scaling of Model Constants to Sway Damper

The damping ratios and damping coefficients obtained by matching test data obtained on the small polyurethane sample must then be extrapolated to the very much larger sway damper configuration. The bulk polyurethane, as shown in Figure 4-33, can be divided in an array of elementary blocks in series and parallel, as shown in Figure 4-36. The size and dynamic properties of each element are the same as those of the test sample. The damping characteristics for the bulk are obtained by summing appropriately the characteristics of the large number of elements. The linearized element is shown in Figure 4-35.

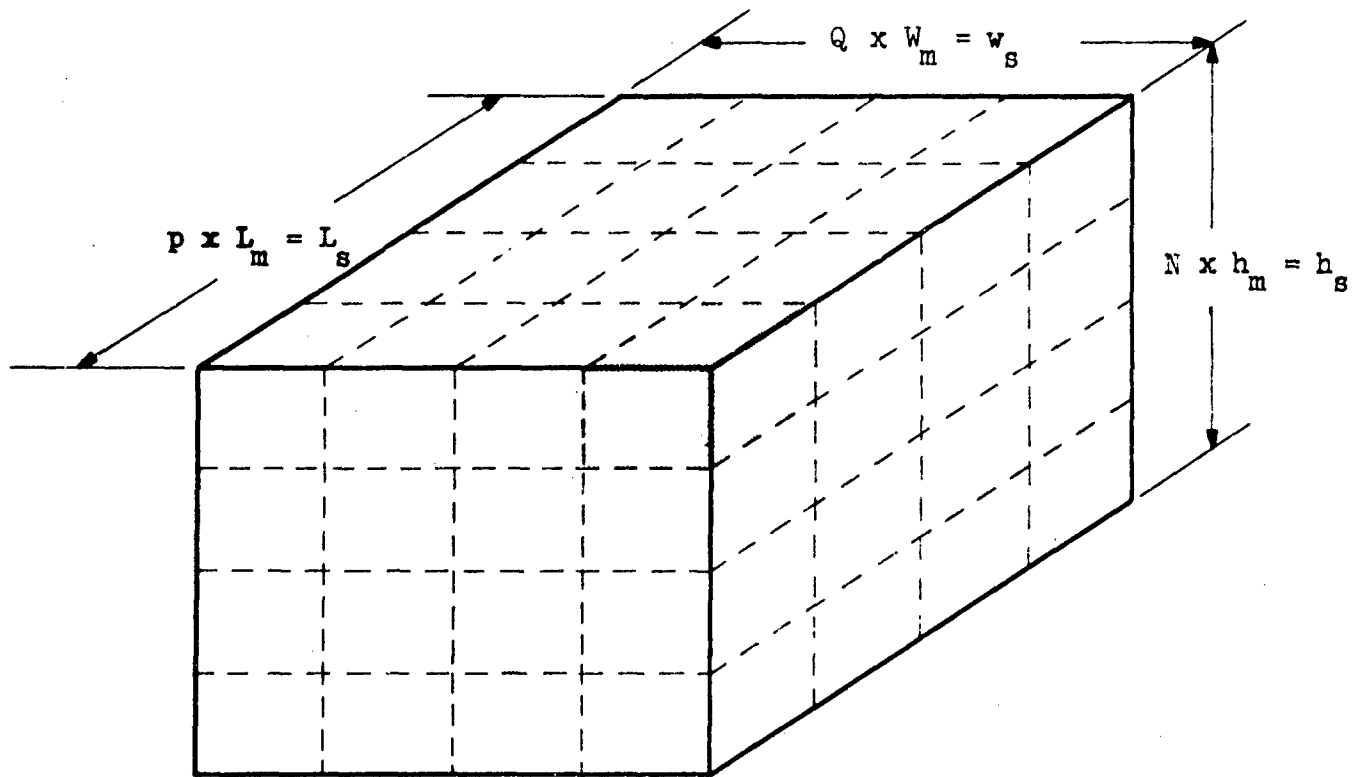


Figure 4-36. Linear Model of Bulk Polyurethane Composed of An $Q \times N \times p$ Array of Elemental Sample.

For equal springs and dampers in series,

$$K_{es} = \frac{K'_m}{N}, \quad C_{es} = \frac{C'_m}{N}$$

For equal springs and dampers in parallel,

$$K_{ep} = Q_p (K'_m), \quad C_{ep} = Q_p (C'_m)$$

Therefore

$$K_e = \frac{Q_p}{N} K'_m, \quad C_e = \frac{Q_p}{N} C'_m$$

Converting into dimensional ratios, we get

$$K_e = K'_m \left\{ \frac{h_m}{h_s} \cdot \frac{L_s}{L_m} \cdot \frac{W_s}{W_m} \right\}$$

$$C_e = C'_m \left\{ \frac{h_m}{h_s} \cdot \frac{L_s}{L_m} \cdot \frac{W_s}{W_m} \right\}$$

As shown in Figure 4-36, it is assumed that the model is a rectangular parallelepiped with the load applied normal to a face. Then for the linear model, the strain and rate of strain of each of the elements are the same and identical to the strain and rate of strain of the entire unit. This assumption will result in some error as the collar in the physical system is a segment of an annulus and is loaded, not radially, but by parallel forces. To correct, in part, for this effect, the stiffness of the actual configuration was determined as a function of displacement and the average value used in the analysis. Note also that in the actual configuration the collar is attached to the capsule but not to the cage. Thus, it can be loaded only in compression.

The average stiffness, K'_s was found to be 8840 pounds per inch and the equivalent damping coefficients were based on the following data:

$$h_m = 0.875 \text{ inch}$$

$$h_s = 56 \text{ inches}$$

$$L_m = 2 \text{ inches}$$

$$L_s = 1410 \text{ inches}$$

$$W_m = 2 \text{ inches}$$

$$W_s = 72 \text{ inches}$$

$$C_{m \text{ max}} = 23.6 \times 10^{-2} \text{ pound seconds per inch}$$

$$C_{m \text{ ave}} = 9.25 \times 10^{-2} \text{ pound seconds per inch}$$

$$C_{s \text{ max}} = 23.6 \times 10^{-2} \left[\frac{(0.875)(1410)(72)}{(56)(2)(2)} \right] = 93.5 \text{ pound seconds per inch}$$

$$C_{s \text{ ave}} = 9.25 \times 10^{-2} \left[\frac{(0.875)(1410)(72)}{(56)(2)(2)} \right] = 36.7 \text{ pound seconds per inch}$$

The system was simplified to a single degree of freedom, as shown in Figure 4-37, for obtaining critical damping ratios.

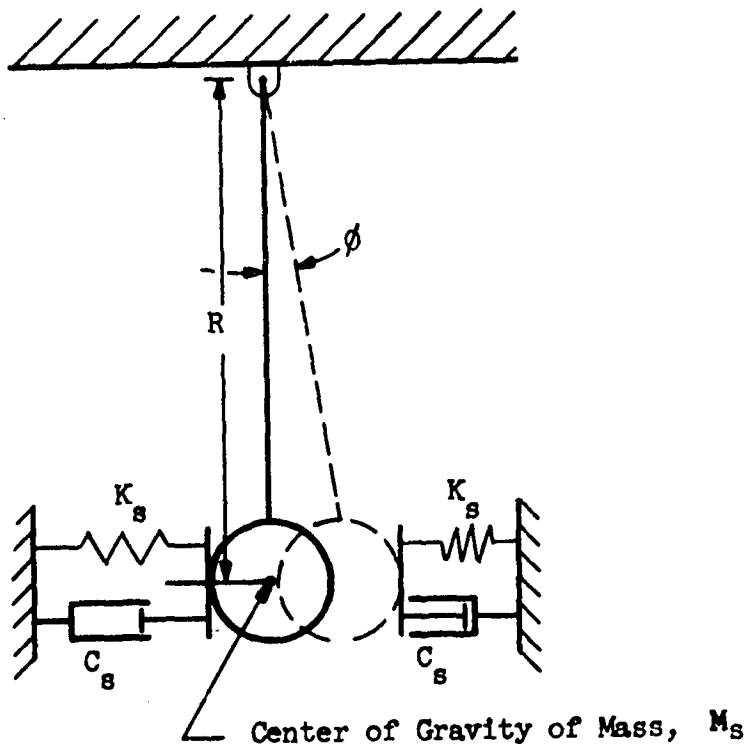


Figure 4-37. Model for Determining Damping Ratio of Bulk Polyurethane in Horizontal Direction.

The equation of motion can be written as

$$M_s R \ddot{\phi} + K'_s R \sin \phi + C_s R \dot{\phi} + M_s g \sin \phi = 0$$

For small angular displacements $\sin \phi \approx \phi$, therefore

$$\ddot{\phi} + \frac{C_s}{M_s} \dot{\phi} + \left[\frac{K'_s}{M_s} + \frac{g}{R} \right] \phi = 0$$

It can be shown that critical damping is

$$C_{sc} = 2m \sqrt{\frac{K'_s}{m} + \frac{g}{R}} = 2(13.1 \times 10^3) \left[\frac{8840}{13.1 \times 10^3} + \frac{386}{840} \right]^{1/2}$$

$$C_{sc} = 27.8 \times 10^3 \text{ pound seconds per inch}$$

Then the damping ratios are

$$\zeta_{\max} = \frac{C_{s \max}}{C_{sc}} = \frac{93.5}{27.8 \times 10^3} = 0.00337 \text{ or } 0.337 \text{ per cent}$$

$$\zeta_{\text{ave}} = \frac{C_{s \text{ ave}}}{C_{sc}} = \frac{36.7}{27.8 \times 10^3} = 0.00132 \text{ or } 0.132 \text{ per cent}$$

Conclusions

The necessity for obtaining dynamic response data of polyurethane foams by approximating test results obtained under different loading conditions on a single small sample of a slightly different material and for extrapolating the properties so obtained to a configuration of different shape and of a size many orders larger of magnitude, must cast serious doubt on the validity of the answers. However, the damping ratio calculated by this method is lower by well over one order of magnitude than that needed in this facility. Thus, while there is insufficient evidence to conclude that the polyurethane foams cannot be used in this application, there is sufficient doubt to encourage investigations of alternate methods.

4.5 Cable/Isolator Interaction

4.5.1 Inherent Problems in Cable Suspension Systems

The suspension system configurations employ the use of an elastic pendulum. Basically, the elastic pendulum consists of cables connected to shock isolators and installed so that the length of the cables can be varied within limits. This implies that for the effective use of a cable as a pendulum, it should always be in tension, as the presence of any compression load will slacken the cable which will deviate considerably from its desired use.

The suspension system is designed in such a way that the acceleration of the center of gravity is not greater than 1.50 and not less than 0.5 g during steady state motions. This assures that the cable will be in tension at all times after a shock. However, due to high ground accelerations it may be entirely possible that the motion of the ground may exceed that of the cable-shock isolator connection resulting in a slackening of the cable. It is apparent that when the cable is slack, it does not transmit any compressive loads. Hence, during the slack period no significant external force is acting on the suspended body except that of gravity. Therefore, the body will fall with the acceleration of gravity. After some time, the motion of the body will exceed that of the ground due to the free fall of the body, and deceleration of ground motion tightening the cable again. This sudden tightening may induce high acceleration on the body and in the cable.

Hence, it is necessary to obtain the response of the cable-isolator suspension system during the transient period to investigate the problem of the slackening of the cable. If the cable goes slack, an investigation should be made of accelerations induced in various components and the parameters causing the slackening.

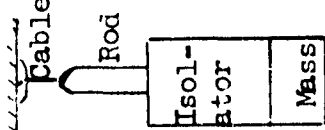
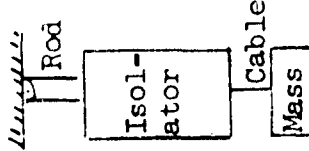
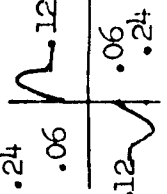
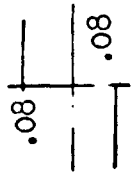
4.5.2 Transient-State Response of the Cable/Isolator System

A single isolator-mass system is selected for the investigation of the transient response. The system is reduced to two degrees of freedom with an appropriate mass. Friction and square law damping are included. The equations of motion are derived and solved by a numerical integration.

The important parameters which affect the response are damping, ratio of the masses of isolator to suspended mass and the position of the isolator in the cable/isolator system, i.e., near top end or bottom end.

Various cases are set up to investigate the effect of the above parameters on the response. Table 4-9 shows the comparison between various cases. Cases 1-A, 1-B, 1-C and 2-A are set up with the isolator at the bottom end of the cable. Cases 1-A and 1-B have 20 per cent equivalent viscous damping with different friction forces. The viscous damping is reduced to 5 per cent in case 1-C and is entirely eliminated in case 2-A, keeping the friction the same as in 1-B. Case 1-R is set up with the isolator at the

Table 4-2 Comparison of Various Cases
Transient Response Investigation

Config- uration	Case No.				
	1-A	1-B	1-C	2-A	1-R
		Same as 1-A	Same as 1-A	Same as 1-A	
					1-ZZ
					1-ZZ*
					Same as 1-ZZ
Friction			Same as 1-B	Same as 1-B	Same as 1-B
Eq. Visc. Damping	20%	20%	5%	0	20%
					0

top of the cable and with 20 per cent viscous damping. It seems interesting to investigate the difference in response when the cable is replaced by a rigid rod capable of taking compression. Cases 1-ZZ and 1-ZZ* are considered with the rigid rod and the variation in damping.

4.5.2.1 Equations of Motion for Cases 1-A, 1-B, 1-C and 2-A

The equations of motion are obtained from the basic system shown on Figure 4-38(a).

Figure 4-38(b) shows the equivalent two-degree of freedom system

$$\sum F_r = P_o A_e - m_r \ddot{Z}_r + F_d - T_c + W_r + (\text{sign } \Delta \dot{L}) F_f = 0$$

$$\sum F_m = -P_o A_e - m \ddot{Z}_m - F_d + W - (\text{sign } \Delta \dot{L}) F_f = 0$$

where the subscripts r and m refer to the rod and supported mass, respectively, and

$$P_o A_e = K_1 (Z_m - Z_r)$$

$$T_c = K_c (Z_r - Z_g)$$

$$\Delta L = Z_m - Z_r$$

$$F_d = c_1 |\Delta \dot{L}| \Delta \dot{L}$$

$$m_r = \text{isolator mass plus one-third of cable mass.}$$

Substituting these identities in the equations of motion, we obtain

$$\ddot{Z}_r = \frac{K_1}{m_r} (Z_m - Z_r) + (\text{sign } \Delta \dot{L}) \frac{F_f}{m_r} - \frac{K_c}{m_r} (Z_r - Z_g)$$

$$+ \frac{c_1}{m_r} |\dot{Z}_m - \dot{Z}_r| (\dot{Z}_m - \dot{Z}_r) + g$$

$$\ddot{Z}_m = g - \frac{K_1}{m} (Z_m - Z_r) - (\text{sign } \Delta \dot{L}) \frac{F_f}{m} - \frac{c}{m} |\dot{Z}_m - \dot{Z}_r| (\dot{Z}_m - \dot{Z}_r)$$

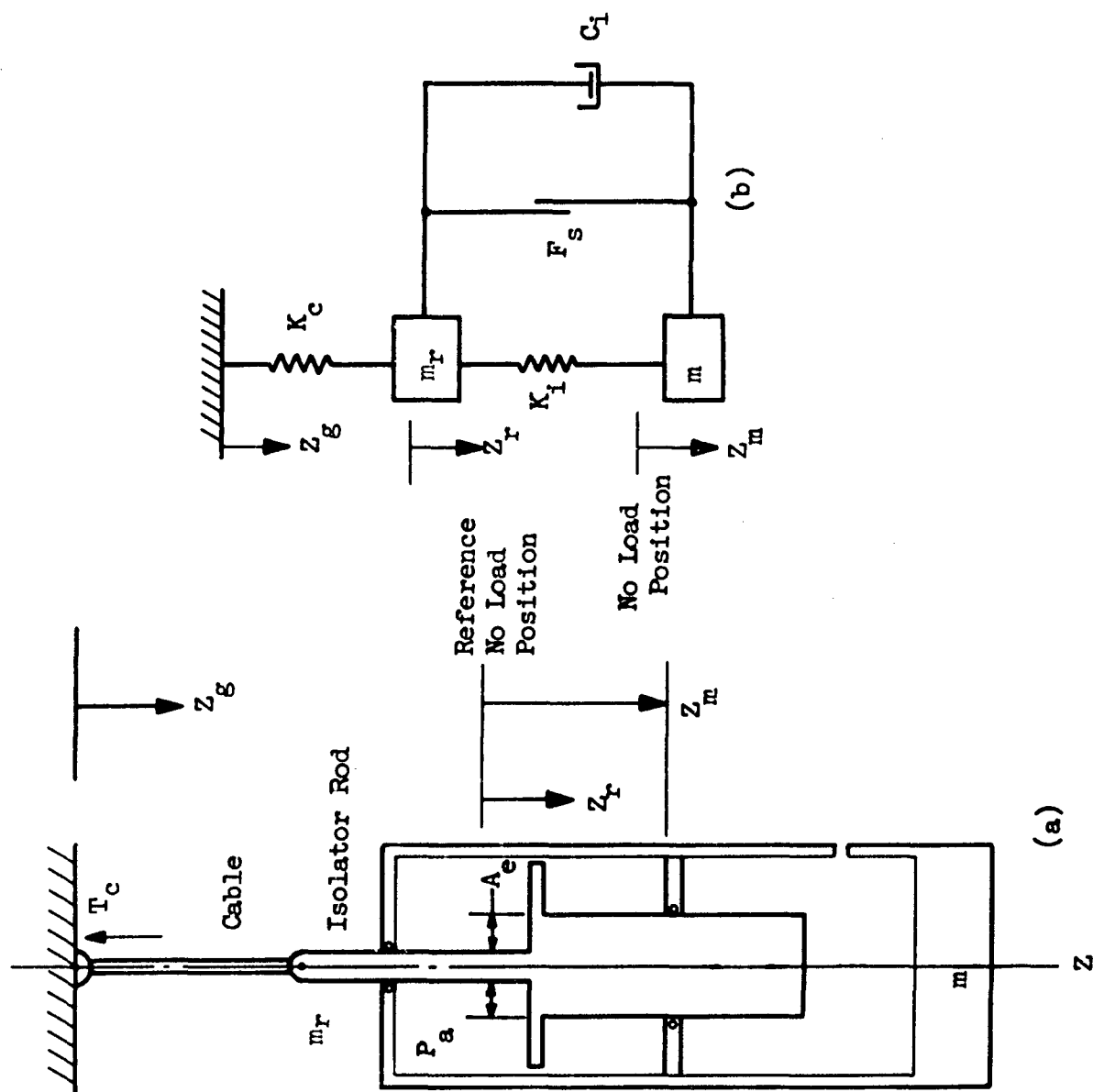


Figure 4-38. Basic Suspension System With Isolator at Bottom and Analog Equivalent.

In this analysis an empirical expression is set up for the friction force as a function of velocity, using data presented by manufacturers as being typical of liquid spring isolator friction characteristics. These data are given in percentage of isolator load, as indicated in Figure 4-39.

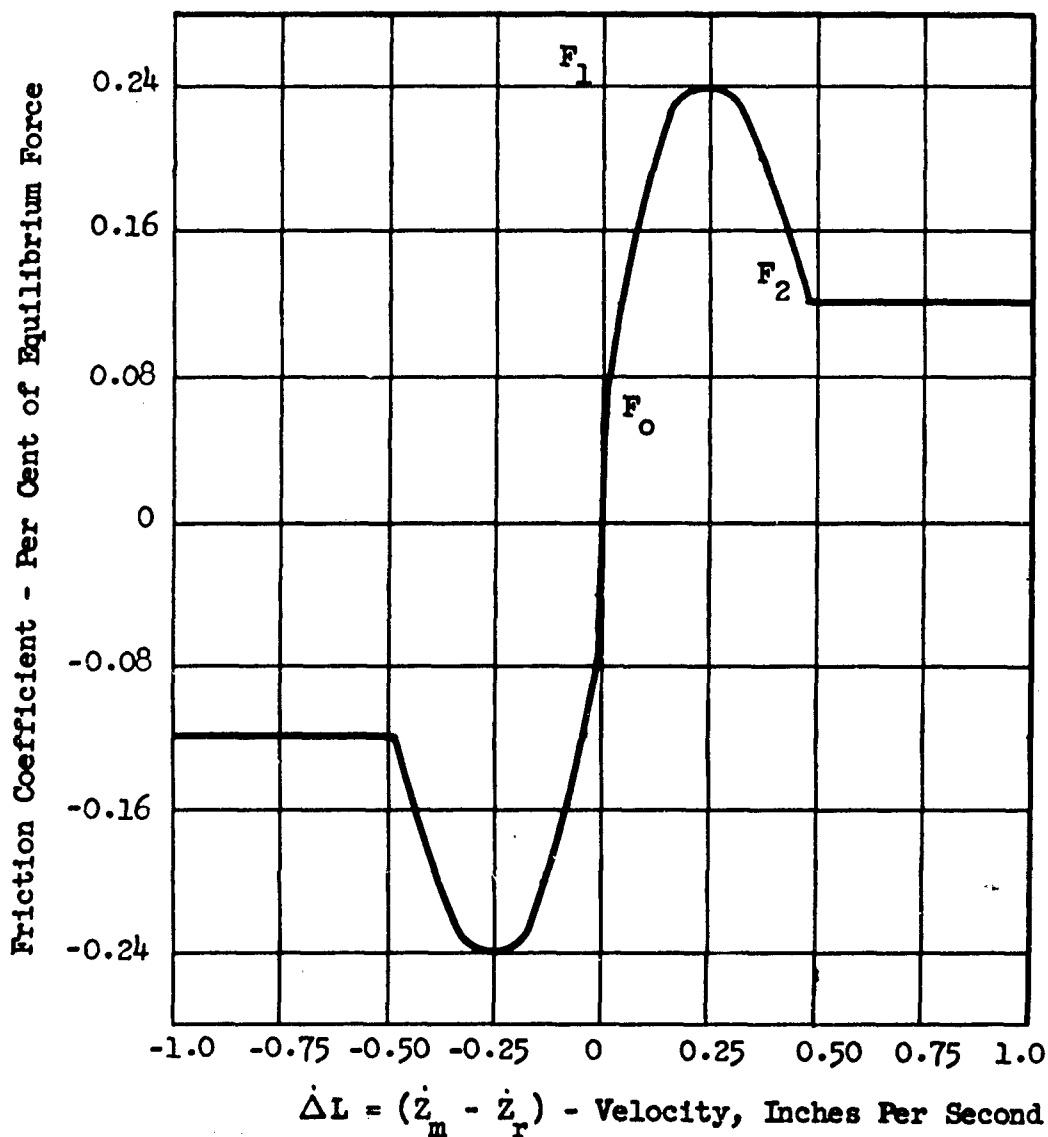


Figure 4-39. Friction Coefficient Versus Velocity For a Typical Liquid Spring.

The friction force can be presented by the following expression:

$$F_f = F_s (\text{sign } \Delta \dot{L}) K_1 (Z_m - Z_r)$$

where F_s is a constant defined within the following limits:

$$\begin{aligned} 0 \leq |\Delta \dot{L}| \leq \Delta \dot{L}_1 & \quad F_s = \pm \left[F_0 + (F_1 - F_0) \left[\sin \left(\frac{\pi}{2} \frac{|\Delta \dot{L}|}{\Delta \dot{L}_1} \right) \right] \right] \\ \Delta \dot{L}_1 \leq |\Delta \dot{L}| \leq \Delta \dot{L}_2 & \quad F_s = \pm \left[F_2 - \frac{1}{2} (F_1 - F_2) \left[-1 + \sin \pi \left(\frac{|\Delta \dot{L}| - (\Delta \dot{L}_2 + \Delta \dot{L}_1)}{(\Delta \dot{L}_2 - \Delta \dot{L}_1)} \right) \right] \right] \\ \Delta \dot{L} \leq |\Delta \dot{L}| & \quad F_s = \pm F_2 \end{aligned}$$

Friction for Case 1-B

The expression for friction force is simplified as shown in Figure 4-40 to reduce computing time.

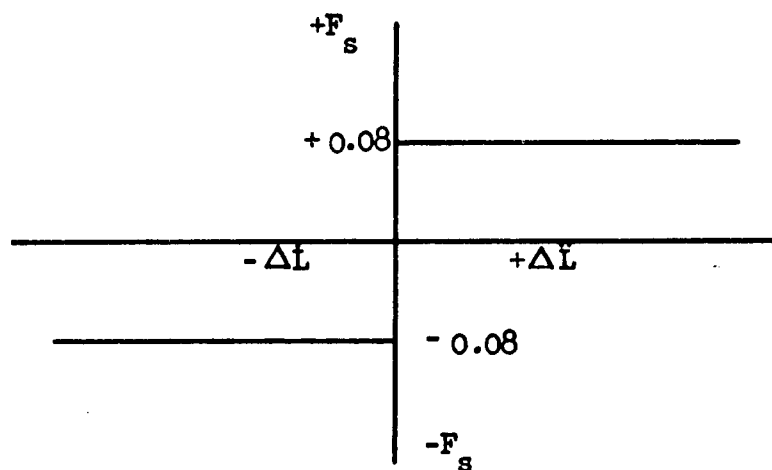


Figure 4-40. Simplified Friction Coefficient Versus Velocity $\Delta \dot{L}$.

Since the friction force is a constant percentage of the isolator load, the term $K_1 [1 + (\text{sign } [\dot{Z}_m - \dot{Z}_r]) F_s] (Z_m - Z_r)$ in the acceleration equations has the load deflection characteristic given in Figure 4-41. This modifies the spring rate as a function of displacement and direction of travel.

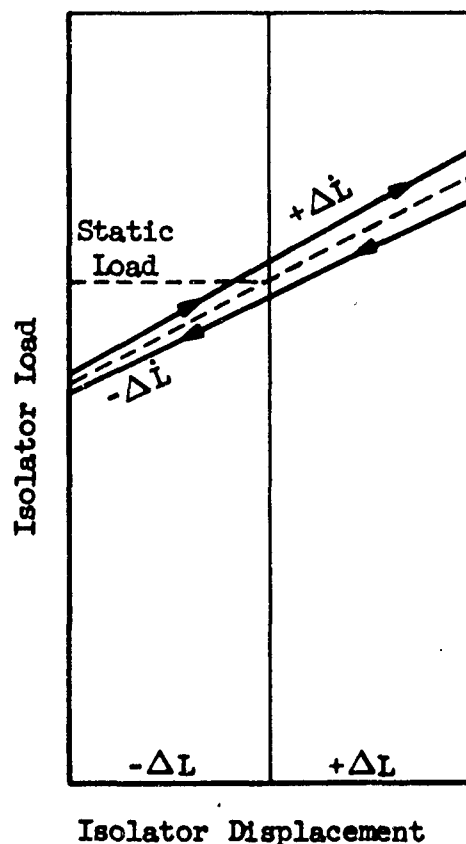


Figure 4-41. Isolator Load Deflection Curve Showing Combined Spring Force, Friction Force, and Velocity Direction Effect.

4.5.2.2 Equations of Motion for Case 1-R

The equations of motion are set up for the configuration shown in Figure 4-42.

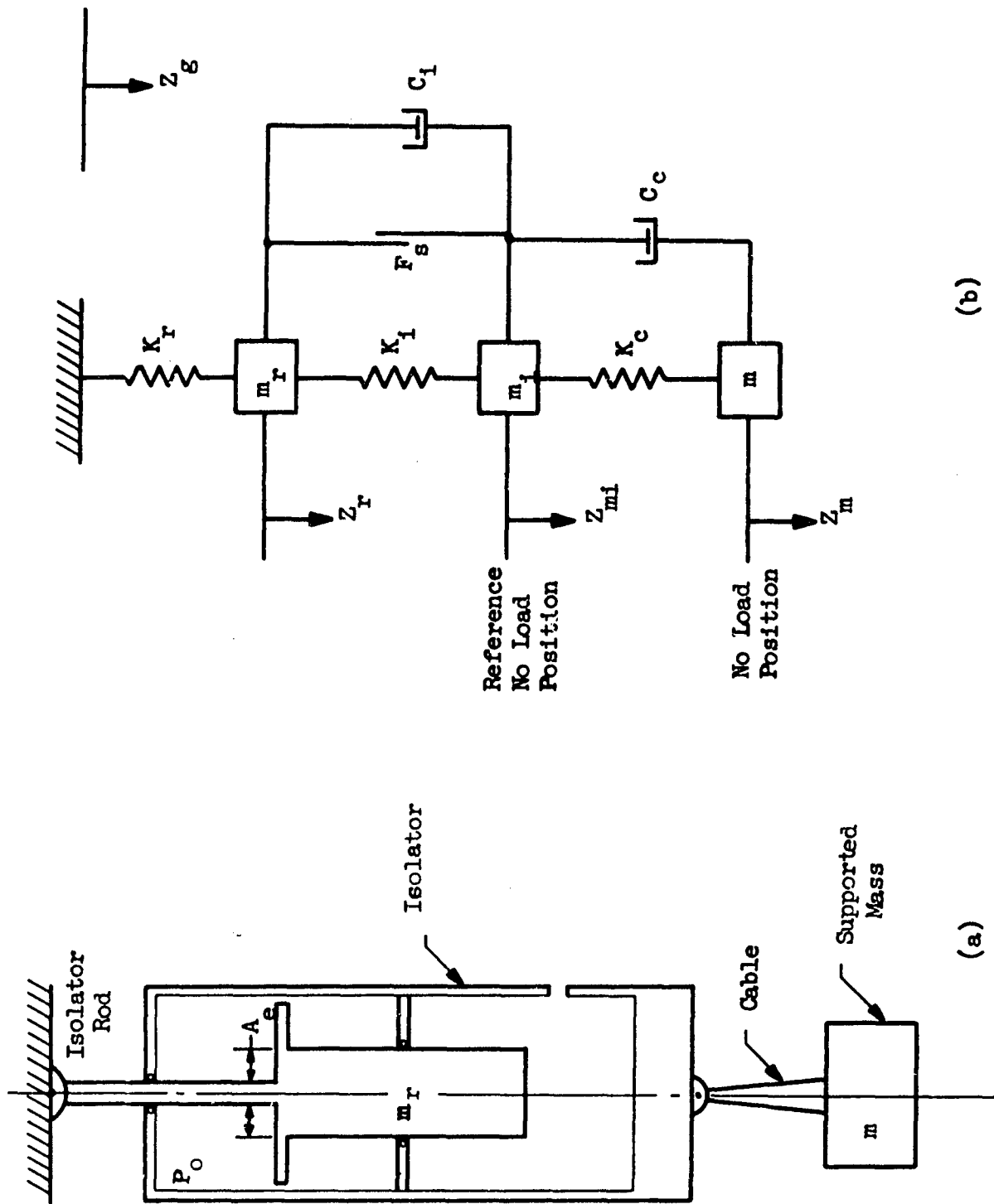


Figure 4-42. Basic Suspension System with Isolator at Top End and Analog Equivalent.

$$\sum F_r = P_{oe} - m_r \ddot{Z}_r + F_d - T_r + W_r + (\text{sign } \dot{\Delta L}) F_s P_{oe} = 0$$

$$\sum F_{mi} = -P_{oe} - m_i \ddot{Z}_{mi} + W_i - (\text{sign } \dot{\Delta L}) F_s P_{oe} - F_d + T_c + F_c = 0$$

$$\sum F_m = -T_c - F_c - m \ddot{Z}_m + W = 0$$

where the subscripts c, r, m and i refer to cable, rod, supported mass, and isolator, respectively; and

$$P_{oe} = K_i (Z_{mi} - Z_r)$$

$$T_r = K_r (Z_r - Z_g)$$

$$\Delta L = Z_{mi} - Z_r$$

$$T_c = K_c (Z_m - Z_{mi})$$

$$F_d = C_d \left| \dot{Z}_{mi} - \dot{Z}_r \right| (\dot{Z}_{mi} - \dot{Z}_r)$$

$$F_c = C_c (\dot{Z}_m - \dot{Z}_{mi})$$

The equations can be rewritten as

$$\ddot{Z}_r = \frac{K_i}{m_r} \left[1 + (\text{sign } [\dot{Z}_{mi} - \dot{Z}_r]) F_s \right] (Z_{mi} - Z_r) - \frac{K_r}{m_r} (Z_r - Z_g) + \frac{C_i}{m_r} \left| \dot{Z}_{mi} - \dot{Z}_r \right| (\dot{Z}_{mi} - \dot{Z}_r) + g$$

$$\ddot{Z}_{mi} = g - \frac{K_i}{m_i} \left[1 + (\text{sign } [\dot{Z}_{mi} - \dot{Z}_r]) F_s \right] (Z_{mi} - Z_r) - \frac{C_i}{m_i} \left| \dot{Z}_{mi} - \dot{Z}_r \right| (\dot{Z}_{mi} - \dot{Z}_r) + \frac{K_c}{m_i} (Z_m - Z_{mi}) + \frac{C_c}{m_i} (\dot{Z}_m - \dot{Z}_{mi})$$

$$\ddot{Z}_m = g - \frac{K_c}{m} (Z_m - Z_{mi}) - \frac{C_c}{m} (\dot{Z}_m - \dot{Z}_{mi})$$

4.5.2.3 Numerical Constants

The shock isolator and cable weight and spring constants are evaluated using Figures 4-43, 4-44 and 4-45 for the nominal design static system weight of 5.05×10^6 pounds. Since minimal supported load appears critical for this analysis, the minimum system weight of 4.545×10^6 pounds was used. The cable weight plotted in Figure 4-44 is one-third of the actual cable weight.

For Case 1-A Isolator

W	$= 378 \times 10^3$ pounds
m	$= .982 \times 10^3$ pound seconds ² /inch
K_r	$= 4.125 \times 10^6$ pounds/inch, spring constant of the shock isolator rod
K_c	$= 1.37 \times 10^5$ pounds/inch, equivalent spring for the isolator rod and cable in series
K'_c	$= 1.42 \times 10^5$ pounds/inch, spring constant of the cable
L_c	$= 26$ feet, length of cable
K_i	$= 4.72 \times 10^3$ pounds/inch, spring constant of the shock isolator
m_r	$= 13.2$ pound seconds ² /inch, rod mass plus one-third of cable mass
C_i	$= 15$ pound seconds ² /inch ² , for 20 per cent equivalent viscous damping

In order to obtain the numerical constants for the suspension system for Case 1-A, the above tabulated values should be multiplied by twelve, the number of isolators.

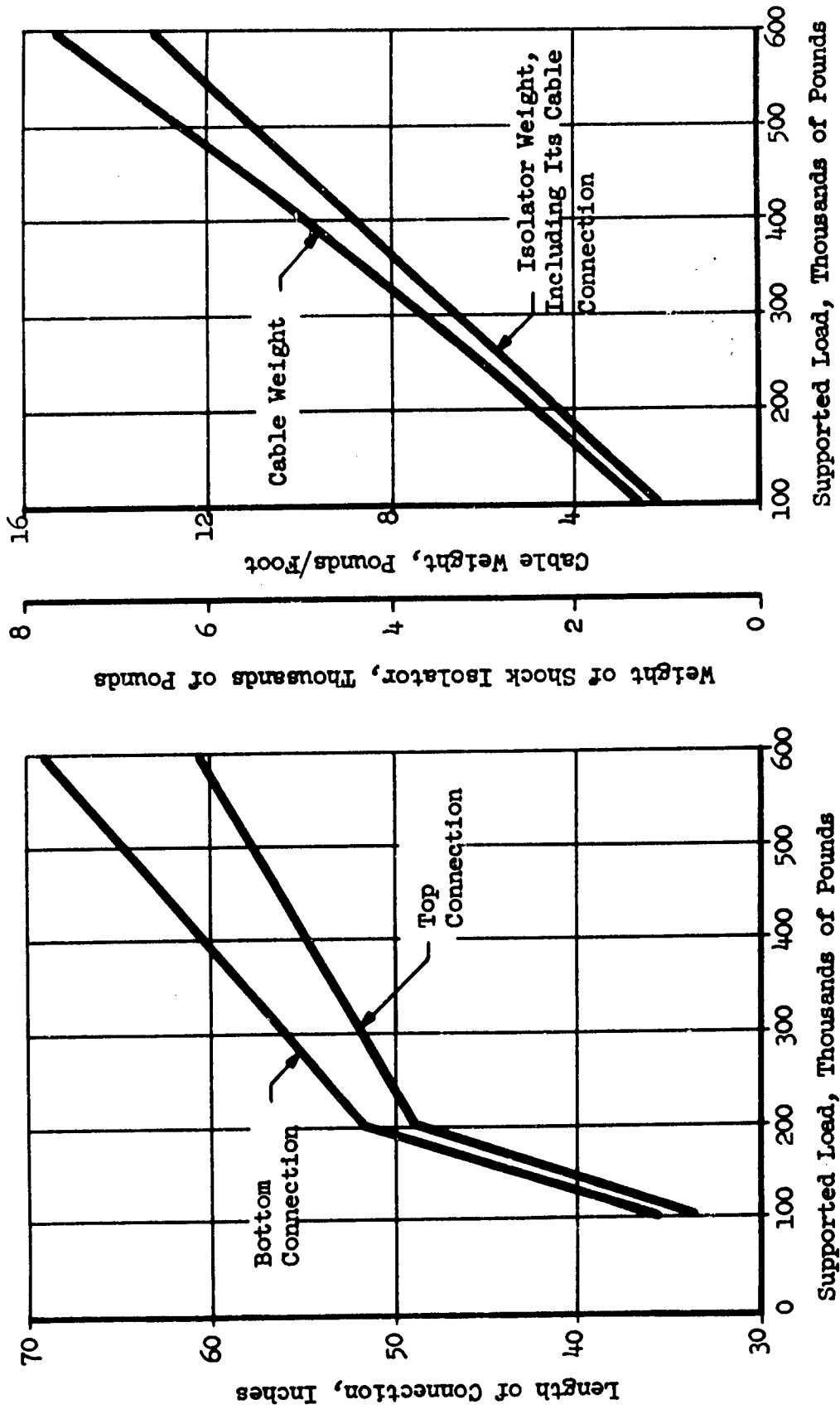


Figure 4-44. Weights For Shock Isolator.

Figure 4-43. Length of Isolator Connections.

NOTE: To obtain cable stiffness divide cable stiffness factor by cable length.

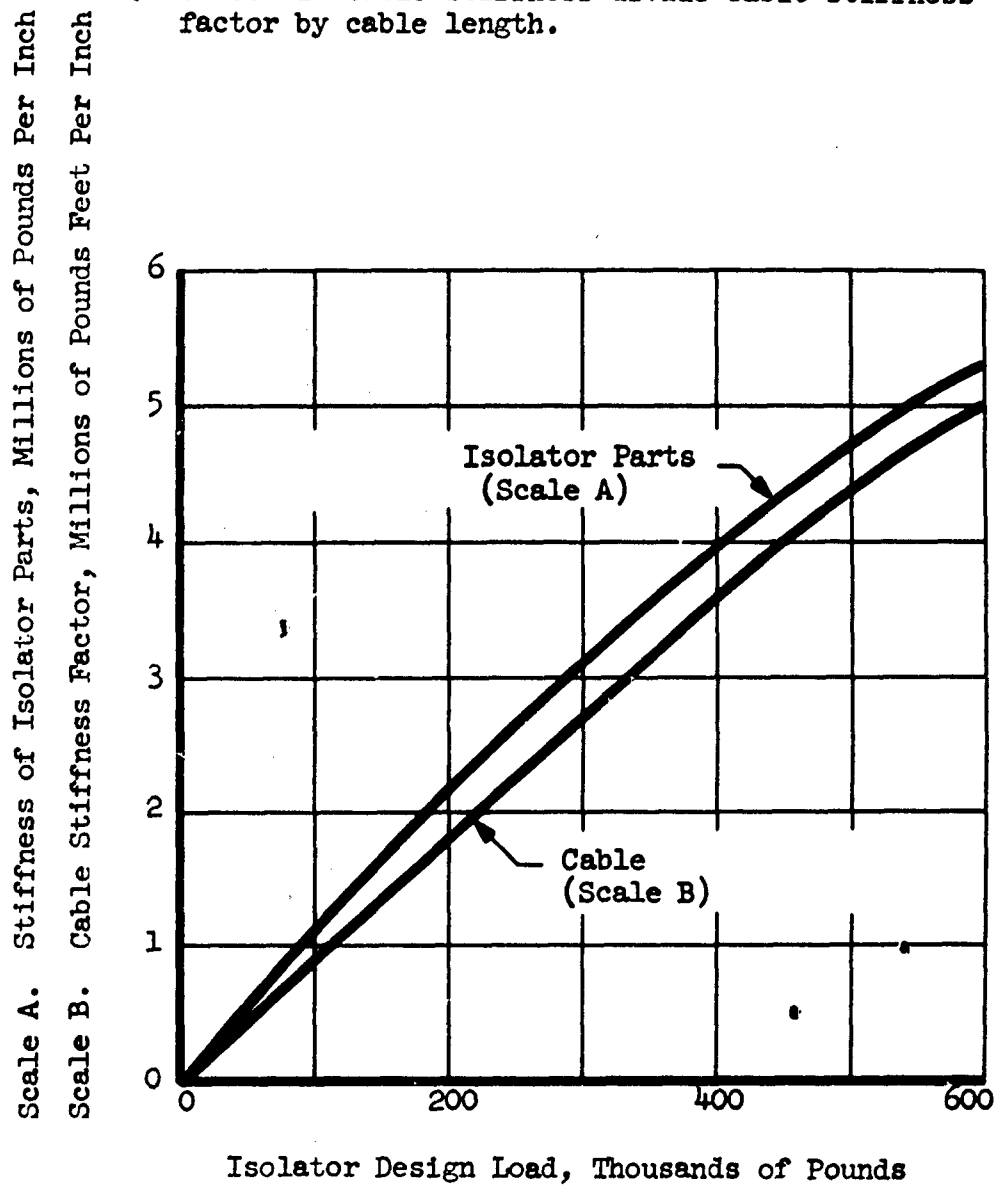


Figure 4-45. Stiffness Data for Isolator and Cable Parts.

Initial Condition for Case 1-A

Z_{ro} = 2.81 inches, static deflection of cable and rod spring

Z_{mo} = 82.81 inches, static deflection of mass (includes Z_{ro})

Z_g = Ground motion input as a function of time and is shown in Figure 2-1

$\dot{Z}_{ro} = \ddot{Z}_{ro} = \dot{Z}_{mo} = \ddot{Z}_{mo} = 0$, initially

For Case 1-R Isolator

W = 378×10^3 pounds

K_r = 4.125×10^6 pounds/inch, spring constant of the isolator rod

C_1 = 15 pound seconds²/inch², for 20 per cent equivalent viscous damping

W_1 = 20×10^3 pounds, isolator weight

m_1 = 52 pound seconds²/inch, isolator mass

W_r = 4.75×10^3 pounds, isolator rod weight

m_r = 12.3 pound seconds²/inch, mass of the isolator rod

In order to obtain the numerical constants for the suspension system for Case 1-R the tabulated values, above, should be multiplied by twelve, the number of isolators.

Initial Conditions for Case 1-R

Z_{ro} = 0.098 inches, static deflection of isolator rod

Z_{mio} = 84.998 inches (includes Z_{ro})

Z_{mo} = 87.678 inches (includes Z_{mio} and static deflection of cable)

$\ddot{Z}_{ro} = \dot{Z}_{ro} = \ddot{Z}_{mio} = \dot{Z}_{mio} = \ddot{Z}_{mo} = \dot{Z}_{mo} = 0$

One per cent equivalent viscous damping was assumed for cable damping. This was converted to an equivalent viscous damping coefficient as shown below.

$$F_c = C_c (\dot{Z}_m - \dot{Z}_{m1}) = 2 \zeta_c \omega_{nm} m (\dot{Z}_m - \dot{Z}_{m1})$$

$$\therefore C_c = 2 \zeta_c \omega_{nm} m$$

$$\omega_{nm} = \sqrt{\frac{K_c}{m}}$$

$$m = 11.8 \times 10^3 \text{ pound seconds}^2/\text{inch, total system}$$

$$K_c = 1.7 \times 10^6 \text{ pounds/inch, total system}$$

$$\omega_{nm} = \sqrt{\frac{1.7 \times 10^6}{11.8 \times 10^3}} = 12 \text{ sec}^{-1}$$

$$C_c = 2.84 \times 10^3 \text{ pound seconds/inch}$$

4.5.2.4 Response Results

The equations of motion for the several cases were solved on a Burroughs 205 Computer by numerical integration. The response results obtained are shown in Table 4-10.

Table 4-10 Comparison of Response Results
Transient Response Investigation

CASE NUMBERS							
	1-A	1-B	1-C	2-A	1-R	1-ZZ	1-ZZ*
Equivalent Viscous Damping	20%	20%	5%	0	20%	20%	0
Cable Slack Time	0.02 Sec. thru 0.15 Sec.	0.02 Sec. thru 0.15 Sec.	0.02 Sec. thru 0.12 Sec.	0.02 thru 0.03 Sec. @ 0.09 Sec. 0.15 thru 0.16 Sec.	0.03 Sec. thru 0.18 Sec.	No Cable	No Cable
Isolator Rod Peak Accel.	-52.8 g's @ 0.17 Sec.	-56.8 g's @ 0.17 Sec.	-83 g's @ 0.15 Sec.	-105 g's @ 0.12 Sec. (Oscillatory)	+31.8g @ 0.02 Sec. -22.3 g @ 0.09 Sec. -22 g @ 0.11 Sec.	+30.8 g @ 0.02 Sec. -28.8 g @ 0.1 Sec.	-77 g @ 0.13 Sec. (Oscillatory)
Mass Peak Accel.	+0.01 g @ 0.03 Sec. thru 0.15 Sec. -1.74 g @ 0.22 Sec.	+1.00 g @ 0.03 Sec. thru 0.15 Sec. -1.73 g @ 0.22 Sec.	+1.00 g @ 0.04 Sec. thru 0.12 Sec. -0.846 g @ 0.16 Sec.	+0.452 g @ 0.11 Sec. -0.194 g @ 0.41 Sec. -0.191 g @ 0.65 Sec.	+1.0 @ 0.03 Sec. thru 0.18 Sec. -2.36 g @ 0.22 Sec.	+6.38 g @ 0.04 Sec. -3.85 g @ 0.15 Sec.	+0.431 g @ 0.1 Sec. -0.154 g @ 0.39 Sec.

4.5.3 Discussion of the Response Results

The condition for slackening of the cable is $(Z_g - Z_r) > 0$. The study of the response of Case 1-A reveals that the cable is slackened from 0.02 to 0.15 second and an acceleration of 52.6 g's is induced in the isolator rod when the cable is tightened. During the slack period the suspended mass shows a tendency to attain accelerations slightly higher than gravity because of the motion of the isolator rod within the cylinder. The peak acceleration induced in the suspended body after tightening of the cable is 1.74 g's, which is greater than the prescribed limit.

Case 1-B differs from Case 1-A only in the friction force. The amount of friction is slightly reduced and the variation of friction force with respect to velocity is eliminated in Case 1-B. The responses of the two cases differ very little. The slack period remains the same. The peak acceleration of the suspended mass shows a slight reduction while that of the isolator rod shows an increase. The comparison of the two results shows that the small variation in the amount of friction force and in the shape of friction-velocity curve has no significant effects on the total response of the system.

Case 1-C differs from Case 1-B only in the amount of damping. In Case 1-B equivalent viscous damping of 20 per cent is used. This is reduced to 5 per cent in 1-C. Comparing the responses of the two cases it can be seen that for Case 1-C the slack period is slightly reduced and the peak acceleration of the isolator rod is increased to 83 g's after the cable is tightened, while the peak acceleration of the suspended mass is reduced to about half that in Case 1-B. This shows that the reduction in damping helps in reducing the acceleration of the suspended mass and the cable slack period.

To reach a limit in reduction in damping, the ratio of equivalent viscous damping is reduced to zero in Case 2-A, keeping friction the same as in Case 1-B. Comparing the responses of Cases 1-C and 2-A, it can be seen that the slack period is further reduced and the peak acceleration of the suspended mass is brought within 1/2 g. The peak acceleration induced in the isolator rod, however, is increased to as high as 105 g's, which seems to be the only disadvantage in extreme reduction in damping.

Even though it is apparent that, for practical application, the isolator cannot be attached at the top-end of the cable because of high bending stresses that will be induced in the rigid isolator rod, the response for Case 1-R is obtained to study the significant changes in behavior. Compared to the response for Case 1-A it can be seen that by introducing the cable between the isolator and the mass, the slack period is increased and the peak acceleration of the suspended mass is also increased after tightening of the cable.

When the cable is replaced by a rigid rod capable of resisting compression loads, the peak acceleration of the suspended mass is considerably increased. Two responses are obtained for rigid rod suspension, one with equivalent damping of 20 per cent and the other with zero damping. The same phenomenon can be observed in these cases as in the cable suspension system; the reduction in damping reduces the peak acceleration on the suspended mass.

It can be seen that for various cases considered for analysis in this section, the cable does slacken for a short time, even though the slack period changes with variation in certain parameters. As discussed earlier, the basic condition to be satisfied to avoid slackening is that the acceleration of the isolator rod shall be greater than that of the ground. To meet this requirement, it is necessary to increase the acceleration of the isolator rod, which can be achieved by reducing its mass.

4.5.4 Conclusions

a. The shape of the friction-velocity curve and the small variation in the amount of friction force have no significant effect on the dynamic response of the system.

b. The increase in amount of damping increases the peak acceleration of the suspended body and also increases the cable slack-period.

c. With the ground shock time history used here, only a reduction in the mass of the isolator rod will eliminate the problem of slackening of the cable.

SECTION 4 SYMBOLS AND NOTATIONS

A	: Area, inches ²
C	: Damping coefficient, pound seconds/inch
C _{ave}	: Model average equivalent viscous damping coefficient, pound seconds/inch
C _e	: System series-parallel equivalent damper, pound seconds/inch
C _{ep}	: System parallel equivalent damper, pound seconds/inch
C _{es}	: System series equivalent damper, pound seconds/inch
C _i	: Isolator damping constant, pound seconds ² /inch ²
C _m	: Linear model equivalent viscous damping coefficient, pound seconds/inch
C _m	: Model damping constant, pound seconds ² /inch ²
C _{max}	: Model maximum equivalent viscous damping coefficient, pound seconds/inch
C _p	: Specific heat of air, Btu/pound-degrees F.
C _s	: System equivalent viscous damping constant, pound seconds/inch
C _{s ave}	: System average equivalent viscous damping coefficient, pound seconds/inch
C _{sc}	: Pendulum horizontal critical damping coefficient, pound seconds/inch
C _{s max}	: System maximum equivalent viscous damping coefficient, pound seconds/inch
D	: Diameter, inches
d _f	: Viscous damper hole size, inches
F	: Force, pounds
F _c	: Liquid spring seal friction force, pounds

F_d	: Damping force, pounds
F_{dm}	: Model equivalent viscous damping force, pounds
F_f	: Friction force, pounds
F_h	: Equivalent pendulum and polyurethane horizontal forces, pounds
$F_{osc.m}$: Model frequency of oscillation, cycles/second
F_r	: Liquid spring rod force, pounds
F_s	: Liquid spring friction coefficient, pound seconds/inch
g	: Gravitational constant, 386 inches/seconds ²
h_L	: Head loss, height of fluid column, feet
h_m	: Model height, inches
h,u,c	: Pneumatic spring dimensions, inches
h_s	: System polyurethane height, inches
K	: System polyurethane spring constant, pounds/inch
K_1	: Model nonlinear spring, pounds/inch
K_2	: Model nonlinear spring, pounds/inch
K_c	: Cable and isolator rod combined spring constant, pounds/inch
K_D	: Model damping coefficient, pound seconds/inch
K_e	: System series-parallel equivalent spring, pounds/inch
K_{ep}	: System parallel equivalent spring, pounds/inch
K_{es}	: System series equivalent spring, pounds/inch
K_i	: Isolator spring constant, pounds/inch
K'_m	: Linear model equivalent spring constant, pounds/inch
K_m	: Model spring constant, pounds/inch

K'_S	: Polyurethane, average, spring rate, pounds/inch
K_S	: System equivalent nonlinear spring constant, pounds/inch
K_{sd}	: Sway damper spring constant, pounds/inch
k	: Liquid spring stiffness, pounds/inch
L	: Pneumatic spring sleeve length, inches
L_m	: Model length, inches
L_s	: System polyurethane depth, inches
l	: Liquid spring stroke, maximum, inches
l_d	: Linear motion damper piston length, inches
l_s	: Liquid spring seal width, inches
M	: System model number of horizontal elements
M_m	: Model mass, pound seconds ² /inch
M_s	: Suspended mass, pound seconds ² /inch
m	: Mass, pound seconds ² /inch
N	: System model number of vertical elements
N_m	: Model height, inches
n	: Polytropic index
P	: Pressure, pounds/inches ²
p	: System model number of horizontal elements
q	: Thermal energy, British thermal units
Q	: System model number of horizontal elements
R	: Pendulum equivalent length, inches
R_{es}	: System series equivalent spring, pounds/inch
r	: Radius, inches
S, a, b, c	: Arbitrary constants

T	: Temperature, absolute, degrees fahrenheit
T_c	: Cable tension, pounds
T_r	: Rod tension, pounds
t	: time, seconds
V	: Volume, inches
V_f	: Fluid velocity, inches/second
V_p	: Piston velocity, inches/second
W	: Load, pounds
W_m	: Model width, inches
W_s	: System polyurethane width, inches
w	: Specific weight, pounds/feet ³
X	: Piston displacement, inches
\dot{X}	: Piston velocity, inches/second
X_1	: Model mass absolute displacement, inches
\dot{X}_1	: Model mass absolute velocity, inches/second
X_2	: Model damper absolute displacement, inches
\dot{X}_2	: Model damper absolute velocity, inches/second
X_3	: Model spring bottom point absolute displacement, inches
Z	: Vertical displacement, inches
γ	: Ratio of specific heats for air
ζ_m	: Model damping ratio
$\zeta_{s \text{ ave}}$: Pendulum average horizontal damping ratio
$\zeta_{s \text{ max}}$: Pendulum maximum horizontal damping ratio
ω	: Frequency, radians/second
ω_{nm}	: Model natural frequency of oscillation, radians/second

$\omega_{osc.m}$: Model frequency of oscillation, radians/second
ω_{sn}	: Pendulum horizontal natural frequency, radians/second
ω_v	: System vertical frequency, radians/second
ϕ	: Pendulum inclination, angle, degrees
$\dot{\phi}$: Pendulum angular velocity, degrees/second
$\ddot{\phi}$: Pendulum angular acceleration, degrees/second ²
ν	: Kinematic viscosity, inches ² /second
ΔL	: Change in isolator length, inches

5.0 RIGID BODY ANALYSIS

5.1 Introduction

In Section 3.0, various types of suspension systems were compared with regard to the amount of coupling they introduced into the system and to their stability. To reduce the problem to a manageable size, the systems were simplified to three degrees of freedom and the comparisons were made on a qualitative rather than a quantitative basis. Two systems were selected for more detailed analysis, Configurations 2 and 3.

For the purpose of selecting the basis configuration of the system and establishing the gross characteristics of the system components, it is believed that the simplified treatment is sufficient. However, it does not establish the bounds of excursions or accelerations of the system nor does it account for the nonlinear stiffnesses of the isolators, the effect of damping, nor the contribution of coupling in the neglected modes. As a second step in the design procedure, then, a formal analysis of the dynamic response of the complete system is essential.

In this section, the complete equations of motion are formulated for the six-degree-of-freedom rigid body system. The assumption that flexibilities in the cage structure itself have negligible effect on the system response is justified by a separate analysis described in Section 6.0. The dynamics of the suspension system elements themselves, that is the cables and isolators, have also been studied separately in Section 4.0. The solution of the equations has not been undertaken here as they are not essential to the demonstration of feasibility but serve to provide design data and a means for refinement of the system parameters.

Another area given special attention is that of control requirements. Variations in loading and environment and off-nominal conditions caused by construction tolerances all tend to displace the suspended cage from its normal equilibrium position. Some displacement of the cage, of course, can be tolerated. But care must be taken to insure that the excursion is not excessive nor the dynamic response of the system compromised.

To limit the excursions, therefore, a control system is needed. Its only function is to maintain the static position of the cage within prescribed tolerances; it is inactive during shock conditions. The requirements for such a system are reviewed in this section. The sensitivity required can be related directly to the permissible rotation of the cage, and from the sensitivity, the maximum permissible friction established.

Two additional factors, presented as appendices, which can influence significantly the dynamic response of the system are the forces exerted on the cage by the resistance of air to its motion and by the sloshing of fluids in the many containers located within the cage.

The motion of the rigid body system comprising the cage structure in space possesses six degrees of freedom; three generalized translations of the center of gravity, and three generalized rotations about the center of gravity. The generalized translations are expressed in polar coordinates by the instantaneous length of the

pendulum (ℓ) with its angles in the horizontal and vertical planes (θ and ϕ). The generalized rotations (α, β, γ) are selected about a set of axes passing through the center of gravity, these axes remaining parallel to their original directions during motion.

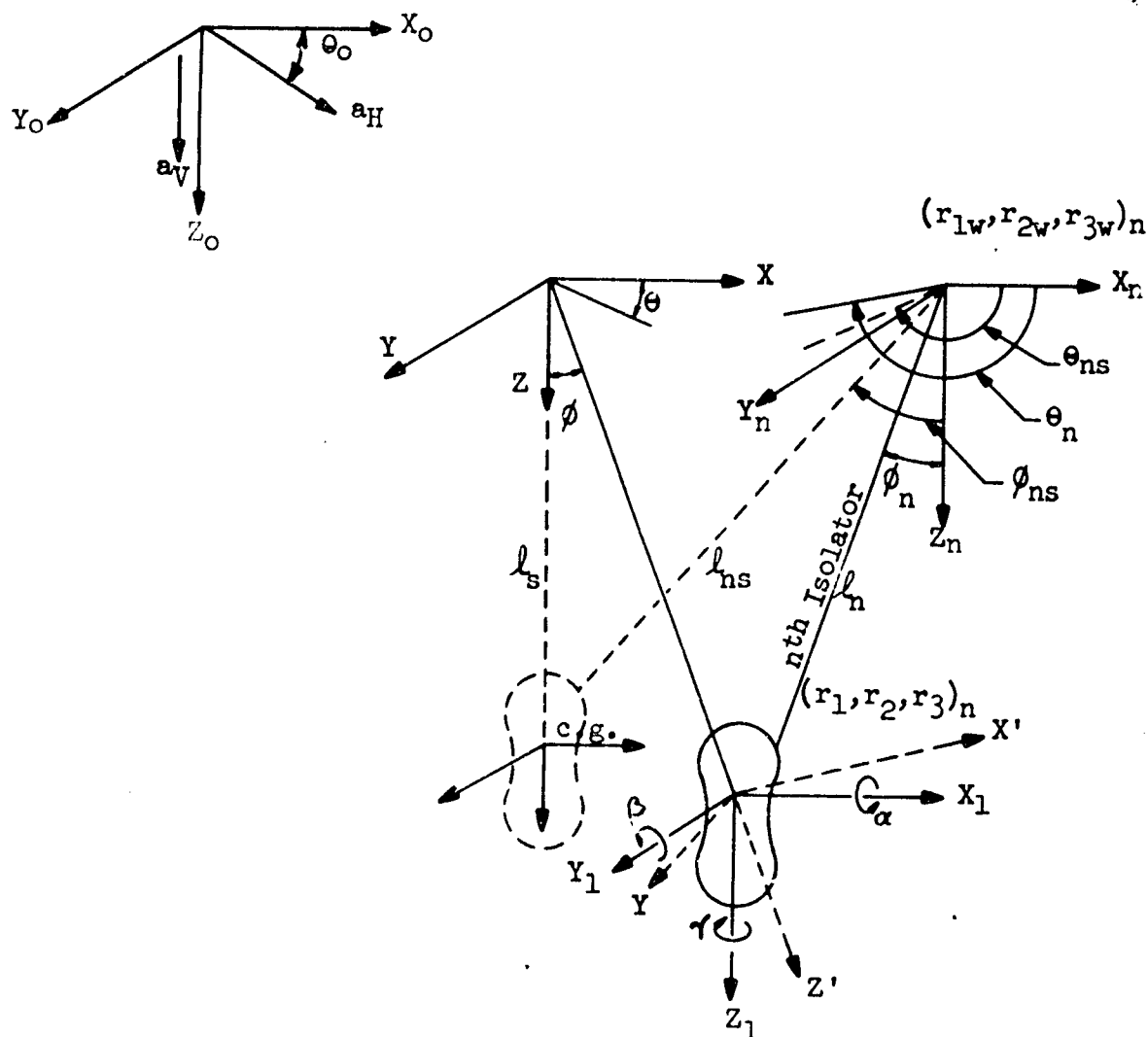
The equations of motion are derived by using tensor analysis and matrix algebra. The transformation from one reference system to another is obtained by linear algebra. The equations account for the couplings in the translations and rotations, including the gyroscopic effects. Hence, they represent the rheo-nonlinear system in relative coordinates with respect to the capsule.

It seems reasonable to assume that the rotations α, β and γ about the X, Y, Z axes, respectively, are small. Hence, the following approximations are made to reduce the computing time without impairing the accuracy.

$$\begin{array}{ll} \sin \alpha \approx \alpha & \cos \alpha \approx 1 \\ \sin \beta \approx \beta & \cos \beta \approx 1 \\ \sin \gamma \approx \gamma & \cos \gamma \approx 1 \end{array}$$

5.2 Reference Systems

Various reference systems are selected for describing the motions. The capsule motion is described in the reference system fixed to the earth's axis (ground reference system $X_0-Y_0-Z_0$). The cage motion is described in the reference system fixed to the capsule (capsule reference system $X-Y-Z$). Two sets of reference systems are selected at the center of gravity; one remaining parallel to its original position (inertial reference system $X_1-Y_1-Z_1$) and the other fixed to the cage which rotates along with the cage rotations (moving reference system $X'-Y'-Z'$), which is related to the inertial reference system by classical Euler's coordinates. These systems are shown on Figure 5-1.



$X_0-Y_0-Z_0$ - Ground reference system

$X-Y-Z$ - Capsule reference system (parallel to $X_0-Y_0-Z_0$)

$X_1-Y_1-Z_1$ - Inertial reference system (origin at center of gravity, parallel to $X-Y-Z$)

$X'-Y'-Z'$ - Moving reference system (origin at center of gravity, fixed to mass)

$X_n-Y_n-Z_n$ - Isolator reference system (origin at capsule attachment point, parallel to $X-Y-Z$).

Figure 5-1. Reference Systems.

5.3 Equations of Motion

$$\left\{ [D]_p [m\ddot{S}]_p \right\} + \sum \left\{ [D]_{pn} [C]_n \left[[S]_{pn} + [D]_{pn}^{-1} [-r_a] [\dot{\phi}] \right] \right\} \\ + \sum \left\{ [D]_{pn} [C^D]_n \left[[\dot{S}]_{pn} + [D]_{pn}^{-1} [-r_a] [\dot{\phi}] \right] \right\} + \left\{ [m\ddot{S}_0 - mg] \right\} = 0 \quad (\text{Eq. 5.1})$$

$$\left\{ \frac{d}{dt} [\phi] \right\} + \sum \left\{ [r_a] [D]_{pn} [C]_n \left[[S]_{pn} + [D]_{pn}^{-1} [-r_a] [\dot{\phi}] \right] \right\} \\ + \sum \left\{ [r_a] [D]_{pn} [C^D]_n \left[[\dot{S}]_{pn} + [D]_{pn}^{-1} [-r_a] [\dot{\phi}] \right] \right\} = 0 \quad (\text{Eq. 5.2})$$

$$[\omega] = [D]_{\omega} [\dot{\lambda}] \quad (\text{Eq. 5.3})$$

$$[\dot{\phi}] = [D]_{\phi} [\dot{\lambda}] \quad (\text{Eq. 5.4})$$

where $[D]_{pn}$ and $[S]_{pn}$ are found by solving the following equation

$$[D]_{pn} [S]_{pn} = [D]_{pns} [S]_{pns} = [D]_p [S - l_s]_p \quad (\text{Eq. 5.5})$$

$$[C]_n = [D]^{-1} [K]_n [D]$$

$$[C^D]_n = [D]^{-1} [K^D]_n [D]$$

$$\frac{d}{dt} [\phi] = \begin{bmatrix} I_{11}\dot{p} + (I_{33} - I_{22}) \cdot qr \\ I_{22}\dot{q} + (I_{11} - I_{33}) \cdot rp \\ I_{33}\dot{r} + (I_{22} - I_{11}) \cdot pq \end{bmatrix}$$

$$[\omega] = \{p \quad q \quad r\}$$

$$[\phi] = \{\alpha \quad \beta \quad \gamma\}$$

$$[\dot{\phi}] = \{\dot{\alpha} \quad \dot{\beta} \quad \dot{\gamma}\}$$

$$[\lambda] = \{\theta \quad \phi \quad \psi\}$$

$$[\dot{\lambda}] = \{\dot{\theta} \quad \dot{\phi} \quad \dot{\psi}\}$$

$$\{[D]_{pn}[S]_{pn}\} = \begin{bmatrix} l_n \cdot \sin \phi_n \cdot \cos \theta_n \\ l_n \cdot \sin \phi_n \cdot \sin \theta_n \\ l_n \cdot \cos \phi_n \end{bmatrix}$$

$$\{[D]_{pns}[S]_{pns}\} = \begin{bmatrix} l_{ns} \cdot \sin \phi_{ns} \cdot \cos \theta_{ns} \\ l_{ns} \cdot \sin \phi_{ns} \cdot \sin \theta_{ns} \\ l_{ns} \cdot \cos \phi_{ns} \end{bmatrix}$$

$$\{[D]_p[S-l_s]_p\} = \begin{bmatrix} l \cdot \sin \phi \cdot \cos \theta \\ l \cdot \sin \phi \cdot \sin \theta \\ l \cdot \cos \phi - l_s \end{bmatrix}$$

$$[D]_{\phi} = \begin{bmatrix} 0 & -\sin \theta & \sin \phi \cdot \cos \theta \\ 0 & \cos \theta & \sin \phi \cdot \sin \theta \\ 1 & 0 & \cos \phi \end{bmatrix}$$

$$[m\ddot{S}']_p = \begin{bmatrix} 2m\ddot{l}\dot{\phi} + m\ddot{l}\phi - m\dot{\theta}^2 \sin \phi \cdot \cos \phi \\ 2m\dot{\theta}\dot{\phi}\sin \phi + 2m\ddot{\phi}\dot{\theta} \cos \phi + m\ddot{\theta} \sin \phi \\ m\ddot{l} - m\dot{\phi}^2 - m\dot{\theta}^2 \sin^2 \phi \end{bmatrix}$$

$$[S]_{pn} = \begin{bmatrix} 0 \\ 0 \\ l_n - l_{no} \end{bmatrix}$$

$$[\dot{S}']_{pn} = \begin{bmatrix} l_n \cdot \dot{\phi}_n \\ l_n \cdot \sin \phi_n \cdot \dot{\theta}_n \\ l_n \end{bmatrix}$$

$$[r_a]_n = \begin{bmatrix} 0 & -r_3 & r_2 \\ r_3 & 0 & -r_1 \\ -r_2 & r_1 & 0 \end{bmatrix}_n$$

$$[-r_a]_n = \begin{bmatrix} 0 & r_3 & -r_2 \\ -r_3 & 0 & r_1 \\ r_2 & -r_1 & 0 \end{bmatrix}_n$$

$$[D]_p = \begin{bmatrix} \cos\phi \cdot \cos\theta & -\sin\theta & \sin\phi \cdot \cos\theta \\ \cos\phi \cdot \sin\theta & \cos\theta & \sin\phi \cdot \sin\theta \\ -\sin\phi & 0 & \cos\phi \end{bmatrix}$$

$$[D]_{pn} = \begin{bmatrix} \cos\phi_n \cdot \cos\theta_n & -\sin\theta_n & \sin\phi_n \cdot \cos\theta_n \\ \cos\phi_n \cdot \sin\theta_n & \cos\theta_n & \sin\phi_n \cdot \sin\theta_n \\ -\sin\phi_n & 0 & \cos\phi_n \end{bmatrix}$$

$$[D]_{pn}^{-1} = \begin{bmatrix} \cos\phi_n \cdot \cos\theta_n & \cos\phi_n \cdot \sin\theta_n & -\sin\phi_n \\ -\sin\theta_n & \cos\theta_n & 0 \\ \sin\phi_n \cdot \cos\theta_n & \sin\phi_n \cdot \sin\theta_n & \cos\phi_n \end{bmatrix}$$

$$[D] = \begin{bmatrix} 1 & -\gamma & \beta \\ \gamma & 1 & -\alpha \\ -\beta & \alpha & 1 \end{bmatrix}$$

$$[D]^{-1} = \begin{bmatrix} 1 & \gamma & -\beta \\ -\gamma & 1 & \alpha \\ \beta & -\alpha & 1 \end{bmatrix}$$

$$[D]_\omega = \begin{bmatrix} -\sin\phi \cdot \cos\psi & \sin\psi & 0 \\ \sin\phi \cdot \sin\psi & \cos\psi & 0 \\ \cos\phi & 0 & 1 \end{bmatrix}$$

Initial Conditions

For resultant pendulum

$$\begin{bmatrix} l \\ \phi \\ \theta \end{bmatrix}_{t=0} = \begin{bmatrix} l_s \\ 0 \\ 0 \end{bmatrix}$$

For n^{th} isolator

$$\begin{bmatrix} l_n \\ \phi_n \\ \theta_n \end{bmatrix}_{t=0} = \begin{bmatrix} l_{ns} \\ \phi_{ns} \\ \theta_{ns} \end{bmatrix}$$

Translation of center of gravity

$$\begin{bmatrix} X \\ Y \\ Z \end{bmatrix} = \begin{bmatrix} l \cdot \sin\phi \cdot \cos\theta \\ l \cdot \sin\phi \cdot \sin\theta \\ l \cdot \cos\phi \end{bmatrix}$$

Displacement of mass-attachment point of the n^{th} isolator

$$\begin{bmatrix} \delta x \\ \delta y \\ \delta z \end{bmatrix}_n = \begin{bmatrix} X \\ Y \\ Z \end{bmatrix} + \begin{bmatrix} 0 & r_s - r_2 \\ -r_3 & 0 & r_1 \\ r_2 & -r_1 & 0 \end{bmatrix}_n \begin{bmatrix} \alpha \\ \beta \\ \gamma \end{bmatrix}$$

Length of n^{th} isolator at time t

$$l_{nf} = \left\{ (r_{1w} - r_1 - \delta x)_n^2 + (r_{2w} - r_2 - \delta y)_n^2 + (r_{3w} - r_3 - \delta z)_n^2 \right\}^{1/2}$$

Stiffness of n^{th} isolator

$$(K_{ZZ})_n = (K)_n \left\{ 1 + C_1 \left[\text{Sign} (\Delta l_{nf}) \right]^0 \right\}$$

Damping stiffness of n^{th} isolator

$$(K_{ZZ}^D)_n = C_2 (\Delta l_{nf})^0$$

5.4 Dynamic Response

The equations of motion for the isolated cage structure with six degrees of freedom are presented in paragraph 5.3. These equations need be solved by numerical integration method on a digital computer. The purpose of numerical analysis is not only to obtain the response of a particular system but also to obtain enough data to study the effects of various parameters on the response of a system. Suspension configurations, locations of the center of gravity, weight of the body input waveforms, damping et cetera, are a few of the important parameters to which most isolation systems are sensitive.

Various computer runs can be planned as shown in Table 5-1. The order of runs is set up in such a way as to arrive at the selection of values of parameters at the end of all runs which will give optimum response of the system.

Run No. 1 and 2 will give the response of systems with one-level and two-level suspension configurations for a direct comparison. These two runs are basically scheduled to confirm the qualitative results obtained in Section 3 by quantitative analysis. Run No. 3 is introduced to check the effect of an increase in computing time interval on total response. To reduce total computing time and in turn reduce the cost of computation, it is desirable to integrate numerically with maximum possible computing time interval, and errors within set limits. With this in mind, the response obtained from Run No. 3 can be compared with that of No. 2 and if the difference is small enough to neglect, the increased time interval can be used in the subsequent runs. Even though the qualitative analysis (Ref. Section 3) shows certain relations between various parameters which will optimize the response, these relations in turn are not sufficient to define the configuration completely. Hence Runs No. 4 and 5 are scheduled to study the effects of a change in the levels of attachment points and in the ratio of stiffness between the top and bottom series of isolators.

It is expected that enough data will be obtained at the end of five runs to decide on the final configuration for the two-level suspension system. To study the effect of variation of damping in the system, Run No. 6 is scheduled to obtain the response with smaller or greater amount of damping. The change in damping can be decided after studying the results of previous runs. The effect of the shift of the center of gravity location and increase or decrease in weight of the body will be obtained from Run No. 7, while Run No. 8 will provide the basis for comparison between responses of the system with different initial inclinations of isolators.

The phase difference between the arrival time of horizontal and vertical waves may increase the response of the system. Run No. 9 is planned to obtain quantitative data on effect of phasing. Depending upon the reliability of the system, it seems possible that one of the isolators carrying the maximum load may break during dynamic motion, in which case it is highly desirable to know the behavior of the body, the response of which is planned in Run No. 10. If the response of the system is completely out of bounds, the reliability of the system should be increased. Runs No. 11 to 13 are scheduled for the static stability check.

The programming of the equations of motion is done in general form, as given in Reference 22 so that for various runs only the numerical data need to be changed.

Table 5-1 Computer Run Schedule - Rigid Body Analysis

Run No	Suspension Configuration See Note 1		Input See Note 2			Center of Gravity Location See Note 3			Damping See Note 4			Liner Attachment Point See Note 5			Cage Attachment Point See Note 6			Remarks
	1	2	1	2	3	1	2	3	1	2	3	1	2	3	1	2	3	
1	X		X	X	X	X	X	X	X	X	X	X	X	X	X	X	X	One level suspension Two level suspension Time interval check - run time = 1 sec. Change attachment points Change in stiffness ratio Adjustment of damping Center of gravity and wt. variation Effect of initial inclination of Isolators Phasing of Input Isolator with max. load, assumed broken Static Stability Check -do- -do- Reserve
2		X	X	X	X	X	X	X	X	X	X	X	X	X	X	X	X	
3		X	X	X	X	X	X	X	X	X	X	X	X	X	X	X	X	
4		X	X	X	X	X	X	X	X	X	X	X	X	X	X	X	X	
5		X	X	X	X	X	X	X	X	X	X	X	X	X	X	X	X	
6		X	X	X	X	X	X	X	X	X	X	X	X	X	X	X	X	
7		X	X	X	X	X	X	X	X	X	X	X	X	X	X	X	X	
8		X	X	X	X	X	X	X	X	X	X	X	X	X	X	X	X	
9		X	X	X	X	X	X	X	X	X	X	X	X	X	X	X	X	
10		X	X	X	X	X	X	X	X	X	X	X	X	X	X	X	X	
11		X	X	X	X	X	X	X	X	X	X	X	X	X	X	X	X	
12		X	X	X	X	X	X	X	X	X	X	X	X	X	X	X	X	
13		X	X	X	X	X	X	X	X	X	X	X	X	X	X	X	X	
14		X	X	X	X	X	X	X	X	X	X	X	X	X	X	X	X	

Note 1 - Suspension Configurations

1. One-Level Suspension (Configuration 2)
2. Two-Level Suspension (Configuration 3)

Note 2 - Inputs

1. Maximum horizontal + maximum vertical with zero phasing
2. Maximum horizontal + maximum vertical with phasing
3. Static stability inputs

Note 3 - Center of Gravity Locations

1. Highest Center of Gravity + greatest eccentricity with min. weight
2. Lowest Center of Gravity + greatest eccentricity with max. weight

(continued next page)

Table 5-1 (Continued)

- Note 4 - Damping
1. Equivalent of 10 percent critical damping
 2. To be determined
- Note 5 - Liner attachment points
1. Short pendulum (as shown in Fig. 3-7)
 2. To be determined
- Note 6 - Cage attachment points
1. As shown in Fig 3-7
 2. As shown in Fig. 3-4
 3. To be determined

5.5 Leveling and Load Balancing Control

5.5.1 Leveling Requirements

As the cage is subjected to changing loads and the suspension system must withstand changes in environment, excursions of the system from its position of balanced equilibrium will occur unless prevented by some type of adjustment. In suspension Configurations 2 and 3 where the pendulum arms are inclined from the vertical, loading eccentricities introduced by shifts of the center of gravity off the vertical centerline can introduce lateral translations of the cage as well as rotations. In Configuration 1 no lateral translations can occur.

Both rotations and translations are undesirable in that they increase the rattlespace requirement; and even small rotations of the cage may create an unpleasant environment for personnel housed within it. Thus a control system, preferably automatic, which will maintain the position of the cage near a nominal location and will insure that the system is properly balanced appears to be warranted.

Conditions which tend to disturb the position of the cage from its equilibrium position are

- . load change (R,T)
- . center of gravity shift (R,T)
- . temperature change (T)
- . leakage of fluid from isolator (R,T)
- . creep of pendulum assemblies, particularly the cables (R,T).

The resulting excursion, rotation or translation, is indicated by (R) or (T) respectively. If the cage is to be restored to its initial position, a correction involving a change in the mass of fluid within the isolator or in the volume of the isolator must be made.

The approximate ranges of conditions influencing the design of the control system are given in the following tabulation.

Load/Isolator

Configuration 2 421,000 lb $\begin{cases} +32\% \\ -28\% \end{cases}$

Configuration 3

Upper 560,000 lb $\begin{cases} +32\% \\ -28\% \end{cases}$

Lower 282,000 lb $\begin{cases} +32\% \\ -28\% \end{cases}$

Center of Gravity Shift

Radial ± 4.0 ft.

Vertical ± 6.0 ft.

Temperature Variation $\pm 10^{\circ}$ F.

Leakage small but finite

Creep $\frac{\Delta L}{L}$ per year = .005 (est.)

The tolerance on the rotation of the platform under equilibrium conditions is established on the bases of

- . human factors: unpleasantness due to sloping floors.
- . rattlespace: translation of corners of cage due to angular displacement.

Quantitative data on the effect on human beings of continued exposure to slightly tilted surroundings have not been located. On the basis of intuition, however, it would appear that a floor sloping six inches in twenty feet would cause some discomfort. Yet this slope amounts to an angle of only 1.5 degrees. In Figure 5-2 the vertical and horizontal displacements of the corners of the cage are shown as functions of the angle of rotation. For an angle of rotation of 1.5 degrees, it is seen that the horizontal displacement is 1.9 feet. Note that this value is greater than the translation of the center of gravity of the system due to the ground shock.

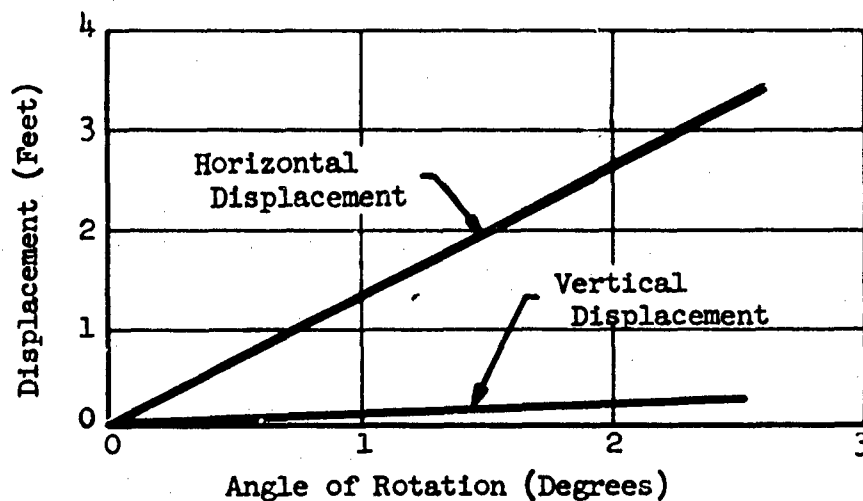


Figure 5-2. Displacement of Corner of Cage vs Angle of Rotation.

It was noted in Section 3.0 that for Configurations 2 and 3 where the pendulum arms are inclined from the vertical, a lateral excursion of the center of gravity will cause a rotation and a lateral translation of the cage. For both configurations a four foot radial excursion of the center of gravity will cause a lateral displacement of the cage relative to the capsule wall of about 1.8 feet.

If the lengths of the pendulum arms are adjusted by a controller so that the angle of rotation is not permitted to exceed 1.5 degrees, the total possible excursion of a corner of the cage resulting from the combined affects of rotation and translation will be 3.9 feet. This static displacement is very near to the amount needed to accommodate the dynamic response and thus would double the rattlespace requirement.

Lateral translation due to the center of gravity shift can be reduced only by decreasing the angle of inclination of the pendulum arms, thus increasing dynamic excursions and reducing the ratio of horizontal to vertical damping. The permissible angularity of 1.5 degrees, however, was fixed arbitrarily and can be reduced. Assuming a maximum permissible lateral excursion of the cage corner of 2.5 feet, the maximum allowable component due to rotation is 0.7 feet and the rotation angle 0.55 degrees. If the pendulum attachments to the cage structure are located on an 80-foot diameter, the vertical excursion to produce this rotation is ± 3.8 inches. It is necessary then that any leveling system be sufficiently sensitive to maintain all pendulum arm lengths within a tolerance of ± 3.8 inches if the 2.5 foot maximum excursion of the cage corner is to be maintained.

The change in the length of a liquid spring due to expansion of the fluid accompanying a 20°F . variation in temperature was shown in Section 4.0 to be 13.1-inches. Assuming the temperature distribution throughout the system is uniform, the change in pendulum arm length would result in a vertical translation of the cage of about $\pm 6\frac{1}{2}$ inches. While rattlespace in the vertical direction is not particularly critical, the incorporation of temperature sensitive adjustment capability in the controller does not add to the cost of the controller and could obviate the need for added length of the isolator as well as for rattlespace.

It was shown in Section 4.0 that the temperature sensitivity of the pneumatic isolator was much less than that of the liquid spring. Here again, however, the same controller which maintains the rotational orientation can be employed to correct for the deviations in isolator piston position due to temperature changes.

However, even if the controller maintains the isolator piston in a fixed position relative to the cylinder, it will not compensate for changes in length of the cable or other metal parts comprising the pendulum arm. Due to the small temperature variation, however, these changes in length will not be large. For Configuration 2 and for the upper arm of Configuration 3, a $\pm 10^{\circ}\text{F}$. temperature variation will result in a length change of about ± 0.05 inches. For the lower arm of configuration the change in length is ± 0.11 inches.

Similarly, while the controller can compensate for isolator displacements due to load changes, it will not compensate for elastic deformations of the cables.

The amount of creep that may be expected to occur in the cables over the expected life span is a function principally of load and vibration. Although it is difficult to calculate the creep with any confidence, it is known to be small. Further, turnbuckles may be installed in the cables to permit readjustment of cable length at very infrequent intervals.

To calculate the elastic deformations of the cables due to variations in loading conditions assume an allowable cable stress (σ_m) of 50,000 psi, a modulus of elasticity (E) of 13×10^6 psi and an effective cross-sectional area equal to

$$A_{eff} = 0.4 d^2$$

where d is the nominal cable diameter (Reference 21). Then the deflection is

$$\delta = \frac{FL}{0.4d^2E} = \frac{FL\sigma_m}{F_m} = (3.84 \times 10^{-3}) \left(\frac{LF}{F_m} \right)$$

where

F = the applied load

L = cable length

F_m = maximum design load

Designating the nominal isolator load by F_o , and as $F_m = 1.32F_o$, the maximum deviations of isolator loads from the equilibrium value are:

Deviation Due To	Minimum	Maximum
Weight Change	$\pm 0.10 F_o$	$- 0.10 F_o$
C.G. Shift	$\pm 0.18 F_o$	$\pm 0.22 F_o$

while for Configuration 3 the ratios for the upper and lower cables will differ slightly from these values, the difference will be small and may be neglected here.

Using the cable geometry given in Section 3, the vertical displacements of isolator attachment points on the cage resulting from load changes and center of gravity shifts are calculated and shown in Table 5-2 together with estimates of excursions due to temperature changes and creep. None of these deviations can be rectified by a controller which maintains the isolator piston in a given position relative to the cylinder.

Table 5-2 Vertical Displacements of Cage
Not Corrected by Controller

	Configuration No. 2		Configuration No. 3	
	Up (in.)	Down (in.)	Up (in.)	Down (in.)
Temperature	.05	.05	.11	.11
Creep (per year)	-	.40	0	.66
Elastic Displacement of Cables				
Due to Translation	.15	.15	.38	.38
Due to Rotation	.33	.33	.83	.83
Total Uncorrected Vertical Displacement	.53	.93	1.32	1.98

Earlier the maximum permissible angular rotation of the platform under static conditions was fixed at 0.55 degrees. This angle will result from vertical differential movements of the isolator attachment points of ± 3.8 inches. If the static elongation of the cables due to center of gravity shifts is ± 0.8 inches as indicated in the Table above, the control band of isolator position must not exceed ± 3.0 inches if the angularity tolerance is to be met.

5.5.2 Leveling Control

As the differential changes in length of the pendulum cables due to temperature, creep and elasticity are relatively small, leveling of the cage can be easily controlled within an acceptable tolerance by a signal proportional to the displacement of the isolator piston relative to a set point in the cylinder. The signal would regulate the volume of oil or air in the cylinder so as to restore the system to its equilibrium position. By this means, changes in fluid pressure due to temperature variations are corrected as are those due to leakages and load changes.

It is possible now to evaluate the maximum static friction the system can possess and still permit the pendulum and length to return to the maximum permissible deviation from the equilibrium position. If the error band half-width, δ , is 3.0 inches, the maximum possible ratio of static friction force F_f to supported weight (η) is

$$\eta = \frac{\delta \omega^2}{g} = \frac{3.0 \times 2.20^2}{386} = .037 \text{ or } 3.7\% \text{ of the static load}$$

Whether or not this amount of static friction will allow the controller to exercise a reasonable degree of control on the equilibrium position of the system depends on the details of the friction force-velocity relationship. If the initial slope of the friction-force curve is negative, the system will exhibit "stick-slip" characteristics i.e. as a control force is applied slowly to the unit, it will remain motionless until the static friction force is exceeded and will then break loose and jump to a new position where the process is repeated. It is evident that if the jump displacement is any sizeable percentage of the control band width, controlability is severely reduced and the system tends to hunt. If for small velocities, the slope of the friction force-velocity curve is positive, no jump will occur and the controller can return the system to any desired position.

In Figure 4-12, the rough outlines of a friction force-velocity relationship as predicted by one liquid spring manufacturer are shown. It may be noted that the slope of the curve in the region $0 < v < 0.25$ inches per second is positive while at greater velocities it is negative. If this curve is truly representative of the character of friction in a liquid spring, "stick-slip" tendencies can be avoided by limiting the flow of fluid to and from the cylinder to those rates which would produce piston velocities less than 0.25 inches per second.

The vital importance of the shape of the friction force-velocity relationship on the controlability of an isolator which develops an appreciable amount of friction is evident. Friction in good pneumatic spring design is relatively small, on the order of one half of one per cent of the static force, so that even if "stick-slip" were to occur, the jumps would be of relatively small displacement.

It has been noted, however, that the total friction associated with the liquid spring may be appreciable. Thus the feasibility of the use of the liquid spring hinges directly on the nature of the friction characteristic. Friction data furnished by manufacturers, however, are inconclusive although they state they have not observed "stick-slip" tendencies.

5.5.3 Load Balancing Requirement

One further requirement of the control system, and, possibly the most difficult to achieve, is that of ensuring that the proper proportion of total load is carried by each of the twelve isolators. It was shown in Section 3 that there is a unique relationship between the loads carried by each of the isolators which will minimize coupling and achieve a dynamic balance. Yet all systems containing more than three supports are statically indeterminate and there are an infinite number of loading arrangements that can be used to obtain static balance. In installing and adjusting the isolators then, either manually or automatically, it is not sufficient that the cage simply be leveled, but that the loads are apportioned correctly.

It is apparent that the problem is not unique with this facility. Yet in no known installation has there been provisions made to maintain the dynamic balance after the system has once been installed.

The degree of accuracy with which the loads should be maintained in proper balance can only be established by a careful comparison of the cost and reliability of the controller with that of the additional rattlespace resulting from greater coupling.

5.5.4 Load Balance Control System

To determine the proper load each isolator should carry, the total weight, W , and the center of gravity location must be known. For example, consider the system, similar to Configuration 2, as shown in Figure 5-3 .

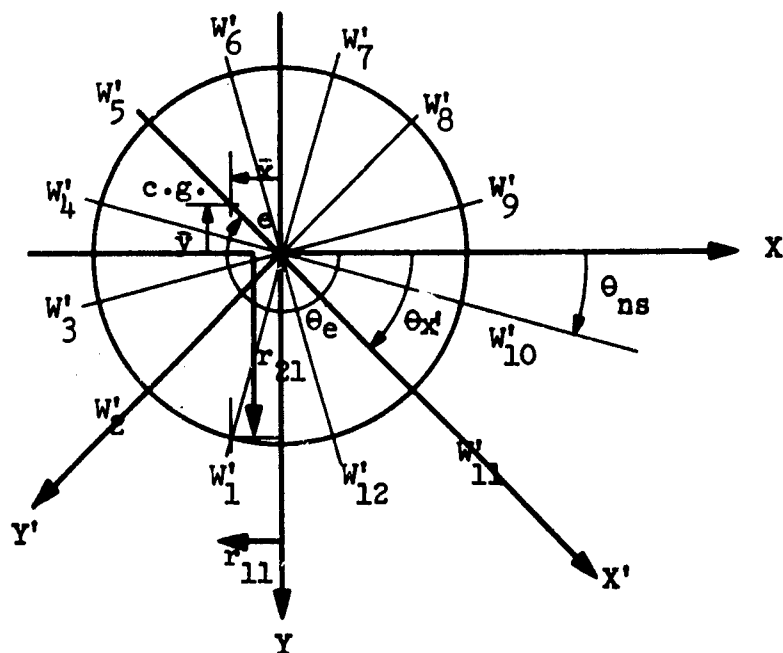


Figure 5-3. Isolator Orientation in Chosen Coordinate System and the Initial Loads Carried by Such Isolator.

The location of the center of gravity can be determined by the following relationship.

$$\bar{X} = - \frac{(W'_1 r_{11} + \dots W'_6 r_{16}) + (W'_7 r_{17} + \dots W'_{12} r_{1-12})}{W_T}$$

$$\bar{Y} = \frac{(W'_1 r_{21} - \dots W'_6 r_{26}) - (W'_7 r_{27} + \dots W'_{12} r_{2-12})}{W_T}$$

$$W_T = W'_1 + \dots W'_{12}$$

where

W'_{1-12} = load carried by each isolator

\bar{X} = distance from y axis to the c.g. location

\bar{Y} = distance from x axis to the c.g. location

r_{1-12} = coordinate of isolator attach points along the x axis

r_{2-12} = coordinate of isolator attach points along the y axis

W_T = total load

Knowing the center of gravity location and the total load, the required load for each isolator can be determined by the relation below.

$$W_{in} = \frac{W_T}{N} + W_T \cdot e \cdot \frac{r'_{in}}{I}$$

W_{in} = required load for each isolator

N = total number of the isolators

n = number of an individual isolator

$$e = \sqrt{\bar{X}^2 + \bar{Y}^2}$$

e = c.g. eccentricity in the x-y coordinate system

r'_{in} = distance to each isolator along the rotated x axis

$$I = \frac{N}{2} R^2 = \text{a constant}$$

ρ = radius of isolator attachment points from geometric center

The location of the center of gravity establishes the direction of the rotated coordinate system, $x'-y'$.

$$\theta'_x = \theta_e - 180.$$

where

θ'_x = angle between the x and the x' axis

θ_e = location of the center of gravity in the x-y coordinate

system $\frac{\bar{X}}{\bar{Y}}$

To use this method as a basis for control, it is necessary to measure the force in each of the isolators; sum them to obtain total weight; calculate the center of gravity location and balanced isolator load; compare the balanced load with the actual load and using the difference as a control signal apply a corrective force to this isolator. Machinery required to accomplish this task would consist of load cells in each of the pendulum arms and a small special purpose computer to generate the error signals. Corrective action could employ the same devices as would be needed for the leveling system.

For the suspension system of Configuration 3, the same basic method could be employed but the equations would have to be modified to insure

the proper load ratio was maintained between the upper and lower pendulum arms.

Two important precautions must be taken during the load balancing process. First, at no time during the process can the rotations or displacement of the cage structure exceed the established tolerances. Second, the facility must remain hard at all times.

5.5.5 Combined Leveling and Load Balancing Control

Satisfactory operation of the control system cannot be obtained if the leveling and the load balancing systems are permitted to operate independently, as many situations would result in conflicting signals being given the servo valve. By means of a simple switching system, however, the two control signals can be made to work together smoothly.

The servo valves are connected so that they always receive their signal from the leveling controller. The load balancing signal then simply acts as a gate to shut out or to permit the leveling signal to be transmitted to the servo valve. In Table 5-3 all combinations of signals are indicated together with the appropriate gate action. The symbols are

- + high level or load
- low level or load
- * correct level or load
- gate open
- gate closed

Table 5-3. Level Signal Gate Command Schedule

Level	+	-	-	+	*	*	+	-
Load	-	+	-	+	+	-	*	*
Gate Position	□	□	○	○	□	○	○	○

The signal would return the system near to the set position but sufficient deadband should be provided to prevent hunting and, in Configuration 3, to accommodate differences in the lengths of the upper and lower cables arising from "noncontrollable" sources listed in Table 5-2. The maximum difference in elongations of the upper and lower cables of Configuration 3

is about 3/4-inch. Thus the minimum deadband width should be on the order of 1/2-inch.

5.5.6 Alternate Load Balancing System

An alternate method of load balancing which obviates the need for any control equipment other than the leveling device has been given some attention but its feasibility has not yet been established. The principle stems from a suggestion made by The Boeing Company regarding the Launch Control Center Shock Isolation System for the Minute-Man Weapon System. In any three-point suspension system, the load carried by each of the three supporting members is uniquely defined. If the system has more than three support points, the suggestion was made that they be interconnected such that they form three groups, each group acting effectively as a single support point.

To obtain a level and balanced equilibrium position it would only be necessary to provide three leveling devices, each device serving a group of isolators. The system retains the advantages of wider load distribution and smaller isolator units than a system employing only three isolators.

The dynamic response of the system, however, is related directly to the manner in which the isolators of a single group are interconnected. If the connection is such that the pressures within all of the isolators of a single group are identical during dynamic as well as static conditions, the entire group then acts as a single unit and the system is balanced dynamically as well as statically. However due to the large fluid flow rates occurring during dynamic excursions, it does not appear practicable to maintain a pressure balance at all times. On the other hand, if the physical connection is made only large enough to maintain equal pressures during small motions, the system is no longer balanced dynamically.

The feasibility of this method of obtaining load balance then is directly dependent on the degree of coupling which can be tolerated in the system. The suitability of the method for this application can only be evaluated by a thorough analysis of the system response.

5.5.7 Liquid Spring Controller

As a general practice in high pressure liquid system design every attempt should be made to reduce the number of external fluid filled accessories to a minimum. Pumps, valves, regulators, and even piping not only present severe design and fabrication problems but also increase the possibility of catastrophic failure. Yet in this design, it has been shown that active position regulation is essential. Thus the physical volume of the cylinder must be controlled in some manner, or fluid must be added and removed.

One concept of a control system which will provide the needed regulation is described here and approximate sizes estimated. The detail mechanical design of the system has not been investigated nor have suppliers of high pressure equipment been consulted. However the basic principle appears to be sound and while some rearrangements would undoubtedly be required, the concept as presented should be sufficient to establish feasibility.

One definite advantage in the design of a controller for this facility is that its response rate should not be high. It was mentioned earlier that this fact permitted the use of piston velocities which were sufficiently low so that the slope of the friction characteristic was positive. The selection of a low response rate is based on two considerations. First, it is desirable not to have to turn the system off during dynamic excursions yet it should not influence significantly the dynamic response. As the primary purpose of the control is to compensate for weight and temperature changes, the second consideration is based on the estimated maximum time rates of change of these variables which are usually very low.

The minimum total stiffness of the isolation system in the vertical direction is about 57,000 pounds per inch. If the load in the cage structure were changed at a rate of 1000 pounds per second, and the controller was to provide continuous compensation, the control velocity need be only about one inch per minute or 0.016 inches per second.

The rate of temperature change for which position compensation could be provided if the maximum piston velocity is 0.016 inches per second is

$$\frac{dT}{dt} = -\left(\frac{A}{\tau V_0}\right) \frac{dV}{dt}$$

where

T = temperature

t = time

A = effective cross section area of piston

V₀ = volume of isolator cylinder

X = piston displacement

τ = coefficient of thermal expansion of the fluid

As A/V₀ is the same for all cylinders and is equal to

$$8.846 \times 10^{-4} \text{ inches}^{-1}, \text{ and } \tau \approx 6 \times 10^{-4} \text{ } ^\circ\text{F.}^{-1}$$

$$\frac{dT}{dt} = 1.47^{\circ}\text{F.}/\text{Min.}$$

which certainly appears to be sufficiently high. A maximum controllable piston velocity of 0.016 inches per second then is considered to be very conservative and could possibly be reduced.

One possible arrangement for a liquid spring controller consists of a small positive displacement pump, a motor with control gear, and a low pressure fluid reservoir all mounted rigidly to the isolator. Limit switches or a displacement transducer attached to the isolator cylinder and piston rod indicate their relative position and serve as a source for the leveling signal. If the balanced load is to be computed, a load cell is installed in each of the pendulum arms. Electronic equipment consists of motor controls, signal conditioners, switching circuits and the load computer.

To gain some idea of the size of the system, assume that due to the isolator friction characteristics, the isolator piston velocity is limited to 0.016 inches per second. The ratios of the maximum and minimum to the nominal load for all isolators is 1.32 and .72 respectively resulting in a change in fluid volume of 12.3% and 8.5%. The change in fluid volume needed to offset the effect of a 10° temperature difference is 0.6 per cent. Using these values, the following system dimensions can be calculated.

	Configuration No. 2	Configuration No. 3	
		Upper	Lower
Pump Capacity (cu. in./sec)	.336	.448	.224
Maximum Static Pressure (psi)	26,400	26,400	26,400
Reservoir Volume (min. cu. in.)	1,000	1,340	680

The problem of removing fluid at very high pressure from the cylinder can be as difficult as that of injecting it. Several methods have been considered all of which involve allowing the fluid to drive the injecting mechanism in reverse and absorbing the energy in a friction device.

SECTION 5 APPENDIX

5A DEVELOPMENT OF EQUATIONS OF MOTION

5A-1 Basic Equations

The basic equations of motion in the inertial reference system can be written as follows:

Translation of the Center of Gravity

$$[m\ddot{S}] + \sum [F]_n + \sum [F]_n^D = - [m\ddot{S}_0 - mg]$$

Rotations about the Center of Gravity

$$\frac{d}{dt} [\phi] + \sum [M]_n + \sum [M]_n^D = 0$$

where

$[m\ddot{S}]$: Inertial forces on the mass

$[F]_n$: Restoring force by n^{th} isolator

$[F]_n^D$: Damping force by n^{th} isolator

$[M]_n$: Moment of restoring force by n^{th} isolator = $[r_a] [F]_n$

$[M]_n^D$: Moment of damping force by n^{th} isolator = $[r_a] [F]_n^D$

$\frac{d}{dt} [\phi]$: Rate of change of angular momentum

$[m\ddot{S}_0 - mg]$: Disturbing force imposed by ground acceleration

5A-2 Transformation Matrices

5A-2.1 Cartesian Transformation

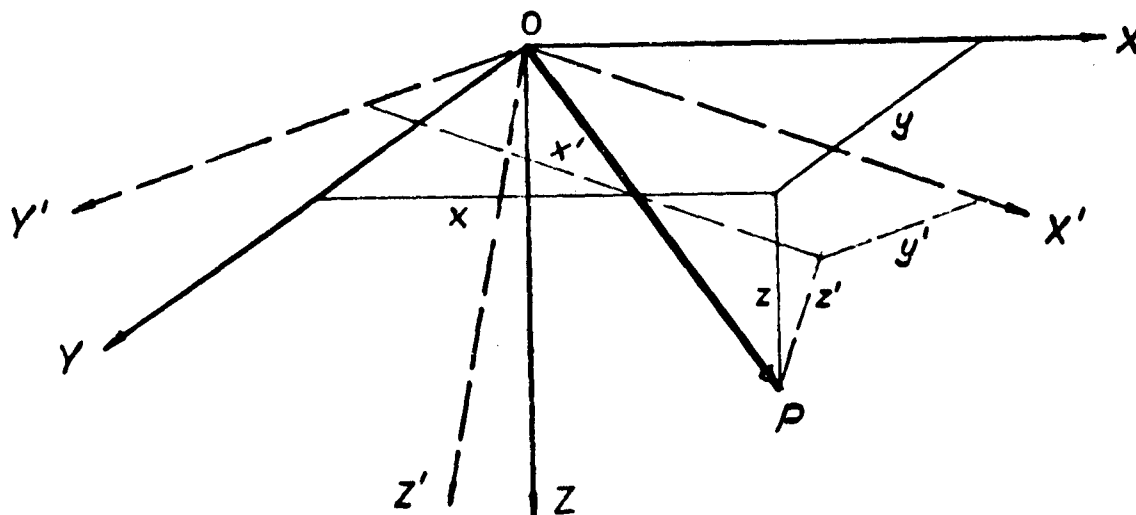


Figure 5A-1. Cartesian Transformation

X-Y-Z : Original reference system.

X'-Y'-Z' : New reference system obtained by γ - β - α rotation about Z-Y-X respectively.

x-y-z : Components of any vector P in original reference system, X-Y-Z.

x'-y'-z' : Components of vector P in new reference system, X'-Y'-Z'.

The relationship between original and new sets of components can be established as follows:

$$\begin{bmatrix} x \\ y \\ z \end{bmatrix} = \begin{bmatrix} \cos\beta \cdot \cos\gamma & -\cos\alpha \cdot \sin\gamma + \sin\alpha \cdot \sin\beta \cdot \cos\gamma \\ \cos\beta \cdot \sin\gamma & \cos\alpha \cdot \cos\gamma + \sin\alpha \cdot \sin\beta \cdot \sin\gamma \\ -\sin\beta & \sin\alpha \cdot \cos\beta \end{bmatrix} \begin{bmatrix} x' \\ y' \\ z' \end{bmatrix}$$

In matrix form

$$[x] = [D] [x'] \quad \text{to obtain original components}$$

$$[x'] = [D]^{-1} [x] \quad \text{to obtain new components}$$

where $[D]$ is the Cartesian transformation matrix -
function of α, β, γ

5A-2.2 Polar Transformation

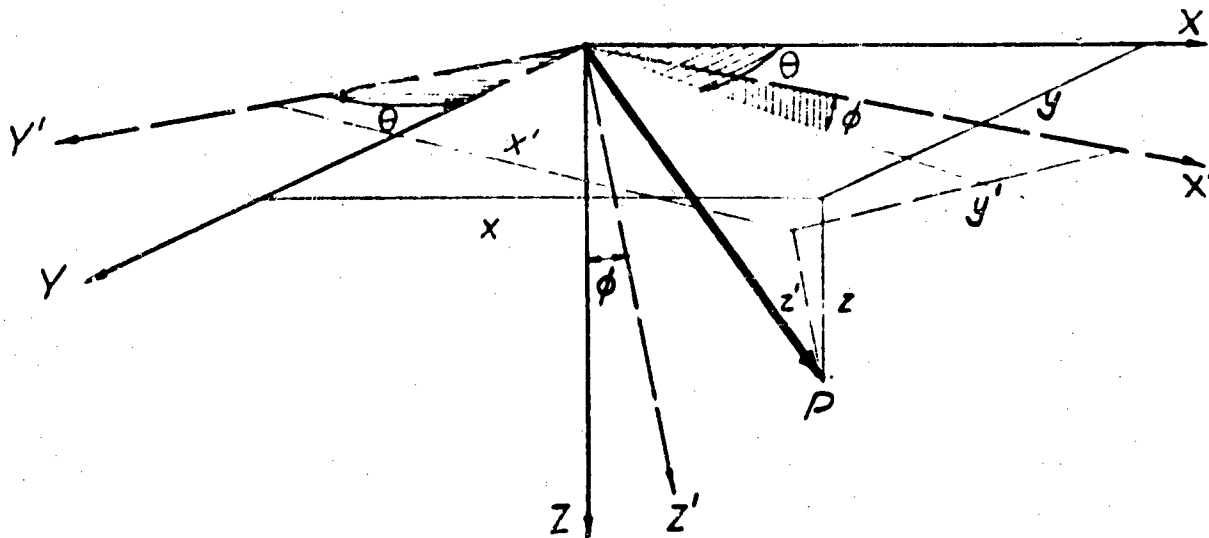


Figure 5A-2. Polar Transformation

X-Y-Z Original reference system.

X'-Y'-Z' New reference system obtained by rotating
 θ - about Z axis.
 ϕ - about Y' axis.

x-y-z Components of any vector P in original
reference system X-Y-Z.

x'-y'-z' Components of P in new reference system
X'-Y'-Z'.

The relation between original and new sets of components
can be established as follows:

Best Available Copy

$$\begin{bmatrix} x \\ y \\ z \end{bmatrix} = \begin{bmatrix} \cos\phi \cdot \cos\theta & -\sin\theta & \sin\phi \cdot \cos\theta \\ \cos\phi \cdot \sin\theta & \cos\theta & \sin\phi \cdot \sin\theta \\ -\sin\phi & 0 & \cos\phi \end{bmatrix} \begin{bmatrix} x' \\ y' \\ z' \end{bmatrix}$$

In matrix form

$$[x] = [D]_p [x'] \quad \text{to obtain original components.}$$

$$[x'] = [D]_p^{-1} [x] \quad \text{to obtain new components.}$$

5A-2.3 Summary

$$[D] = \begin{bmatrix} \cos\beta \cdot \cos\gamma & -\cos\alpha \cdot \sin\gamma + \sin\alpha \cdot \sin\beta \cdot \cos\gamma \\ \cos\beta \cdot \sin\gamma & \cos\alpha \cdot \cos\gamma + \sin\alpha \cdot \sin\beta \cdot \sin\gamma \\ -\sin\beta & \sin\alpha \cdot \cos\beta \end{bmatrix}$$

$$\begin{bmatrix} \sin\alpha \cdot \sin\gamma + \cos\alpha \cdot \sin\beta \cdot \cos\gamma \\ -\sin\alpha \cdot \cos\gamma + \cos\alpha \cdot \sin\beta \cdot \sin\gamma \\ \cos\alpha \cdot \cos\beta \end{bmatrix}$$

$$[D]_p = \begin{bmatrix} \cos\phi \cdot \cos\theta & -\sin\theta & \sin\phi \cdot \cos\theta \\ \cos\phi \cdot \sin\theta & \cos\theta & \sin\phi \cdot \sin\theta \\ -\sin\phi & 0 & \cos\phi \end{bmatrix}$$

5A-3 Inertial Forces

$$[S]_p = \{0 \ 0 \ \ell\} \text{ coordinates in polar reference system.}$$

$$[S] = \{X \ Y \ Z\} \text{ coordinates in X-Y-Z reference system.}$$

By using polar transformation, we get

$$[S] = [D]_p [S]_p$$

$$\therefore [\dot{S}] = [\dot{D}]_p [S]_p + [D]_p [\dot{S}]_p$$

$$\therefore [\ddot{S}] = [\ddot{D}]_p [S]_p + 2[\dot{D}]_p [\dot{S}]_p + [D]_p [\ddot{S}]_p$$

The expressions for $[\dot{S}]$ and $[\ddot{S}]$ can be solved and reduced to the following form:

$$[\dot{S}] = \begin{bmatrix} \cos\phi \cdot \cos\theta & -\sin\theta & \sin\phi \cdot \cos\theta \\ \cos\phi \cdot \sin\theta & \cos\theta & \sin\phi \cdot \sin\theta \\ -\sin\phi & 0 & \cos\phi \end{bmatrix} \begin{bmatrix} l\ddot{\phi} \\ l\sin\phi \cdot \ddot{\theta} \\ \dot{l} \end{bmatrix}$$

$$= [D]_p [\dot{S}']_p$$

and

$$[\ddot{S}] = \begin{bmatrix} \cos\phi \cdot \cos\theta & -\sin\theta & \sin\phi \cdot \cos\theta \\ \cos\phi \cdot \sin\theta & \cos\theta & \sin\phi \cdot \sin\theta \\ -\sin\phi & 0 & \cos\phi \end{bmatrix} \begin{bmatrix} 2\dot{l}\dot{\phi} + l\ddot{\phi} - l\dot{\theta}^2 \sin\phi \cdot \cos\phi \\ 2\dot{l}\dot{\theta} \sin\phi + 2l\dot{\phi}\dot{\theta} \cos\phi + l\ddot{\theta} \sin\phi \\ \ddot{l} - l\dot{\phi}^2 - l\dot{\theta}^2 \sin^2\phi \end{bmatrix}$$

$$= [D]_p [\ddot{S}']_p$$

where

$$[\dot{S}']_p = \begin{bmatrix} l\ddot{\phi} \\ l\sin\phi \cdot \ddot{\theta} \\ \dot{l} \end{bmatrix}$$

and

$$[\ddot{S}']_p = \begin{bmatrix} 2\dot{l}\dot{\phi} + l\ddot{\phi} - l\dot{\theta}^2 \sin\phi \cdot \cos\phi \\ 2\dot{l}\dot{\theta} \sin\phi + 2l\dot{\phi}\dot{\theta} \cos\phi + l\ddot{\theta} \sin\phi \\ \ddot{l} - l\dot{\phi}^2 - l\dot{\theta}^2 \sin^2\phi \end{bmatrix}$$

$$\therefore \underline{[m\ddot{S}]} = [D]_p [m\ddot{S}']_p$$

Note: $[S]_p = \{ 0 \ 0 \ l \}$ when it is premultiplied by $[C]_H$: Horizontal stiffness matrix.

and $[S]_p = \{ 0 \ 0 \ l - l_0 \}$ when it is premultiplied by $[C]_V$: Vertical stiffness matrix.

5A-4 Rate of Change of Angular Momentum

Let \vec{G} be angular momentum

$$\therefore \vec{G} = \vec{I} \cdot \vec{\omega}$$

$$\text{Now } \frac{d}{dt} [\vec{G}] = \frac{\partial}{\partial t} [\vec{G}] + \vec{\omega} \times \vec{G}$$

where operator $\frac{d}{dt}$ refers to absolute time variation

$\frac{\partial}{\partial t}$ refers to relative time variation

and $\vec{\omega} \times \vec{G}$ refers to drag time variation

$$\begin{aligned} \therefore \frac{d}{dt} [\vec{I} \cdot \vec{\omega}] &= \frac{\partial}{\partial t} [\vec{I} \cdot \vec{\omega}] + \vec{\omega} \times \vec{I} \cdot \vec{\omega} \\ &= \vec{I} \frac{\partial}{\partial t} [\vec{\omega}] + (\epsilon_{ijk} \omega_k) \vec{I} \cdot \vec{\omega} \end{aligned}$$

$$\begin{aligned} &= \begin{bmatrix} I_{11} & 0 & 0 \\ 0 & I_{22} & 0 \\ 0 & 0 & I_{33} \end{bmatrix} \begin{bmatrix} \dot{p} \\ \dot{q} \\ \dot{r} \end{bmatrix} \\ &+ \begin{bmatrix} 0 & -r & q \\ r & 0 & -p \\ -q & p & 0 \end{bmatrix} \begin{bmatrix} I_{11} & 0 & 0 \\ 0 & I_{22} & 0 \\ 0 & 0 & I_{33} \end{bmatrix} \begin{bmatrix} p \\ q \\ r \end{bmatrix} \\ &= \begin{bmatrix} I_{11} \cdot \dot{p} + (I_{33} - I_{22}) \cdot qr \\ I_{22} \cdot \dot{q} + (I_{11} - I_{33}) \cdot rp \\ I_{33} \cdot \dot{r} + (I_{22} - I_{11}) \cdot pq \end{bmatrix} \end{aligned}$$

These are Euler's equations.

The position of the moving reference system can be obtained by

1. Rotating axes by Euler's angles - θ, ϕ, ψ

θ about Z_1 axis

ϕ about y axis

ψ about Z' axis

2. Rotating axes by α, β, γ about X_1, Y_1, Z_1 , respectively.

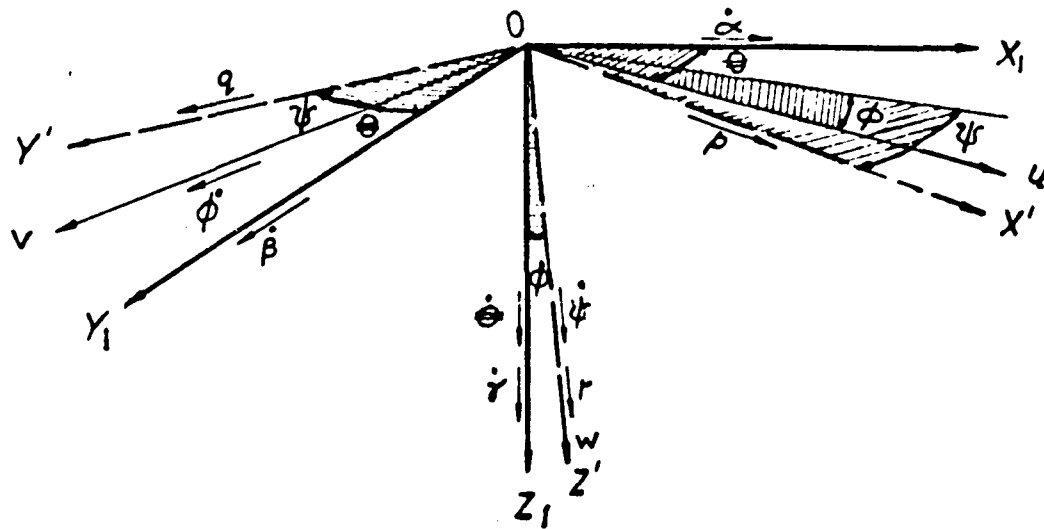


Figure 5A-3. Euler's Reference System

Relating p, q, r and $\dot{\theta}, \dot{\phi}, \dot{\psi}$ we get

$$\begin{bmatrix} p \\ q \\ r \end{bmatrix} = \begin{bmatrix} -\sin \phi & \cos \psi & \sin \psi & 0 \\ \sin \phi & \sin \psi & \cos \psi & 0 \\ \cos \phi & 0 & 0 & 1 \end{bmatrix} \begin{bmatrix} \dot{\theta} \\ \dot{\phi} \\ \dot{\psi} \end{bmatrix}$$

$$\text{or } [\omega] = [D]_{\omega} [\dot{\lambda}]$$

relating $\dot{\alpha}, \dot{\beta}, \dot{\gamma}$ and $\dot{\theta}, \dot{\phi}, \dot{\psi}$, we get

$$\begin{bmatrix} \dot{\alpha} \\ \dot{\beta} \\ \dot{\gamma} \end{bmatrix} = \begin{bmatrix} 0 & -\sin \theta & \sin \phi \cos \theta \\ 0 & \cos \theta & \sin \phi \sin \theta \\ 1 & 0 & \cos \phi \end{bmatrix} \begin{bmatrix} \dot{\theta} \\ \dot{\phi} \\ \dot{\psi} \end{bmatrix}$$

$$\text{or } [\dot{\phi}] = [D]_{\phi} [\dot{\lambda}]$$

5A-5 Restoring Forces

5A-5.1 Stiffness Matrix

The stiffness matrix $[K]_n$ of n^{th} isolator undergoes the transformation due to the translation of center of gravity and the rotations about center of gravity.

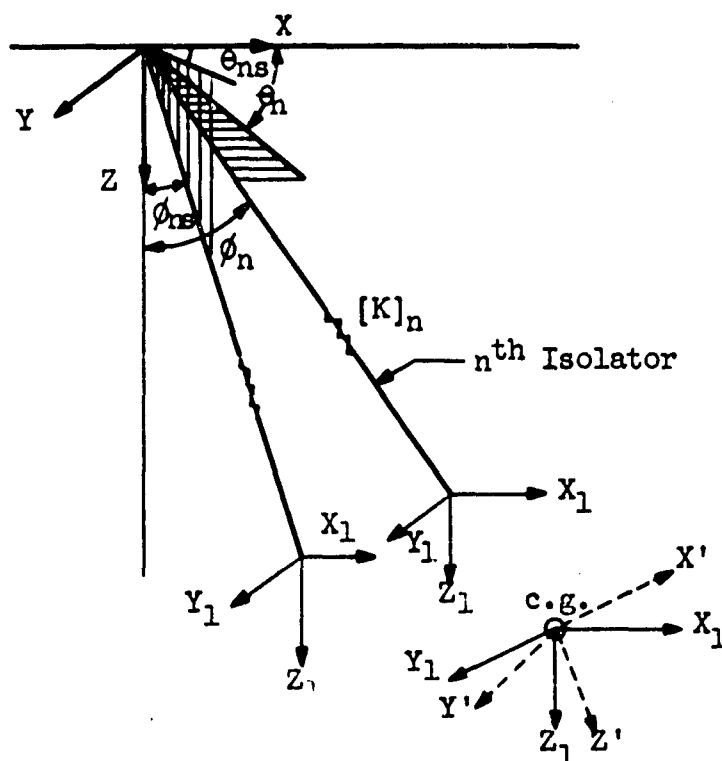


Figure 5A-4. Transformation of Stiffness Matrix.

$[K]_n$ transforms into

$\{[D]_{\text{pns}} [K]_n [D]_{\text{pns}}^{-1}\}$ due to the initial position

$[D]^{-1} \{[D]_{\text{pns}} [K]_n [D]_{\text{pns}}^{-1}\} [D]$ due to rotation about center of gravity

$[D]_{\text{p}(\phi_n - \phi_{\text{ns}})} [D]^{-1} \{[D]_{\text{pns}} [K]_n [D]_{\text{pns}}^{-1}\} [D] [D]_{\text{p}(\phi_n - \phi_{\text{ns}})}^{-1}$
due to translation of mass.

$$\begin{aligned}
&= [D]_{pn} [D]_{pns}^{-1} [D]^{-1} \left\{ [D]_{pns} [K]_n [D]_{pns}^{-1} \right\} [D] [D]_{pns} [D]_{pn}^{-1} \\
&\quad \text{as } [D]_{p(\phi_n - \phi_{ns})} = [D]_{pn} [D]_{pns}^{-1} \\
&= [D]_{pn} \left\{ [D]^{-1} [K]_n [D] \right\} [D]_{pn}^{-1}
\end{aligned}$$

Hence $[K]_n$ is transformed into $[\bar{C}]_n$ due to translation of center of gravity and rotations about center of gravity, where

$$\begin{aligned}
[\bar{C}]_n &= [D]_{pn} [C]_n [D]_{pn}^{-1} \\
\text{and } [C]_n &= [D]^{-1} [K]_n [D]
\end{aligned}$$

5A-5.2 Displacement Matrix

The displacement of any point in mass may be considered to consist of that due to

1. translation of center of gravity
2. rotation about center of gravity

In matrix form

$$[\delta]_n = [S]_n + [\Delta r]_n$$

$$\text{Now } [S]_n = [D]_{pn} [S]_{pn}$$

$$[\Delta r]_n = [r']_n - [r]_n$$

where $[r]_n$ initial coordinates of n^{th} point

$[r']_n$ coordinates of n^{th} point at time t

$$= [D] [r]_n$$

$$\therefore [\Delta r]_n = [D] [r]_n - [r]_n$$

$$= [D] - [I] [r]_n$$

For small values of α , β , and γ making the approximations

$$\sin \alpha \approx \alpha \quad \cos \alpha \approx 1$$

$$\sin \beta \approx \beta \quad \cos \beta \approx 1$$

$$\sin \gamma \approx \gamma \quad \cos \gamma \approx 1$$

and neglecting second order quantities in $[D]$, we get

$$\begin{aligned}
 [D] &\cong \begin{bmatrix} 1 & -\gamma & \beta \\ \gamma & 1 & -\alpha \\ -\beta & \alpha & 1 \end{bmatrix} \\
 \therefore [\Delta r]_n &= [D] - [I] \quad [r]_n \\
 &= \begin{bmatrix} 0 & -\gamma & \beta \\ \gamma & 0 & -\alpha \\ -\beta & \alpha & 0 \end{bmatrix} \begin{bmatrix} r_1 \\ r_2 \\ r_3 \end{bmatrix}_n \\
 &= \begin{bmatrix} 0 & r_3 & -r_2 \\ -r_3 & 0 & r_1 \\ r_2 & -r_1 & 0 \end{bmatrix}_n \begin{bmatrix} \alpha \\ \beta \\ \gamma \end{bmatrix}
 \end{aligned}$$

$$= [-r_a] [\phi]; \text{ where}$$

$$[-r_a] = \begin{bmatrix} 0 & -r_3 & r_2 \\ r_3 & 0 & -r_1 \\ -r_2 & r_1 & 0 \end{bmatrix}_n$$

$$\begin{aligned}
 \therefore [\delta] &= [s]_n + [\Delta r]_n \\
 &= [D]_{pn} [s]_{pn} + [-r_a] [\phi] \\
 &= [D]_{pn} \left\{ [s]_{pn} + [D]_{pn}^{-1} [-r_a] [\phi] \right\}
 \end{aligned}$$

5A-5.3 Restoring Force Matrix

Restoring force in the inertial reference system

$$\begin{aligned}
 [F]_n &= [\bar{C}]_n [\delta]_n \\
 &= [D]_{pn} [C]_n [D]_{pn}^{-1} [D]_{pn} \left\{ [s]_{pn} + [D]_{pn}^{-1} [-r_a] [\phi] \right\} \\
 &= [D]_{pn} [C]_n \left\{ [s]_{pn} + [D]_{pn}^{-1} [-r_a] [\phi] \right\}
 \end{aligned}$$

5A-6 Moment of Restoring Force

The restoring force matrix as obtained above is

$$[F]_n = [D]_{pn} [C]_n \{ [S]_{pn} + [D]_{pn}^{-1} [-r_a] [\Phi] \}$$

The moment of this restoring force about center of gravity can be obtained by premultiplying $[F]_n$ by $[r_a]_n$

$$\begin{aligned} \therefore [M]_n &= [r_a]_n [F]_n \\ &= [r_a]_n [D]_{pn} [C]_n \{ [S]_{pn} + [D]_{pn}^{-1} [-r_a] [\Phi] \} \end{aligned}$$

5A-7 Damping Force

The restoring force $[F]_n$ which is the function of displacement is represented as

$$[F]_n = [\bar{c}]_n [\delta]_n$$

where $[\bar{c}]_n$ is stiffness matrix, having elements representing force/displacement

$[\delta]_n$ is displacement matrix, having elements representing displacement

Similarly the damping force $[F]_n^D$ which is the function of velocity can be represented as

$$[F]_n^D = [\bar{c}]_n^D [\dot{\delta}]_n$$

where

$[\bar{c}]_n^D$ is the damping stiffness matrix having elements representing force/velocity

$[\dot{\delta}]_n$ is velocity matrix having elements representing rate of change of displacement

Also, it can be represented as

$$[F]_n^D = [\bar{c}^D \frac{d}{dt}] [\delta]_n$$

where

$[\bar{c}^D]$ is damping coefficient, function of velocity

$\frac{d}{dt}$ is the differential operator acting on displacement matrix $[\delta]_n$

Referring to #5A-5.3 it can be seen that $[K]_n$ is transformed into

$$[\bar{C}]_n = [D]_{pn} [D]^{-1} [K]_n [D] [D]_{pn}^{-1}$$

due to translation of center of gravity and rotations about center of gravity.

Similarly it can be shown that $[K]_n^D$, damping stiffness is transformed into

$$[\bar{C}]_n^D = [D]_{pn} [D]^{-1} [K]_n^D [D] [D]_{pn}^{-1}$$

or

$$[C^D \frac{d}{dt}] = [D]_{pn} [D]^{-1} [K^D \frac{d}{dt}] [D] [D]_{pn}^{-1}$$

due to translation of center of gravity and rotation about center of gravity

$$\begin{aligned} \text{now } [F]_n^D &= [\bar{C}]_n^D [\dot{\delta}]_n \\ &= [\bar{C}^D \frac{d}{dt}] [\dot{\delta}]_n \\ &= [D]_{pn} [D]^{-1} [K^D \frac{d}{dt}]_n [D] [D]_{pn}^{-1} [\dot{\delta}]_n \\ &= [D]_{pn} [D]^{-1} [K^D \frac{d}{dt}]_n [D] [D]_{pn}^{-1} [D]_{pn} \left\{ [S]_{pn} + [D]_{pn}^{-1} [-r_a] [\dot{\Phi}] \right\} \\ &= [D]_{pn} [D]^{-1} [K^D \frac{d}{dt}]_n [D] \left\{ [S]_{pn} + [D]_{pn}^{-1} [-r_a] [\dot{\Phi}] \right\} \\ &= [D]_{pn} [D]^{-1} [K^D]_n [D] \left\{ \frac{d}{dt} [S]_{pn} + [D]_{pn}^{-1} [-r_a] \frac{d}{dt} [\dot{\Phi}] \right\} \\ &= [D]_{pn} [D]^{-1} [K^D]_n [D] \left\{ [\dot{S}]_{pn} + [D]_{pn}^{-1} [-r_a] [\dot{\Phi}] \right\} \\ &= [D]_{pn} [C^D]_n \left\{ [\dot{S}]_{pn} + [D]_{pn}^{-1} [-r_a] [\dot{\Phi}] \right\} \end{aligned}$$

where $[C^D]_n = [D]^{-1} [K^D]_n [D]$

5A-8 Moment of Damping Force

The moment of damping force about center of gravity can be obtained by premultiplying $[F]_n^D$ by $[r_a]_n$

$$\begin{aligned}
 \therefore [\dot{M}]_n^D &= [r_a]_n [F]_n^D \\
 &= [r_a]_n [D]_{pn} [D]^{-1} [K^D]_n [D] \left\{ [\dot{S}]_{pn} + [D]_{pn}^{-1} [-r_a] [\dot{\Phi}] \right\} \\
 &= [r_a]_n [D]_{pn} [C^D]_n \left\{ [\dot{S}]_{pn} + [D]_{pn}^{-1} [-r_a] [\dot{\Phi}] \right\}
 \end{aligned}$$

where

$$[C^D]_n = [D]^{-1} [K^D]_n [D]$$

5A-9 Disturbing Forces

The disturbing force matrix can be written as

$$[m\ddot{S}_O - mg] = \begin{bmatrix} m\ddot{X}_O \\ m\ddot{Y}_O \\ m\ddot{Z}_O - mg \end{bmatrix}$$

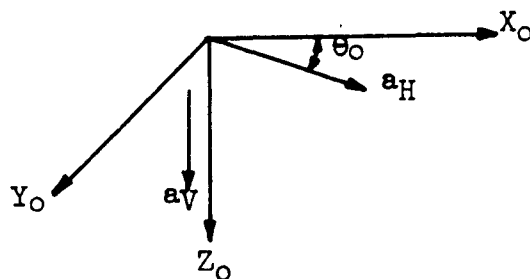


Figure 5A-5. Ground Accelerations.

where

$$\ddot{X}_O = a_H \cos \theta_O$$

$$\ddot{Y}_O = a_H \sin \theta_O$$

$$\ddot{Z}_O = a_v$$

The moment of disturbing forces about center of gravity is zero.

5A-10 Determination of Transformation Matrix $[D]_{pn}$.

The polar coordinates of the n^{th} isolator in dynamic position can be obtained by adding the static position vector of the n^{th} isolator and the displacement vector of mass attachment point.

Referring to Figure 5A-6 we get

$$\begin{aligned} \vec{O_{nw}O_p} &= \vec{O_{nw}O_{nm}} + \vec{O_{nm}O_p} \\ \therefore [D]_{pn} [S]_{pn} &= [D]_{pns} [S]_{pns} + [D]_p [S]_p \\ \therefore \begin{bmatrix} l_n \sin \phi_n \cos \theta_n \\ l_n \sin \phi_n \sin \theta_n \\ l_n \cos \phi_n \end{bmatrix} &= \begin{bmatrix} l_{ns} \sin \phi_{ns} \cos \theta_{ns} \\ l_{ns} \sin \phi_{ns} \sin \theta_{ns} \\ l_{ns} \cos \phi_{ns} \end{bmatrix} + \begin{bmatrix} l \sin \phi \cos \theta \\ l \sin \phi \sin \theta \\ l \cos \phi - l_s \end{bmatrix} \end{aligned}$$

The above simultaneous equations can be solved for l_n , ϕ_n and θ_n for the use in transformation matrix $[D]_{pn}$

5A-11 Equations of Motion.

5A-11.1 Basic Equation for Translation of Center of Gravity.

$$[m\ddot{S}] + \sum [F]_n + \sum [F]_n^D = -[m\ddot{S}_0 - mg]$$

where

$$[m\ddot{S}] = [D]_p [m\ddot{S}']_p \quad (\text{Ref. 5A-3})$$

$$[F]_n = [D]_{pn} [C]_n \left\{ [S]_{pn} + [D]_{pn}^{-1} [-r_a] [\Phi] \right\} \quad (\text{Ref. 5A-5.5})$$

$$[F]_n^D = [D]_{pn} [C^D]_n \left\{ [\dot{S}]'_{pn} + [D]_{pn}^{-1} [-r_a] [\dot{\Phi}] \right\} \quad (\text{Ref. 5A-7})$$

therefore compiling the equation we get

$$\begin{aligned} [D]_p [m\ddot{S}']_p + [D]_{pn} [C]_n \left\{ [S]_{pn} + [D]_{pn}^{-1} [-r_a] [\Phi] \right\} \\ + [D]_{pn} [C^D]_n \left\{ [\dot{S}]'_{pn} + [D]_{pn}^{-1} [-r_a] [\dot{\Phi}] \right\} = -[m\ddot{S}_0 - mg] \end{aligned}$$

5A-11.2 Basic Equation for Rotation About Center of Gravity.

$$\frac{d}{dt} [\mathcal{O}] + \sum [M]_n + \sum [M]_n^D = 0$$

where

$$\frac{d}{dt} [\mathcal{O}] = \frac{d}{dt} [I \omega] \quad (\text{Ref. 5A-4})$$

$$[M]_n = [r_a]_n [D]_{pn} [C]_n \left\{ [s]_{pn} + [D]_{pn}^{-1} [-r_a] [\dot{\Phi}] \right\} \quad (\text{Ref. 5A-6})$$

$$[M]_n^D = [r_a]_n [D]_{pn} [C^D]_n \left\{ [\dot{s}]_{pn} + [D]_{pn}^{-1} [-r_a] [\dot{\Phi}] \right\} \quad (\text{Ref. 5A-8})$$

therefore compiling the equation we

$$\begin{aligned} \frac{d}{dt} [\mathcal{O}] + \sum [r_a] [D]_{pn} [C]_n \left\{ [s]_{pn} + [D]_{pn}^{-1} [-r_a] [\dot{\Phi}] \right\} \\ + \sum [r_a] [D]_{pn} [C^D]_n \left\{ [\dot{s}]_{pn} + [D]_{pn}^{-1} [-r_a] [\dot{\Phi}] \right\} = 0 \end{aligned}$$

5B AIR RESISTANCE

5B-1 Introduction

The motion of the large cage relative to the capsule, where the clearance between the cage and the capsule walls is small, can produce air pressures which yield high forces and moments on the cage. In the shock isolated Control Center of the Titan II (LGM-25C) facilities this effect has been observed to be very pronounced, damping vertical oscillations after only a few cycles and producing significant side loads. In this facility where very large areas are exposed to air pressures, it was believed that the problem might be particularly acute and that their magnitude should be investigated.

As a result of the relative motion of the cage and the capsule, the distribution of air pressures about the cage may produce on it lift and drag forces and a pitching moment where lift and drag are measured normal to, and in the direction of, the relative motion of the body.

Any or all of these effects may exert a significant influence on the dynamic response of the cage. The lift force will tend to move the cage in a horizontal direction closer to the capsule wall. The pitching moment is destabilizing and will amplify rotations of the cage about the horizontal axis. The net effect of the drag force will be to oppose the motion of the oscillations of the cage.

Due to the influence of the capsule walls on the flow pattern around the cage it is very difficult to calculate the magnitudes of the lift force and pitching moment. Force and moment coefficients should be obtained by experiment. However, a reasonably close approximation of the drag force can be obtained by considering the cage as a piston oscillating in a cylinder, the ends of which are connected to permit crossflow of air. An analysis of this model has been made and is presented here.

Air Cylinder with Capillary Cross-Flow

Consider a piston oscillating harmonically in an air-filled cylinder whose ends are connected by a capillary tube (Figure 5B-1). We assign these dimensionless ratios defining the geometry

$$\frac{h}{d} = \bar{\theta}; \quad \frac{h_1}{d} = \bar{\phi}$$

The oscillation of the piston is described

$$Z = \bar{\beta}d \sin \omega t$$

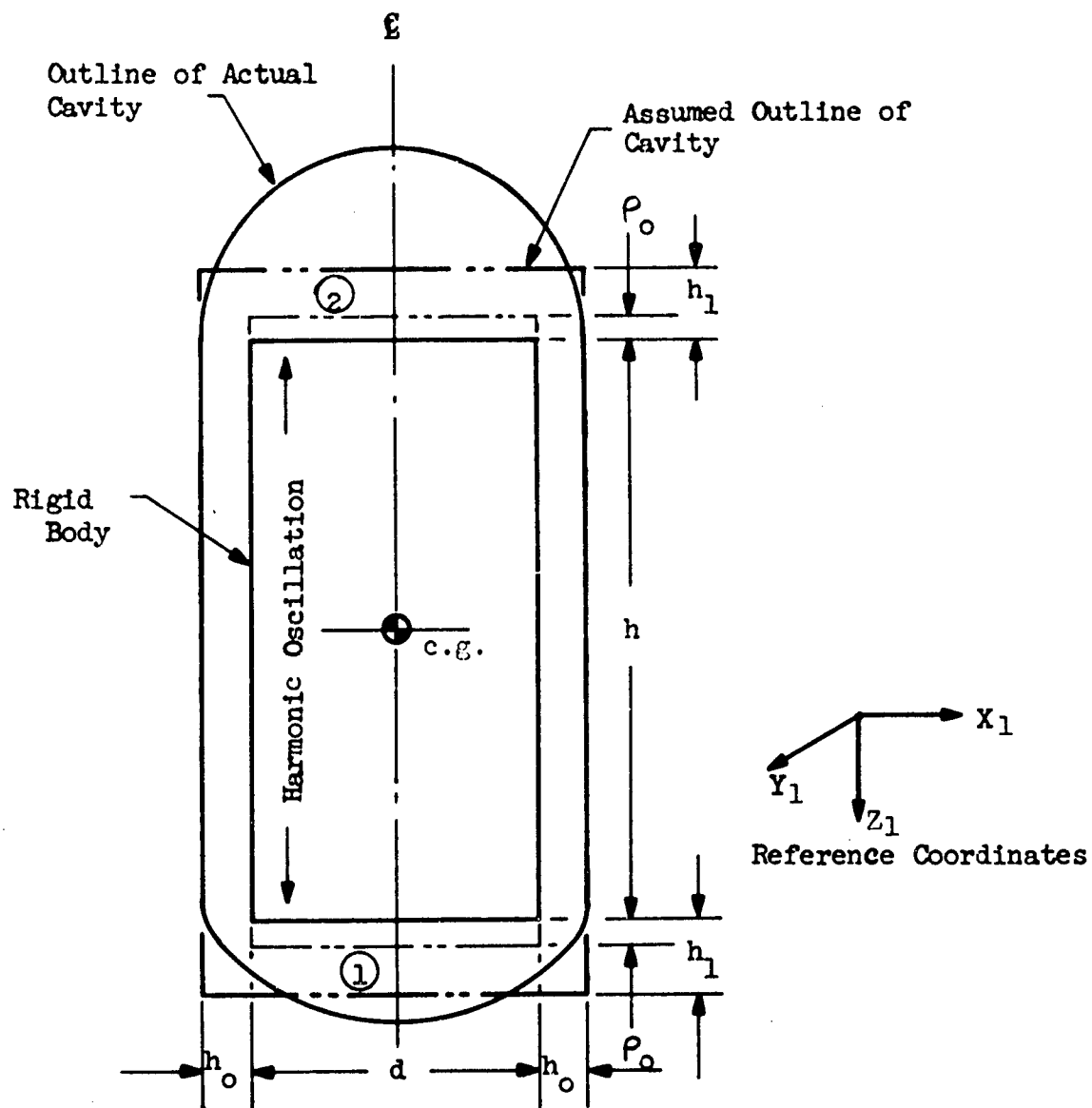


Figure 5B-1. Model of Cage Oscillating Vertically in Capsule.

where

$$\bar{\rho} = \frac{\rho_o}{d}$$

We further define the capillary dimensions as

$$\text{length} = h = \bar{\theta}d$$

$$\text{width} = \pi d(1 + \bar{\alpha})$$

where

$$\bar{\alpha} = \frac{h_o}{d}$$

$$\text{thickness} = \bar{\alpha}d$$

The incremental force exerted on the piston by an incremental change in pressure caused by a downward displacement is

$$dF = \frac{\pi d^2}{4} (dP_1 - dP_2) \quad (\text{Eq. 5B-1})$$

where

F = force acting on piston

P_1 = absolute pressure in side (1)

P_2 = absolute pressure in side (2)

To evaluate the pressures, we write the equations for the state of air in sides (1) and (2). Thus

$$\frac{dP_1}{P_1} = \frac{dw_1}{w_1} + \frac{dT_1}{T_1} - \frac{dV_1}{V_1} \quad (\text{Eq. 5B-2a})$$

$$\frac{dP_2}{P_2} = \frac{dw_2}{w_2} + \frac{dT_2}{T_2} - \frac{dV_2}{V_2} \quad (\text{Eq. 5B-2b})$$

From the geometry,

$$V_1 = \frac{\pi d^2}{4} (\bar{\phi}d - Z), \quad dV_1 = - \frac{\pi d^2}{4} dZ \quad (\text{Eq. 5B-3a})$$

$$V_2 = \frac{\pi d^2}{4} (\bar{\phi}d + Z), \quad dV_2 = \frac{\pi d^2}{4} dZ = -dV_1 \quad (\text{Eq. 5B-3b})$$

The air flow dw_1 from side (1) to side (2) is

$$dw_1 = - \frac{c_r}{2RT_1} (P_1^2 - P_2^2) \quad (\text{Eq. 5B-4})$$

where

R = gas constant

$$c_r = \frac{\pi d^3 \bar{\alpha}^3 (1 + \bar{\alpha})}{(12)^6 \mu \bar{\theta}} \quad (\text{Eq. 5B-5})$$

μ = dynamic viscosity of air

then $dw_2 = - dw_1$

To determine the rate of change of temperature of the gas, we assume there is no heat transferred to or from the air during the process. The energy equation for the air in side (1) then is

$$c_p dT_1 = v_1 dP_1$$

where

c_p = specific heat at constant pressure

v = specific volume

Since

$$v = \frac{V}{w}$$

$$c_p dT_1 = \frac{V_1 dP_1}{w_1} = RT_1 \frac{dP_1}{P_1}$$

then

$$\frac{dT_1}{T_1} = \left[\frac{\bar{T} - 1}{\bar{T}} \right] \frac{dP}{P}$$

Substituting in Eq. 5B-2a, we obtain

$$\frac{dP_1}{P_1} = \bar{T} \left[\frac{dw_1}{w_1} + \frac{dV_1}{V_1} \right] \quad (\text{Eq. 5B-6a})$$

$$= \bar{T} \left[\frac{dw_1}{w_1} + \frac{dZ}{\bar{\phi}d - Z} \right] \quad (\text{Eq. 5B-6b})$$

Similarly, for side (2)

$$\frac{dP_2}{P_2} = - \bar{T} \left[\frac{dw_1}{w_2} + \frac{dZ}{\bar{\phi}d + Z} \right] \quad (\text{Eq. 5B-6c})$$

where

$$dw_1 = \left[\frac{-\pi(\bar{\alpha}d)^2(1 + \bar{\alpha})}{(2)(12)^6 \mu R T_1 \bar{\theta}} (P_1^2 - P_2^2) \right]$$

$$Z = \bar{\beta}d \sin \omega t$$

$$dZ = \omega \bar{\beta}d \cos \omega t dt$$

A case was then considered where

$$d = 75 \text{ feet}$$

$$R = 53.3 \text{ feet/degrees } R$$

$$\bar{\beta} = 0.0377$$

$$\bar{T} = 1.4$$

$$\bar{\theta} = 2.0$$

$$\mu = 37.5 \times 10^{-8} \text{ pounds second feet}^2$$

and with the initial conditions

$$t(0) = P_1 (2116) = P_2 (2116)$$

Solutions were obtained on the Burroughs 205 computer varying $\bar{\alpha}$, $\bar{\phi}$ and ω .

In Figures 5B-2 through 5B-4 the peak drag forces acting on the cage are plotted as a function of side clearance ratio $\bar{\alpha}$. It may be noted that at low values of $\bar{\alpha}$ (i.e., $\bar{\alpha} = .06$) the force on the cage becomes very large, about 800,000 lbs. The deceleration of the cage due to a force of this magnitude would be 0.15 g. When the side clearance ratio is increased to 0.10, the force is reduced to less than one fourth the previous value.

It may also be noted in the figures that end clearance ratio $\bar{\phi}$ and frequency of cage oscillation ω have only a slight effect on the magnitude of the force generated.

A typical force-displacement diagram for one cycle of oscillation is shown in Figure 5B-5. The large amount of damping afforded by the flow of air around the cage is clearly portrayed by the large enclosed area.

On the basis of this analysis it is concluded that the final selection of rattlespace should be made only after a careful consideration of the air pressures. Although it may be desirable to take advantage of high drag forces to provide extra damping in the vertical direction, the attendant higher velocities of air moving through the clearance will amplify the lift force and pitching moment. Since both the lift force and the pitching moment excite modes in the cage which have low stiffnesses, significant displacements relative to the capsule wall may result. It is therefore recommended that, in the design of facilities of the general configuration considered here, aerodynamic force and moment data be obtained experimentally on scale models before a final selection of rattlespace is made.

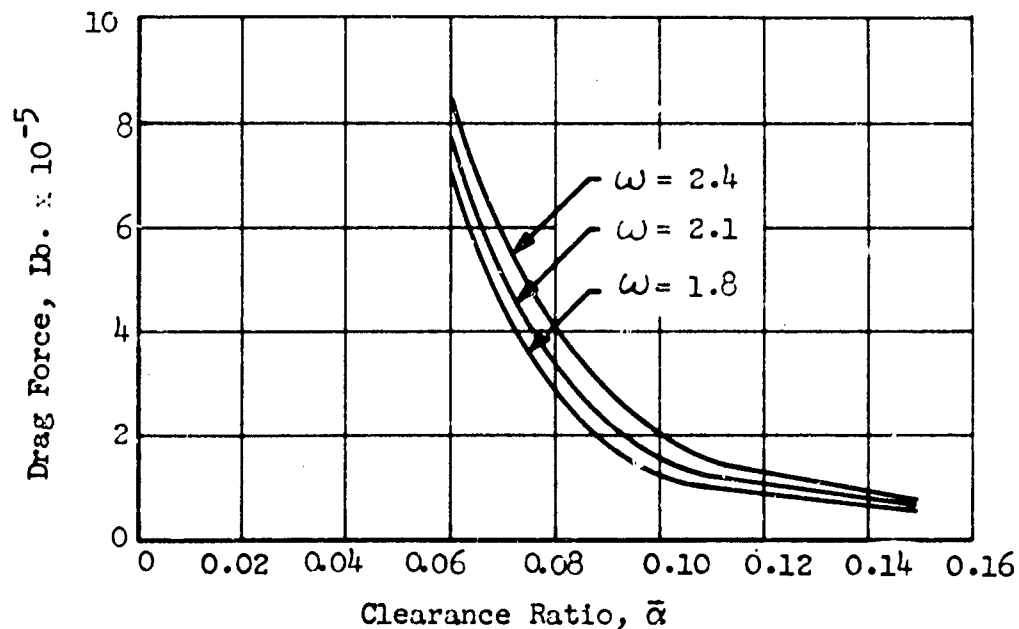


Figure 5B-2. Effect of Clearance Ratio $\bar{\alpha}$ on Drag Force, $\bar{\phi} = 0.6$

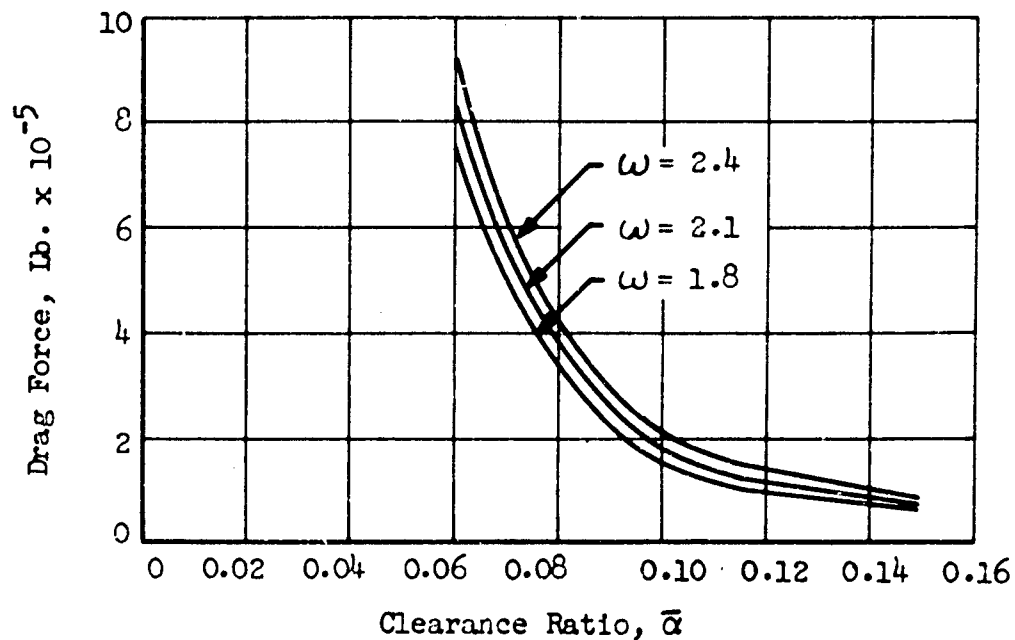


Figure 5B-3. Effect of Clearance Ratio $\bar{\alpha}$ on Drag Force, $\bar{\phi} = 0.4$

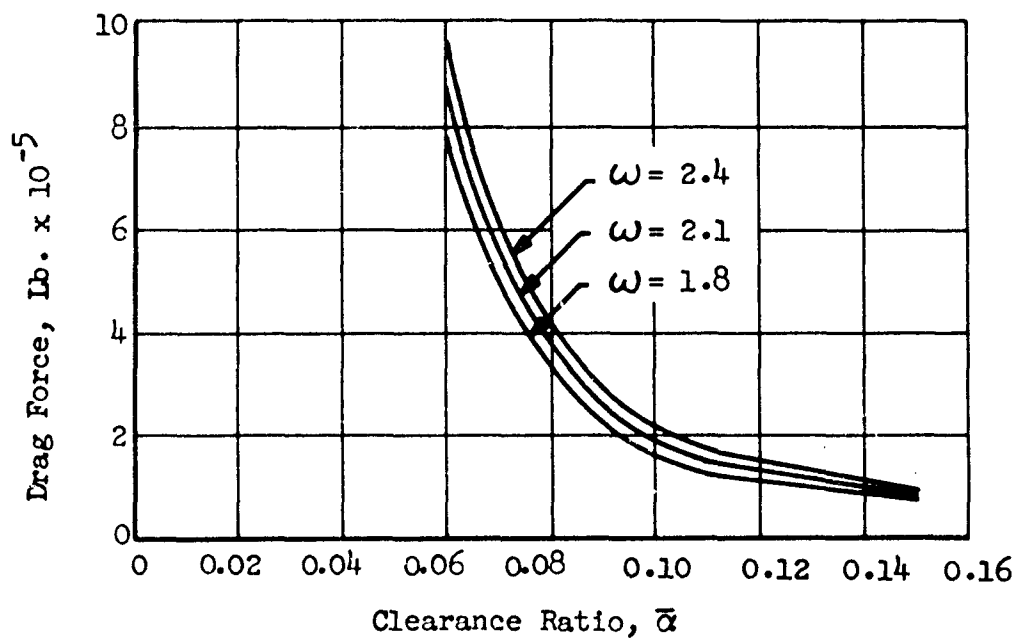


Figure 5B-4. Effect of Clearance Ratio $\bar{\alpha}$ on Drag Force, $\bar{\phi} = 0.2$

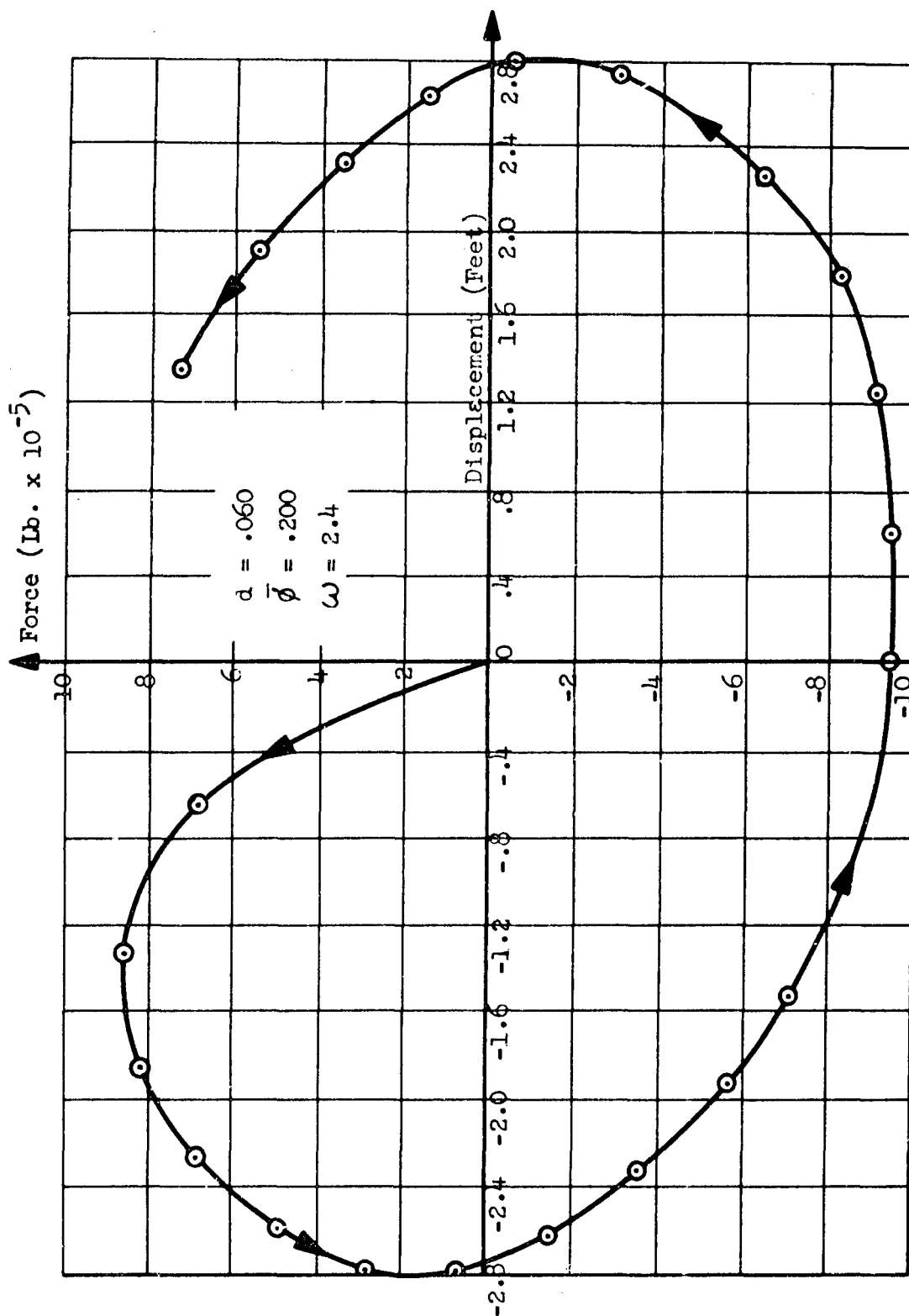


Figure 5B-5. Typical Force-Displacement Diagram for Drag Air Resistance Due to Cage Oscillating in Capsule.

5C THE EFFECT OF LIQUID SLOSHING ON THE RESPONSE OF THE CONTAINER AND SUPPORTING STRUCTURE

5C-1 Introduction

In most facilities of the nature of the one under consideration here, the shock isolated structure contains a number of fairly large containers partially filled with various fluids. During the response of the structure to a shock, the oscillations of the fluid within the container not only impose severe loads on the container itself, but also, if the mass of the oscillating fluid is sufficiently large, exert a significant influence on the dynamic response of the entire shock isolated system.

The total weight of fluids which may be stored in this facility is about one million pounds, or 20 per cent of the total suspended weight. This figure, however, is based on containers which are completely filled. Since the most severe dynamic condition occurs when the container is only about half full, the critical fluid weight is about one half million pounds. This quantity of fluid is distributed among seven vessels as shown in Table 5C-1.

Table 5C-1 Stored Fluid Quantities

Vessel	No. Of Identical Vessels	Weight of Fluid Per Vessel (Half Full) Pounds	Total Fluid Weight (Half Full) Pounds
H ₂ SO ₄	2	115,000	230,000
NaOH	2	53,000	106,000
Waste	2	67,000	134,000
Aerator	1	27,500	27,500
Total Half-Full Weight			497,500

As the sizes of the vessels are different, the frequencies of the fluid oscillations will not be the same and the entire fluid system will not be sharply tuned. On the other hand, the range of frequencies is not as broad as it could have been if dynamic response had been given greater consideration in establishing their sizes and orientations.

In this Appendix, the general problem of liquid sloshing is reviewed. The effects of tank shape and of baffles on damping and frequency of the fluid oscillations are discussed and equations presented. The pendulum analogy to the sloshing problem is described and employed to calculate the natural frequencies of the vessels listed above.

5C-2 Analysis Procedures

The dynamic analysis of partially-filled liquid tanks subjected to impulsive motions must consider the motion of the tank relative to its base as well as the motion of the liquid relative to the tank. If a closed tank is completely full of liquid or completely empty, the representative mechanical system is essentially a single-mass system. However, if the tank has a free liquid surface, there will occur a sloshing of the liquid in the tank during the impulsive motion and thus the configuration becomes effectively a two-mass system. In the latter, the dynamic behavior of the liquid tank may be quite different from that of the former. For certain proportions of the tank and the structure the sloshing of the liquid may be a dominant factor, whereas for other proportions the sloshing may have only a small effect. In this case then the survival of the tanks depends on the dynamic forces associated with the sloshing of the liquid in the tank.

The effects of the movement of large fluid masses on the stability of their container or the structure on which they are mounted are a matter of common experience, having long been a factor in the stability of ships. The oscillation of free-surface liquid masses exert forces and moments which may couple with those of the supporting system and cause instability. These fluid oscillations are the most critical when the excitation frequency is in the region of a natural frequency of lower mode oscillations. The frequencies of fluid oscillations may coincide with the frequencies of structural modes and induce resonance conditions leading to amplified structural deformations.

The knowledge of natural frequencies of liquids in liquid tanks of various configurations offers the designer sufficient information to avoid resonant conditions. However simple, exact, closed form solutions for the natural frequencies of the liquid are available at this time only for a few simple configurations, such as rectangular, cylindrical, or spherical tanks. For more complicated configurations, dimensionless frequency parameters, expressing the ratio of experimentally determined liquid frequencies to the simple, exact closed form solutions, have been derived. Such expressions result from the fact that at various liquid depths, the liquid has physical boundaries relatively similar to those of liquids in containers for which information concerning natural fluid frequencies is available.

5C-3 Damping

The damping of the fundamental antisymmetric mode of contained, sloshing liquids usually results from two sources:

1. the relative motion of the liquid and the tank wall.
2. the relative motion of liquid and baffles (if any).

Although, in general, the contribution of the smooth-wall damping is assumed to be small for certain configurations, it may be found to be significant. For upright circular cylinders of radius, R , the damping of the fundamental antisymmetrical liquid mode is independent of liquid depth for depths ratios $h/R \geq 1$, but increases as the depth ratio decreases below $h/R = 1$. By experiment, the damping effect of smooth-walls has been found to vary with the square root of the liquid kinematic viscosity, $(\nu)^{1/2}$ and the tank size $(R)^{-3/4}$.

The following relationship has been found to be adequate for the prediction of the damping factor, ξ

$$\xi = K (\nu)^{1/2} (R)^{-3/4} (g)^{-1/4} \left[1 + 2(1 - \frac{h}{R}) \operatorname{cosech} (3.68 \cdot \frac{h}{R}) \right] \left[\frac{1}{\sqrt[4]{\tanh(1.84 \frac{h}{R})}} \right] \quad (\text{Eq. 5C-1})$$

where the proportionality constant, K , has been found by experiment to have the numerical value, $5.23 \cong \frac{2}{3} \pi$. For small values of $h/R < 1$, the bracketed terms in the above expression become dominant and

$$\delta \cong \frac{1}{n} \log \frac{A_0}{A_n} \quad (\text{for } \frac{h}{R} < 1) \quad (\text{Eq. 5C-2})$$

where

n = number of cycles

A_0 = initial liquid amplitude

A_n = liquid amplitude after the n th cycle

For large values of $h/R > 1$, the bracketed terms in the above expression become insignificant; and the damping factor, ξ , is invariant with further increases in depth. Then

$$\xi = 3.52 (\nu)^{1/2} (R)^{-3/4} (g)^{-1/4} \quad (\text{for } \frac{h}{R} > 1) \quad (\text{Eq. 5C-3})$$

A time variant liquid depth does not have an important effect on liquid sloshing damping. Further, in the range of amplitudes covered by experiments the damping also appears to be independent of the liquid amplitude.

5C-3.1 Effect Of Baffles On Damping

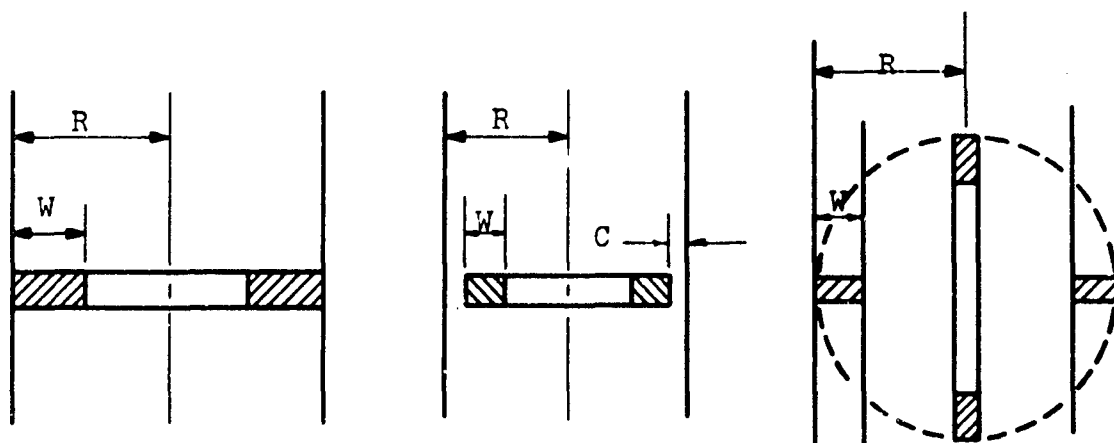
Analytical means for predicting damping effects due to baffles are limited to special cases because of the complexity of the boundary conditions. Moreover analytical expressions for the natural frequency of a sloshing liquid are limited to tanks without baffles. Prime variables to be taken into consideration when investigating the baffle effects are width, configuration, location, and orientation, together with liquid kinematic viscosity, and amplitude of oscillation.

The effects of baffle width, configuration and location on the damping characteristics and frequency of the fundamental antisymmetric mode of liquid oscillations in upright circular cylindrical tanks have been investigated experimentally for upright, inverted and perforated baffles having fixed rings, rings with fixed clearance, and cruciform and conic sections, (Figure 5C-1. It has been found that the associated damping factor, ξ , is independent of the kinematic viscosity and that baffle thickness does not appear to influence sensibly the damping factor. However, the flexibility of the baffle may be an important factor in the sense that the damping may increase with some increase in the flexibility of the baffle. In view of the obvious relationship between baffle thickness and flexibility, additional research is necessary to isolate the effects of these and other parameters before definite conclusions are drawn.

For a ring baffle of given width and location, the damping factor decreases as the radial clearance increases. The damping factor for the inverted and perforated conic-sections is less than that for the upright conic section of same area. Based on the total surface area of a baffle, the highest mean damping factor appears to be offered by the fixed ring baffle. A comparison of the damping values measured for the fixed ring baffle with those predicted by the theoretical expression

$$\xi = \left(\frac{1}{2W} \right) 2.83(d)^{-4.6d/R} \cdot (a)^{3/2} \left(\frac{A}{R} \right)^{1/2}$$

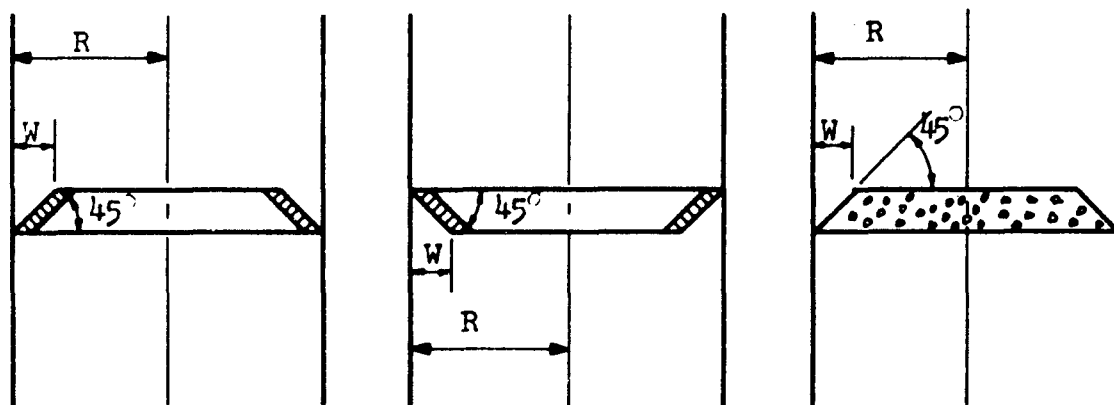
(Eq. 5C-4)



Fixed Ring

Ring with Clearance

Cruciform



Conic Upright

Conic Inverted

Conic Upright and Perforated

Figure 5C-1. Conventional Baffle Shapes.

where

$$a = \frac{R^2 - (R - W)^2}{R^2}$$

d = baffle location below the liquid free surface

W = width of the annulus projected on the liquid free surface

A = liquid wave amplitude

R = radius of cylindrical tank

shows that both the trends and the magnitudes of damping predicted by the above equation agree closely with measured results, thus the above method of predicting damping factors for this configuration, where the baffle remains below the surface, is considered to be adequate.

5C-3.2 Effect Of Baffles On Frequency

The frequency of the fundamental mode of oscillation varies with the baffle location, since the baffle effectively changes the tank geometry. As the baffle is lowered below the free surface, the frequencies of the liquid motion decrease from a maximum value at $d/R = 0$, when the baffle is located at the surface $d = 0$, until a minimum value is reached at which time, the baffle depth, d , corresponds to a value where the damping factor is maximum. As the baffle is lowered further, the frequency increases to the free surface value. The decrease in frequency may be caused by a tendency of the baffle to restrict the motion of the liquid in a manner equivalent to that of a shallow tank of the same diameter, the effect decreasing as the baffle moves to greater depth.

Therefore, the location of flat ring and conic section baffles, necessary for a substantial increase in damping, is restricted to a narrow range near the liquid free surface. For locations near the liquid free surface, the damping factor increases with the size of the flat ring and conic section baffles. However, for baffle locations well below the liquid surface, increases in the baffle size do not result in substantial increases in damping.

5C-3.3 Other Attenuation Methods

In order to decrease the instability conditions caused by the sloshing of liquids in tanks several other methods can be employed. The introduction of conventional ring baffles mounted on the tank walls breaks up the flow and creates enough turbulence to damp the oscillations. The dividing of the tank in several sub tanks by means of

separating cross-inner-walls will increase the natural frequencies of the liquid but, since the resonance frequencies will remain the same for all sub tanks, superposition of forces and moments due to liquid motion still may occur. However, dividing the tank in concentric sub tanks by means of concentric-inner-walls, thus dividing the tank in an inner cylindrical tank and an outer ring tank, will separate the frequencies. In that case the relative phase shift between the liquid oscillations in the inner and outer tanks will make possible a reduction in the resultant forces and moments.

5C-3.4 Capillarity and Viscosity

If the tank diameter is comparatively large, the effects of viscosity and capillarity (surface tension) are of minor importance to the liquid flow pattern. However, if baffles are used in the tank to damp the oscillations, the turbulence and pressure forces acting on these surfaces may have a pronounced influence on the motion of the liquid. In this case an approximation may be made by using the undamped results with damping factors introduced in the resonance terms. However, these damping factors must be obtained by tests for various types of suppressors.

5C-4 Method of Solution

In analyzing theoretically, the nature of the liquid motion is considered to be irrotational, $\nabla \times \vec{v} = 0$, in the sense that the velocity vector is considered to be the gradient of a potential $\vec{v} = \nabla \phi$. Furthermore the liquid is assumed to be an incompressible fluid, $\nabla \cdot \vec{v} = 0$, and as such the velocity potential is a solution of the Laplace equation $\nabla^2 \phi = 0$, not involving explicitly the time variable. Under these conditions, the flow pattern in the tank is defined at each moment only by the instantaneous boundary conditions. This implies then that a solution for the motion of the liquid sloshing in the tank may be found by solving the Laplace equation for various time-and-space dependent boundary conditions, in a linearized form, including the free-liquid surface boundary condition. The free-liquid surface boundary conditions is obtained by combining the nonstationary Bernoulli equation, using the zero pressure condition at the free surface of the liquid, with the kinematic condition of the liquid-free surface.

If the velocity potential is known, the shape of the free surface, together with the pressure and velocity distribution of the liquid can be obtained by simple differentiations and integrations of infinite series. Furthermore, the assumed linearization makes it possible to superimpose all modal motions.

During roll oscillations of the tank about its centroidal axis, part of the resulting oscillation is due to friction at the walls and baffles. By assigning an "effective moment of inertia" and with the damping of the liquid solutions may be obtained by employing the Navier-Stokes equations.

5C-4.1 Mechanical Analogs

The results obtained by the analytical procedure based on the dynamics of the fluid can also be obtained by replacing the fluid system by its mechanical equivalent. The equivalent mechanical model is chosen in such a way that it exerts the same forces and moments and has the same natural frequencies as the oscillating liquid in the container. Two mechanical equivalents are the simple pendulum and the spring-bob, the size and the location of their inertias being determined by matching forces and moments on the tank surfaces with those obtained by the linearized hydrodynamic theory.

The two mechanical analogs imply that no damping is applied to the liquid. The incorporation of damping in these analogies to simulate damping of the liquid has been limited because available methods for including the damping provided by a baffle are questionable and because quantitative data on the damping offered by baffles have only recently become available. Damping effects in the fundamental antisymmetrical mode have been evaluated, as described earlier, in terms of baffle configuration, size and location for the case of a liquid oscillating in a static upright-circular-cylindrical tank. Emphasis has been placed on the damping of the wave amplitude provided by annular ring baffles at various locations with respect to the free surface in terms of the logarithmic decrement. As a result an equivalent damping coefficient could be extrapolated which would provide a similar decrement for the mechanical analysis.

These damping coefficients apply, however, only to the first antisymmetrical liquid mode. However, it has been shown by experiment that this mode is of primary importance because of the ease with which large amplitude liquid motions can be induced and because of the large forces which the liquid pressure imparts to the tank wall.

For small displacements the two mechanical models are identical and provide good simulation of the stiffness and inertia terms for liquid sloshing. However, the pendulum analogy appears to be a better approach in some applications, such as those involving a varying acceleration field, because the pendulum frequencies exhibit the same dependence on the longitudinal accelerations of the tank as do the liquid natural frequencies. As a consequence it appears that the liquid sloshing can be treated as a single-degree-of-freedom system simulated by a simple damped pendulum or a simple mass-spring-dashpot configuration plus a fixed mass having a certain moment of inertia.

These mechanical analogs provide a very effective method for the determination of coupled natural frequencies of partially filled tanks undergoing planar translatory and pitching oscillations. They yield valid modal damping for systems in which the tank experiences purely translatory motions so that its decrement is equal to the decrement of the liquid amplitudes in an identical static tank filled with the same baffle configuration. However, mechanical analogs, incorporating damping values, do not yield valid modal damping for the same system undergoing pitching oscillations. This apparent discrepancy is due principally to a basic difference in the behavior of damping in a liquid exposed to translatory or to pitching motions. This difference in the damping characteristics is a direct result of the dissimilarity in the relative motions existing between the liquid and the tank with two cases. In a translatory tank, relative motion exists between the liquid and the tank wall primarily in the region of the liquid surface, while in a pitching tank, relative motion takes place at all points of the liquid-tank contact. As such a baffle in a pitching tank has a greater effective depth range and thus an entirely different damping characteristic.

5C-4.2 Equations of Pendulum Analog

The physical parameters involving the analogous pendulum duplicating the hydrodynamic forces and moments obtained by the foregoing procedure for an upright circular cylinder tank, partially-filled with liquid (Figure 5C-2a) and corresponding to the mechanical scheme are shown in Figure 5C-2b. The following notations have been used:

m = total mass of liquid

R = tank radius

h_1 = distance from the bottom of the tank to the tank pitch axis

$e_1 = 1.84 \approx \frac{7}{12} \pi$ = The first zero of the first derivative of the Bessel function of first kind and of first order

The nondimensional parameter, k_1 , defines the geometry of the configuration in the fundamental mode and can be represented in the form

$$K_1 = e_1 \frac{h}{R}$$

(Eq. 5C-5)

The natural frequency in the fundamental mode is then given by

$$\omega^2 = \frac{g}{h} k_1 \tanh k_1 \quad (\text{for } e_1 = \frac{7}{12}\pi) \quad (\text{Eq. 5C-6})$$

then m_p = mass of pendulum = $m A_1$;
 m_o = fixed liquid mass = $m (1-A_1)$
 I_o = mass moment of inertia of the fixed liquid mass =
 $mh^2 \left(\frac{1}{3} + A_3 - A_1 \right) - m (h_1 - \ell_o)^2$
 ℓ_p = g/ω^2 = length of the pendulum
 ℓ_o = distance from tank pivotal axis to the centroid of the fixed mass =

$$h_1 = \frac{h}{1-A_1} \left(\frac{1}{2} + \frac{R^2}{4h^2} - A_2 \right) \quad (\text{Eq. 5C-7})$$

ℓ_h = distance from tank pivotal axis to pendulum pivot =

$$h_1 - h A_2/A_1$$

where A_1, A_2, A_3 are quantities defined by the fundamental antisymmetrical mode of the liquid oscillation in the form

$$\begin{aligned} A_1 &= \frac{2 \tanh K_1}{K_1 (e_1^2 - 1)} \\ A_2 &= 2 \frac{1}{K_1^2} \cdot \frac{2 + \sinh K_1 - \cosh K_1}{(e_1^2 - 1) \cosh K_1} \\ A_3 &= 4 \frac{1}{K_1^3} \cdot \frac{2 \sinh K_1 - K_1}{(e_1^2 - 1) \cosh K_1} \end{aligned} \quad (\text{Eq. 5C-8})$$

Equations 5C-5, -6, and -7 may be also used in a first approximation for horizontal circular cylindrical tank (Figure 5C-2c) of length, $l = 2R$, partially-filled with liquid to the level, h , when the sloshing occurs in the direction of the longitudinal axis. In this case, however, the parametric quantity, e_1 , has the value, $\pi/2$. Then the natural frequency of the liquid sloshing in the fundamental mode is given by

$$\omega^2 = \frac{g}{h} K_1 \tanh K_1 \quad (\text{for } e_1 = \frac{\pi}{2})$$

(Eq. 5C-9)

The above result is equally valid for liquid sloshing in the fundamental mode in vessels of rectangular shape of length, l , partially-filled with liquid to the level, h , where the sloshing occurs in the longitudinal direction (Figure 5C-2d).

For the case of horizontal circular cylindrical tanks of radius, R , partially-filled with liquid to the level, h , where sloshing occurs in a transverse direction (Figure 5C-2e) there is no known explicit closed form expression for the natural frequency, ω , of the liquid sloshing in the fundamental mode. However, analytical values have been obtained in numerical form, corresponding to the eigenvalues for various depths of the liquid in the tank resulting from a numerical solution of certain integral equations by a matrix iteration procedure.

The geometrical parameters for a partially-filled circular cylindrical tank are shown on Figure 5C-2f. The depth of the liquid is measured by, e , which varies from -1 for the empty tank to +1 for the full vessel. The eigenvalues, λ_n thus obtained are related to the natural frequencies of the liquid sloshing in various modes in the form

$$\lambda_n = \omega_n^2 \frac{R}{g}$$

(Eq. 5C-10)

The eigenvalues thus obtained for the fundamental sloshing modes are given in Table 5C-2 in terms of the geometrical parameters shown in Figure 5C-2f.

Table 5C-2 Eigenvalues

	e										
	-1.0	-0.8	-0.6	-0.4	-0.2	0.0	0.2	0.4	0.6	0.8	1.0
a	0.0	0.6	0.8	0.917	0.980	1.0	0.980	0.917	0.8	0.6	0.0
$a\lambda_1$	0.0	0.627	0.879	1.068	1.224	1.360	1.482	1.596	1.706	1.822	2.018
λ_1	1.0	1.045	1.099	1.165	1.249	1.369	1.513	1.742	2.130	3.040	∞

Thus, it is apparent that the analytical solution just described infers that the frequencies tend to infinity as the full condition is approached.

5C-4.3 Higher Modes

For higher frequencies than the fundamental the variation in frequency with e is not monotonic. The minimum frequency of a given higher mode appears to occur slightly below the half-full condition, whereas the fundamental mode has its lowest frequency in the nearly empty state. The finite values of λ_n under near-empty conditions may be interpreted physically as the result of the fluid acting as a compound pendulum for the case of the first mode and a multiple pendulum for the higher modes, the center of rotation being the center of the circular cross section of the cylinder. That λ_n should approach infinity at the higher depths may be physically interpreted as the result of the reduction of the free surface area as the tank is filled. The above results show that the transverse natural frequencies of liquid in horizontal cylinders are independent of the container length. The theoretical values obtained from the analytical results (given above) show good agreement with the experimental data obtained, especially for the half-full case.

5C-4.4 Spherical Container

The general trend and the physical explanation of the boundary values are similar to the case of a spherical configuration. An alternative method for computing, in a first approximation, the natural frequency of the fundamental mode of liquid sloshing in circular cylindrical or spherical vessels in lateral direction consists of replacing such a configuration by an equivalent liquid system approximated by an upright circular cylinder having a radius, r , equal to the radius aR of the liquid-free surface in the sphere and a liquid depth, h_c , which will yield a cylindrical volume equal to the volume of the liquid contained in the sphere. In this case the natural frequency of the liquid in such a cylinder is given by the equation 5C-6. This method appears to yield excellent correlation between the frequencies of a liquid when the equilibrium surface is circular.

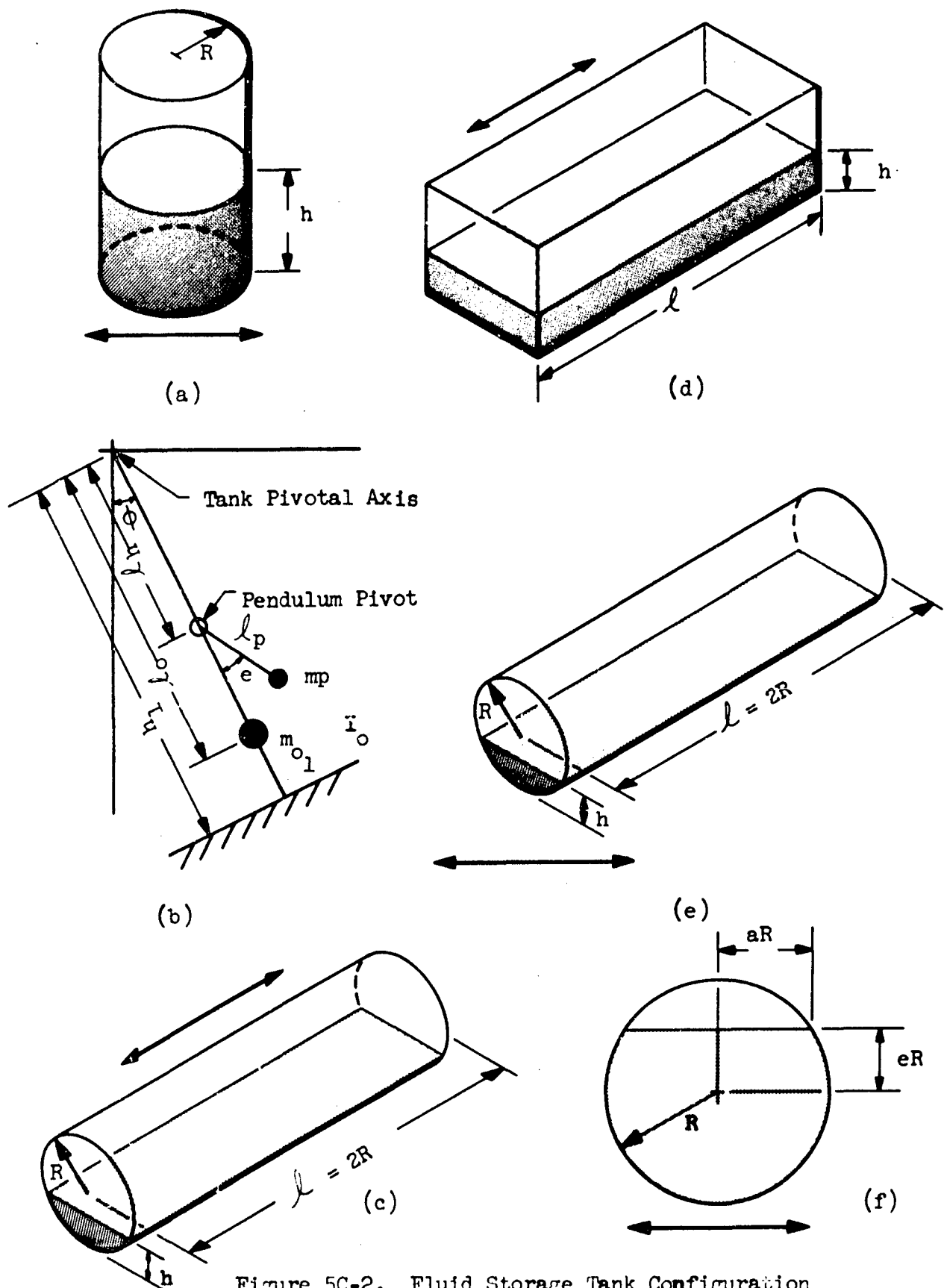


Figure 5C-2. Fluid Storage Tank Configuration

5C-4.5 Elliptical Container

More generally if the equilibrium surface has an elliptical shape such as in oblate spheroidal tanks subjected to oscillations parallel and perpendicular to the plane of the spheroid equator, the above method infers the substitution of the actual configuration by an equivalent liquid system consisting of an upright elliptical cylinder whose cross section is congruent to the equilibrium liquid surface in the spheroid; the liquid depth, h_e , assigned to the hypothetical cylinder being adjusted so that the volume of liquid contained in the cylinder is equal to the liquid volume in the spheroid. The natural frequency of the n th mode of the liquid in such a cylinder is then given by

$$\omega^2 n^2 = \frac{g}{\alpha} K_n \tanh \frac{h_e}{\alpha} K_n$$

(Eq. 5C-11)

Where Q is defined as the semimajor axis of the cylinder section and the constant K_n is proportional to the positive parametric zeros of the first derivative of the Mathieu functions related to the system. This method appears to correlate satisfactorily with experimental data for frequencies of liquids in oblate spheroidal tanks within the region of practical interest.

Experimental evidence agrees in general with the foregoing results of the available theory, and confirm that the characteristic variations of the natural frequencies with tank fullness vary considerably with tank orientation and mode of fluid oscillation.

The analytical expression for the natural frequencies of a fluid undergoing transverse oscillations in an upright circular cylinder is found to yield results in close agreement with the experimental data obtained, over a wide range of fluid depths and container sizes.

5C-4.6 Horizontal Cylindrical and Spherical Containers

In the case of longitudinal oscillations in fluids in horizontal circular cylinders, the natural frequencies of all modes increase monotonically with tank fullness. No exact theoretical results are available for comparison for this configuration.

In the case of transverse oscillations of liquids in spheres and horizontal cylinders, a monotonic increase in frequency from a finite value is noted for the first mode as the tank is filled. For the higher modes, the frequencies decrease from finite values for the empty conditions to minimum values when the tank is approximately half full. As the tank is filled further, the frequencies again increase. As the full condition is approached the frequencies of all modes approach infinite values.

Good agreement is shown between the experimental data and the results of available theory. In order to investigate the coupled dynamic response of a liquid-tank combination undergoing free and forced oscillations a mathematical model of the complete system must be set up in form of differential equations based on the mechanical analog described earlier whereby the basic phenomena associated with the effects of this motion on the dynamic stability of the liquid-carrying vehicles may be determined. By solving in an appropriate manner these differential equations of motion there will be obtained the coupled natural frequencies of the system in question which in general may be different from the above descriptive values. The mathematical work involved in this approach is laborious due to the complexity of the differential equations describing the complete system and as such will not be presented here.

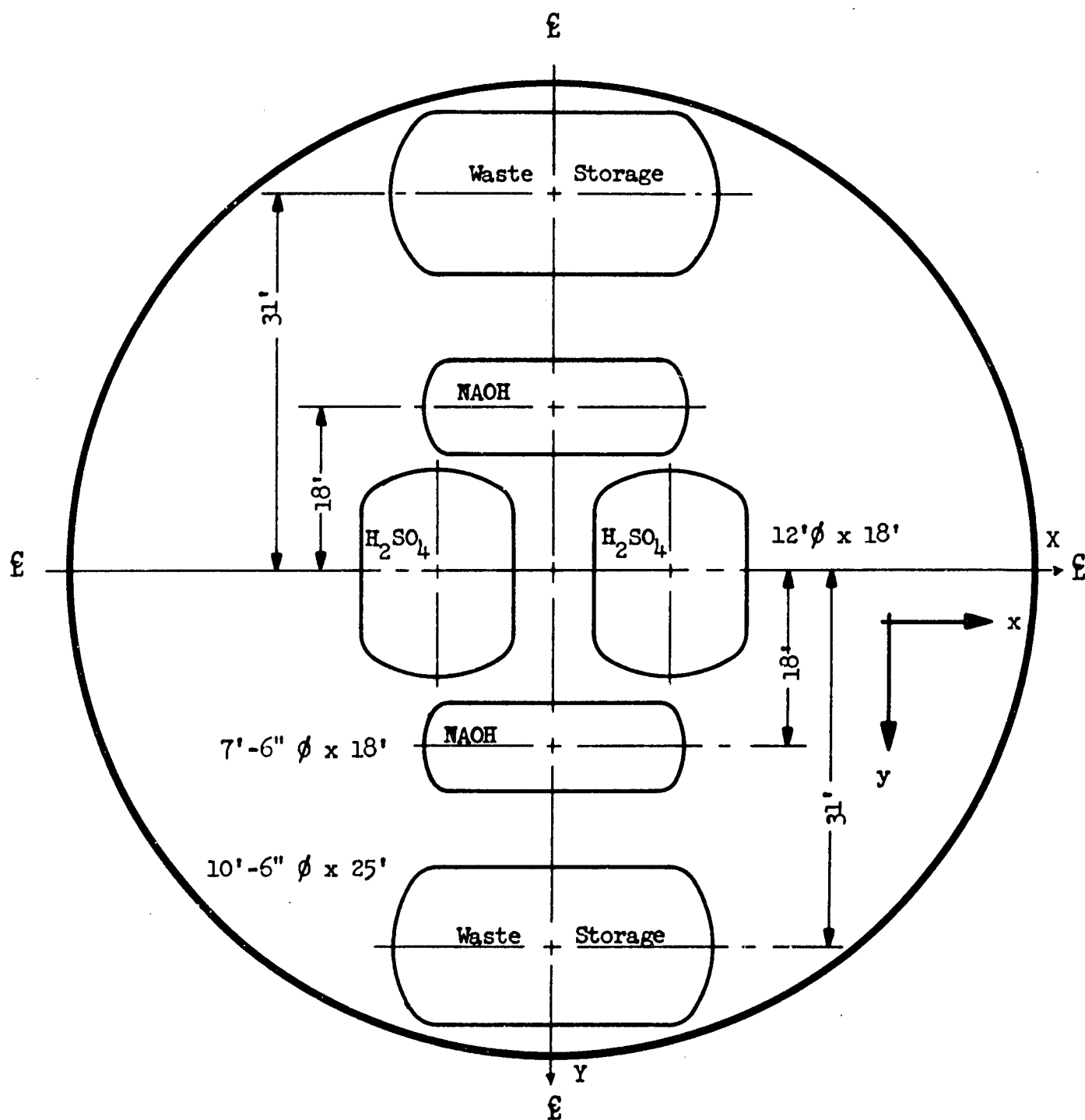
5C-5 Natural Frequencies of Sloshing in Tank for This Facility

Applying the foregoing results (Eq. 5C-5, 6, 9, and 10) for the various partially-filled liquid vessels incorporated in the structure as shown on Figures 5C-3 and 5C-4, the following natural frequencies for the liquid sloshing in the fundamental modes in X and Y directions have been obtained.

Table 5C-3 Fundamental Liquid Sloshing Natural Frequencies

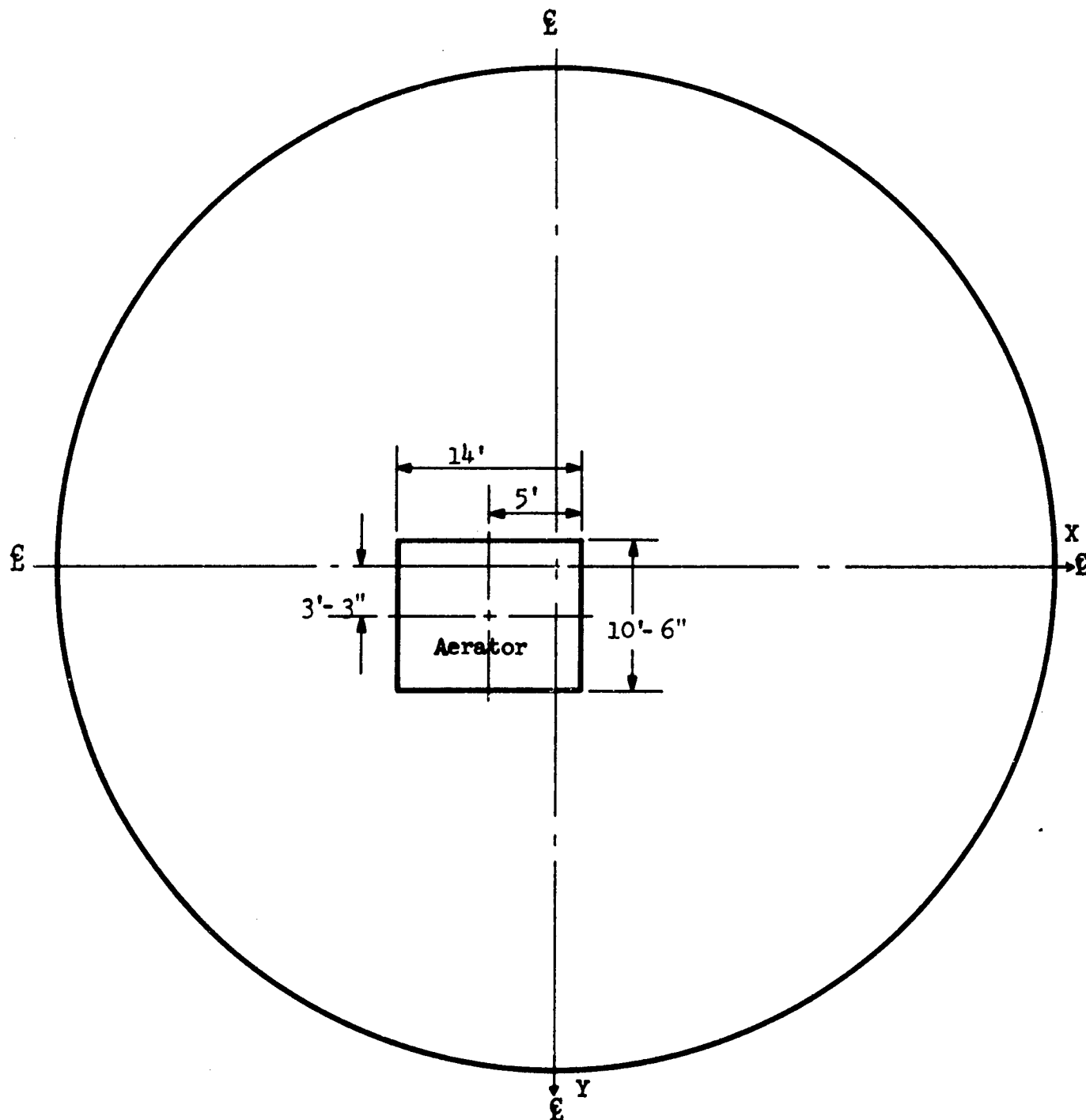
	Vessel	R_{ft}	l_{ft}	h_{ft}	$e_{\%}$	k_1	λ	ω^2	f_{cps}
X-Direction	H ₂ SO ₄	6	18	7	0.166	-----	1.488	7.985	0.449
	NaOH	3.75	18	4.75	-----	0.828	-----	3.812	0.310
	Waste Storage	5.25	25	6.25	-----	0.785	-----	2.651	0.259
	Aerator		14	2	-----	0.448	-----	3.031	0.277
Y-Direction	H ₂ SO ₄	6	18	7	-----	1.221	-----	4.717	0.345
	NaOH	3.75	18	4.75	0.266	-----	1.588	13.635	0.587
	Waste Storage	5.25	25	6.25	0.190	-----	1.505	9.230	0.483
	Aerator	----	10.5	2	-----	0.598	-----	5.156	0.361

Should the above natural frequencies coincide with the natural frequencies of the cage, antisloshing devices must be installed to avoid resonance.



Note: All Liquid Levels are $\phi + 1$ ft. Above Floor.

Figure 5C-3. First Level Plan.



Note: Liquid Level = 5' Above Floor.

Figure 5C-4. Second Level Plan.

SECTION 5 SYMBOLS AND NOTATIONS

Generalized Coordinates

ℓ : Instantaneous length of the resultant pendulum

ϕ : Inclination of the resultant pendulum with vertical axis

θ : Inclination of vertical plane containing resultant pendulum with X-axis.
(ℓ, ϕ, θ are polar coordinates of the center of gravity in capsule reference system X-Y-Z)

$\left. \begin{matrix} \alpha \\ \beta \\ \gamma \end{matrix} \right\}$: Rotations of the suspended mass about inertial reference system $X_1-Y_1-Z_1$, respectively

$\left. \begin{matrix} p \\ q \\ r \end{matrix} \right\}$: Angular velocities of the suspended mass along $X'-Y'-Z'$, respectively

$\left. \begin{matrix} \theta \\ \phi \\ \psi \end{matrix} \right\}$: Euler angles defining $X'-Y'-Z'$ with respect to $X_1-Y_1-Z_1$

$\left. \begin{matrix} X_0 \\ Y_0 \\ Z_0 \end{matrix} \right\}$: Ground reference system

$\left. \begin{matrix} X \\ Y \\ Z \end{matrix} \right\}$: Capsule reference system (parallel to $X_0-Y_0-Z_0$)

$\left. \begin{matrix} X_1 \\ Y_1 \\ Z_1 \end{matrix} \right\} : \text{Inertial reference system, origin at center of gravity}$
 (parallel to X-Y-Z)

$\left. \begin{matrix} X_n \\ Y_n \\ Z_n \end{matrix} \right\} : \text{Isolator reference system, origin at capsule attachment}$
 point (parallel to X-Y-Z)

$\left. \begin{matrix} u \\ v \\ w \end{matrix} \right\} : \text{Euler's reference system}$

$\left. \begin{matrix} X' \\ Y' \\ Z' \end{matrix} \right\} : \text{Moving reference system origin at center of gravity fixed}$
 to mass

Ground Accelerations

a_v : Vertical ground acceleration
 a_H : Horizontal ground acceleration
 θ_o : Angle between a_H and X_o axis

$\left. \begin{matrix} \ddot{X}_o \\ \ddot{Y}_o \\ \ddot{Z}_o \end{matrix} \right\} : \text{Ground accelerations along } X_o-Y_o-Z_o \text{ respectively}$

Physical Constants for Suspension System

l_s : Length of the resultant pendulum in static position (with
 dead load)

$\left. \begin{matrix} l_{ns} \\ \phi_{ns} \\ \theta_{ns} \end{matrix} \right\} :$ Polar coordinates of n^{th} isolator in static position
 (Origin of reference system at r_{1w} , r_{2w} , r_{3w} wall attachment point, parallel to X-Y-Z)

$\left. \begin{matrix} l_n \\ \phi_n \\ \theta_n \end{matrix} \right\} :$ Polar coordinates of n^{th} isolator at time "t" due to translation of center of gravity (Reference system as above)

$l_{no} :$ Length of n^{th} isolator with zero load

$l_{nf} :$ Final length of n^{th} isolator at time "t", due to translation of and rotation about center of gravity

$m :$ Mass of the suspended body

$\left. \begin{matrix} I_{11} \\ I_{22} \\ I_{33} \end{matrix} \right\} :$ Moment of inertia of the suspended body about X'-Y'-Z' respectively

$\left. \begin{matrix} r_1 \\ r_2 \\ r_3 \end{matrix} \right\} :$ Co-ordinates of mass-attachment point of n^{th} isolator
 n

$\left. \begin{matrix} r_{1w} \\ r_{2w} \\ r_{3w} \end{matrix} \right\} :$ Co-ordinates of wall-attachment point of n^{th} isolator
 n

$\left. \begin{matrix} x \\ y \\ z \end{matrix} \right\} : \text{Translation of center of gravity in } X_1-Y_1-Z_1 \text{ reference system}$

$\left. \begin{matrix} \delta x \\ \delta y \\ \delta z \end{matrix} \right\}_n : \text{Displacement of mass-attachment point of the } n^{\text{th}} \text{ isolator in } X_1-Y_1-Z_1 \text{ reference system due to translation of and rotations about center of gravity}$

$[F]_n : \text{Restoring force in } X_1-Y_1-Z_1 \text{ reference system by } n^{\text{th}} \text{ isolator}$

$[F]_n^D : \text{Damping force in } X_1-Y_1-Z_1 \text{ reference system by } n^{\text{th}} \text{ isolator}$

$[M]_n : \text{Moment of the restoring force in } X'-Y'-Z' \text{ reference system by } n^{\text{th}} \text{ isolator}$

$[M]_n^D : \text{Moment of the damping force in } X'-Y'-Z' \text{ reference system by } n^{\text{th}} \text{ isolator}$

$[\mathcal{O}] : \text{Angular momentum in } X'-Y'-Z' \text{ reference system}$

$\frac{d}{dt}[\mathcal{O}] : \text{Rate of change of angular momentum}$

$[S] : \text{Position matrix of the resultant pendulum in } X'-Y'-Z' \text{ reference system}$

$[S]_p : \text{Position matrix of the resultant pendulum in polar reference system}$

$[S]_{pn} : \text{Position matrix of the } n^{\text{th}} \text{ isolator in the polar reference system}$

$[S_0] : \text{Displacement due to ground translation in } X_0-Y_0-Z_0 \text{ reference system}$

$[D] : \text{Cartesian transformation matrix}$

$[D]_p : \text{Polar transformation matrix for center of gravity}$

$[D]_{pn} : \text{Polar transformation matrix for } n^{\text{th}} \text{ isolator}$

$[K]_n : \text{Stiffness matrix of the } n^{\text{th}} \text{ isolator}$

$[K]_n^D : \text{Damping stiffness matrix of the } n^{\text{th}} \text{ isolator}$

$[\delta]_n$: Displacement of mass-attachment-point of the n^{th} isolator
$[r_a]_n$: Moment arm for mass attachment point of the n^{th} isolator
$[K_{ZZ}]_n$: Axial stiffness of the n^{th} isolator
$[K_{ZZ}]_n^D$: Axial damping stiffness of the n^{th} isolator
ξ	: Damping ratio
C_1	: Friction damping coefficient
C_2	: Square-law damping coefficient
h	: Height of the cage or tank
d	: Diameter of the cage or baffle location below the liquid free surface
h_1	: Equivalent clearance at top and bottom
h_o	: Equivalent clearance on sides
P	: Absolute pressure
W	: Weight of air
V	: Volume
T	: Absolute temperature
R	: Gas constant
μ	: Dynamic viscosity of air
v	: Specific volume
C_p	: Specific heat for air at constant pressure
C_v	: Specific heat for air at constant volume
γ	: Ratio of specific heats for air = c_p/c_v
R	: Radius of circular tank

ν	:	Liquid kinematic viscosity
g	:	Acceleration due to gravity
n	:	Number of cycles
A	:	Liquid wave amplitude

6.0 CAGE STRUCTURAL ANALYSIS

6.1 Introduction

The selection of the suspension system configuration (Section 3.0) and the derivation of the equations for the system response (Section 5.0) were both based on the assumption that the cage structure was absolutely rigid. In many systems which are isolated from ground shock and where the natural frequencies of the system are so much lower than the fundamental mode frequencies of the supported structure, negligible error is introduced by the rigid body approximation. In this application, however, where the cage is very large and contains relatively long beams and tension members, the possible interaction of the motions of the cage with those of the isolation system warranted further investigation.

The structure of the cage (Figures 6-1, 6-2 and 6-3) is of a fairly conventional design. Twelve vertical members are spaced nearly equally around the periphery of the cylinder, and to these are attached both the shock isolators and the floor beams. To add to the rigidity of the 75-foot diameter floors, eight tension members are attached at the top of the structure to crossed Pratt trusses and to each floor. The exterior of the structure is entirely covered by a shell of 1/4-inch steel.

The exterior shell provides tremendous shear stiffness to the structure as a whole, but the long spans of the floors and the large proportion of weight represented by the floors and their contents, aroused some suspicion that the effect of their dynamic response might be significant to the system motion.

One approach to the solution of this problem involves, first, a calculation of the normal unrestrained vibration modes of the complete spaceframe for the various loading conditions. Second, if the calculated mode frequencies are found to be near the frequencies of the isolation system, an analysis of their effect on the system response can be made by introducing in the spaceframe, at the isolator attachments, forces obtained by a rigid body analysis of the isolation system. A comparison of the attachment point displacements obtained in this manner with those obtained in the rigid body analysis would serve as an indication of the magnitude of the coupling between systems.

In this study, only the unrestrained vibrational modes of the cage structure were obtained and compared with the frequencies of the isolation system.

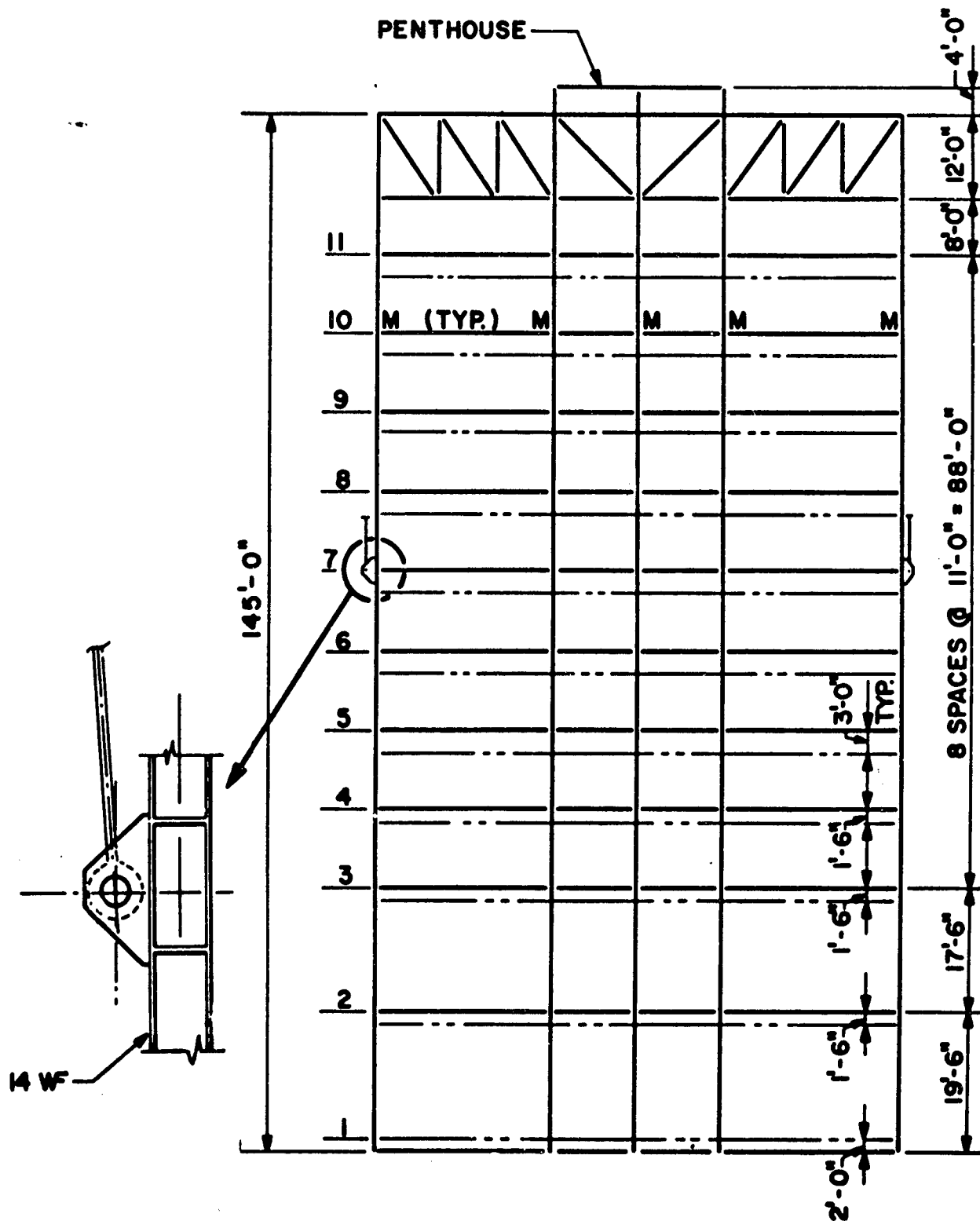
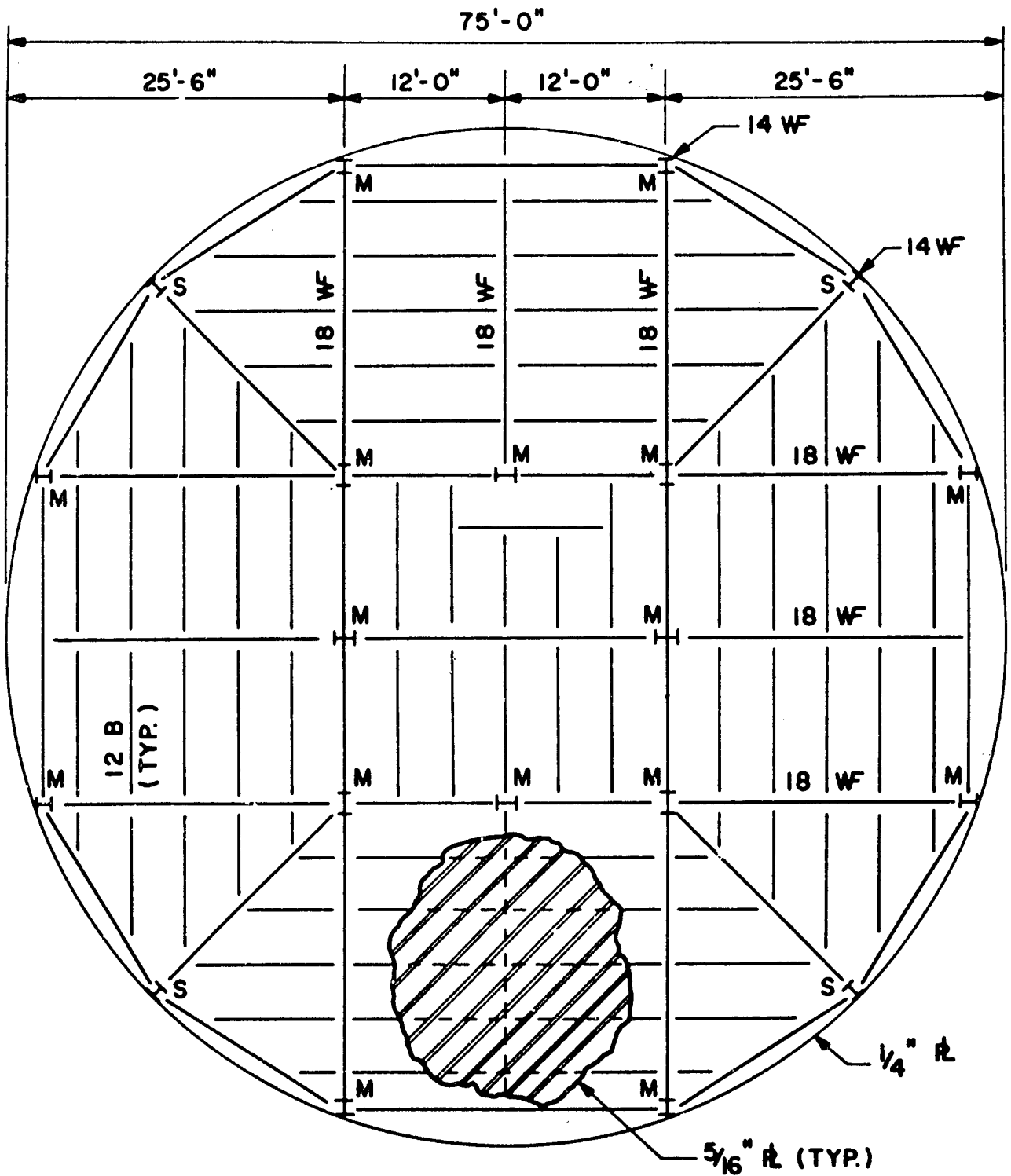


Figure 6-1 Elevation of Suspended Structure



M = MOMENT CONN.
S = SIMPLE CONN.

Figure 6-2 Typical Floor Framing of Suspended Structure

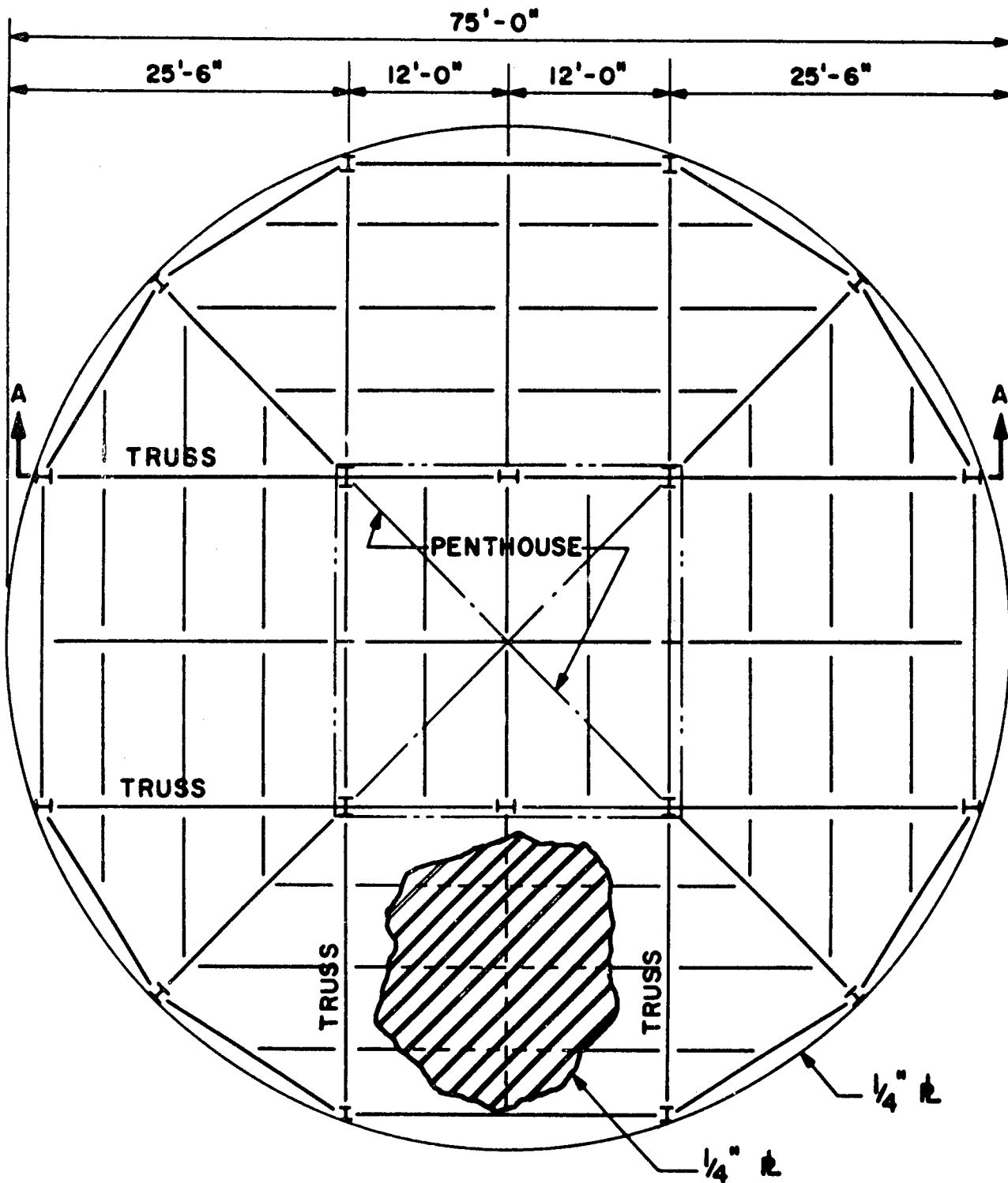


Figure 6-3 Top Framing Plan of Suspended Structure

6.2 Structural Arrangement

As noted previously, the suspended structure is assumed to be an eleven-story cage, 75 feet in diameter and 145 feet high (Figure 6-1). It is supported by twelve pendulum arms for each of the three configurations. A principal structural feature is twelve vertical ribs, to which the pendulum arms are attached, running full height on the outside of the structural cage. These ribs are loaded in compression over a part of their length, and in tension for the remainder. Floor beams are attached directly to the ribs.

The basic framing consists of two pairs of crossed Pratt trusses at the very top (Figure 6-4). Eight tension columns are hung from the points of intersection of the trusses and halfway between, outlining the sides of a 24-foot square core in the center of the cage. The core serves as an elevator shaft and a housing for duct and cable ways, stairs, and piping. By concentrating practically all the vertical stiffness of the floor framing in one place (i.e., the trusses), the span of the floor framing is greatly reduced, and results not only in a stiffer floor, but considerably reduces the overall weight of steel required for the cage as a whole.

The exterior of the cage is a thin steel plate built integrally with the framing and stiffened as necessary for compressive forces. The chief advantage of the shell is that it stiffens the structure more economically and with less weight than could be done by continuous framing or with bracing. The particular issue involved is the required rigidity of the structure. Conventional framing could be made strong enough to take the applied loadings, but would be so flexible as to couple with the oscillations of the shock isolators. To provide sufficient stiffness to avoid coupling by bracing or continuous framing, very heavy steel sections would be required.

Other advantages of the steel shell are that it

- . provides more unobstructed space
- . doubles as an EMP shield
- . reduces relative motion between points of attachment of the isolators
- . forms an outer wall
- . provides protection against the remote possibility of spallation of concrete from the inner face of the liner.

The main beams of the floor framing run approximately radially from the central tension columns. Secondary framing members span between the main beams, forming a pattern of successively larger concentric squares.

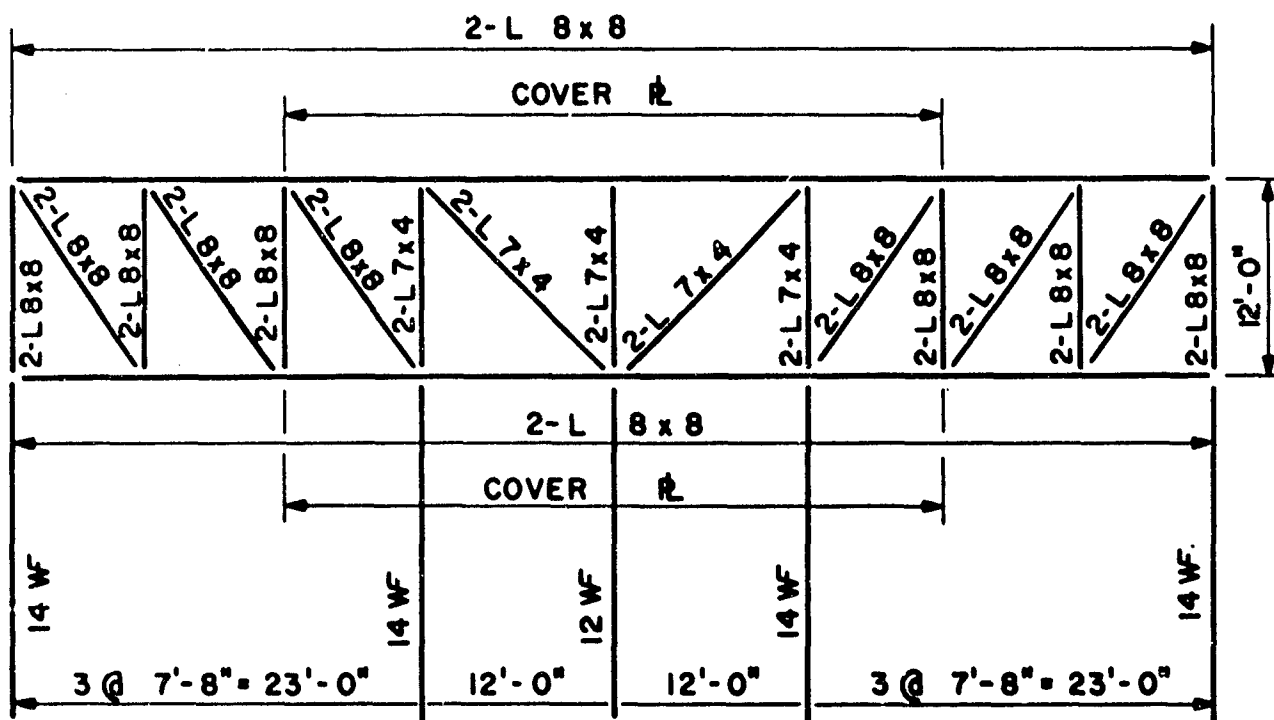


Figure 6-4 SECTION A-A ELEVATION OF TRUSS

Approximately 1.5 to 2.0 feet depth has been allowed for structural framing in the first three floors. The remaining floors have an allowance of three feet each to provide space for mechanical, electrical and other utility items, as well as for structural framing.

6.3 Member Sizes

Before an analysis could be made, it was necessary to determine the approximate sizes of the principal structural members. These are presented in Table 6-1.

Table 6-1 Principal Structural Member Size for Cage

Location	Item	Size
Trusses	Upper Chords	2L - 8 x 8 x 1-1/8 + 27 square inches of cover plates
	Lower Chords	2L - 8 x 8 x 1-1/8 + 12 square inches of cover plates
	Verticals	2L - 8 x 8 x 1 and 2L - 7 x 4
	Diagonals	2L - 8 x 8 x 7/8 and 2L - 7 x 4
Periphery	Vertical Ribs	14 WF 111
Core	Tension Columns	12 WF 40 to 14 WF 84
Typical Floor	Main Girders	18 WF 50
	Secondary Beams	12 B 14
	Floor Plate	5/16 inch
Roof	Beams	12 B 14
	Plate	1/4 inch
Exterior	Shell Plate	1/4 inch reinforced as required

All columns are considered as being continuous, as are the main girders, which are parallel to the overhead trusses. All other connections are shear connections.

6.4 Weight and Balance

Dead Load

An estimate of approximately 1618 tons of dead load has been made for the structural cage. Of this, 1060 tons were structural steel and the remaining 558 tons were miscellaneous items, such as floor cover, ceiling, partitions, stairways, elevators, toilets, and other utilities.

Live Load

An estimate of approximately 907 tons of live load was made for the cage. This was predicated on an average applied actual load of 20 psf over most of the floor area. (Preliminary sizing of members was based on 150 percent of dead load plus 100 psf live load.) On the third floor, a live load of 100 psf was used to account for electronic equipment. On the first floor, the live load used was 128 psf, which approximated the load in the first floor tanks, exclusive of the capacity of the sewage storage tanks.

Variation in Mass Properties of Cage

An increase in live load of 133 tons was applied to the first floor to account for the filling of the sewage tank after an initial attack. This lowered the center of gravity about three feet, increased the mass moment of inertia about the center of gravity by 10.0 percent, and the polar moment of inertia about the vertical axis by 6.4 percent.

On the other hand, if both the sodium hydroxide and sulphuric tanks should become emptied, the center of gravity would be raised about 7.3 feet, the total weight decreased 11.2 percent, and the polar moment of inertia decreased 3.7 percent.

Concerning a horizontal shift in the center of gravity, it was assumed that a decrease of approximately 25 percent of the live load near the perimeter of the cage could shift the center of gravity as much as four feet for an extreme case. The resulting decrease in total weight would be about 10 percent and the center of gravity would be raised 0.7 feet, the mass moment of inertia would be decreased 13.7 percent, and the polar moment of inertia decreased 14.7 percent.

In order to base response studies on an even basis above and below the "normal" cage characteristics, the following changes were adopted:

Weight	\pm 10 percent
Vertical center of gravity	\pm 6 feet

Horizontal center of gravity	\pm 4 feet
Mass moment of inertia	\pm 14 percent
Polar moment of inertia	\pm 15 percent

Weight and Balance Summary

Table 6-2 presents a tabulation of the dead and live loads, the position of the vertical center of gravity, the mass moment of inertia about the center of gravity, and the polar mass moment of inertia about the vertical axis for an assumed "normal" cage.

Table G-2a Nominal Vertical Center of Gravity of Cage

Location	Item	Center of Gravity		
		Weight (Kips)	Height (Feet)	Wt. x Ht.
Shell	D	547.0	72.5	39658
Top Cover	D	71.0	145.0	10295
Top Chord Truss	D	40.5	145.0	5872
Top Chord Truss	D	40.5	145.0	5872
Lower Chord Truss	D	40.5	133.0	5387
Lower Chord Truss	D	40.5	133.0	5387
Ceiling	D	22.0	133.0	2926
11th Floor	D	223.0	125.0	27875
	L	94.0	125.0	11750
10th Floor	D	223.0	114.0	25422
	L	94.0	114.0	10716
9th Floor	D	223.0	103.0	22969
	L	94.0	103.0	9682
8th Floor	D	223.0	92.0	20516
	L	94.0	92.0	8648
7th Floor	D	223.0	81.0	18063
	L	94.0	81.0	7614
6th Floor	D	223.0	70.0	15610
	L	94.0	70.0	6580
5th Floor	D	223.0	59.0	13157
	L	94.0	59.0	5546
4th Floor	D	223.0	48.0	10704
	L	94.0	48.0	4512
3rd Floor	D	223.0	37.0	8251
	L	402.0	37.0	14874
2nd Floor	D	223.0	19.5	4348
	L	94.0	19.5	1833
1st Floor	D	132.0	2.0	264
Na OH Tank	L	206.0	7.0	1442
H ₂ SO ₄ Tank	L	360.0	7.0	2520
Bottom Cover	D	71.0	0	0
	I.	1814	47.253	85,717
	D	<u>3235</u>	<u>74.985</u>	<u>242,576</u>
		5049	65.021	328,293

Table 6-2b Nominal Movements of Inertia of Suspended Cage

Location	Item	Moment of Inertia					
		Z (feet)	Z ² (feet ²)	WZ ² (Kip Feet ²)	K (Feet)	K ² (Feet ²)	WK ² (Kip Feet ²)
Shell	D	7.5	56	30,769	26.52	703.3	384,705
Top Cover	D	80.0	6400	454,400	18.75	351.6	24,964
Top Chord	D	80.0	6400	259,200	20.21	408.4	16,540
Top Chord	D	80.0	6400	259,200	12.00	144.0	5,832
Lower Chord	D	68.0	4624	187,272	20.21	408.4	16,540
Lower Chord	D	68.0	4624	187,272	12.00	144.0	5,832
Ceiling	D	68.0	4624	101,728	18.75	351.6	7,735
11th Floor	D	60.0	3600	802,800	18.75	351.6	78,407
	L	60.0	3600	338,400	18.75	351.6	3,050
10th Floor	D	49.0	2401	535,423	18.75	351.6	78,407
	L	49.0	2401	225,694	18.75	351.6	33,050
9th Floor	D	38.0	1444	322,012	18.75	351.6	78,407
	L	38.0	1444	135,736	18.75	351.6	33,050
8th Floor	D	27.0	729	162,567	18.75	351.6	78,407
	L	27.0	729	68,526	18.75	351.6	33,050
7th Floor	D	16.0	256	57,088	18.75	351.6	78,407
	L	16.0	256	24,064	18.75	351.6	33,050
6th Floor	D	5.0	25	5,575	18.75	351.6	78,407
	L	5.0	25	2,350	18.75	351.6	33,050
5th Floor	D	- 6.0	36	8,028	18.75	351.6	78,407
	L	- 6.0	36	3,384	18.75	351.6	33,050
4th Floor	D	-17.0	289	64,447	18.75	351.6	78,407
	L	-17.0	289	27,166	18.75	351.6	33,050
3rd Floor	D	-28.0	784	174,832	18.75	351.6	78,407
	L	-28.0	784	315,168	18.75	351.6	141,343
2nd Floor	D	-45.5	2070	461,666	18.75	351.6	78,407
	L	-45.5	2070	194,604	18.75	351.6	33,050
1st Floor	D	-63.0	3969	523,908	18.75	351.6	46,411
NaOH Tank	L	-58.0	3364	692,984	11.00	121.0	24,926
H ₂ SO ₄ Tank	L	-58.0	3364	1,211,040	11.00	121.0	43,560
Bottom Cover	D	-65.0	4225	299,975	18.75	351.6	24,964

L 3,239,116
D 4,898,162
8,137,278

507,279
1,317,593
1,824,872

Tables 2a and 2b (continued)

NOTES

An item noted as D is Fixed Weight.

An item noted as L is a Movable Weight.

$$\text{Center of Gravity} = \frac{\text{Wt.} \times \text{Ht.}}{\text{Weight}} = \frac{328,293}{5049}$$

= 65.021' above the lowest point on cage structure.

Z is dimension above or below center of gravity.

Moment of inertia of the weight about the center of gravity in any vertical plane through the cage centerline is

$$\begin{aligned} I_z &= \frac{WZ^2 + WK^2}{g} = \frac{8,137,278 + 1,824,872}{32.17} \\ &= 309,672 \text{ Kip-sec}^2\text{-ft.} \end{aligned}$$

Moment of inertia of the weight about the vertical centerline is

$$I_k = \frac{2 \times 1,824,872}{32.17} = 113,452 \text{ Kip-sec}^2\text{-ft.}$$

6.5 Stiffnesses

The theoretical basis for the computer program used to determine the unrestrained vibration frequencies is presented in Appendix 6A, together with the results which are summarized in Table 6-3.

Table 6-3 Unrestrained Mode Frequencies

Weight Configuration	Unrestrained Mode Frequency (cps)	
	Vertical	Lateral
Heavy		
First Mode	4.25	} Response is Negligible
Second Mode	5.11	
Light		
First Mode	4.72	

In comparing these frequencies with the estimated frequency of the isolation system in the vertical mode (0.35 cps), it is seen that they are higher by a factor of 12. It would be expected, then, that the effect of internal motions of the mass on the system response would be small.

SECTION 6 APPENDIX

6A RESPONSE OF SPACE FRAME STRUCTURE

6A-1 Introduction

This appendix presents the theoretical basis, computer programs, and digital output for the following task:

1. Development of the stiffness equations for a space frame with both uniform and nonuniform members of arbitrary orientation.
2. Programming the formation of the stiffness matrix of the space frame.
3. Development of the unrestrained vibration equation for the space frame and programming for their solution.
4. Development of the equations required to determine the dynamic response of the unrestrained space frame to applied transient forces and programming for their solution.
5. Formation of the stiffness matrix for a space frame.
6. Determination of the normal unrestrained vibration modes of the frame for two weight configurations.

6A-2 Summary

All programming tasks were completed and the programs were checked out. The listings of the FORTRAN programs are included in this appendix.

The space frame equations were solved for the stiffness coefficients of the joints at which mass was concentrated. The resulting stiffness matrix was checked by postmultiplying by vectors of rigid body displacements. The resulting vectors were nearly null in relation to the magnitude of the products of the stiffness coefficients and the elements of the postmultiplying vectors. Thus, the stiffness matrix appears to have been calculated with good accuracy.

The vibration analysis was performed using a power method after sweeping out the rigid body modes by means of a matrix transplant of conservation of momentum equations into the unrestrained stiffness matrix. Apparently, because of the large order and relatively close eigenvalues only two accurate modes were obtained for one mass configuration and only one for the other configuration. Only vertical vibration modes were obtained, consequently, the lateral vibration modes appear to be above 6 cps, the highest frequency calculated accurately.

An alternative solution for the vibration modes by determinant iteration (trial and error) might provide more accuracy for both eigenvalues and eigenvectors.

6A-3 Formulation of the Space Frame Structural Equations

The structural equations for a general space frame are developed using the stiffness method for an arbitrarily oriented element in three-dimensional space. Figure 6A-1 illustrates the geometry of element ij and the rotation angles used to transform vectors from the space coordinate system $x-y-z$ into the $x''-y''-z''$ element coordinate system or vice versa.

To determine the transformation equations the first rotation, β , is taken about the z axis (using right-hand rule for signs) to intermediate axis positions x' and y' :

$$\begin{aligned}x' &= x \cos \beta - y \sin \beta \\y' &= y \cos \beta + x \sin \beta \\z &= z\end{aligned}\tag{Eq. 6A-1}$$

The second rotation, $-\phi$, is taken about the x' axis to the intermediate axis z' and the axis y'' which is an element axis:

$$\begin{aligned}x' &= x' \\z' &= z \cos (-\phi) + y' \sin (-\phi) \\y'' &= y' \cos (-\phi) - z \sin (-\phi)\end{aligned}\tag{Eq. 6A-2}$$

The third rotation, θ , is taken about the y'' axis to the other element axes z'' and x'' :

$$\begin{aligned}x'' &= x' \cos \theta - z' \sin \theta \\y'' &= y'' \\z'' &= z' \cos \theta + x' \sin \theta\end{aligned}\tag{Eq. 6A-3}$$

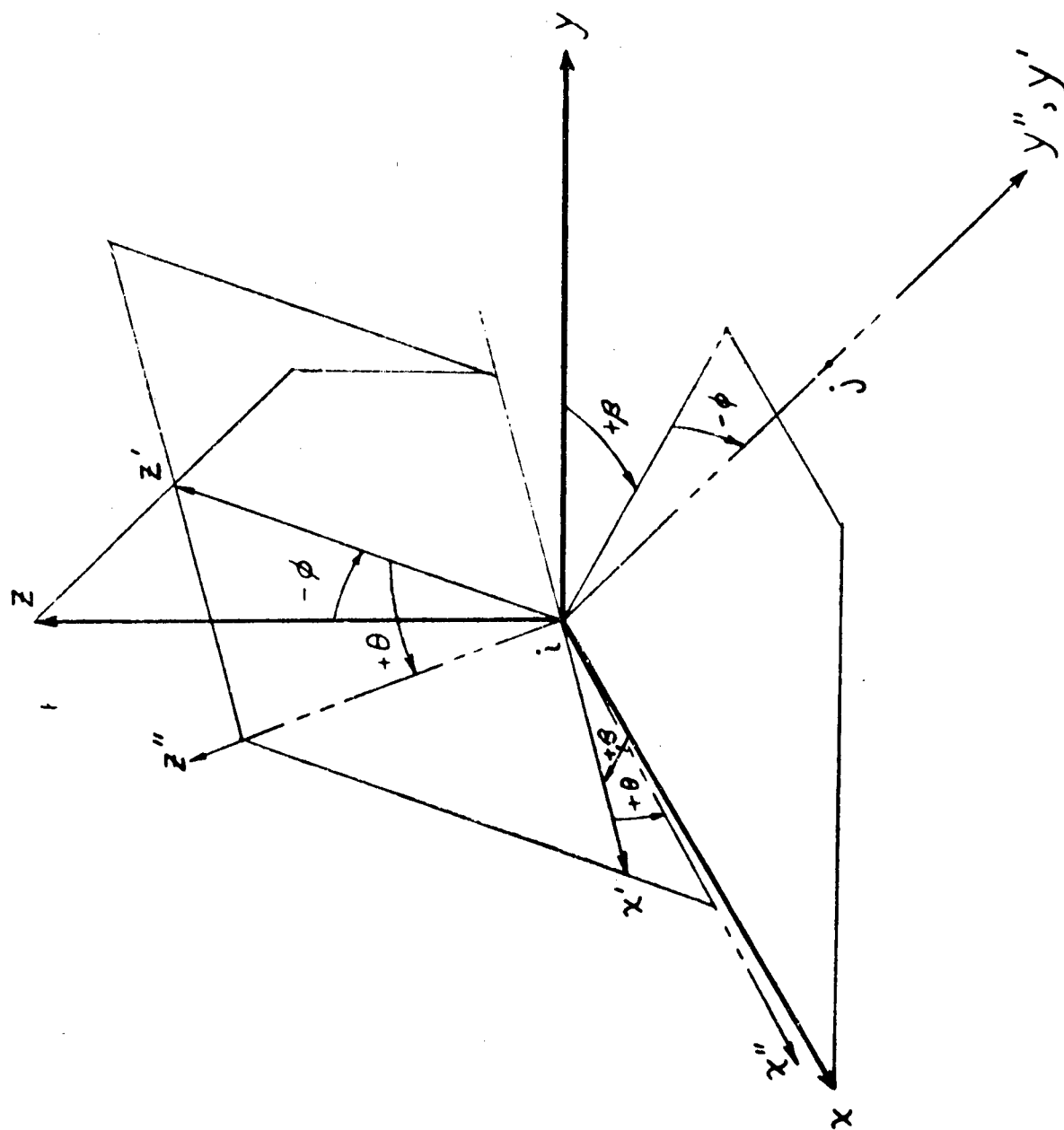


Figure 6A-1. Geometry of Element ij Arbitrarily Oriented in XYZ Space.

Substituting Equation 6A-1 and 6A-2 in Equation 6A-3, yields the final transformation equations:

$$\begin{aligned} x'' &= (\sin \beta \sin \phi \sin \theta + \cos \beta \cos \theta)x \\ &\quad + (\cos \beta \sin \phi \sin \theta - \sin \beta \cos \theta)y \\ &\quad + (-\cos \phi \sin \theta)z \\ y'' &= (\sin \beta \cos \phi)x + (\cos \beta \cos \phi)y + (\sin \phi)z \\ z'' &= (\cos \theta \sin \theta - \sin \beta \sin \phi \cos \theta)x \\ &\quad + (-\sin \beta \sin \theta - \cos \beta \sin \phi \cos \theta)y \\ &\quad + (\cos \phi \cos \theta)z \end{aligned} \quad (\text{Eq. 6A-4})$$

In matrix form* Equation 6A-4 may be expressed as

$$\begin{aligned} d'' &= T^T d \text{ for displacement vectors, and} \\ F'' &= T^T F \text{ for force vectors,} \end{aligned} \quad (\text{Eq. 6A-5})$$

where T is defined on Table 6A-3.

Now the force-displacement equations in the element coordinate system may be transformed into the space coordinate system in the following manner:

$$F'' = K d'' \quad (\text{Eq. 6A-6})$$

where K is the stiffness matrix in the element coordinate system; substituting Equation 6A-5, yields

$$T^T F = K T^T d. \quad (\text{Eq. 6A-7})$$

Since the elements of the columns of T are, in fact, the direction cosines of the orthogonal x'' , y'' , and z'' axes, respectively, it can be shown that

$$T T^T = I, \text{ and thus} \quad (\text{Eq. 6A-8})$$

$$F = T K T^T d. \quad (\text{Eq. 6A-9})$$

*NOTE: Superscript T indicates transposed, double primes indicate element coordinate system.

Hence, Equation 6A-9 yields the submatrix TKT^T for each element which must be located in the space coordinate stiffness matrix for the total frame according to the i-j designation of the element.

The stiffness equations for fixed-fixed, pinned-fixed, and pinned-pinned elements are found on Tables 6A-1 and 6A-2. They include biaxial bending and shearing, torsional, and axial stiffness and provide for members with variable moment of inertia.

A description of the input parameters and the program computations required to find the stiffness matrix of the complete frame is found below:

K-Matrix Formation Program - Input Parameters

1st card set - Joint and element counters (once per case)

1st card No. of fixed joints
 No. of pinned joints
 Order of complete stiffness matrix
 Number assigned to complete stiffness matrix
 No. of sections read in matrix

2nd and 3rd cards are title cards

2nd card set - Joint locations (once per case)

1 card for every two joints in the following format with the fixed joints listed before the pinned joints:

Joint no. (1-5)
 x (6-15)
 y (16-25)
 z (26-35)

Joint no. (36-40)
 x (41-50)
 y (51-60)
 z (61-70)

3rd card set - section counters (one card precedes each section read in matrix)

Last row read into core storage
 Last row read out of core storage
 Left columns deleted between subsequent sections
 Width of matrix band
 No. of uniform fixed-fixed elements
 No. of uniform pinned-fixed elements

Table 6A-1a
Stiffness Equations for Pinned-Pinned Elements

$$\begin{aligned} (F_{V_Y''})_i &= [K_A] [V_Y'']_i + [-K_A] [V_Y'']_j \\ (F_{V_Y''})_j &= [-K_A] [V_Y'']_i + [K_A] [V_Y'']_j \end{aligned}$$

Table 6A-2 Stiffness Equations for Fixed-Fixed Elements

$$(F_{ux})_i = [K_3(C_1 + 2C_2 + C_3)/l^2] [u_x]_i + [-K_B(C_1 + C_2)/l] [\alpha_z]_i + [K_B(C_1 + 2C_2 + C_3)/l^2] [u_x]_j + [K_B(C_2 + C_3)/l] [\alpha_z]_j$$

$$(F_{vy})_i = [K_A] [V_y]_i + [-K_A] [V_y]_j$$

$$(F_{Wz})_i = [K_B(C_1 + 2C_2 + C_3)/l^2] [W_z]_i + [K_B(C_1 + C_2)/l] [\alpha_x]_i + [K_B(C_1 + 2C_2 + C_3)/l^2] [W_z]_j + [K_B(C_2 + C_3)/l] [\alpha_x]_j$$

$$(F_{\alpha_x})_i = [K_B(C_1 + C_2)/l] [W_z]_i + [K_B C_1] [\alpha_x]_i + [K_B(C_1 + C_2)/l] [W_z]_j + [K_B C_2] [\alpha_x]_j$$

$$(F_{\alpha_y})_i = [K_G J/l] [\alpha_y]_i + [-K_G J/l] [\alpha_y]_j$$

$$(F_{\alpha_z})_i = [-K_B(C_1 + C_2)/l] [u_x]_i + [K_B C_1] [\alpha_z]_i + [K_B(C_1 + C_2)/l] [u_x]_j + [K_B C_2] [\alpha_z]_j$$

$$(F_{ux})_j = [-K_B(C_1 + 2C_2 + C_3)/l^2] [u_x]_j + [K_B(C_1 + C_2)/l] [\alpha_z]_j + [K_B(C_1 + 2C_2 + C_3)/l^2] [u_x]_i + [K_B(C_2 + C_3)/l] [\alpha_z]_i$$

$$(F_{vy})_j = [-K_A] [V_y]_j + [K_A] [V_y]_i$$

$$(F_{Wz})_j = [-K_B(C_1 + 2C_2 + C_3)/l^2] [W_z]_j + [-K_B(C_1 + C_2)/l] [\alpha_x]_j + [K_B(C_1 + 2C_2 + C_3)/l^2] [W_z]_i + [K_B(C_2 + C_3)/l] [\alpha_x]_i$$

$$(F_{\alpha_x})_j = [K_B(C_2 + C_3)/l] [W_z]_j + [K_B C_2] [\alpha_x]_j + [-K_B(C_2 + C_3)/l] [W_z]_i + [K_B C_3] [\alpha_x]_i$$

$$(F_{\alpha_y})_j = [-K_G J/l] [\alpha_y]_j + [K_G J/l] [\alpha_y]_i$$

$$(F_{\alpha_z})_j = [K_B(C_1 + C_2)/l] [u_x]_j + [K_B C_2] [\alpha_z]_j + [K_B(C_1 + C_2)/l] [u_x]_i + [K_B C_3] [\alpha_z]_i$$

292

No. of pinned-pinned elements
 No. of nonuniform fixed-fixed elements
 No. of nonuniform pinned-fixed elements

1st card set after section counters - Uniform fixed-fixed element properties.

1 card for each element in the following format:

i joint no.	(1-4)
j joint no.	(5-8)
$I_x'' = I_z'' z''$	(9-16)
$I_z'' = I_x'' x''$	(17-24)
$(KAG)_x''$	(25-32)
$(KAG)_z''$	(33-40)
KGJ	(41-48)
A	(49-56)
E	(57-64)
G	(65-72)

2nd card set after section counters - Uniform pinned-fixed element properties.

1 card for each element in the same format as the fixed-fixed uniform elements.

3rd card set after section counters - Pinned-pinned element properties.

One element per card in the following format:

i joint no.	(1-4)
j joint no.	(5-8)
A	(9-16)
E	(17-24)

4th card set after section counters - Nonuniform, fixed-fixed element properties.

2 cards for each element with the first card the same as the uniform elements. The second card has the following format:

i joint no.	(1-4)
j joint no.	(5-8)
$(PC_1)_x''$	(9-16)
$(PC_2)_x''$	(17-24)
$(PC_3)_x''$	(25-32)

$(PC_1)_z''$	(33-40)
$(PC_2)_z''$	(41-48)
$(PC_3)_z''$	(49-56)

5th card set after section counters - Nonuniform, pinned-fixed element properties.

2 cards for each element in the same format as the nonuniform fixed-fixed set. After the 5th card set a new section counter card is read in until all sections have been read into the matrix.

K-Matrix Formation Program - Computation

Elements are operated on in the order in which they appear in each section unless one of the joint numbers (i or j) exceeds the bounds of the joint numbers being read into the computer for the section.

Calculate for each structural element:

$$\begin{aligned} \ell &= ((x_j - x_i)^2 + (y_j - y_i)^2 + (z_j - z_i)^2)^{\frac{1}{2}}, \\ \phi &= \arcsin((z_j - z_i)/\ell), \\ \theta &= \arctan((x_j - x_i)/(y_j - y_i)). \end{aligned}$$

and the elements of the appropriate T matrix-(12 x 12)* for fixed-fixed, (12 x 12) for pinned-fixed with i a fixed joint, (9 x 9)** for pinned-fixed with i a pinned joint, (6 x 6) for pinned-pinned. Note that Theta is input. For all elements other than pinned-pinned calculate:

$$\begin{aligned} (C_1)_x'' &= (PC_1)_x'' - K^*_x'' \left\{ (PC_1)_x'' + (PC_2)_x'' \right\} 2/(KAG)_x'' \\ (C_2)_x'' &= (PC_2)_x'' - K^*_x'' \left\{ (PC_1)_x'' + (PC_2)_x'' \right\} \left\{ (PC_2)_x'' + (PC_3)_x'' \right\} / (KAG)_x'' \\ (C_3)_x'' &= (PC_3)_x'' - K^*_x'' \left\{ (PC_2)_x'' + (PC_3)_x'' \right\} 2/(KAG)_x'' \end{aligned}$$

and similarly for z". If $(KAG) = 0$ then let $C_k = PC_k$.

The above equations account for the effect of shearing stiffness on the slope-deflection equation coefficients.

$$1/K^* = \Delta^2/EI + (PC_1 + 2PC_2 + PC_3)/KAG$$

*Table 6A-5

**Table 6A-4

Table 6A-4

(xxc) T Matrix for Pinned-Fixed Elements Where i is a Pinned Joint

[illegible]

Now the elements of the stiffness matrix K_s may be found from $T K T^T$ for each element $i j$ where K is evaluated according to the following description for either fixed-fixed, pinned-fixed or pinned-pinned elements*. Note that the position of the elements in the K_s matrix is shown in the column-row designation of the elements of the K matrix. The complete program listing is contained in Reference 22.

K-Matrix Formation Program - Actual Input Data

The actual input for the space frame structure, shown upside down in Figure 6A-2, is contained in Reference 22 and corresponds to the input previously described.

Joints 1-99 are fixed and the numbering and elements shown in the bottom story (joints 1-18) are typical up to the level at the bottom of the trusses. At that level both numbering and elements change to that shown in the figure and all joints (100-125) are pinned.

The heavy lines indicate fixed-fixed and pinned-fixed elements. The lighter lines are all pinned-pinned elements. For clarity the diagonal members are omitted for the intermediate stories.

It should be noted that the stiffnesses of the panels of the wall are taken into account by the lattice analogy of Hrennikoff. Using this analogy a rectangular panel a by b and t thick can be replaced by 4 bars around the periphery and two diagonals.

The areas of these bars are determined by

$$A_d = (3at/16k) (1 + k^2)^{3/2}$$

$$A_a = (3at/16k) (3k^2 - 1)$$

$$A_b = (3at/16k) (3 - k^2)$$

where $k = b/a$.

6A-4 Solution of the Space Frame Equations for Stiffness Coefficients.

Once the complete stiffness matrix is obtained for the space frame, another stiffness matrix may be determined for any group of joints in the frame including any number of the six degrees of freedom of each joint. Since the structure to be analyzed possesses double symmetry about the x - z and y - z planes and the mass is assumed to be symmetric about the x - z plane, symmetry and antisymmetry are utilized to reduce the order of the K_s matrix.

*See Tables 6A-6 through 6A-9

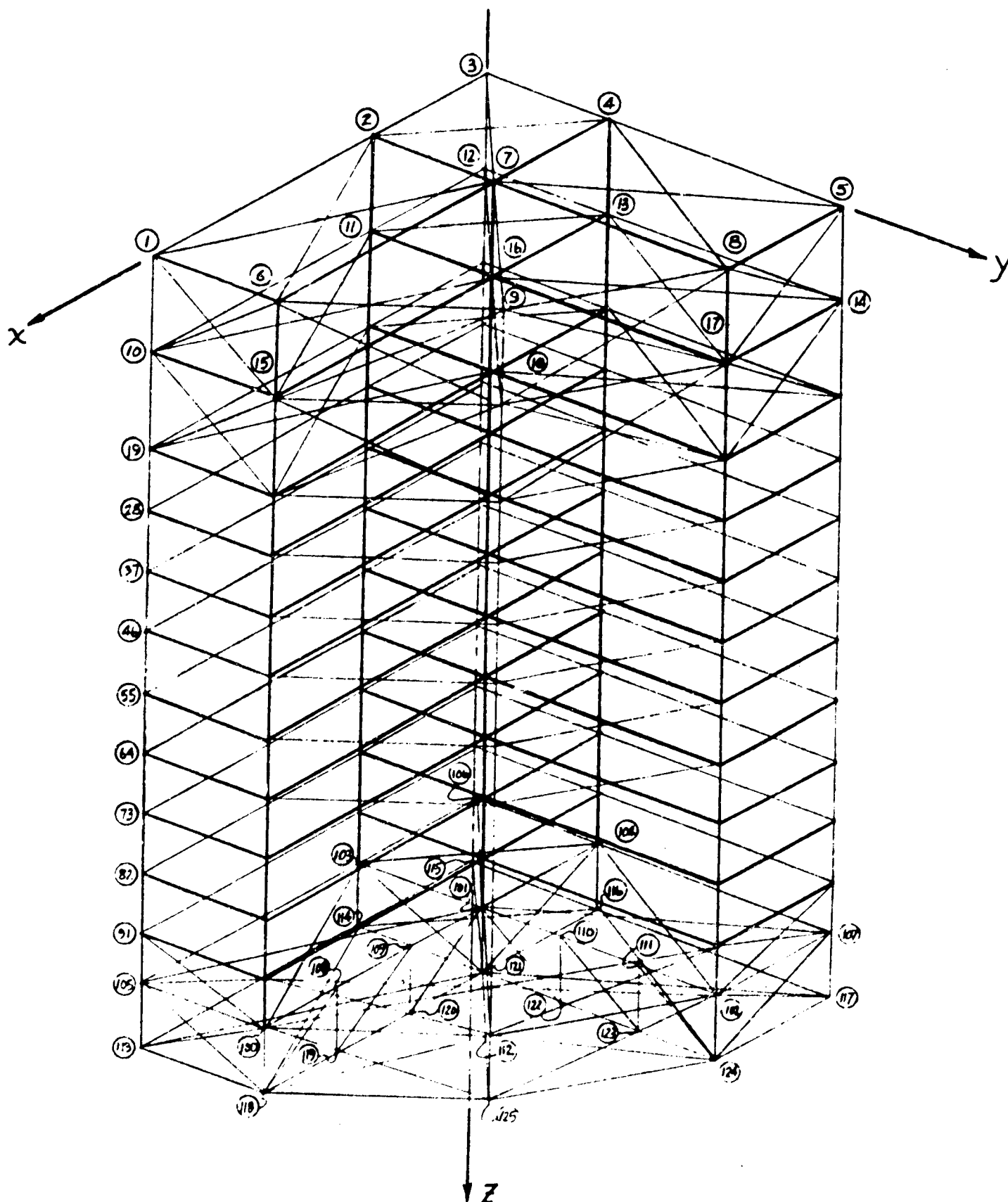


Figure 6A-2. Typical Quarter of the Structural Frame.

Table 6A-6

(12x12) Upper Triangular of K Matrix for Fixed-Fixed Elements

												K _{sf} Matrix Column Row
6i-5	6i-4	6i-3	6i-2	6i-1	6i	6j-5	6j-4	6j-3	6j-2	6j-1	6j	
$[K_B(C_1+2C_2+C_3)/L^3]x''$					$[K_B(C_1+C_2+C_3)/L^3]x''$	$[K_B(C_1+2C_2+C_3)/L^3]x''$					$[K_B(C_2+C_3)/L]x'$	6i-5
	KA						-KA					6i-4
		$[K_B(C_1+2C_2+C_3)/L^3]z''$	$[K_B(C_1+C_2)/L^3]z''$					$[K_B(C_1+2C_2+C_3)/L^3]z''$	$[K_B(C_2+C_3)/L]z'$			6i-3
			$(K_B C_1)/L^3$					$[K_B(C_1+C_2)/L^3]z''$	$(K_B C_2)/L^3$			6i-2
				KGJ/L						-KGJ/L		6i-1
					$(K_B C_1)/L^3$	$[K_B(C_1+C_2)/L^3]x''$					$(K_B C_2)/L^3$	6i
						$[K_B(C_1+2C_2+C_3)/L^3]x''$					$[K_B(C_2+C_3)/L]x'$	6j-5
							KA					6j-4
								$[K_B(C_1+2C_2+C_3)/L^3]z''$	$[K_B(C_2+C_3)/L]z'$			6j-3
									$(K_B C_3)/L^3$			6j-2
										KGJ/L		6j-1
											$(K_B C_3)/L^3$	6j

Table 6A-7

(12x12) Upper Triangular of K Matrix for Pinned-Fixed Elements with i a Fixed Joint

												K _{ij} Matrix Column	Row _i
$G i-5$	$G i-4$	$G i-3$	$G i-2$	$G i-1$	$G i$	$G j-5$	$G j-4$	$G j-3$	$G j-2$	$G j-1$	$G j$		$G i-5$
$[K_B(G_3-C_3^2)/C_1/l^2] x''$						$[K_B(G_3-C_3^2)/C_1/l^2] x''$							$[K_B(G_3-C_3^2)/C_1/l^2] x''$
	K_A						$-K_A$						$G i-4$
		$[K_B(G_3-C_3^2)/C_1/l^2] x''$						$[K_B(G_3-C_3^2)/C_1/l^2] x''$					$G i-3$
													$G i-2$
				$K G J / l$						$-K G J / l$			$G i-1$
													$G i$
						$[K_B(G_3-C_3^2)/C_1/l^2] x''$					$[K_B(G_3-C_3^2)/C_1/l^2] x''$		$G j-5$
							K_A						$G j-4$
								$[K_B(G_3-C_3^2)/C_1/l^2] x''$	$[K_B(G_3-C_3^2)/C_1/l^2] x''$				$G j-3$
									$[K_B(G_3-C_3^2)/C_1/l^2] x''$				$G j-2$
										$K G J / l$			$G j-1$
											$[K_B(G_3-C_3^2)/C_1/l^2] x''$		$G j$

Table 6A-8

(9x9) Upper Triangular of K Matrix for Pinned - Fixed Elements With 1 a Pinned Joint

[illegible]

Note: N = no. of fixed joints in the frame.

Table 6A-9

(6x6) K Matrix For Pinned - Pinned Elements

K Matrix					
s_2					
Column					
Row					
$3N+3i-2$	$3N+3i-1$ p-p	$3N+3i$	$3N+3j-2$	$3N+3j-1$ p-p	$3N+3j$
	$(3N+3i-1) p-f$ $(6i-4) f-f$			$(6j-4) p-f$ $(6j-4) f-f$	
	K_A			$-K_A$	$(3N+3i-1) p-f$ $(6i-4) f-f$
	$-K_A$			K_A	$(6j-4) p-f$ $(6j-4) f-f$

Notes: N = no. of fixed joints in the frame.

p - p indicates indices for K matrix for i pinned, j pinned
 p - f " " " " i pinned, j fixed
 f - f " " " " i fixed, j fixed

The appropriate boundary conditions are no deflection through either plane for symmetry and no deflection through the x-z plane and no vertical deflection in the y-z plane for antisymmetry.

The procedure used to determine stiffness coefficients is to restrain all joints in the degrees of freedom to be considered with one degree of freedom excepted. The unrestrained degree of freedom is deflected a unit amount and the reactions in all the restrained degrees of freedom are determined. These reactions have the magnitude and sign of the stiffness coefficients. Since the force applied to the restraint, the stiffness coefficient for the degree of freedom being deflected must be determined from the sum of the reactions in all the other degrees of freedom. By repeating this procedure for all the degrees of freedom to be considered, the stiffness matrix can be determined. So that all coefficients can be determined in one operation the unit deflection of each degree of freedom is obtained by imposing a load on the restraint in the appropriate units and in the positive direction of the degree of freedom.

The matrix operations required for the above-described procedures are outlined below for the actual space frame, one quarter of which is shown in Figure 6A-2.

<u>Matrix Designation</u>	<u>Matrix Order</u>	<u>Matrix Definition</u>
K_s	672 x 672	unrestrained stiffness matrix of 1/4 of frame.
K_{ar}	672 x 672	diagonal matrix of antisymmetric restraints
K_{sr}	672 x 672	diagonal matrix of symmetric restraints
K_{mpr}	672 x 672	diagonal matrix of mass point restraints
F_s	672 x 73	matrix of forces equal to mass point restraint, one per column for each of 73 mass points
\bar{d}_s	672 x 73	matrix of deflections for symmetric loading
\bar{d}_a	672 x 73	matrix of deflections for antisymmetric loading
K_a	73 x 73	antisymmetric stiffness matrix
K_b	73 x 73	symmetric stiffness matrix

<u>Matrix Designation</u>	<u>Matrix Order</u>	<u>Matrix Definition</u>
$K_{d_i} (i=1,2,3,4)$	1 x 73 73 x 73	matrices which are formed as rows and converted to diagonals to provide the diagonal elements of K_a and K_b
K_{11}	73 x 73	upper left quadrant of complete stiffness matrix
K_{12}	73 x 73	upper right quadrant of complete stiffness matrix with duplicated columns included
R_s	73 x 73	diagonal matrix used to null and double some rows and columns in K_b matrix
R_a	73 x 73	diagonal matrix used to null and double some rows and columns in K_a matrix
E	73 x 48	matrix used to eliminate some rows and columns of K_{11} and K_{12} matrices in the formation of the complete stiffness matrix
K_c	121 x 121	complete stiffness matrix for all degrees of freedom to be considered in the vibration analysis

The following operations were performed for the actual structure using the Lockheed proprietary FAMAS matrix algebra programming system:

Antisymmetric operations

1. Three stiffness matrices are added and inverted and postmultiplied

$$1/2(K_s + K_{ar} + K_{mpr})^{-1} F_s = d_a \quad (\text{Eq. 6A-10})$$

2. The resulting deflection matrix is premultiplied by the transpose of the force matrix, the diagonal eliminated by an element by element multiply, and the columns are summed.

$$\begin{bmatrix} K_{d_1} \end{bmatrix} = \begin{bmatrix} 1 \end{bmatrix} (F_s^T d_a)(e.e) * \left\{ \begin{bmatrix} 1 \end{bmatrix} - \begin{bmatrix} 1 \end{bmatrix} \right\} \quad (\text{Eq. 6A-11})$$

3. The deflection matrix is also premultiplied by the matrix of antisymmetric restraints and the columns summed

$$\begin{bmatrix} K_{d_2} \end{bmatrix} = \begin{bmatrix} 1 \end{bmatrix} K_{ar} d_a \quad (\text{Eq. 6A-12})$$

*The term (e.e) indicates an element by element multiply of the matrices on either side of it.

4. The antisymmetric stiffness matrix is now formed by converting the resulting row matrices of operations 2 and 3 to diagonals, adding them and subtracting the matrix with the nulled diagonal.

$$\begin{aligned}
 \left[K_{d_1} \right] &\rightarrow \left[K_{d_1} \right] \\
 \left[K_{d_2} \right] &\rightarrow \left[K_{d_2} \right] \\
 K_a &= \left[K_{d_1} \right] + \left[K_{d_2} \right] - (F_s^T d_a) (e.e) * \left\{ \left[1 \right] - \left[1 \right] \right\} \\
 &\hspace{15em} \text{(Eq. 6A-13)}
 \end{aligned}$$

Symmetric operations

The procedure is the same as that used in the antisymmetric operations; however, the following matrices are replaced:

K_{ar} is replaced by K_{sr}

d_a is replaced by d_s

K_{d_1} is replaced by K_{d_3}

K_{d_2} is replaced by K_{d_4}

K_a is replaced by K_b

Combining operations

Certain requirements of symmetry and antisymmetry must be accounted for prior to combining the antisymmetric and symmetric stiffness matrices to form the stiffness matrix of one half of the structure. Specifically, the rows and columns of all vertical (z) degrees of freedom in the boundary plane must be nulled in the antisymmetric stiffness matrix, since there can be no reactions at the boundary under antisymmetric loading. The same rows and columns must be doubled in the symmetric stiffness matrix except for the elements in the row-column intersections which must be quadrupled. The reasons for this are that the boundary reactions must be doubled for unit deflections of non-boundary joints, and boundary reactions and the unit deflections must both be doubled when the deflected joint is a boundary joint.

*The term (e.e), indicates an element by element multiply of the matrices on either side of it.

Horizontal (x) degrees of freedom must be treated in a similar manner if breathing modes are not considered. The procedure is reversed, however, in that the rows and columns are nulled in the symmetric matrix and doubled in the antisymmetric matrix (again intersection elements are quadrupled).

$$\begin{aligned} K_{11} &= R_s K_b R_s + R_a K_a R_a \\ K_{12} &= R_s K_b R_s - R_a K_a R_a \end{aligned} \quad (\text{Eq. 6A-14})$$

To eliminate duplication of rows and columns of the vertical boundary and horizontal degrees of freedom the stiffness matrix is formed as follows:

$$K_c = \begin{bmatrix} K_{11} & K_{12}E \\ E^T K_{12}^T & E^T K_{11} E \end{bmatrix}$$

where the matrix E eliminates the columns and E^T eliminates the rows.

6A-5 Determination of the Unrestrained Vibration Modes of the Space Frame.

The basic equations of free vibration are for the conservation of linear and angular momentum and the internal equilibrium equations. Obviously, for the space frame in question an equal vertical or horizontal deflection of all points or a rigid body rotation results in no strain energy being put into the structure. Hence, three of the internal equilibrium equations are not independent and must be replaced by three conservation-of-momentum equations. These latter three equations are chosen as the summation of vertical and horizontal inertial forces about the center of gravity equal zero. In matrix form

$$\begin{aligned} e_1 M \ddot{d} &= 0 \\ e_2 M \ddot{d} &= 0 \\ e_3 M \ddot{d} &= 0 \\ M \ddot{d} + K_c d &= 0 \end{aligned} \quad (\text{Eq. 6A-16})$$

Since the vibration is sinusoidal it is possible to reduce Equation 6A-16 to

$$\begin{aligned} e_1 M d &= 0 \\ e_2 M d &= 0 \\ e_3 M d &= 0 \\ (M - \lambda K_c) d &= 0 \end{aligned} \quad (\text{Eq. 6A-17})$$

and by eliminating the first three rows of Equation 6A-17 and replacing them with the first three rows of Equation 6A-16

$$\left\{ \begin{bmatrix} e_1 \\ \vdots \\ e_2 \\ \vdots \\ e_3 \\ 0 \quad \vdots \quad I \end{bmatrix} M - \lambda \begin{bmatrix} \vdots & 0 & \vdots \\ 0 & \vdots & 0 \\ \vdots & I & \vdots \end{bmatrix} K_c \right\} d = 0 \quad (\text{Eq. 6A-18})$$

By scalar multiplying the first three equations by λ

$$\begin{bmatrix} e_1 \\ e_2 \\ e_3 \end{bmatrix} \begin{bmatrix} M \end{bmatrix} \quad \text{may be transplanted}$$

in the first three rows of the K_c matrix to form K_T . Although the K_c matrix has three singularities the K_T will have none provided the order of elements is chosen such that e_1 , e_2 , and e_3 provide elements on the diagonal. Consequently Equation 6A-18 can be modified to

$$(M_T - \lambda K_T) d = 0 \quad (\text{Eq. 6A-19})$$

and since K_T can be inverted Equation 6A-19 can be put in the form

$$K_T^{-1} M_T d = \lambda d \quad (\text{Eq. 6A-20})$$

which is suitable for solution for eigenvalues and eigenvectors by the power method.

The procedure described above was utilized in attempting to obtain the first three vibration modes of the unrestrained space frame in two weight configurations. All matrix operations were accomplished using the FAMAS matrix algebra programming system. Two modes were obtained accurately for the heavyweight configuration; however, only one was obtained accurately for the lightweight configurations. In the latter case the second and third mode frequencies were extremely close. Since the accuracy of the power method is severely degraded for modes whose frequencies nearly coalesce, the loss of accuracy may be attributable to this fact. Two hundred iterations for each mode failed to provide the desired accuracy in the eigenvector.

All eigenvalues, eigenvectors, and other vibration data which were obtained are contained in Reference 22. However, the three accurate mode shapes which were obtained are plotted in Figures 6A-3, 6A-4, and 6A-5. The two mass matrices, M , and the rigid body eigenvectors e_1 , e_2 (two cases), and e_3 , which were used are contained in Reference 22.

WL TDR 64-53

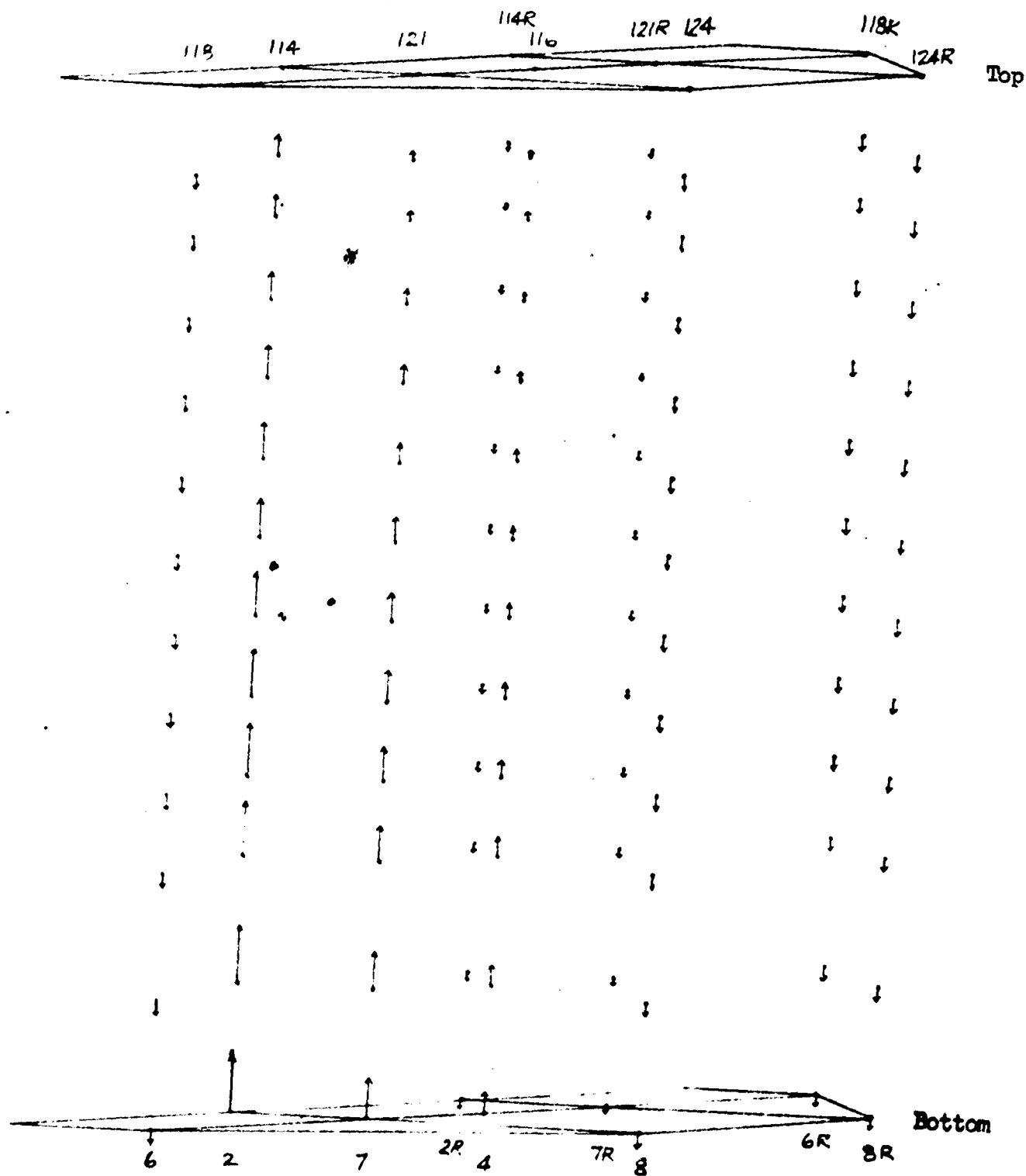


Figure 6A-3. Heavyweight Configuration First Vibration Mode.
Frequency = 4.25 cps; Lateral Response - Negligible.

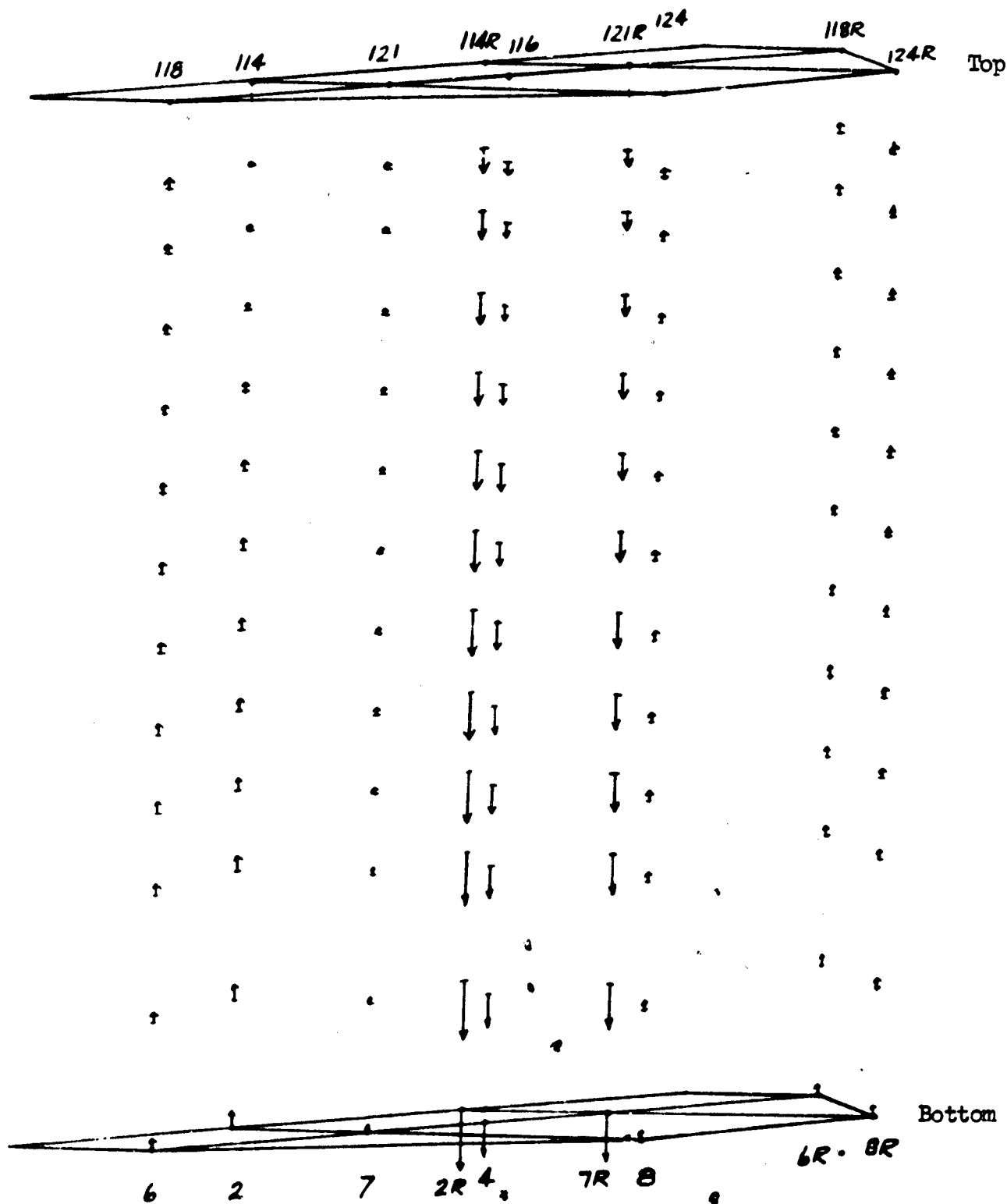


Figure 6A-4. Heavyweight Configuration Second Vibration Mode.
Frequency = 5.11 cps; Lateral Response - Negligible.

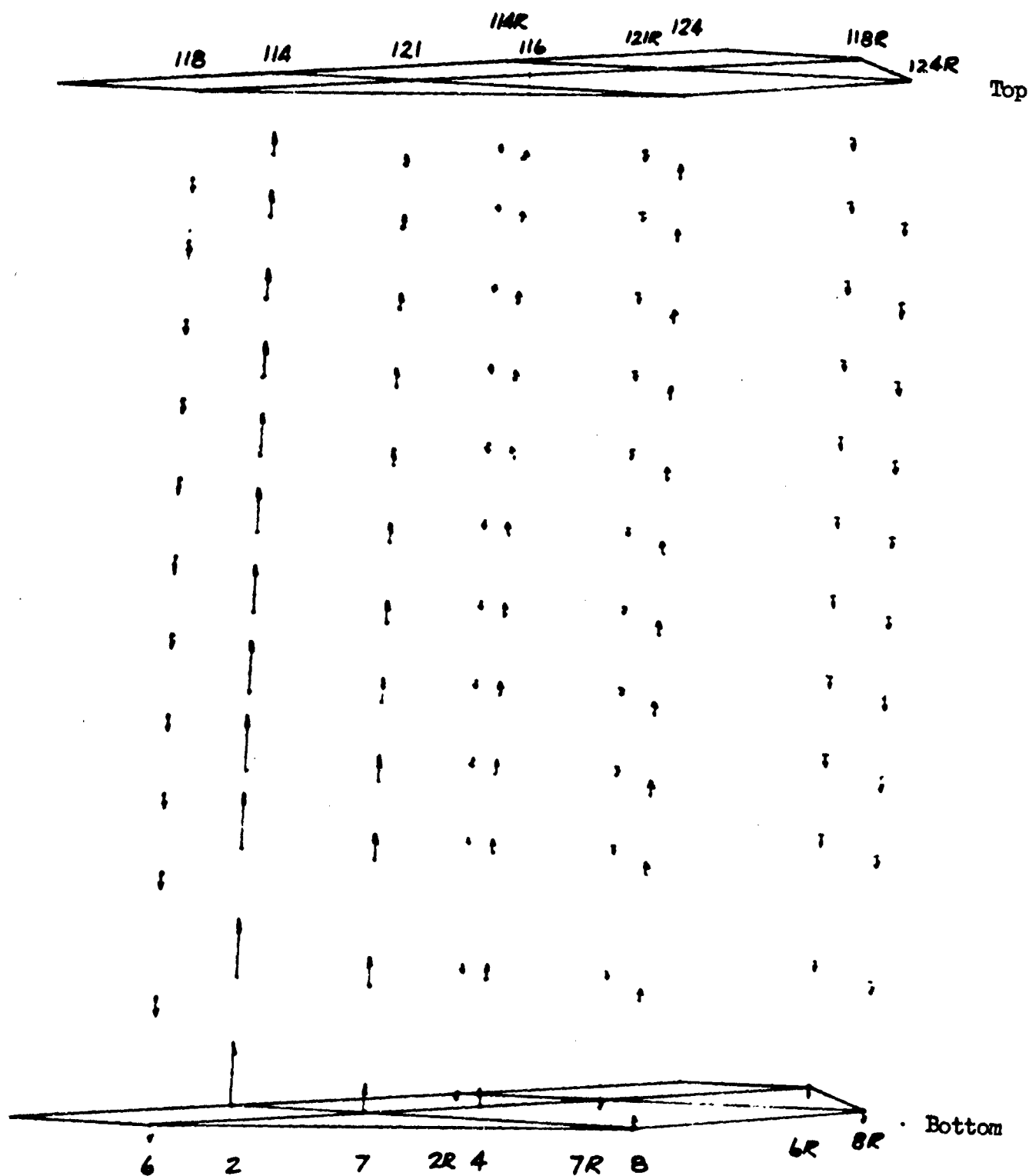


Figure 6A-5. Lightweight Configuration First Vibration Mode.
Frequency = 4.72 cps; Lateral Response - Negligible.

TABLE 6A-10
DEGREES OF FREEDOM

<u>Degree of Freedom</u>	<u>Joint No.</u>	<u>Direc.</u>	<u>Degree of Freedom</u>	<u>Joint No.</u>	<u>Direc.</u>
1	2	z	31	47	z
2	4	z	32	49	z
3	6	x	33	51	x
4	6	z	34	51	z
5	7	z	35	52	z
6	8	z	36	53	z
7	11	z	37	56	z
8	13	z	38	58	z
9	15	x	39	60	x
10	15	z	40	60	z
11	16	z	41	61	z
12	17	z	42	62	z
13	20	z	43	65	z
14	22	z	44	67	z
15	24	x	45	69	x
16	24	z	46	69	z
17	25	z	47	70	z
18	26	z	48	71	z
19	29	z	49	74	z
20	31	z	50	76	z
21	33	x	51	78	x
22	33	z	52	78	z
23	34	z	53	79	z
24	35	z	54	80	z
25	38	z	55	83	z
26	40	z	56	85	z
27	42	x	57	87	x
28	42	z	58	87	z
29	43	z	59	88	z
30	44	z	60	89	z

TABLE 6A-10 (continued)
DEGREES OF FREEDOM

<u>Degree of Freedom</u>	<u>Joint No.</u>	<u>Direc.</u>	<u>Degree of Freedom</u>	<u>Joint No.</u>	<u>Direc.</u>
61	92	z	91	42R	z
62	94	z	92	43R	z
63	96	x	93	44R	z
64	96	z	94	47R	z
65	97	z	95	51R	z
66	98	z	96	52R	z
67	100	x	97	53R	z
68	100	z	98	56R	z
69	101	z	99	60R	z
70	102	z	100	61R	z
71	103	z	101	62R	z
72	104	z	102	65R	z
73	118	x	103	69R	z
74	2R	z	104	70R	z
75	6R	z	105	71R	z
76	7R	z	106	74R	z
77	8R	z	107	78R	z
78	11R	z	108	79R	z
79	15R	z	109	80R	z
80	16R	z	110	83R	z
81	17R	z	111	87R	z
82	20R	z	112	88R	z
83	24R	z	113	89R	z
84	25R	z	114	92R	z
85	26R	z	115	96R	z
86	29R	z	116	97R	z
87	33R	z	117	98R	z
88	34R	z	118	100R	z
89	35R	z	119	101R	z
90	38R	z	120	102R	z
			121	103R	z

The degrees of freedom for the stiffness matrix and eigenvectors are related to the joints of Figure 6A-2 in Table 6A-10. The R indicates the reflected point in the other quarter of the structure.

The magnitude and direction of the arrows in Figures 6A-3, 6A-4 and 6A-5, indicate the relative deflection of vertical degrees of freedom in the vibration mode. The lateral deflections are small and are not plotted for all three modes. For clarity the intermediate joints are not connected and only the top and bottom joints are numbered. Also for convenience the structure has been turned top-side up.

6A-6 Dynamic Analysis of the Unrestrained Space Frame.

In order to determine the elastic response of the space frame to isolator loads determined by a six degree of freedom rigid body analysis, the following transient response program was developed. A complete listing of the program is contained in Reference 22; however, the input and computational requirements are described below:

Transient Response Program - Input

$$\begin{aligned} [M_j] &= \underbrace{nxn}_{\text{diagonal matrix of generalized masses.}} \\ [W_j] &= \underbrace{nxn}_{\text{diagonal matrix of circular frequencies.}} \\ [\psi_j^{(1)}] &= \underbrace{3xn}_{\text{matrices of n columns of 3 element (x,y,z) eigen-}} \\ &\quad \text{vectors for each joint of m joints.} \\ \left\{ \begin{matrix} x^{(1)} \\ y^{(1)} \\ z^{(1)} \end{matrix} \right\} &= \left\{ \begin{matrix} x^{(1)} \\ y^{(1)} \\ z^{(1)} \end{matrix} \right\} = \text{matrix of three coordinates for each joint } i^* \end{aligned}$$

*NOTE: The first K joints are isolator attach points

$$(1) \begin{matrix} F^{(1)} \\ x_{rb} \\ y_{rb} \\ z_{rb} \end{matrix} \text{ vs. } t \text{ for the first } k \text{ joints at fixed intervals of time.}$$

$$(2) \begin{matrix} x_{rb}^{cg} \\ y_{rb}^{cg} \\ z_{rb}^{cg} \\ \alpha^{cg} \\ \beta^{cg} \\ \gamma^{cg} \end{matrix} \text{ vs. } t \text{ for the c.g. only at the same time intervals.}$$

Transient Response Program - Computation

The following set of differential equations is solved

$$[M_j] \left(\left\{ \ddot{\eta}_j \right\} + [\omega_j^2] \left\{ \eta_j \right\} \right) = - \sum_{i=1}^k \begin{bmatrix} F^{(1)} \end{bmatrix} \begin{bmatrix} \psi_j^{(1)} \end{bmatrix} \quad (\text{Eq. 6A-21})$$

$$\text{where } \begin{bmatrix} F^{(1)} \end{bmatrix} = \begin{bmatrix} F_x^{(1)} & F_y^{(1)} & F_z^{(1)} \\ r_b & r_b & r_b \end{bmatrix}$$

and η is evaluated at the fixed time intervals.

Now for each joint i at each time interval finds:

$$\begin{Bmatrix} x_{rb}^{(1)} \\ y_{rb}^{(1)} \\ z_{rb}^{(1)} \end{Bmatrix} = \begin{Bmatrix} x_{rb}^{cg} \\ y_{rb}^{cg} \\ z_{rb}^{cg} \end{Bmatrix} + \begin{bmatrix} 0 & r_z^{(1)} & -r_y^{(1)} \\ -r_z^{(1)} & 0 & r_x^{(1)} \\ r_y^{(1)} & -r_x^{(1)} & 0 \end{bmatrix} \begin{Bmatrix} \alpha^{cg} \\ \beta^{cg} \\ \gamma^{cg} \end{Bmatrix}$$

and

$$\begin{Bmatrix} x_T^{(1)} \\ y_T^{(1)} \\ z_T^{(1)} \end{Bmatrix} = \begin{Bmatrix} x_{rb}^{(1)} \\ y_{rb}^{(1)} \\ z_{rb}^{(1)} \end{Bmatrix} + \begin{bmatrix} \psi_j^{(1)} \end{bmatrix} \begin{Bmatrix} \eta_j \end{Bmatrix}$$

SECTION 6 SYMBOLS AND NOTATION

F	=	force scalar or vector, pounds
d	=	deflection vector, inches
A	=	cross-sectional area, inches ²
E	=	modulus of elasticity, pounds per inch ²
KAG	=	shearing stiffness, pounds per inch
KGJ	=	torsional stiffness, inch pounds per radian
I	=	moment of inertia, inches ⁴
C_1, C_2, C_3	=	slope-deflection equation coefficients
e_1, e_2, e_3	=	rigid body deflection vectors, inches
M	=	matrix of concentrated masses, pound seconds per inch
l	=	element length, inches
K_c	=	unrestrained stiffness matrix of mass point degrees of freedom, pounds per inch
K_T	=	transplanted K_c
M_T	=	transplanted M
$F_{x_{rb}}, F_{y_{rb}}, F_{z_{rb}}$	=	isolator forces, pounds
$x_{rb}^{cg}, y_{rb}^{cg}, z_{rb}^{cg}$	=	rigid body c.g. displacements, inches
$\alpha_{rb}^{cg}, \beta_{rb}^{cg}, \gamma_{rb}^{cg}$	=	rigid body c.g. rotations, radians
ϕ, θ, ψ	=	rotations, radians
K_B	=	$\frac{EI}{l}$, inch pounds
K_A	=	$\frac{AE}{l}$, inch pounds

WL TDR 64-53

7.0 SUMMARY AND RECOMMENDATIONS

7.1 Principal Conclusions

The purpose of this study was to investigate the feasibility of isolating very large structures from the effects of severe ground shock. As a result of the study it is concluded that such shock isolation is feasible and, although no shock isolation systems of this magnitude have been constructed to date, it appears that no new engineering or fabrication techniques are required.

As a basis for this statement, and to summarize some of the more important conclusions reached during the investigation, the following points are presented.

Isolator

1. The fluid filled isolator (liquid or gas) is a smaller more easily controlled device than pure mechanical systems with the same force and stiffness variation characteristics.
2. In a system maintained in the equilibrium position by an automatic controller, moderate amounts of coulomb type friction are desirable if the slope of the friction-force/velocity curve is positive in the range from zero velocity to a value above the maximum desired control velocity.
3. Velocity damping in a rigidly connected simple system can produce very high transient forces in the supported mass. If used in a viscoelastic system, the system properties can be adjusted so as to achieve a more favorable transient response and at the same time provide the required damping in residual oscillations.
4. The coulomb friction inherent in most liquid springs is sufficient to provide the system with the needed insensitivity to input waveform.
5. With all usual types of damping, the amount of damping needed to achieve an acceptable insensitivity to waveform is more severe than the requirements for reducing the oscillations to 10 per cent amplitude in 30 seconds.
6. The response of the cable/isolator pendulum arm to the high velocity phase of the ground motion can produce very high accelerations in the arm and in the suspended mass. The transient accelerations can be reduced to a negligible value only by reducing the mass of the moving parts.

Isolation System

1. Drag forces resulting from the compression of air in the capsule by the oscillatory motion of the cage can be very large for small capsule-cage clearances. While no data are available on the magnitudes of the side force and pitching moment, the low restoring forces of the suspension system in these modes and the destabilizing influence of the side forces and moments could lead to large lateral and rotational excursions.
2. In selecting pendulum suspension system configurations the principal criterion of performance is system stability. The ratio of restoring force to coupling force is a more significant parameter of relative displacement than coupling alone.
3. The effect on the response of the system of sloshing of fluids in containers mounted on the supported mass can be easily reduced to a negligible value by reasonable care in selecting tank size, orientation, and, if warranted, baffles, even though the total mass of the fluids is as much as 20 per cent of the total suspended mass.
4. The two-level, inclined pendulum suspension system appears to offer greater stability and a lesser rattlespace requirement than the two other systems considered, if both systems are assumed to contain linear or near linear isolators.

Structure

1. By exercising reasonable care in design, conventional structural construction methods are adequate to provide the rigidity needed in these installations. Note, however, that the 1/4-inch steel shell enclosing the cage was a major factor in achieving high rigidity.

7.2 Recommendations

If a selection of an isolation system for use in an application similar to that considered here were to be made today, the pneumatic isolator would be recommended as the elastic element on the basis of three considerations.

1. The degree of position control which can be achieved over any isolator is directly related to its "stick-slip" characteristics which in turn are functions of the amount of friction and the slope of the friction-force-velocity curve. If the friction forces are very small, close control may be obtained regardless of the slope of the curve. If the friction forces are appreciable, however, the jump displacements become quite large for small negative slopes and positioning sensitivity is compromised.

It was shown in Section 5.0 that in order to conserve rattlespace the band of excursions from equilibrium within which the isolator must be controlled is fairly narrow. Yet few quantitative data are available on the friction characteristics of liquid springs, and these data are insufficient to give more than a gross indication of the nature of the curve. Further, nothing is known about the change in the friction forces or the curve shape with wear or aging. It would seem, then, that comprehensive experiments must be conducted before sufficient information is available on which to base a decision regarding the suitability of the liquid spring in this respect.

The friction forces on the rolling sleeve pneumatic isolator, however, are very low. Unpublished data from tests conducted on a unit of this type at the Air Force Special Weapons Center, Kirtland Air Force Base, indicate that the coulomb friction is less than 1/4 per cent of the static force and that there is no tendency to jump.

2. The injection or withdrawal of liquid from a cylinder pressurized to 20,000 pounds per square inch is much more severe problem than that of regulating air to a 600 psi storage vessel. In fact for the latter case, the air regulation equipment now in use in the WS 133A Launch Control Center shock isolation system would be more than adequate for this application. Thus, while the regulation of pressure in the liquid spring does not exceed current practice, special equipment calling for experienced engineering, fabrication and maintenance is required. The pneumatic control equipment is commercially available.

3. It is considered highly probable that the weight of the piston and shaft assembly for the pneumatic spring can be reduced to a lower value than those parts for the liquid spring. The general arrangement and the lower pressures of the pneumatic device appear to make the use of stiffened-shell type structure and light weight alloys more feasible than in the liquid spring. This point, of course, can only be determined by a careful comparison of the detail designs of both systems.

The type of suspension system including the number of isolators, the pendulum attach points, and the pendulum arm inclination can be established only after a thorough analysis of the system has been made. It is recommended, however, that principal attention be directed toward the use of the two-level suspension method and that as a starting point, the arrangement of configuration 3 be employed.

An automatic positioning system should be provided to maintain the cage near equilibrium. It is necessary only that position be detected by relative displacement of the isolator piston relative to the cylinder, changes in length of the cable due to temperature, creep or load adjustment being negligible. Turnbuckles should be provided in the cables to enable periodic but infrequent realignments to be made.

7.3 Problem Areas

It is firmly believed that all problems which may arise in connection with the development of a shock isolation system for the general type of application considered in this study can be met without the need for extending the state of the art in engineering design, fabrication or installation techniques. If the system is to be well designed, economical and reliable, many technical challenges must be met successfully, but these challenges are no different in kind or degree than those which have faced the designers of many of the shock isolation systems now in operation in our present underground protective structures.

Areas needing further work, then, are those which involve the accumulation of engineering information, rather than knowledge, as related to a system of this particular type. Some of the areas might be labeled as problems simply because the time required to assemble the information by test or analysis is much longer than the time usually allowed for the design of the complete facility.

Specific areas in which it is recommended that early work be done are:

- . Dynamic analysis of six degree of freedom rigid body system and optimization of two-level pendulum configuration with respect to relative displacement, acceleration and damping.
- . Development and test of pre-prototype (or scale model) of pneumatic isolator with the objective of verifying the analytical expression for restoring force and damping characteristics.
- . Tests to determine the aerodynamic forces and moments produced on a cylindrical piston oscillating in a confined cylindrical cavity.
- . If there is further interest in the liquid spring, determine the friction force-velocity characteristics of liquid spring using typical construction methods and sealing materials. Determine effect on friction of wear and aging. Investigate the mechanical design of fluid injection and withdrawal systems.

REFERENCES

1. Air Force Weapons Laboratory Letter WLRS/Capt. Merkle/2682/
27 Nov. 1963.
2. The Ralph M. Parsons Company: A Guide for the Design of Shock
Isolation Systems for Underground Protective Structures; Air Force
Special Weapons Center, Kirtland Air Force Base, AFSWC-TDR-62-64;
December 1962.
3. Bridgman, P. W.: The Physics of High Pressure; G. Bell and Sons,
London, 1949.
4. Cosgrove, S. L. and Duetlgen, R. L.; The Effect of Nuclear
Radiation on Lubricants and Hydraulic Fluids; Report No. 19,
Radiation Effects Information Center, Battelle Memorial Institute,
Columbus, Ohio, May 31, 1961.
5. Dow Corning Corporation: Silicone Notes; Bulletin 05-041,
April 1963.
6. Bridgman, P. W.: Proceedings of the American Academy of Arts
and Sciences, pp. 115-146, 1949.
7. Dow Corning Corporation: Silicone Notes; Bulletin 05-014,
June 1962.
8. Union Carbide Corporation: Physical Properties of L-45 and L-527;
Data Sheet SF-1116-1, July 1, 1959.
9. Union Carbide Corporation: Compressibility of L-45 and L-527;
Data Sheet SF-1116-4, July 1, 1959.
10. Taylor Devices, Inc.: Supplementary Calculations on Dynamic
Performance for The Boeing Company; North Tonawanda, New York.
11. Stroud, V. and Volz, W. A.: A Combined Analytical and Testing
Method for Obtaining a Mathematical Representation for Nonlinear
Shock Absorbers; prepared for the 30th Symposium on Shock, Vibra-
tion and Associated Environments, 10 - 12 October 1961; Westinghouse
Electric Corporation, Sunnyvale, California.
12. Cavanaugh, R. D.: Air Suspension and Servo-Controlled Isolation
Systems; Shock and Vibration Handbook, Volume 2, Chapter 33;
McGraw-Hill Book Company, Inc., New York, 1961.

13. Saffell, H. R.: Preliminary Performance Analysis of the Model 133AB Pneumatic Shock Isolator; The Ralph M. Parsons Company, June 1963.
14. Drawing 1005359, Cage Shock Isolation Space Allocation, and NavDocks Specification No. 53142/65, Section 50, Special Items, prepared by The Ralph M. Parsons Company under Contract No. NBy-45849.
15. Daugherty, R. L. and Ingersoll, A. C.: Fluid Mechanics; McGraw-Hill Book Company, Inc., New York, 1954.
16. Dombrow, Bernard: Polyurethanes; Reinhold Publishing Corporation, New York, 1957.
17. Kaminsky, Philip J.: Physical Characteristics of Some Resilient Materials; Research and Development Division, Avco Corporation, Wilmington, Massachusetts; DDC Document No. AD-248 800, December 12, 1960.
18. PFSIM Tests of Prototype Segmented Foam Covers; Westinghouse Electric Corporation Control No. 17431. (Confidential)
19. Riley, M. W.: What's New in Plastics, Materials in Design Engineering, pp. 119-134, March 1961.
20. Ved, J. G.; Epure, S. T.; and Saffell, H. R.: WS 133A Launch Equipment Room Platform Dynamic Response Analysis; Report No. RMP-FR-3132-58/2, The Ralph M. Parsons Company, October 1963.
21. United States Steel Corporation: Handbook for Western Wire Rope Users; Columbia-Geneva Steel Division, San Francisco, California.
22. The Ralph M. Parsons Company: Computer Programs, RMP-CP-3295/1; March 1964.